VHPC Material Characterization and Recommendations for the Buffalo Branch Bridge Rehabilitation

Carrie S. Field

Thesis submitted to the Faculty of the Virginia Polytechnic Institute and State University in partial fulfillment of the requirements for the degree of

Master of Science

In

Civil Engineering

Carin L. Roberts-Wollmann, Chair

Thomas E. Cousins

David W. Mokarem

August 10, 2015

Blacksburg, VA

Keywords: Adjacent Box Beam Bridges, UHPC, Shear Key, Live Load Test

VHPC Material Characterization and Recommendations for the Buffalo Branch Bridge Rehabilitation

Carrie S. Field

ABSTRACT

Adjacent box beam bridges are economical bridge systems for accelerated bridge construction. The box beams are constructed at precast plants and are traditionally connected by a shear key filled with grout. This system is ideal for short spans with low clearance restrictions. However, due to the grout deteriorating and debonding from the precast concrete in the shear key, reflective cracking propogates through the deck allowing water and chemicals to leak down into the joints. This can lead to the prestressing steel inside the precast member and the transverse tie steel corroding. This necessitates the bridge being rehabilitated or replaced which shortens the life-span of the bridge system and negates the economical value it had to begin with.

This research project aimed to design a rehabilitation plan for an adjacent box beam bridge with deteriorated joints using Very High Performance Concrete (VHPC). VHPC was chosen as an economical alternative to the proprietary Ultra High Performance Concrete (UHPC) and extensive material tests were performed. The results of the material testing of VHPC and grout revealed that VHPC had higher compressive and tensile strengths, a higher modulus of elasticity, gained strength faster, bonded better to precast concrete, was more durable over time, and shrank less than conventional grout.

The results of this research project were applied to rehabilitate the Buffalo Branch Bridge and further testing will be completed to determine the effectiveness of the rehabilitation.

ACKNOWLEDGEMENTS

First, I would like to thank Dr. Cousins and Dr. Roberts-Wollmann for taking a chance on me and affording me the opportunity to do research. I am grateful for your guidance and patience throughout this whole experience. Without your expertise, I would not have completed this project or learned nearly as much in the process.

Next I wish to say a special thank you to David Mokarem, Brett Farmer, and Dennis Huffman. Your experience and direction you provided when ordering the right materials, designing formwork, mixing concrete, and everything else in the lab were essential in completing the testing. Concrete is heavy and messy; without your care and supervision, I would not have made it through these two years injury free.

Additionally I'm grateful for all the help I received from other students. Amey, Kedar, and Aritra: thanks for teaching me everything I know about Abaqus. Kedar and Pat: thanks for showing me the ins and outs of the lab and helping me test. Jimmy: thanks for being my right-hand man and working tirelessly on my behalf mixing concrete, testing in the middle of the night, and assisting me with the live load test.

Lastly, I would like to thank my friends and family for all your encouragement. Thanks for visiting, hiking, and playing outside with me and for the phone calls that helped keep me sane and focused on the big picture. Your support has been more than I could have ever asked for.

I am really blessed to be able to continue my education here. Thanks y'all for making my graduate school experience rewarding and enjoyable.

Table of Contents

List of Figures

List of Tables

INTRODUCTION

Motivation

Adjacent prestressed girder bridges are comprised of either precast adjacent box beams or voided slab sections as the superstructure with a deck or topping placed directly on top. The precast members are traditionally connected with a shear key filled with grout and transversely tied at intermittent diaphragm locations. This ensures transverse load transfer between neighboring adjacent members. By using precast members, these bridges are fairly simple and can be rapidly constructed due to a significant amount of work done beforehand offsite at a precast plant. Adjacent box beam bridges are an efficient design for short spans and bridge locations with low vertical clearance requirements. However, over time the traditional grout shear key tends to deteriorate causing reflective cracking to propogate through the deck and into the wearing surface as shown in Figure 1.

Figure 1. Reflective cracking

These reflective cracks allow for water and corrosive agents such as deicer salts to seep down into the joints which, if left untreated, can eventually cause the reinforcing and prestressing steel in the precast members to corrode. This leads to the need for bridge repair or replacement well before its design life, negating the assessed economic value of the adjacent member system. Reflective cracking allowing water to leak through the joint can be seen in Figure 2, which is the underside of the joint in Figure 1.

Figure 2. Leaking joint

Purpose and Scope

Due to the problems that arise when reflective cracking appears, the purpose of this project is to recommend an alternative connection that can be used to rehabilitate the adjacent member bridges. The goal of the improved connection is to increase the service life of the bridge well beyond that obtained by simply replacing the deteriorated shear key with an identical shear key design. Graybeal (2014) with the Federal Highway Administration, FHWA, has suggested

replacing the grout shear key with Ultra High Performance Concrete, UHPC. Graybeal (2014) defines UHPC as “a cementitious composite material composed of an optimized gradation of granular constituents, a water-to-cementitious materials ratio less than 0.25, and a high percentage of discontinuous internal fiber reinforcement. The mechanical properties of UHPC include compressive strength greater than 21.7 ksi and sustained post-cracking tensile strength greater than 0.72 ksi”. Additionally Graybeal asserts that the discontinuous pore structure of UHPC significantly enhances the durability compared to traditional concrete or grout because it reduces the liquid ingress. Graybeal’s suggestion for a UHPC connection of adjacent box beams is shown in Figure 3.

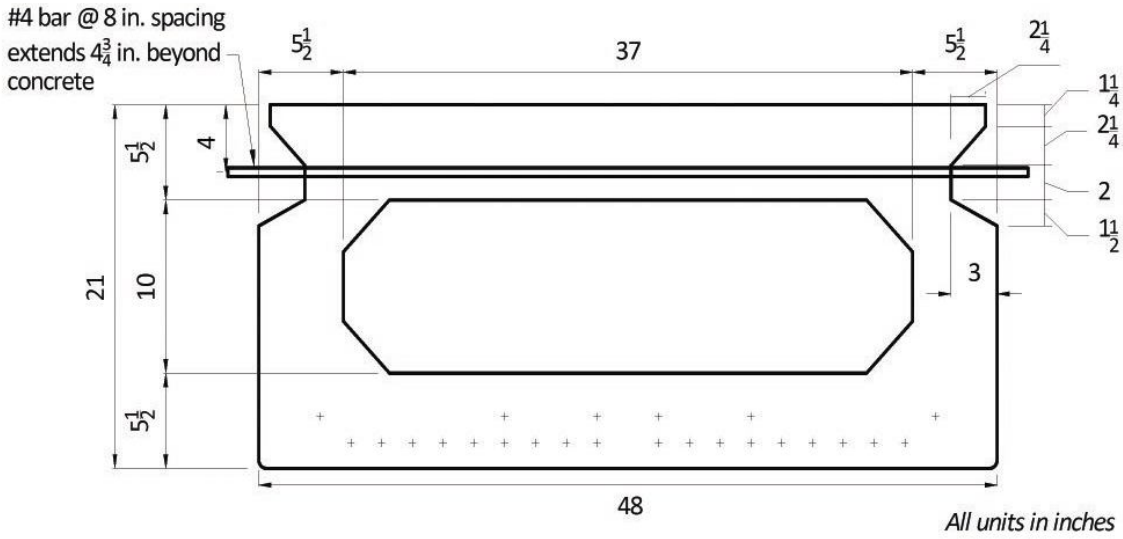

Figure 3. Graybeal's UHPC adjacent box beam connection (Graybeal, 2014)

The adjacent members are formed at the precast plant with reinforcing steel extending into the shear key every 8 in. When the precast members are placed in the field, the overlapping reinforcing steel is spliced together eliminating the need for transverse post-tensioning. The joint is then filled with UHPC instead of grout ultimately allowing the top flange level of the box beams to act as a continuous slab.

Previous research done at Virginia Tech by Halbe (2014) developed a very similar design compared to Graybeal's. However, instead of designing the connection exclusively for new construction, the objective was to design a connection that could be also be used to rehabilitate existing bridges. The recommended connection design from Halbe (2014) is shown in Figure 4. It specifies either using UHPC or Virginia Tech's more economical Very High Performance Concrete (VHPC).

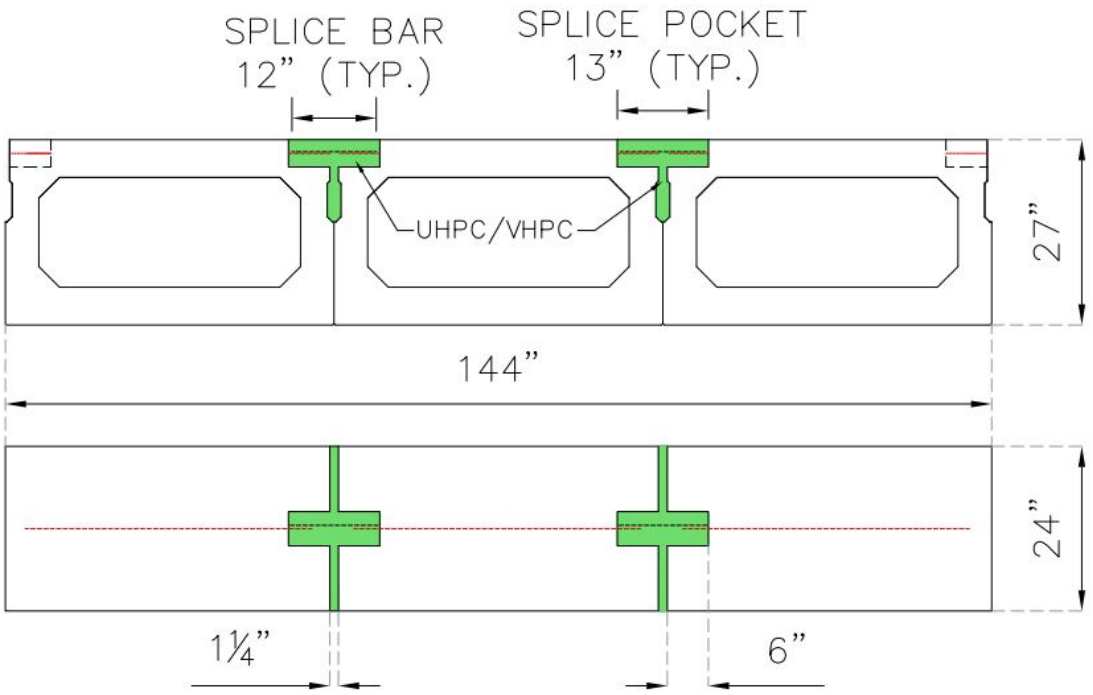

Figure 4. Halbe's UHPC/VHPC adjacent box beam connection (Halbe, 2014)

The scope of this research project was to continue the work presented in Halbe (2014) to determine an improved rehabilitation method for adjacent box beam bridges. Specifically the Virginia Department of Transportation (VDOT) provided the Buffalo Branch Bridge near Staunton, VA as a test build for development of the improved connection. To begin this, more material testing of the VHPC mix was needed to better understand if it was a viable long-term replacement to the UHPC. Additionally, the work currently being completed by researchers at

Virginia Tech helped shape the scope of the final recommendation by exploring different geometric shapes of the improved shear key.

Organization

This thesis is organized into 5 chapters. Chapter 2 provides a literature review of adjacent member bridges, UHPC, VHPC, lap splice lengths, and Girder Distribution Factors. Chapter 3 describes the experimental procedures that were used to obtain the results. Chapter 4 presents and compares the results. Chapter 5 ends with the conclusions and implications for the results obtained.

LITERATURE REVIEW

Adjacent Member Bridges

VDOT stipulates the design requirements for adjacent box beam bridges in Part 2 of the Manual of Structure and Bridge Division Volume V, VDOT (2015). Adjacent box beam bridges may be used in the roadway functional classifications shown in Table 1, but are not allowed on bridges classified as freeways or urban/rural principal arterials.

Table 1. When adjacent box beam bridges can be used (VDOT, 2014)

Design Year ADT	ADTT	Deck/Overlay
≤ 4000	≤ 100	Asphalt Overlay
> 4000	100< ADTT ≤ 200	Concrete deck 5 in. thick with single layer of reinforcement
> 4000	> 200	Concrete deck 7 ½ in. thick with two layers of reinforcement

VDOT requires transverse post tensioned tendons to tie the precast members together prior to grouting and provides two different scenarios. First, if the ends of the prestressed concrete box beams are constrained from lateral movement by wing haunches, the following tendon layouts are required:

For spans ≤ 30 ft.. 1 tie at midspan

For spans ≤ 60 ft.: 2 ties at third points

For spans > 60 ft.: 3 ties at quarter points

Second, if the ends of the prestressed concrete box beams are not constrained from lateral movement, the following tendon layouts are required:

For spans ≤ 30 ft.: 3 ties at midspan and each end

For spans ≤ 60 ft.: 4 ties at third points and each end

For spans > 60 ft.: 5 ties at quarter points and each end

The typical 4 ft. wide box beam section is shown in Figure 5. The smallest depth that VDOT allows is 27 in., which makes adjacent box beam bridges a favorable option in places with low clearance restrictions. The bottom of the precast concrete box beams also provide a smooth bottom which allows greater passage of debris under the bridge compared to beam/girder spans, making it an ideal option for heavy debris laden streams/rivers.

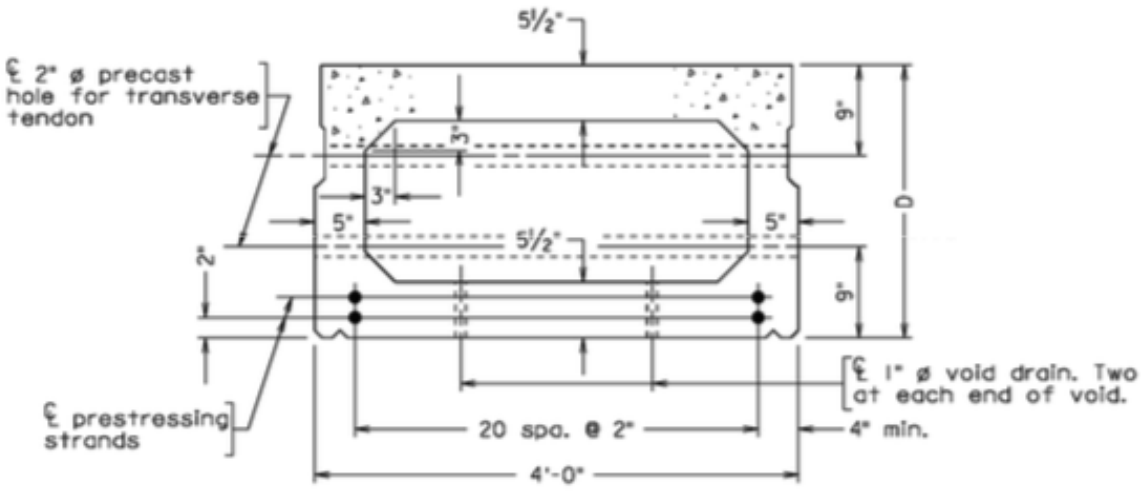

Figure 5. VDOT 4 ft. wide box beam (VDOT, 2015)

The typical connection that VDOT specifies is a partial depth shear key shown in Figure 6. Prior to placing the grout, the shear key is prepared by cleaning, sandblasting, and by creating

a saturated surface drying condition. This has been shown to improve the bond between the grout and the precast member.

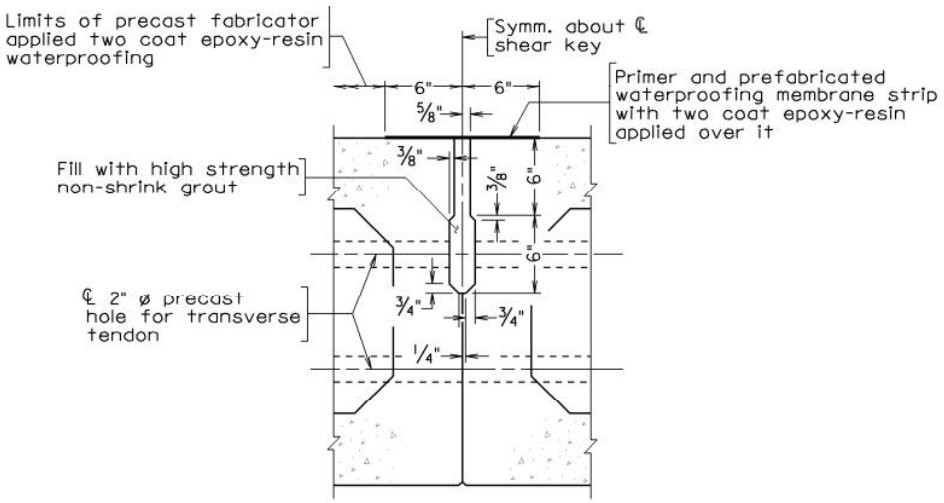

Figure 6. VDOT shear key detail (VDOT, 2015)

VDOT outlines the waterproofing requirements for adjacent box beam bridges in Section 416 of the Road and Bridge Specifications, VDOT (2007). VDOT outlines different procedures using epoxy-resin compounds and aggregates and also a membrane and primer.

Ultra High Performance Concrete

Graybeal (2014) suggests using UHPC for field-cast connections between precast bridge members in accelerated bridge construction because it gains strength quickly and will not create weak points in the structure. Another advantage for using UHPC in connections is that the bond is stronger and therefore the development length required for reinforcing steel is greatly reduced as compared to normal concrete. Because of the superplasticizer in UHPC, it is able to flow efficiently and be self-consolidating while still keeping a low water to cementitious ratio and high strength properties. It should be noted that although UHPC is self-consolidating and can be placed in small connections where normal concrete is not an option, it is still not as fluid as grout, which is the currently accepted material for precast member connections. According to

Yuan and Graybeal (2014), as of 2013, field-cast UHPC connections had been used in 32 bridges in the United States.

Very High Performance Concrete

Research completed at the University of Nebraska by Akhnoukh (2008) aimed to develop a cost efficient non-proprietary high performance concrete. The methods explored to reduce costs were using locally available materials, eliminating the steel fibers, and replacing some of the cement with class C fly ash. The average cost per cubic yard of the high performance mixes developed was $360. As fibers account for a majority of the mixture's cost, eliminating them was the greatest economic value. Akhnoukh tested 19 mixes in three stages. The first stage included material testing on four mixes that had already been developed elsewhere. The second stage involved developing seven mixes to improve the compressive strength and slump flow from the first stage. The third stage further developed seven more mixes and focused on reducing the material costs without altering the compressive strength and slump flow. After studying the 19 mixes, Akhnoukh concluded that the most important qualities of a high performance concrete were:

Early compressive strength at release $\geq$ 10 ksi

Final compressive strength $\geq$ 15 ksi

Self-consolidating with an average spread $\geq$ 26 in.

Mixing time $\leq$ 20 minutes

Material costs per cubic yard $\leq$ $200

No special casting or curing conditions required

Researchers at Virginia Tech continued Akhnoukh's work by further testing the second stage of mixes. Virginia Tech reviewed the compressive strengths of these mixes and found Mix

11 to have the highest 28 day compressive strength. This mix was then modified by adding 2% steel fibers by volume, replacing the Type III cement with Type I/II, replacing the class C fly ash with class F fly ash, and the name was changed to Mix B. The original and modified mixes are displayed in Table 2.

Table 2. VHPC mix design development, Mix 11 and Mix B

Material	Akhnoukh's Mix 11, lb/yd^3	Material	Virginia Tech Mix B, lb/yd^3
Sand	1449	Sand	1450
¼ in. limestone	616	¼ in. limestone	621
Type III Cement	1120	Type I/II Cement	1121
Class C Fly Ash	240	Class F Fly Ash	240
Silica Fume	240	Silica Fume	240
HRWR	75	HRWR	67.5
Water	240	Water	319
w/c	0.189	w/c	0.20
		Steel Fibers	265

The tensile strength of Mix B was then investigated using a modified method of AASHTO T132; instead of using cement mortar as specified in the standard, Mix B of the high performance concrete was tested. The mortar briquette test uses a 3 in. long x 1 in. thick dog bone shaped specimen with a 1 in.^{2} area at midspan. The dog bone is placed in self-aligning grips, which pull apart the dog bone specimen and the load applied and the crosshead extension are recorded. The material properties of Mix B are shown in Table 3.

Table 3. Mix B material properties

Material Property	Age, days	Strength, psi
Compressive Strength	≈ 28	16800
Splitting Tensile Strength	≈ 28	2000
Mortar Briquet Test	>> 28	916

Other variations of Akhnoukh's Mix 11 were also tested by changing the ratio of the cementitious materials and adding different quantities of slag, however Mix B was determined to be best. The material properties of Mix B met all of Akhnoukh's original strength requirements. The name was then changed to VHPC because it didn't quite meet the strength requirements of UHPC, but it was still very strong.

The VHPC was originally designed using ¼ in. aggregate and 1.2 in. steel fibers and used in closure pours. However, when trying to use the VHPC in the connections of precast member bridges, it was discovered that the aggregate and fibers originally selected were too large to fit in the narrow shear keys. Due to this size restriction, a second VHPC mix was designed using 1/8 in. aggregate and ½ in. steel fibers. The original mix with the larger aggregate and fibers was renamed VHPC-Large and the mix with the smaller aggregate and fibers was renamed VHPC-Small.

Lap Splices in UHPC and VHPC

Halbe et al. (2014) report on tests performed to determine the minimum lap splice length required to fully develop No. 4 bars in UHPC and VHPC-Large. Adjacent box beam bridges can have rigid connections at the top flange, causing transverse tensile stresses to develop due to traffic loads and long-term effects (from shrinkage and temperature). A test method was developed to mimic the lap splice region in adjacent precast members shown in Figure 7.

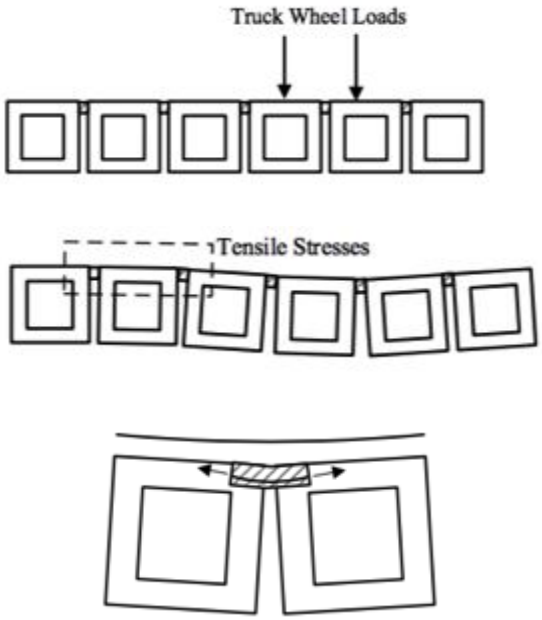

Figure 7. Splice location in adjacent box beam bridges (Halbe et al., 2014)

A total of 11 specimens were tested to failure and the specimen matrix is given in Table 4.

Table 4. Lap splice test specimens

Filler Material	Number of Specimens	Minimum Splice Length, in	Maximum Splice Length, in
UHPC	5	3	6
VHPC	6	3	6

The test specimens were comprised of a 10 in. x 12 in. x 8.5 ft. precast reinforced concrete member with a blockout pocket of varying size at midspan shown in Figure 8.

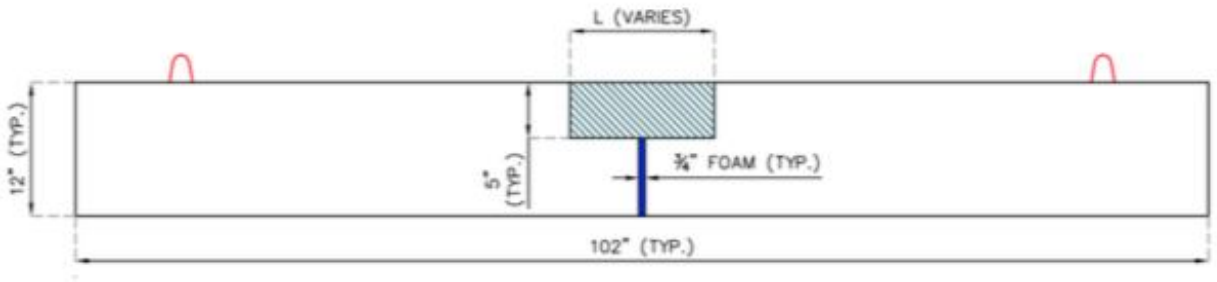

Figure 8. Elevation view of splice test specimens (Halbe et al., 2014)

The reinforcing steel was spliced in the pocket and filled with either UHPC or VHPC. It was then loaded in the configuration shown in Figure 9 so that the splice was in a region of constant moment and remained in tension until failure.

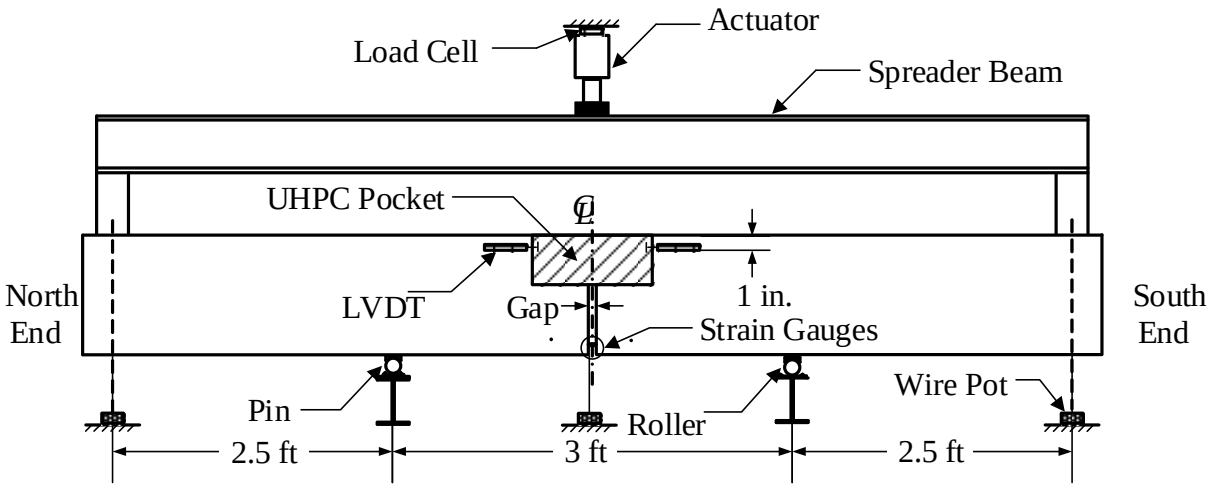

Figure 9. Lap splice test setup (Halbe et al., 2014)

The specimens were instrumented with wire pots at the ends and midspan to measure the vertical deflection. The displacement at the interface of the precast member and pocket was measured using LVDTs on one side of the specimen and locating discs for a DEMEC (DEmountable MEChanical) extensometer on the top and other side of the specimen. The compression zone reinforcing bars were instrumented with strain gauges. The spliced bars were not instrumented with strain gauges because the gauge protective coating would disrupt the bond

between the rebar and concrete. Instead the compression reinforcing steel was instrumented with strain gauges at midspan where a ¾ in. foam pad was located; the compression reinforcing steel carried all of the compression load at midspan. Loading started at increments of 1,000 to 2,000 lbs. until the first crack in the pocket was observed. The load increment was then increased to 2,500 to 3,000 lbs. until failure was reached where the specimen could no longer carry load. Table 5 shows the test results from the lap splice tests.

Table 5. Lap splice test results (Halbe et al., 2014)

Specimen Designation	Splice Length, in.	Compression Reinforcement	First Cracking Load, lbs	Maximum Load, lbs	Nominal Load to Yield Steel, lbs	Failure Modes
U-4-5-I-E	5	2 No. 4s	7200	27900	12800	NA
U-4-6-I-E	6	2 No. 4s	6900	26500	12800	NA
U-4-3-I	3	2 No.7s and 1 No. 6	5800	15700	12800	Rebar slip
U-4-4-I	4	2 No.7s and 1 No. 6	7500	24600	12800	Splitting
U-4-5-II	5	2 No.7s and 1 No. 6	9000	29600	12800	Splitting
V-4-5-I	5	2 No. 8s	3200	24600	12800	Splitting
V-4-6-I	6	2 No. 8s	3000	28700	12800	Splitting
V-4-5-II	5	2 No. 8s	1500	28300	12800	Rupture
V-4-3-I	3	2 No. 8s	1000	21300	12800	Splitting
V-4-4-I	4	2 No. 8s	2000	21800	12800	Rebar slip
V-4-4-II	4	2 No. 8s	1500	23800	12800	Splitting

The failure modes labeled in Table 5 are the typical failure modes exhibited by the specimens. All specimens failed at the interface of the pocket and the precast concrete member. Ten of the specimens failed due to bond failure, while one failed from the reinforcing steel rupturing.

The load vs. the deflection behavior is shown in Figure 10 and Figure 11. The peak loads for all the specimens were far beyond the design capacity calculated using the nominal strength based on the yield strength of the tension reinforcing steel splice bar. The deflection did not increase significantly until the interface of the pocket filler material and the precast beam began

to separate. This can be seen by comparing the deflection plots to Figure 12, when the interface gap starts to increase around 16000 lbs, the deflection also starts to increase.

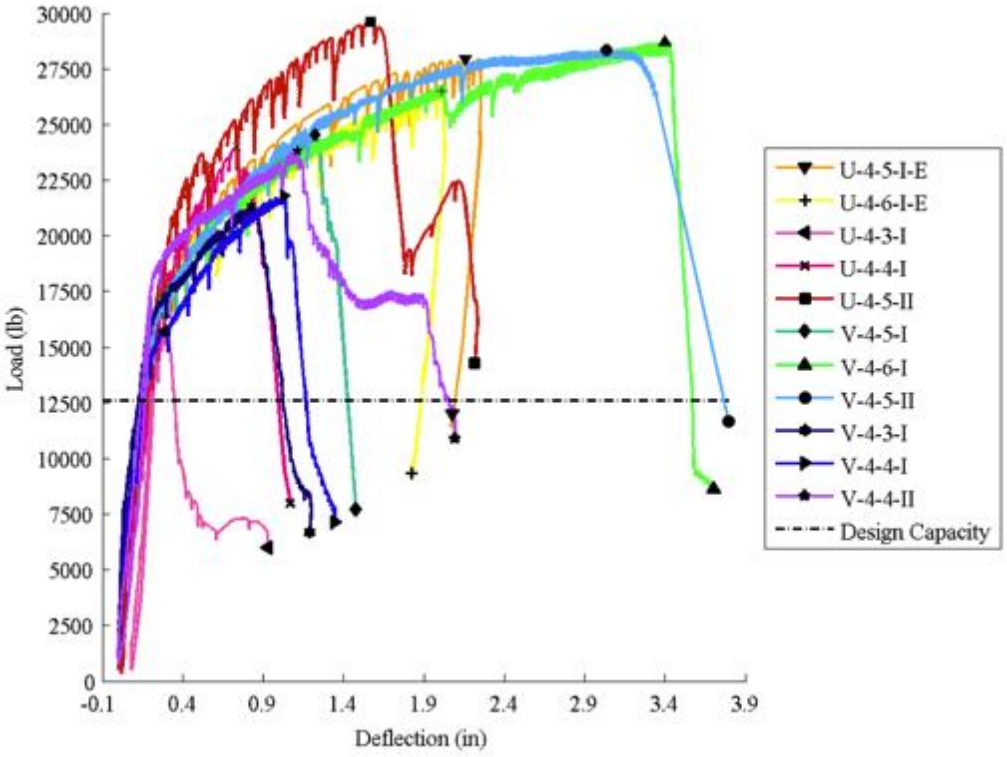

Figure 10. Load vs. average end deflection (Halbe et al., 2014)

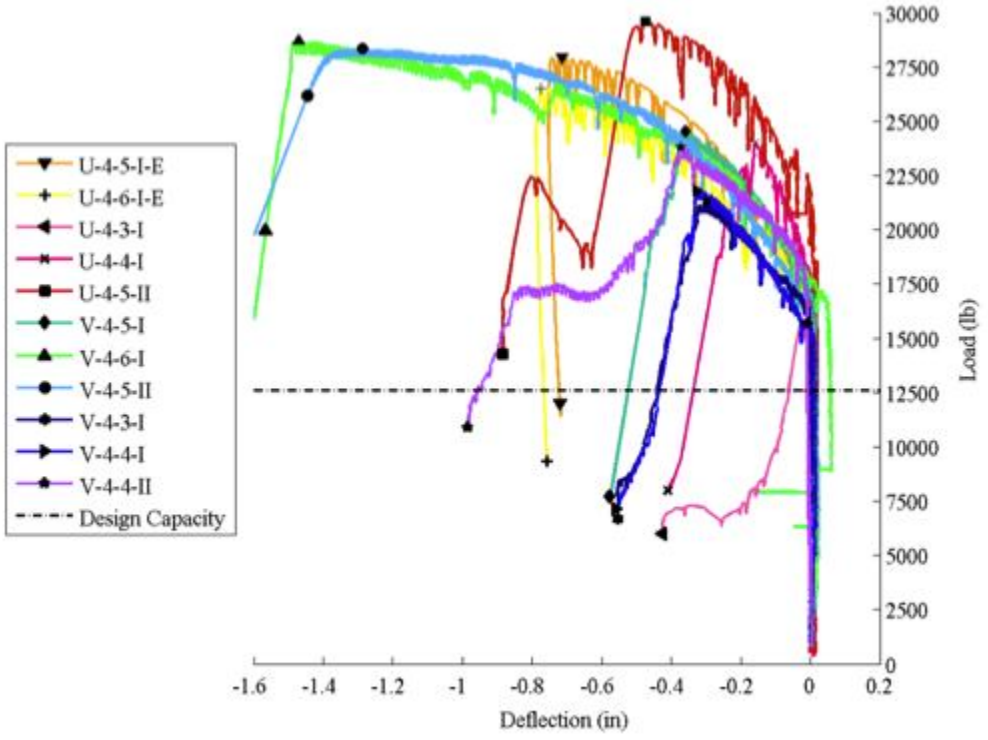

Figure 11. Load vs. midspan deflection, negative is upwards deflection (Halbe et al., 2014)

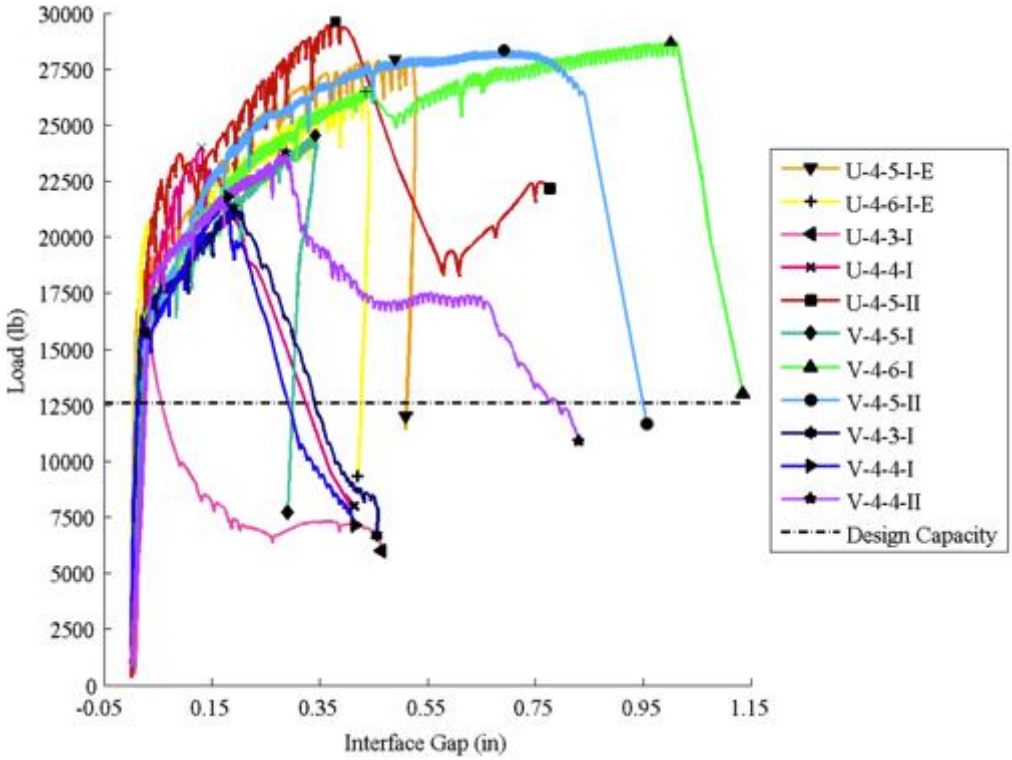

Figure 12. Load vs. interface displacement (Halbe et al., 2014)

Figure 13 shows the load vs. compression strain where the two compression strain gauges for each specimen were averaged together to be plotted. Like the deflections, the compression strain results remain linear until the interface gap begins to open, with the exception of the first two specimens tested. These UHPC specimens with equal area of steel in tension and compression the compression reinforcement yielded at much lower loads than expected. After these results were examined, the amount of compression steel was increased as to avoid the compression reinforcing steel from yielding. However, as the compression steel continues to go nonlinear, the additional area of steel did not seem to prevent yielding.

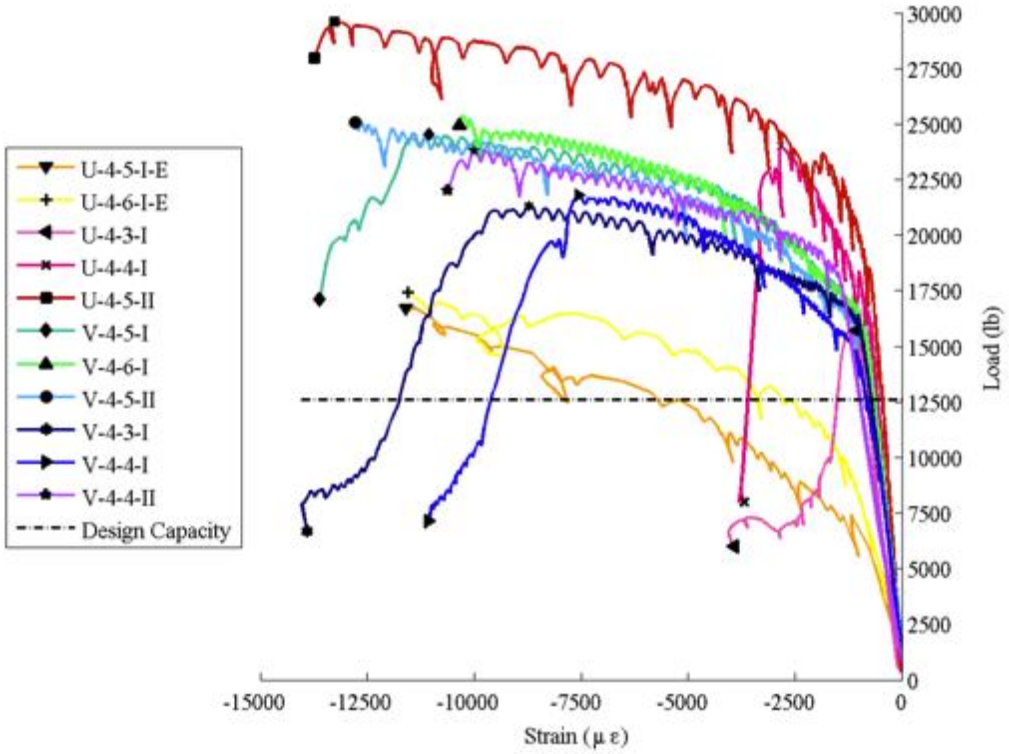

Figure 13. Load vs. average compression reinforcing steel strain (Halbe et al., 2014)

Because the compression reinforcing steel still appeared to yield, a strain compatibility analysis was performed. The constitutive relationships of steel and the pocket filler materials were determined from material property tests and both were simplified: the steel curved plot was

linearized with strain hardening being modeled by a bilinear relationship and the pocket filler material being bilinear in tension. Both are shown in Figure 14.

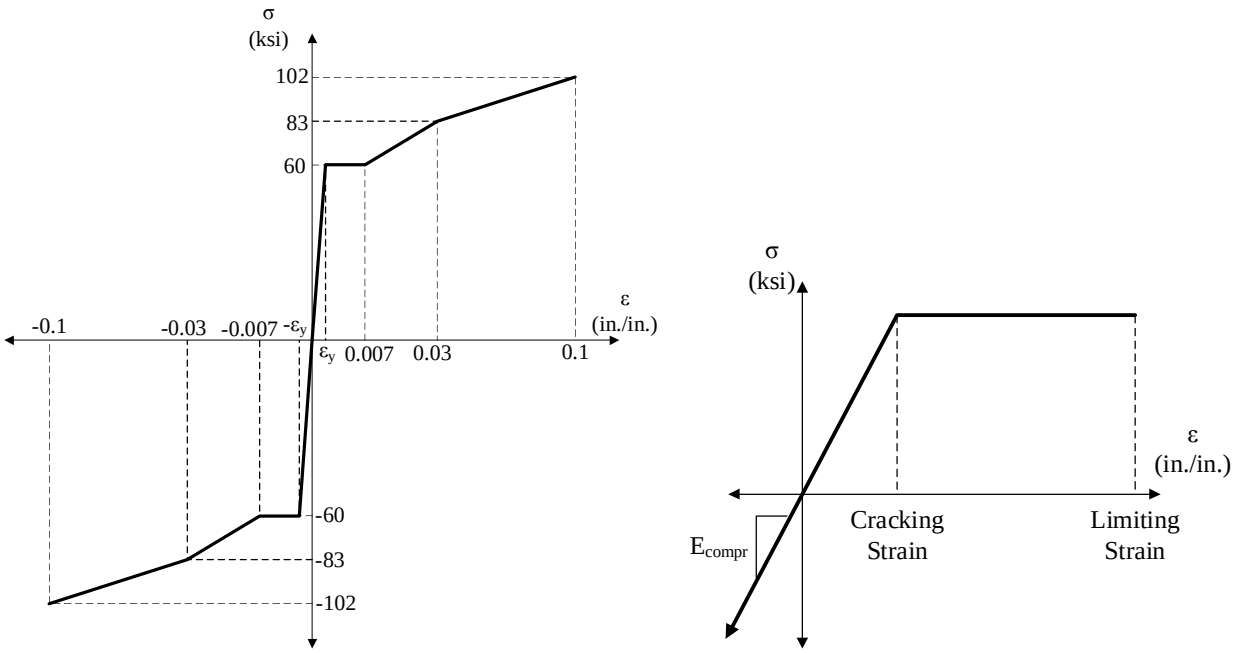

Figure 14. Constitutive model for reinforcing steel (left) and pocket filler material (right) (Halbe et al., 2014)

Using the constitutive models, the tension strains were calculated and are presented in Table 6.

Table 6. Maximum strains and stresses in tension reinforcement (Halbe et al., 2014)

Specimen Designation	Splice Length, in.	Selected Strain in Compression, in. /in.	Maximum Strain in Tension Steel, in. /in.	Maximum Tension Stress, ksi
U-4-5-I-E	5	0.0115	0.01	63.3
U-4-6-I-E	6	0.0107	0.009	62.2
U-4-3-I	3	0.0011	0.016	69.8
U-4-4-I	4	0.00315	0.04	87.1
U-4-5-II	5	0.0079	0.1	100
V-4-5-I	5	0.008	0.092	98.3
V-4-6-I	6	0.008	0.092	98.3
V-4-5-II	5	0.008	0.092	98.3
V-4-3-I	3	0.008	0.092	98.3
V-4-4-I	4	0.005	0.092	92.8
V-4-4-II	4	0.005	0.092	92.8

As observed, all of the tension reinforcement exceeded the yield stress of 60 ksi, therefore, a 3 in. lap splice distance is enough to yield the steel. However, due to ductility concerns, the recommended lap splice length for a No. 4 reinforcing bar in UHPC or VHPC was recommended as 5 in.

Girder Distribution Factors

Girder distribution factors (GDFs) determine the fraction of load that each individual girder is expected to carry. According to Collins (2010), GDFs are influenced by the system stiffness, topping conditions, skew, and deterioration of joints. Two methods for calculating the GDFs of the Buffalo Branch Bridge are presented. First, is the method outlined in the AASHTO LRFD Bridge Design Specifications to calculate the GDFs of the interior and exterior beams. Second, is the method presented by Collins (2010) to calculate the GDFs based on test results for midspan vertical deflection and longitudinal strain.

To begin with AASHTO, the Buffalo Branch Bridge was classified as a type (g) cross-section shown in Figure 15. Type (g) includes precast solid, voided or cellular concrete box with shear keys and with or without transverse post-tensioning and having an integral concrete deck.

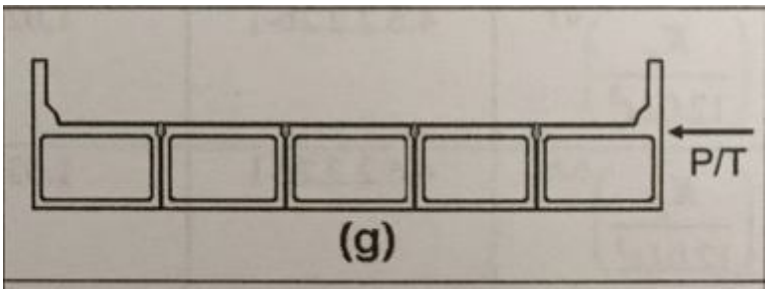

Figure 15. AASHTO Type (g) cross-section

The following formulas associated with concrete beams used in multibeam decks and type (g) cross-sections were used to calculate the GDFs for moments in interior beams.

One design lane loaded:

$$GDF = k\left(\frac{b}{33.3L}\right)^{0.5}\left(\frac{I}{J}\right)^{0.25} \quad \text{(Eq. 1)}$$

$$k = 2.5(N_b)^{-0.2} \geq 1.5 \quad \text{(Eq. 2)}$$

where N_b is the number of girders, b is the girder width in in, L is the span length in ft, I is the moment of inertia in in^4, and J is the St. Venant torsional inertia in in^4.

Two or more design lanes loaded:

$$GDF = k\left(\frac{b}{305}\right)^{0.5}\left(\frac{b}{12.0L}\right)^{0.2}\left(\frac{I}{J}\right)^{0.06} \quad \text{(Eq. 3)}$$

The range of applicability of Eq. 4 through Eq. 6 was:

$$35 \leq b \leq 60 \quad \text{(Eq. 4)}$$

$$20 \leq L \leq 120 \quad \text{(Eq. 5)}$$

$$5 \leq N_b \leq 20 \quad \text{(Eq. 6)}$$

To calculate the GDFs for moments in the exterior beams, the following formulas were used.

$$GDF = eGDF_{interior} \quad \text{(Eq. 7)}$$

One design lane loaded:

$$e = 1.125 + \frac{d_e}{30} \geq 1.0 \quad \text{(Eq. 8)}$$

where d_e is the horizontal distance from the centerline of the exterior web of exterior beam at deck level to the interior edge of curb or traffic barrier in ft.

Two or more design lanes loaded:

$$e = 1.04 + \frac{d_e}{25} \geq 1.0 \quad \text{(Eq. 9)}$$

The range of applicability of Eq. 10 and Eq. 11 was:

$$d_e \leq 2.0 \quad \text{(Eq. 10)}$$

Due to the 30 ^{o} skew of the Buffalo Branch Bridge, the GDFs were reduced using the reduction factor, r:

$$r = 1.05 - 0.25\tan(\theta) \leq 1.0 \quad \text{(Eq. 11)}$$

$$\text{If } \theta > 60^{o}, \text{ use } \theta = 60^{o} \quad \text{(Eq. 12)}$$

where θ is the angle of skew in degrees.

The range of applicability of Eq. 13 was:

$$0° \leq \theta \leq 60° \quad \text{(Eq. 13)}$$

The second method outlined in Collins (2010) was used to calculate the GDFs using the midspan vertical deflections and longitudinal strains obtained from the live load tests and FEA model. The following formula was used:

$$GDF = \frac{R_{max} n}{\sum_{j=1}^{m} R_{peakj}} \quad \text{(Eq. 14)}$$

where R_{max} is the maximum response of the girder, n is the number of trucks applying the load, m is the number of girders, and R_{peakj} is the maximum response of the jth girder. To account for

the skew of the bridge, the sum of the maximum responses of all of the girders was used in the denominator.

Summary

The current VDOT method to connect adjacent member bridges needs updating. The shear keys are deteriorating and older bridges must be rehabilitated or replaced. To save money and time, rehabilitating the existing bridges is more advantageous. The high strength of both UHPC and VHPC make them both suitable options to replace the grouted shear keys. The smaller lap splice distance required to develop the reinforcing steel also helps to increase the advantages to using UHPC or VHPC instead of grout as the shear key material.

EXPERIMENTAL METHODS

This chapter explains the details of the tests performed for this project. The first section explains the material tests executed. The second section reviews the research done by Joyce (2014) to develop a more durable connection in adjacent voided slab bridges. The third section explains the finite element modeling that was completed for this project. The last section outlines the initial live load test of the Buffalo Branch Bridge.

Material Tests

An overview of the material tests performed is presented in Table 7.

Table 7. Material tests overview

Test	Specimen	Material	ASTM Standard	Reference
Compressive Strength	4 in. x 8 in. Cylinders	UHPC, VHPC-Small VHPC-Large, A4 Deck Concrete, Grout	C39	ASTM (2014)
Compressive Strength	2 in. Cubes	VHPC-Small	C109	ASTM (2013)
Splitting Tensile Strength	4 in. x 8 in. Cylinders	UHPC, VHPC-Small VHPC-Large, A4 Deck Concrete, Grout	C496	ASTM (2011)
Modulus of Elasticity	4 in. x 8 in. Cylinders	UHPC, VHPC-Small VHPC-Large, A4 Deck Concrete, Grout	C469	ASTM (2014)
Bond with Rebar	6 in. x 6 in. x 12 in. Block	VHPC-Small and VHPC-Large	N/A	Johnson (2010)
Bond with Concrete	2 in. x 1 in. Pucks	VHPC-Small, VHPC-Large, and Grout	D7234	ASTM (2012) and Scholz et al. (2007)
Workability	N/A	VHPC-Small and VHPC-Large	C1611	ASTM (2014)
Durability	3 in. x 4 in. x 16 in. Bars	UHPC, VHPC-Small VHPC-Large, A4 Deck Concrete, Grout	C666	ASTM (2008)
Free Shrinkage	3 in. x 3 in. x 11 ¼ in. Bars	UHPC, VHPC-Small VHPC-Large, A4 Deck Concrete	C157	ASTM (2011)
Free Shrinkage	3 in. x 3 in. x 12 in. Bars	A4 Deck Concrete, Grout	N/A	N/A

Material Mix Designs and Mixing Procedures

Material tests were performed on five different mix designs. The mix designs for one cubic yard of each material tested and the mixing procedures are outlined below.

UHPC

Ultra High performance Concrete (UHPC) was made using the proprietary premix Ductal. Ductal is a high strength, fiber reinforced, self-consolidating concrete. The mix design is outline in Table 8.

Table 8. UHPC mix design

Constituent	lb/yd^3
Ductal Premix	3700
Water	219
Premia 150 (Superplasticizer)	51
½ in. Steel Fibers (2%)	263
w/cm	0.06

The mixing procedure for UHPC was precisely outlined and followed. To begin the mixer needed to be dry, not damp. The Ductal Premix was added and mixed for two minutes to disperse any large pack-set clumps. Next the water and Premia 150 Superplasticizer were added and mixed for one minute until it was wet and had the consistency of bread dough. The mixer was then stopped and quickly scrapped. Mixing continued until the mix was flowable and no material was sticking to the sides of the mixer, typically three minutes. Fibers were then added while trying to avoid adding them in clumps and the mixer continued for another four minutes until fibers were evenly distributed. The total mix time was approximately ten minutes.

VHPC

Very High Performance Concrete with large aggregate (VHPC-Large) was created at the University of Nebraska and modified at Virginia Tech as a non-proprietary high strength, fiber reinforced, self-consolidating concrete. It is a more economical option than UHPC because of the addition of coarse aggregate and because it is non-proprietary. The High Range Water Reducer (HRWR) is specified in ounces of HRWR per hundred pounds of cementitious materials (oz/cwt.). A range is given for the HRWR amount because it varied each batch. The mix design is outlined in Table 9, and is essentially the same mix presented in as Mix B in Table 2, but with the HRWR dosed in oz/cwt. instead of lbs.

Table 9. VHPC-Large mix design

Constituent	lb/yd^3
Water	319
Cement	1121
Fly Ash	240
Silica Fume	240
Sand	1450
¼ in. Limestone	621
1.2 in. Steel Fibers (2%)	265
HRWR	22-26 oz/cwt.
w/cm	0.20

Very High Performance Concrete with small aggregate (VHPC-Small) was created by modifying the VHPC-Large mixture to contain smaller aggregate and fibers so that it could be placed into smaller joints. The mix design is shown in Table 10.

Table 10. VHPC-Small mix design

Constituent	lb/yd^3
Water	319
Cement	1121
Fly Ash	240
Silica Fume	240
Sand	1345
⅛ in. Limestone	660
½ in. Steel Fibers (2%)	260
HRWR	22-26 oz/cwt.
w/cm	0.20

Both VHPC mixes were mixed using the same procedure. Initially the mixer was sprayed down to be damp. The coarse and fine aggregate and half the water were added and mixed for five minutes until damp. The mixer was then scraped and continued mixing for another two minutes. The cement, fly ash, silica fume, and remaining water were then added and mixed for five minutes before scraping the sides of the mixer again. The HRWR was then added slowly

and mixed for three minutes to validate that it was the desired consistency. Finally the fibers were added and mixed for two minutes before placing. The total mix time was approximately seventeen minutes.

Deck Concrete

VDOT class A4 modified concrete is a standard Virginia bridge deck concrete. This mix design was chosen so that the durability test results could be compared to a more comprehensive group of data. The mix design is shown in Table 11.

Table 11. A4 deck concrete mix design

Constituent	lb/yd^3
Water	286
Cement	635
Fine Aggregate	1286
Coarse Aggregate (# 57 Stone)	1734
Air Entraining Admixture	141 mL.
HRWR	1880 mL.
Retarder	564 mL.
w/cm	0.45

The mixing procedure for the A4 deck concrete mix was performed similarly to the VHPC mixes. Initially the mixer was dampened and the fine and coarse aggregate and half the water were added and mixed until damp. The cement and remaining water were then added and mixed. Finally the AEA, HRWR, and retarder were added and mixed until the concrete reached a slump of 2 in. to 4 in. and the air content was between 5% and 8% as per VDOT specifications.

Grout

Quikrete's non-shrink precision grout was chosen for the grout because it meets the VDOT Bridge Specifications requirement of a grout that meets ASTM C1107. The mix design is in Table 12. The amount of water added was based on the grout being flowable.

Table 12. Grout mix design

Constituent	lb/yd^3
Water	23
Premix Quikrete's Non-Shrink Precision Grout	111

The mixing procedure for grout was the by far the easiest. The mixer was dampened and the Premix and water were added. It was then mixed for five minutes and was ready to be placed.

Material Properties

Compressive Strength

Compressive strength tests were performed in accordance with ASTM C39 with 4 in. x 8 in. cylinders. The cylinders were cured by placing 4 mil plastic over the top to ensure that the moisture did not escape. On the day of testing, cylinders were typically saw cut to obtain a uniform loading surface. The ends were either capped in sulfur or neoprene end caps were used for loading. Cylinders were typically tested in groups of three and at ages ranging from 12 hrs. to 28 days. A cylinder test using the neoprene end caps is shown in Figure 16.

Figure 16. Compressive Test

The compressive strength of the UHPC and VHPC-Small mixtures were also tested following ASTM C109 using 2 in. cubes.

Splitting Tensile Strength

Tensile strength was measured using the procedure outlined in ASTM C496 with 4 in. x 8 in. cylinders. The cylinders were cured and saw cut in the same fashion as the compressive cylinders, but they were not capped. Shown in Figure 17 is the setup for the test. The cylinders were placed between thin bearing strips made of plywood in a jig for aligning the concrete cylinder and loaded to failure. Cylinders were typically tested in pairs at ages ranging from 12 hrs. to 28 days.

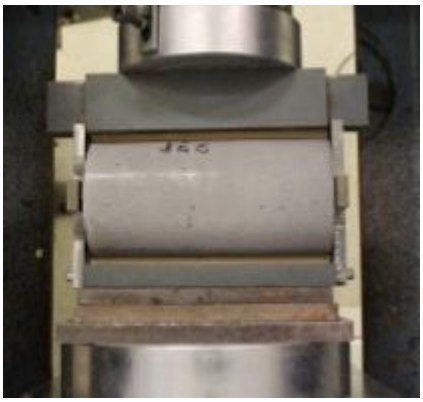

Figure 17. Splitting Tensile Test

Modulus of Elasticity

Cylinders used for compressive strength tests were also used to determine the modulus of elasticity with ASTM C469. A modulus collar was attached to the cylinders and the cylinders were loaded slowly while recording the gauge readings and load. The test set-up is shown in Figure 18.

Figure 18. Modulus of Elasticity Test

Reinforcing Steel Bond

A modified version of the pull out tests presented in Johnson (2010) was performed to determine the bond of the VHPC mixes with reinforcing steel. Johnson did not place the reinforcing steel in the center of the concrete blocks. The tests performed here were simplified with slightly smaller blocks and centered reinforcing steel, as the only objective was to measure if the reinforcing steel slipped out of the concrete or yielded. In the pull out tests, the reinforcing steel was embedded into a block of VHPC and pulled out using a center-hole ram. The forces induced inside the VHPC block are shown in Figure 19.

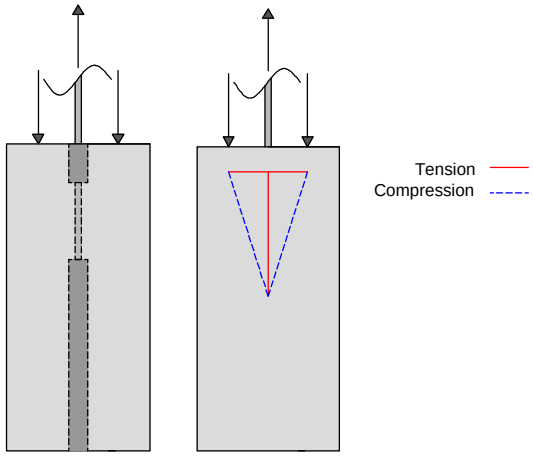

Figure 19. Forces in pull out test (Johnson, 2010)

To prevent the reinforcing steel from pulling out the top section of the VHPC in a cone failure, the top of the reinforcing steel was only bonded towards the center of the VHPC block. The reinforcing steel was debonded in the bottom 4 in. and top 3 in. of the VHPC block so that the 5 in. bond was more centrally located. The steel was debonded by covering it with PVC pipe in these regions. This is shown in Figure 20.

Figure 20. Bonded vs debonded reinforcing steel for pull out specimen

Several pull out specimens were cast at the same time so that the tests could be performed at different early ages. The instrumentation for the pull out tests consisted of Linear Variable Differential Transformers (LVDTs) and wire pots, which were installed to measure displacement. The bottom LVDT was used to determine if the reinforcing steel was slipping through the VHPC and being pulled out the top. The top LVDT and the wire pot were both attached to the top of the ram to measure how far the steel had been stretched. The load cell was used to determine the load that was applied by the ram. As the ram was manually pump controlled, the approximate load rate ranged from 100 lbs./second to 500 lbs./second and the

load cell also helped to monitor the load rate. The test set-up and instrumentation is shown in Figure 21. The pull out specimens were tested 12 hrs, 1 day, 2 day, and 7 days after placing.

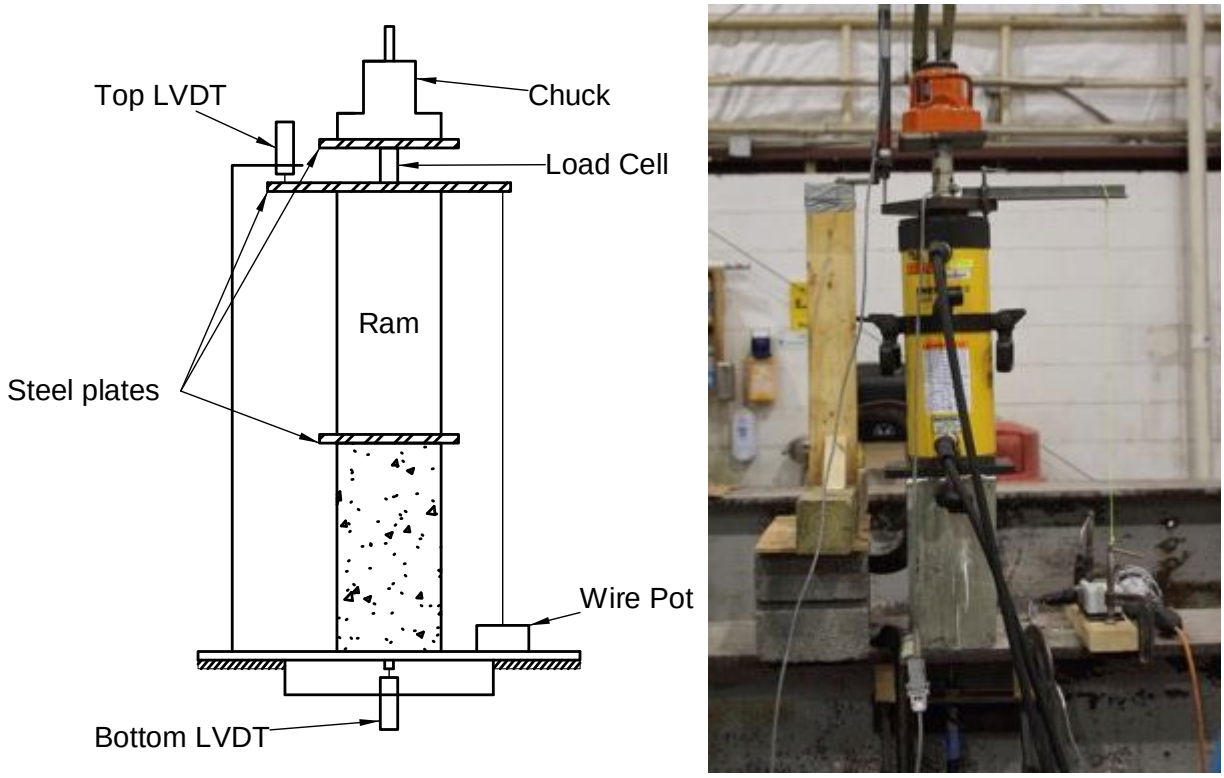

Figure 21. Pull out test setup

Bond with Concrete

To quantify the bond strength of the VHPC with the precast concrete members, a modified version of ASTM D7234 was performed. The ASTM procedure, shown in Figure 22, requires a continuous layer of coating on a concrete substrate. Cuts are then made through both the coating and concrete substrate to attach the loading fixture and a tension force is then applied normal to the test surface.

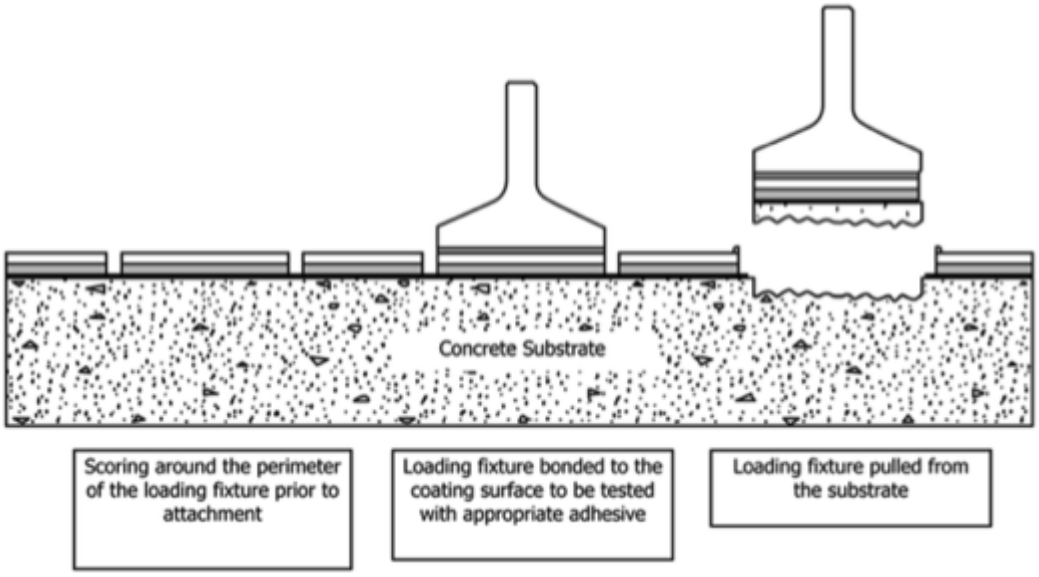

Figure 22. ASTM D7234 Procedure (ASTM D7234, 2012)

The results presented here were obtained by casting 2 in. diameter x 1 in. tall pucks of VHPC on the bottom of precast concrete members. The bottom of the precast member was chosen because it was the largest surface area that allowed for more pucks to be cast on the same member. It also accurately represented the shear key because the precast plant where the members were obtained used the same metal formwork at the shear keys and bottom of the member. The pucks were cast on a horizontal surface because it was not practical to cast them vertically and the results of tension pull off bond are believed to be the same. Also, the test results were to be compared to the results obtained by Joyce (2014) and so the test was set up in an identical method. An overview of multiple VHPC pucks being cast on the bottom of a precast member is shown in Figure 23.

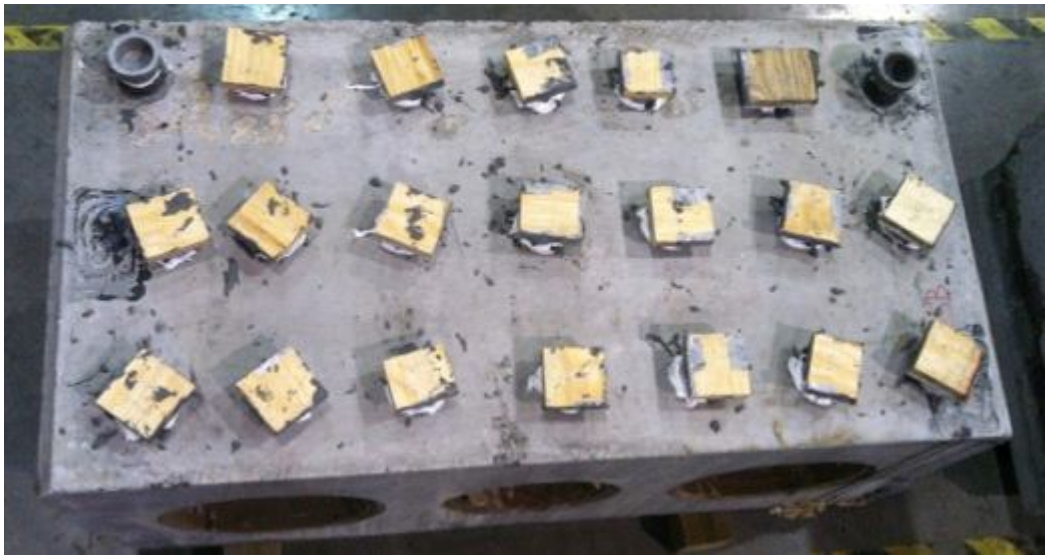

Figure 23. Bond Overview

After VHPC is placed, it immediately starts to form a skin-like layer at the surface. To prevent this from happening with the pucks, a piece of duct-tape covered wood was set on the surface of the puck immediately after placing and is shown in Figure 24. The objective of this was to ensure that the epoxy bonded with the entire puck, instead of just the skin. A threaded metal cap was typically epoxied to the top of the pucks 12 to 24 hours before testing and is shown in Figure 25.

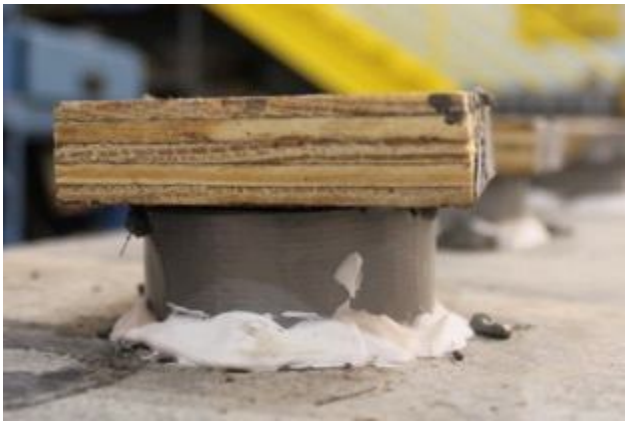

Figure 24. Bond Puck with wood top

Figure 25. Bond puck with hook attached

A hook was screwed into the metal cap and attached to a tension load cell and the tension load was applied by twisting the jack. The test set-up is shown in Figure 26.

Figure 26. Bond Test

By making individual pucks instead of casting a continuous surface, the surface preparation could also be assessed. The two factors examined were sand blasted vs not sand blasted and saturated surface dry (SSD) vs dry.

Workability and Flow

The workability was quantified using ASTM C1611. The inverted slump test is shown in Figure 27. The spread was measured at different times during the mixing procedure.

Figure 27. Inverted Cone and Slump Testing

The flow was measured in other, more unique ways. The box test was created to mimic a closure pour and determine the distance the VHPC-Large could reasonably be expected to flow. A 6 in. x 6 in. x 5 ft. box was made and six large scoops of the VHPC-Large were placed into one end. The distance it flowed was recorded after 15 seconds. The test setup is shown in Figure 28.

Figure 28. Box test

The shear key slope flow test was made to replicate the depth and slope of the shear keys along the length of the Buffalo Branch Bridge to determine if the shear key at the low end of the bridge would need to be covered to prevent the VHPC-Small from overflowing. A 1.5 in. x 12 in. x 8 ft. box was made and initially placed on supports at the same 0.8% grade slope as the bridge. The VHPC-Small was placed in the top of the slot starting at the low end and moving to the high end. Because the VHPC-Small did not overflow on the low end after 5 min. with continued tapping on the sides to agitate it, the elevation difference was changed to 5 in. to represent the full elevation change of the bridge. The shear key slope flow test is show in Figure 29.

Figure 29. Shear key flow test

The transverse slope of the bridge was also replicated by creating formwork for the geometric cutouts recommended to be used in the Buffalo Branch Bridge rehabilitation. Both a dog bone and a bowtie shaped shear key were made and are shown in Figure 30.

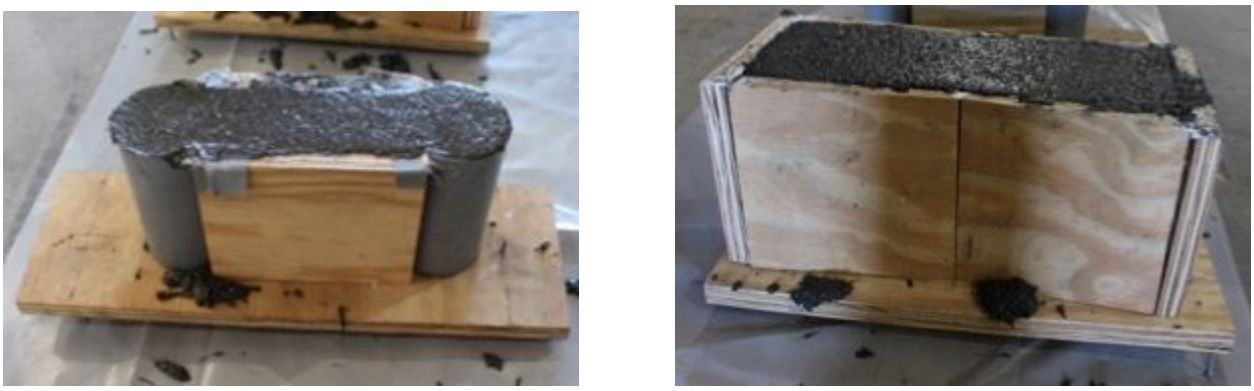

Figure 30. Dog bone and bowtie flow setup

Durability

The durability was measured following ASTM C666 Procedure A. Three freeze/thaw specimens 3 in. x 4 in. x 16 in. were cast for each of the five mixes. Typically every 35 cycles the specimens were removed and their weight and resonant frequencies were recorded. They were then returned to the freeze/thaw machine. The specimens in the freeze/thaw machine are shown in Figure 31.

Figure 31. Freeze/Thaw Machine

Data was recorded from 0 cycles to 306 cycles when the freeze/thaw machine would no longer cycle temperatures. The freeze/thaw machine exhibited problems maintaining a constant freezing and thawing rate.

Shrinkage

Shrinkage tests were performed in accordance with ASTM C157. Prisms (3 in. x 3 in. x 11¼ in.) were cast in pairs and the shrinkage was typically measured daily for the first 14 days after demolding. The comparator is shown in Figure 32. Measurements were then taken weekly until 50 days when the measurements were taken monthly.

Figure 32. Shrinkage testing comparator

The ASTM C157 comparator to measure length change had a very small tolerance on acceptable lengths. Three of the shrinkage specimens cast were out of that range and were not able to be measured. These bars were instrumented with locating discs for a DEMEC extensometer on the top and bottom of the specimen to measure the surface shrinkage. Both the shrinkage bars and DEMEC are shown in Figure 33. Measurements were taken at the same time interval as the rest of the shrinkage prisms.

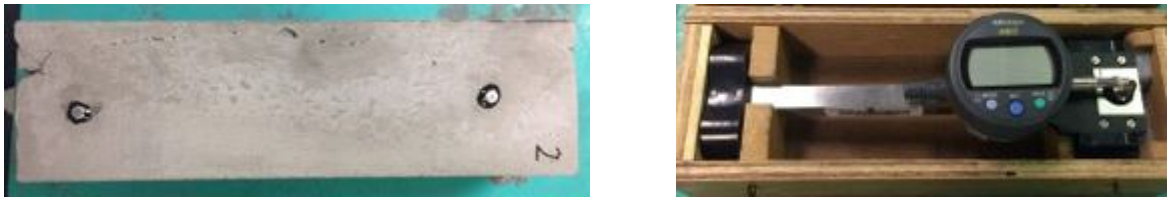

Figure 33. Shrinkage bar with discs and DEMEC extensometer

Non-Contact Lap Splice Tests

The focus of the research of Halbe and Joyce (2014) was developing a durable adjacent member shear key for new construction. Their test set-up and protocol was designed to mimic the transverse tension in the shear key in these types of bridges cause by design loads. Halbe

focused on adjacent box beam bridges and Joyce on voided slab bridges. At the conclusion of their testing, one voided slab test specimen was available for further testing. The test specimen was a sub-assemblage of three adjacent voided slab precast members. Finite element models of both a representative voided slab bridge and the sub-assemblage were used to determine the imposed deflection. It was determined that the transverse tensile stresses in the shear keys of the bridge system subjected to an AASHTO design truck loading was replicated by imposing a vertical displacement of 0.03 in. on the specimen as supported by W8x15 beams. A schematic of the test set-up is shown in Figure 34.

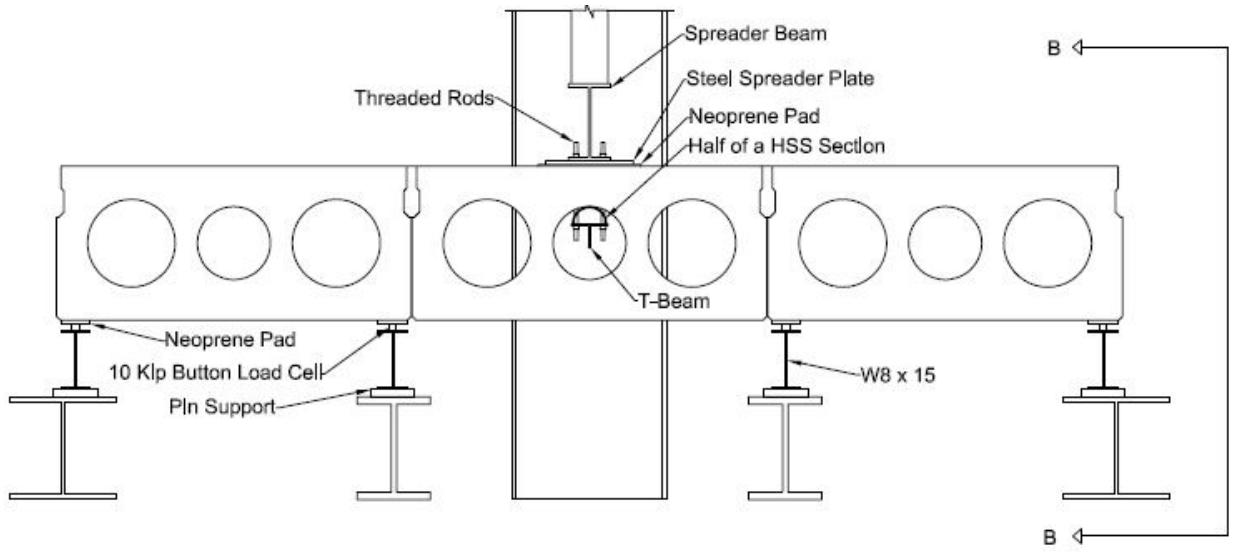

Figure 34. Sub-Assemblage test setup (Joyce, 2014)

The voided slab sub-assemblage was connected by a traditional shear key but also included a 6 in. long blockout pocket with a 6 in. non-contact lap splice over the joint. The joint and shear key were filled with VHPC-Large. The connection pocket can be seen in Figure 35 with a non-contact splice bar in place.

Figure 35. Non-contact voided slab connection

The sub-assemblage was instrumented with LVDTs at the bottom of the shear keys on both sides of each joint, which can be seen in Figure 36. The purpose of the LVDTs was to monitor the amount the joints opened during the testing.

Figure 36. Joint instrumentation

Testing began with an initial static test in which the center voided slab was lowered at a slow rate to a vertical displacement of 0.03 in. and then raised back up by 0.03 in. so that the specimen returned to its initial “zero point”. After the initial static test, cyclic tests began by lowering the specimen by 0.015 in. and then cycling it between 0.03 in. and the “zero point” at a frequency of 3 hertz. Cyclic testing was performed in groups of cycles starting at 10 cycles and ending at 1,000,000 cycles. The groups for cyclic testing were 10 cycles, 100, 1,000, 10,000, and then every 100,000 cycles until the test reached 1,000,000 cycles. Static tests were performed after each group of cyclic testing, with the initial static test being performed before the specimen underwent any cyclic testing and the final static test being performed after the 1,000,000 cycles. During testing, water was ponded on top of the joint to monitor if cracking was occurring. This can be seen in Figure 37.

Figure 37. Water ponding for voided slab

Finite Element Analysis

Overview of Buffalo Branch Bridge

The VDOT visual inspection of the Buffalo Branch Bridge performed in January 2014 stated that water and efflorescence were seeping through the furthest downstream joint for the full length and for the second downstream joint and the furthest upstream joint within six feet of the abutments. A picture of the leaking downstream joint included in the inspection report is shown in Figure 38.

Figure 38. VDOT visual inspection report picture of downstream joint leaking

To determine the current state of the bridge beyond visual inspection, a live load test and finite element analysis (FEA) were performed. The goal of the FEA model was to predict the midspan vertical deflections and longitudinal strains that would result from the live load tests. Another objective was to validate the accuracy of the FEA model with the live load test results to

be able to change the model to match the rehabilitated bridge joints and calculate the stresses experienced in the new shear keys. The commercial FEA program Abaqus was used to model the full scale Buffalo Branch Bridge. The plan and transverse views of the bridge plans are shown in Figure 39 and Figure 40.

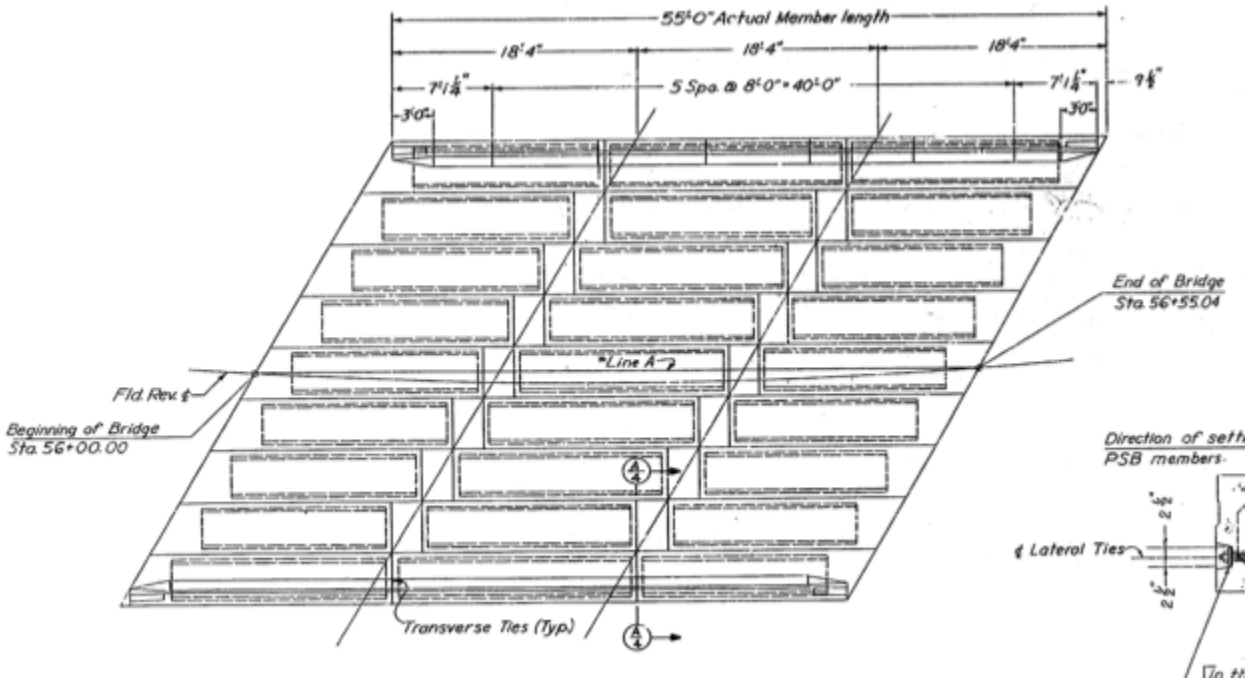

Figure 39. Plan view of Buffalo Branch Bridge plans

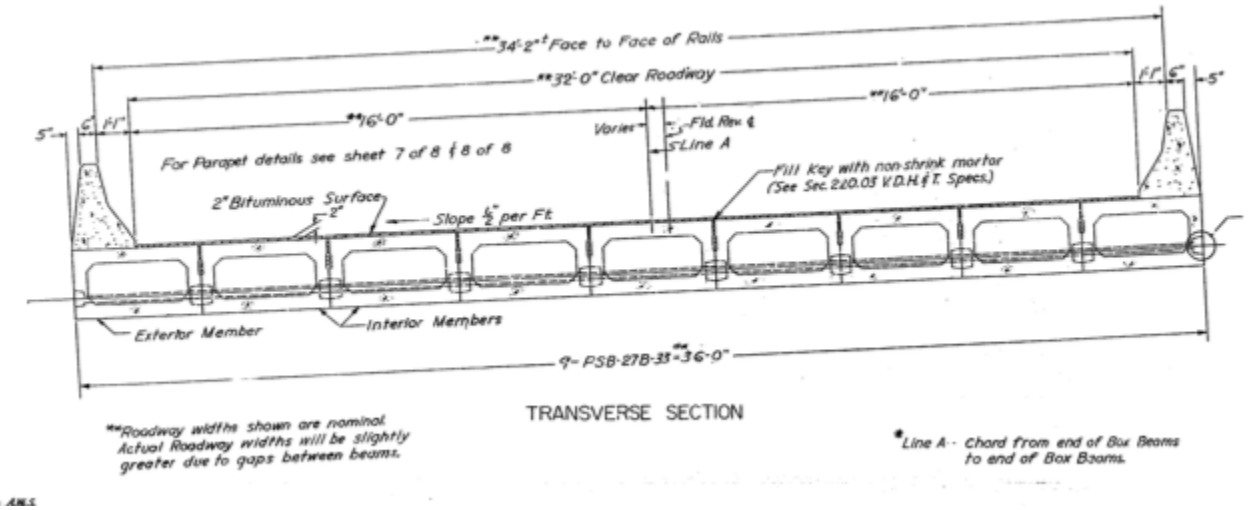

Figure 40. Transverse view of Buffalo Branch Bridge plans

The 55 ft. span bridge consists of nine adjacent box beams with transverse ties at the third points. The FEA model incorporated the diaphragms as 2.25 ft wide solid concrete sections centered at the ties. The analysis performed was linear elastic and the material properties used are shown in Table 13.

Table 13. FEA material properties (Halbe, 2014)

Material	Modulus of Elasticity, ksi	Poisson's Ratio
Barrier Concrete	3640	0.2
Precast Concrete	4100	0.2
Grout	3500	0.2
Neoprene Pad	9	0.5
Prestressing Steel	28500	0.3

The bridge model was broken down into five separate individual parts: a shear key made of grout, exterior precast concrete beams, interior precast concrete beams, concrete barrier rails, and neoprene bearing pads. These parts were connected using master-slave surface ties and are outlined in Table 14. The surface tie connects the two surfaces together so that they are essentially perfectly bonded together; as the master surface deflects, the slave surface deflects the same amount.

Table 14. FEA model connections

Master	Slave
Precast concrete beam	Shear key
Precast concrete beam	Barrier rail
Precast concrete beam	Bearing pads

Using master-slave surface ties was not thought to be the most accurate representation of the Buffalo Branch Bridge deteriorated joints. Because of this, several different methods were attempted to model the bond in the joints more realistically. To initially test these connection methods, they were applied to a simple 3D model of the 2 in. x 1 in. puck placed on concrete member test set-up described in the Bond with Concrete section. A tension load was applied to

the puck to pull the two concretes apart. The intended outcome was for the bond to slowly weaken and then fail at the specified stress, however none of the connection methods modeled were able to produce this outcome. Therefore, the master-slave surface tie was used.

Simulation of Truck Load

Originally, the truck load was the three axle AASHTO design truck. However, after the initial live load test was performed, the loads in the model were changed to match those of the actual trucks used. The model was also adjusted to match the loading pattern of the truck in the field. Data was recorded throughout the duration of the truck's trip across the bridge, but was marked whenever the front left tire reached the start of the bridge, quarterspan, midspan, quarterspan, and finally when it left the bridge. Figure 41 shows FEA results for when the test truck was at quarterspan and midspan. The corresponding deflections are shown in Figure 42 with the spectrum going from blue to white and 0 in. to 0.05 in. respectively. The FEA results compared to the live load test data were the vertical deflection and longitudinal strain at midspan on the bottom of each of the beams.

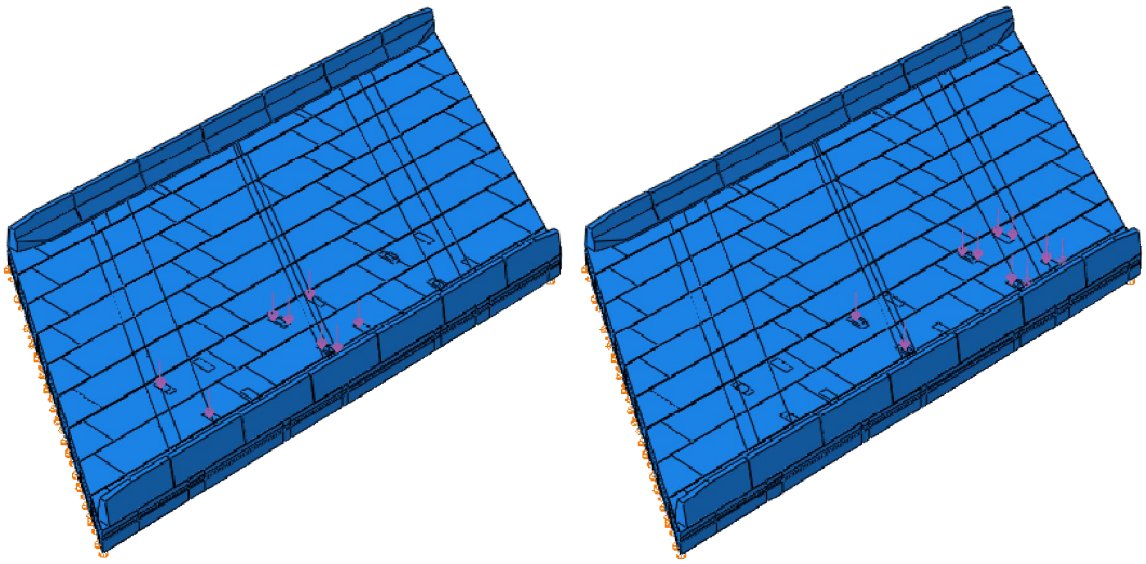

Figure 41. Truck load

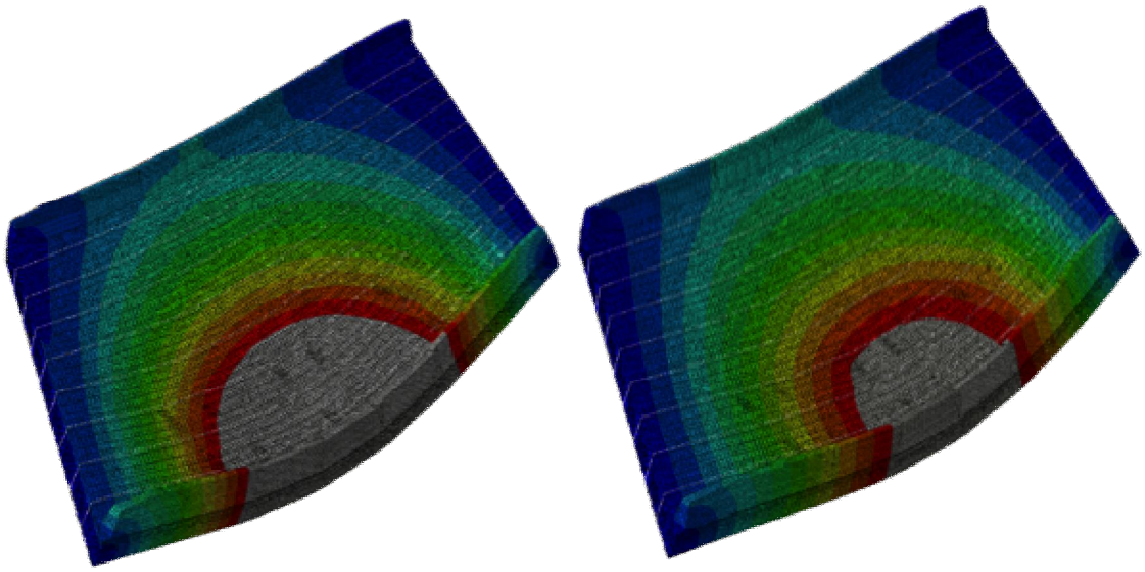

Figure 42. Deflection caused by truck

Buffalo Branch Bridge Live Load Test

Desired Data

With a finite number of sensors available to use for the bridge test, it was important to plan out what data was most pertinent to record. The parameters decided to be most relevant were the box beam vertical deflections and longitudinal strains and the relative vertical and horizontal joint movements.

Data Acquisition

The data acquisition system (DAS) and software used was the Structural Testing System (STS) by Bridge Diagnostics Incorporated (BDI). The STS consisted of three main components: the computer software, DAS base station, and nodes. The sensors were wired directly to the nodes shown in Figure 43. Each node was capable of connecting to four sensors.

Figure 43. BDI nodes

The BDI nodes transmitted the data wirelessly to the computer through the DAS base station shown in Figure 44.

Figure 44. DAS base station

The nodes were placed under the bridge with the instrumentation and the computer was located on top of the bridge to be able to better monitor truck location.

Instrumentation

Glue and Accelerant

Loctite 410 glue and Loctite 7452 accelerant were used to attach all sensors onto the bottom of the box beam members. The glue and accelerant system took seconds to bond sensors to the box beams.

Strain Transducers

Strains were recorded at the midspan of each box beam using nine BDI strain transducers. These gauges are comprised of four strain gauges in a full Wheatstone bridge configuration and BDI provides calibration factors for each. The metal feet on the bottom of the BDI strain transducers were glued to the bottom of the box beam members. A bonded BDI strain transducer is shown in Figure 45. The gauges were placed to measure the longitudinal strain of the box beam members. Therefore, they are not perpendicular to the midspan line that is drawn with the bridge skew.

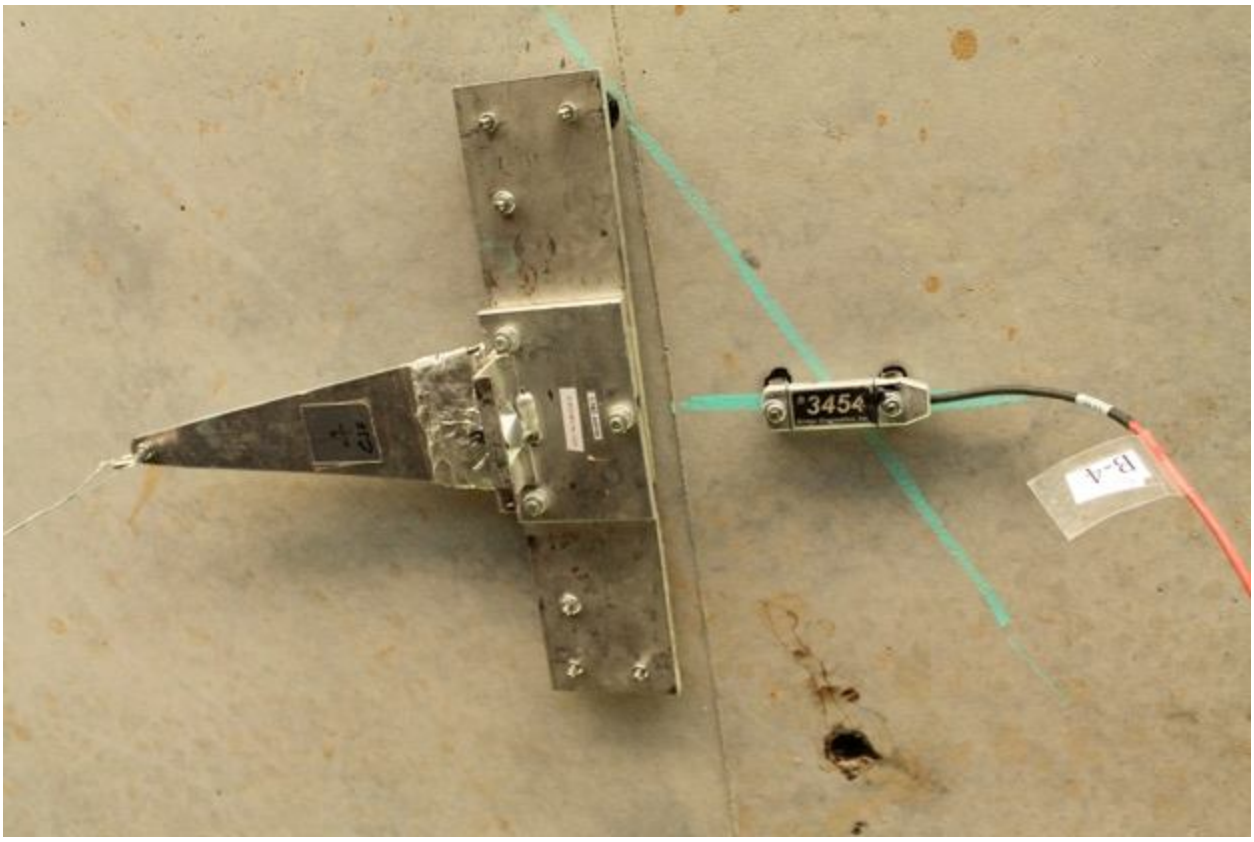

Figure 45. BDI and deflectometer

Deflectometers

Deflections were measured using the home-made sensors, deflectometers as shown in Figure 45. The deflectometers consisted of a flexible aluminum plate with four strain gauges in a full bridge configuration sandwiched between two rigid aluminum plates to create a cantilever. To measure the deflection, the deflectometers were calibrated by deflecting the end of cantilever a known amount and recording the corresponding strain gauge value. The DAS was then calibrated to translate the strain values as deflections. The deflectometers were attached to the bridge by gluing the metal feet to the box beam members. A concrete cylindrical weight was then attached to the end of the deflectometer cantilever to pre-deflect it so that when the truck load is applied and the bridge deflects, the tension applied to the end of the deflectometer by the

weight will be released and the change in strain will measure the deflection. The deflectometers with the weights attached are shown in Figure 46.

Figure 46. Deflectometers with weights attached

Linear Variable Differential Transformers

LVDTs were used to measure the horizontal and vertical relative displacements of adjacent box beam members. The LVDTs were strategically placed at the location of the highest expected relative girder displacements. A horizontally oriented LVDT is shown in Figure 47.

Figure 47. Horizontal LVDT

The horizontal LVDT was glued to the bottom edge of a box beam and a wooden block was glued to the bottom edge of the neighboring box beam so that the LVDT measured differential horizontal movement between the two box girders. Likewise, the vertical LVDT attachment was glued to the bottom edge of a box beam and a piece of steel was glued to the bottom edge of the neighboring box beam. The vertical LVDT was then bolted into a hole to stay in place at the center of the joint as to measure the relative vertical displacement, as seen in Figure 48.

Figure 48. Vertical LVDT

Truck Marker

The location of the truck was marked by using a LVDT as a clicker. The LVDT was depressed and quickly released when the truck reached the six locations shown in Table 15.

Table 15. Truck marker locations

Click	Part of Truck	Bridge Location in Terms of Length, L	Label in Figures
1	Front left tire	0 (Entering bridge)	0L
2	Front left tire	0.25 L	0.25L
3	Front left tire	0.5 L	0.50L
4	Front left tire	0.75 L	0.75L
5	Front left tire	L	L
6	Back right tire	L (Leaving bridge)	L+Wb

The direction of the trucks combined with the skew was such that the front right tire was the first to reach a location and the back right tire was the last to leave. Figure 49 shows the location of the trucks being marked.

Figure 49. Marking location of truck

Instrumentation Layout

BDI strain transducers and deflectometers were placed at midspan on the bottom of each box beam to measure the longitudinal strain and vertical deflection. Due to the visible signs of deterioration in the two external downstream joints, vertical LVDTs and horizontal LVDTs were placed at midspan and quarterspan, where the most leaking appeared to have occurred, on the two external downstream joints. To be able to compare the results of the relative displacement in deteriorated joints to seemingly undamaged joints, the two external upstream joints were also instrumented with vertical LVDTs and horizontal LVDTs. An overall look at the actual instrumentation is shown in Figure 50 and the instrumentation plan is shown in Figure 51.

Figure 50. Overview of instrumentation

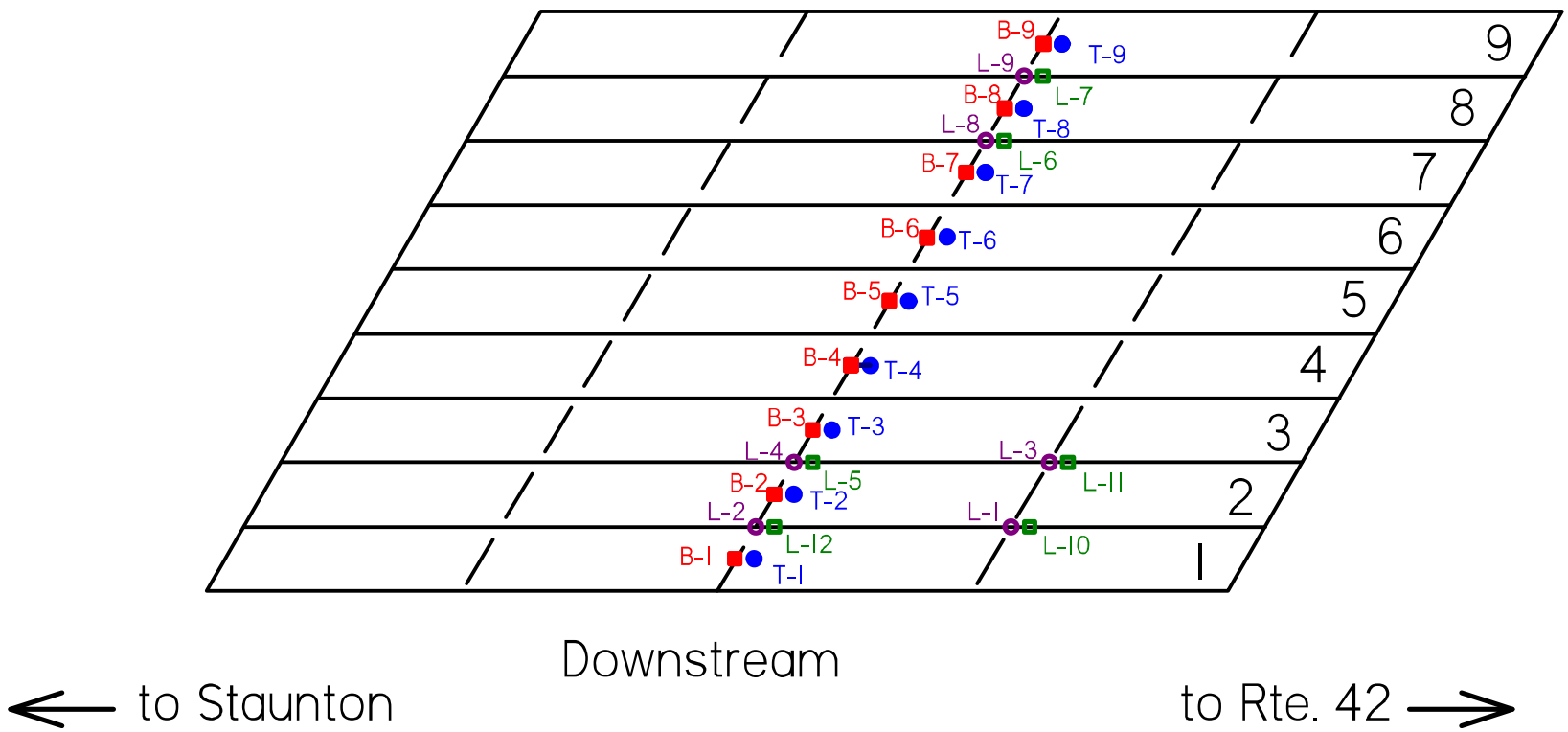

Figure 51. Instrumentation plan

Loading Procedure

A total of six quasi-static load cases were tested by driving the same loading truck over the bridge in three separate runs. Brightly colored chalk lines were drawn on the bridge deck at the joints where the truck load ideally would be applied. The chalk line marked the outside edge of the front left tire so that the driver could follow it more easily and focus on maintaining the slowest possible speed of two to three mph. Figure 52 shows the truck applying the load at the joint by driving along this line.

Figure 52. Truck following line

Trucks

The load was provided by two VDOT dump trucks approximately loaded to 23 tons each. The actual load of each truck is shown in Figure 53. These trucks were chosen as the standard VDOT trucks weighing the legal load limit as to produce the maximum legal deflections and strains in the bridge.

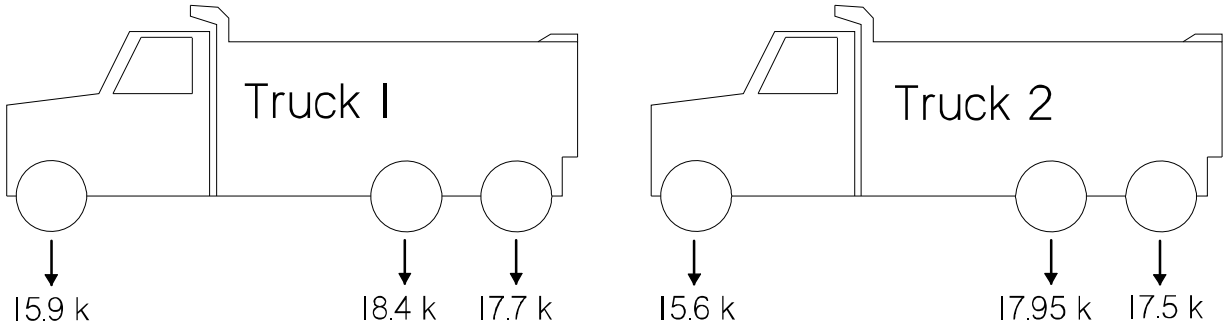

Figure 53. Axel weights of loading trucks

Both loading trucks had the same dimensions and are shown in Figure 54. The width of each of the rear tires was 1 ft, therefore the overall width of the truck was 8 ft.

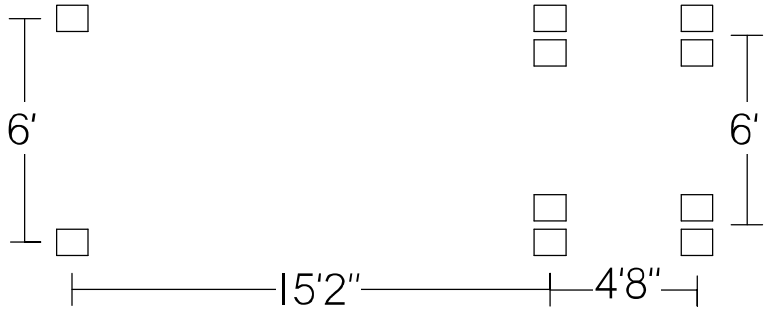

Figure 54. Dimensions of loading trucks

Load Cases

The two exterior downstream joints, joint 1 located between beam 1 and beam 2 and joint 2 between beam 2 and beam 3, showed the most signs of deterioration. Load case 1 shown in Figure 55, and load case 2 shown in Figure 56, were chosen to maximally load joints 1 and 2 in an attempt to record the largest relative joint displacements experienced.

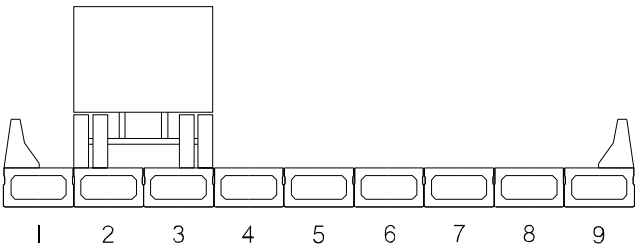

Figure 55. Load case 1

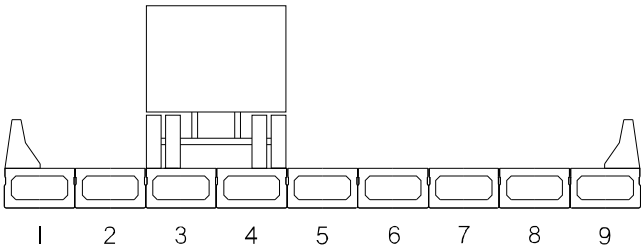

Figure 56. Load case 2

Load case 3 shown in Figure 57, was chosen to obtain the maximum midspan deflections and longitudinal strains in the downstream beams.

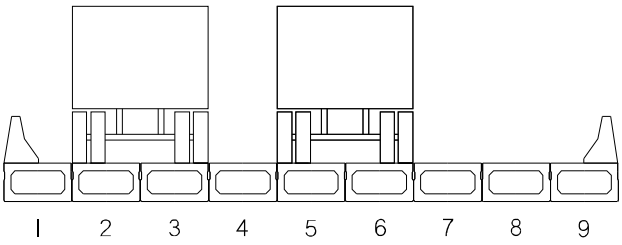

Figure 57. Load case 3

The first three load cases were mirrored to the upstream side of the bridge in an attempt to gather the same information. Load cases 4, 5, and 6 are shown in Figure 58, Figure 59, and Figure 60.

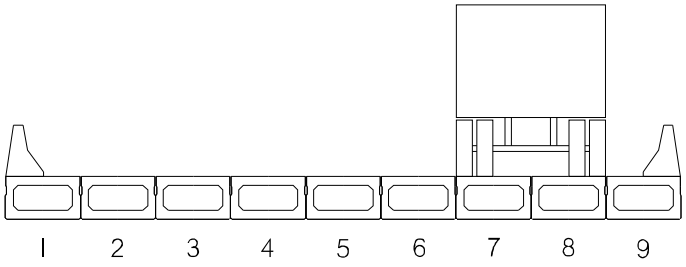

Figure 58. Load case 4

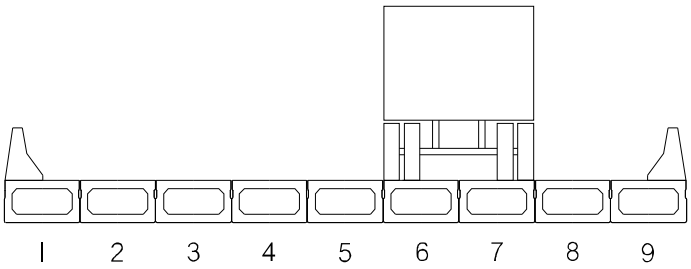

Figure 59. Load case 5

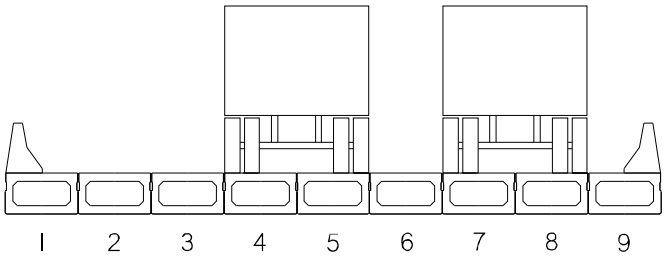

Figure 60. Load case 6

RESULTS AND DISCUSSION

This chapter presents the results obtained from testing and is divided into six sections. The first section presents the results from the material tests performed. The second section presents the results from the splice tests. The third section shows the results from the non-contact splices in sub-assemblage test. The fourth section presents the box beam displacement and strains obtained from the finite element analysis. The finite element analysis results are further

discussed in the fifth section with the Buffalo Branch Bridge live load test results. The sixth section presents the process and findings from the Buffalo Branch Bridge rehabilitation.

Material Tests

The results from the material tests described in the experimental methods chapter are presented here. Part of the objective of the material tests was the material characterization of the VHPC mixes; therefore the two VHPC mixes are plotted separately with more detail in each section. These plots include error bars that show the values associated with the 95 percent confidence intervals, which were obtained using a one-sample t-test.

Compressive Strength

The results from all of the compressive strength tests performed with VHPC-Large and VHPC-Small are shown in Figure 61. Both mixes gain strength quickly and then plateau by 14 days at about 16,000 psi. The higher variability for the VHPC-Large results is most likely due to only testing a few cylinders between 7 and 14 days. The VHPC-Large batch that produced the weakest strengths at all ages was the only one used to obtain the strength at 12 days. Therefore the strength at 12 days is not the best representation of the VHPC-Large mix overall.

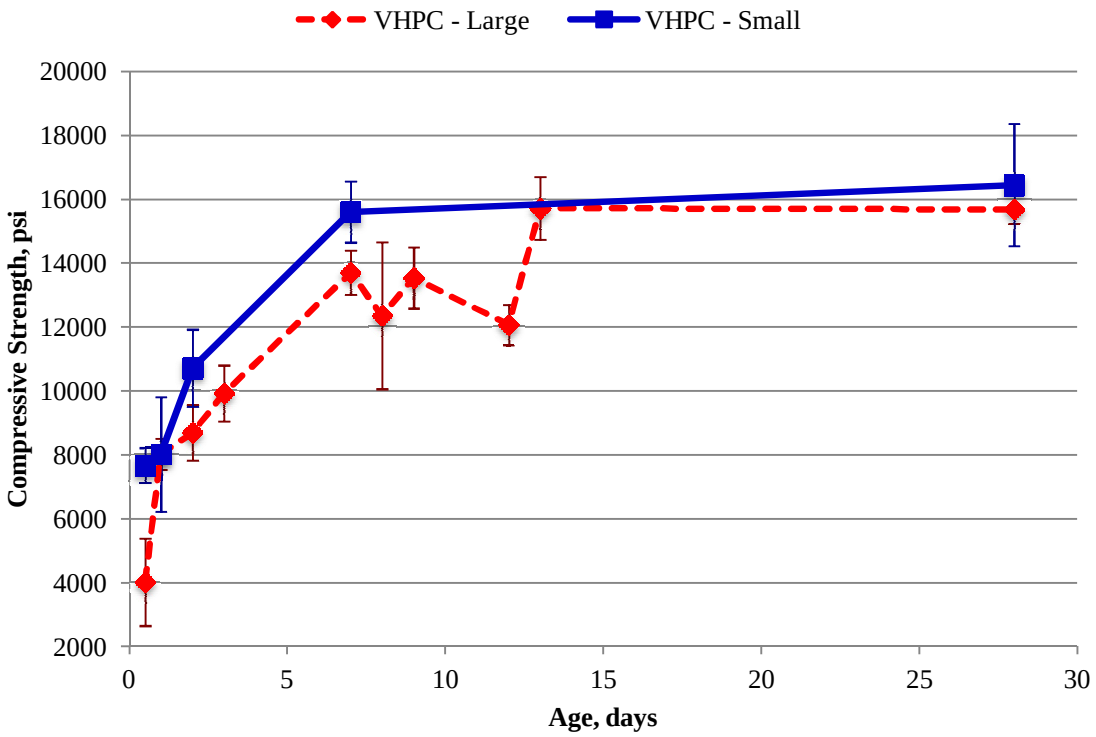

Figure 61. VHPC Compressive Strength Results

The compressive strength results from all of the mixes are shown in Figure 62. The grout mixture gained strength the slowest. At 7 days, the grout had only gained about 50% of its 28 day strength while all of the other mixes had gained about 80% of their 28 day strength. The 28 day compressive strength of the UHPC does not meet the definition of at least 21.7 ksi. This is most likely due to the small sample size of only mixing one batch of the UHPC and testing three cylinders at each age.

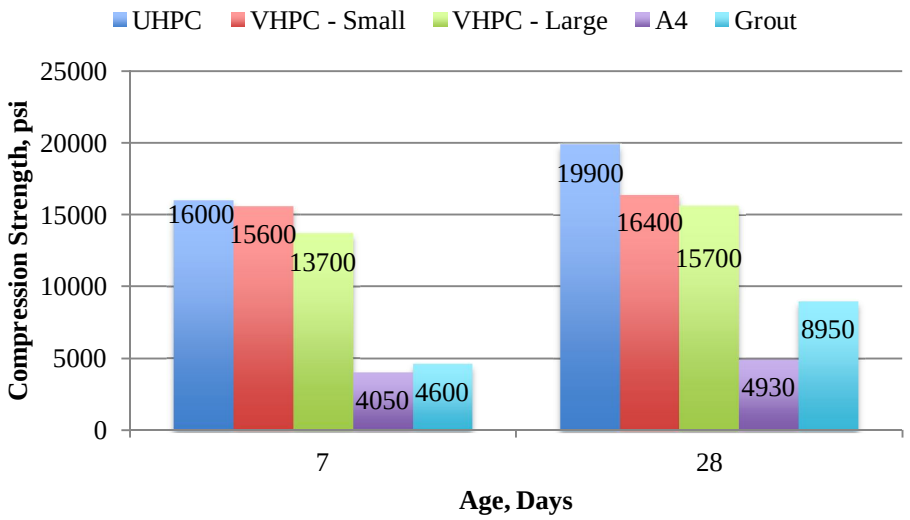

Figure 62. Compressive strengths

The temperature effects on compressive strength gain of the VHPC-Small mixture were investigated to gain a better understanding of how it would remain workable, cure, and gain strength in different temperatures. Three VHPC-Small batches were mixed and left to cure outside in varying temperatures, which mimicked the anticipated temperature environment for the Buffalo Branch Bridge rehabilitation. The high and low temperatures on the day of mixing, one day after, and two days after are presented in Table 16. The results from the compressive strength tests are also shown in Figure 63 and the mean of all the VHPC-Small batches mixed is included in the plot. As seen, the VHPC-Small mixture gained strength faster with warmer temperatures and slower in colder temperatures. Using VHPC in bridge repairs requires rapid strength gain. Most likely, the bridge would not be closed for more than just the night, with the typical scenario being the bridge is only closed for a few hours when the construction crew leaves and traffic is allowed back over the bridge. With the low temperatures in September not producing the mean strengths normally obtained, the VHPC should not be placed with

temperatures in the 40s because it would not gain strength fast enough for a repair project. Another note is that while the VHPC gains strength faster in the warmer temperatures, it also starts to set up quicker while placing, decreasing the workability. This was further examined by mixing several batches outside in the summer heat and investigating the addition of retarder and is explained in the Workability and Flow section. VDOT (2007) specifies that concrete used in the construction of bridge decks shall have a temperature between 40 °F and 85 °F.

Table 16. VHPC-Small temperatures

	Day of Mixing		1 Day		2 Day	
Mixing Date	**Low, °F**	**High, °F**	**Low, °F**	**High, °F**	**Low, °F**	**High, °F**
6/16/14	61	87	62	88	63	85
7/1/14	65	88	66	89	65	84
9/23/14	42	60	46	67	56	75

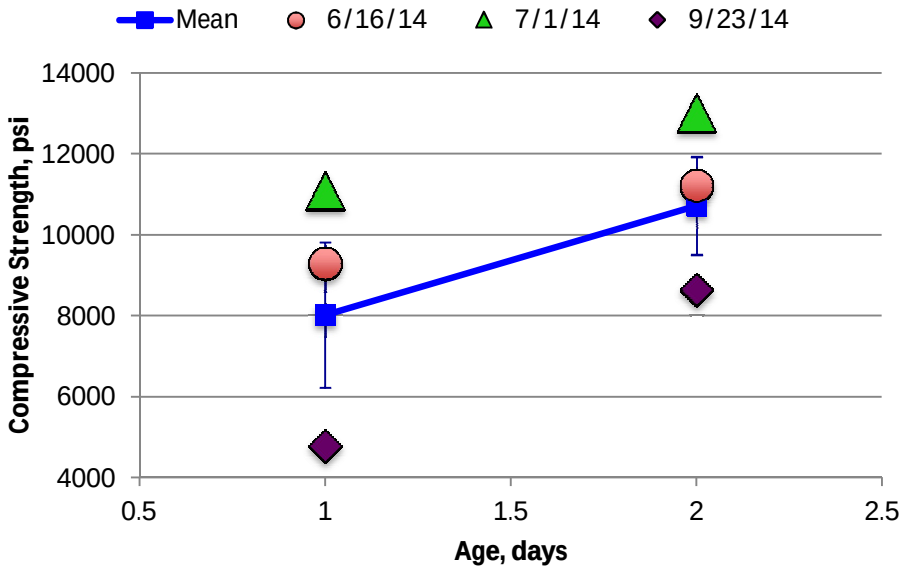

Figure 63. VHPC-Small compressive temperature comparison

Splitting Tensile Strength

The splitting tensile results for both VHPC mixes are shown in Figure 64. Both VHPC mixes plateau around 2,000 psi.

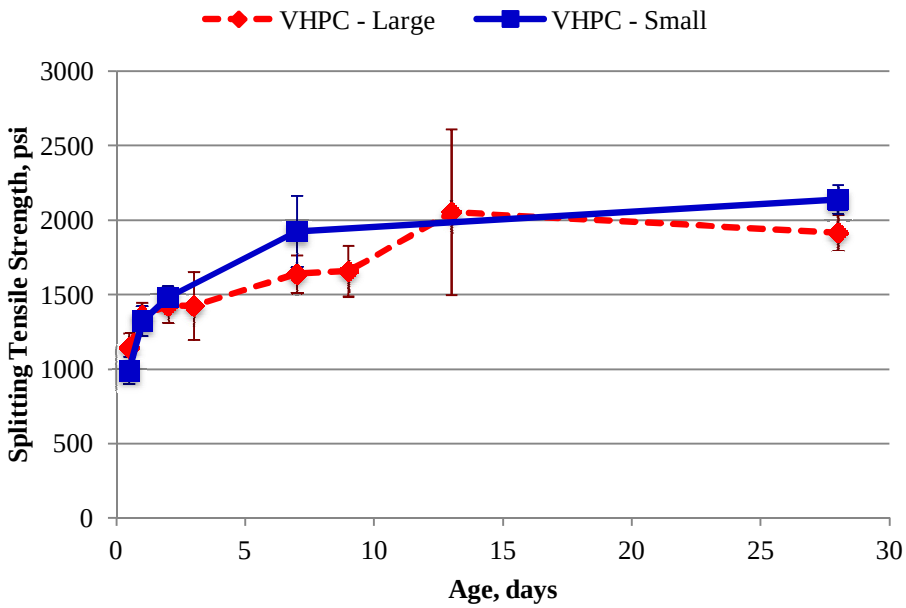

Figure 64. VHPC Splitting Tensile Results

The splitting tensile results for all of the mixes are present in Figure 65. All of the fiber reinforced concrete, UHPC and both VHPC mixes, have significantly higher splitting tensile strengths than the grout and normal concrete. This is to be expected because when cracks start to form in the fiber reinforced concretes, the fibers bridge the openings. The strong tensile strength and post cracking behavior is one of the advantages to using fiber reinforced concretes in adjacent precast member connections instead of grout. The fibers bridging the cracks can be seen in Figure 66 where the VHPC-Large cylinder is still completely intact as compared to the grout and A4 deck concrete that splits in half at failure.

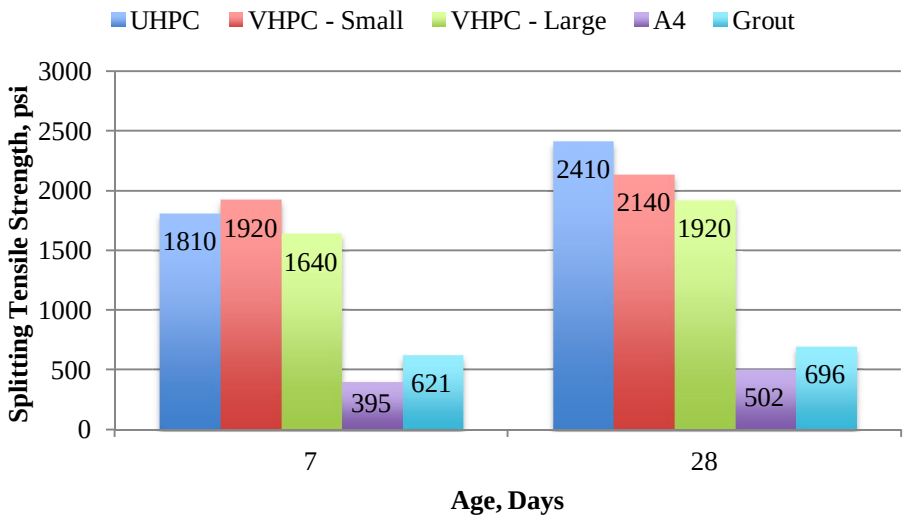

Figure 65. Splitting Tensile

Figure 66. Splitting tensile grout, A4, and VHPC-Large

Modulus of Elasticity

The modulus of elasticity results for both VHPC mixes are shown in Figure 67. The same cylinders tested for compressive strength were first used in the modulus of elasticity test.

Therefore the lower modulus of elasticity at 12 days is also explained by the weakest batch being the only one tested.

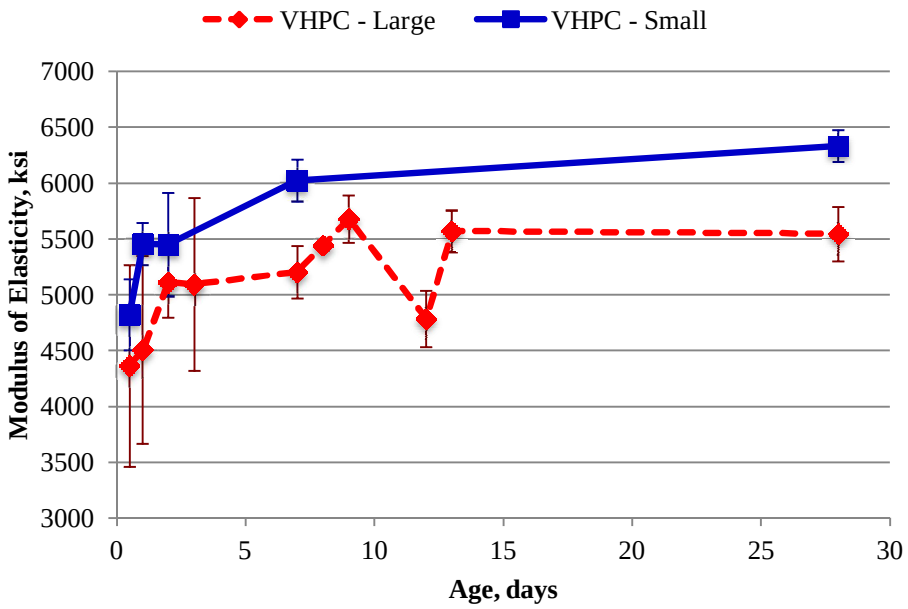

Figure 67. VHPC Modulus of Elasticity

The modulus of elasticity results for all of the mixes are shown in Figure 68. The modulus of elasticity for UHPC relative to the other mixes is a larger difference than previously seen in the strength tests. It is also worth noticing that grout had a 28 day compressive strength almost double that of the A4 deck concrete, but the modulus of elasticity for grout is lower than the A4 deck concrete.

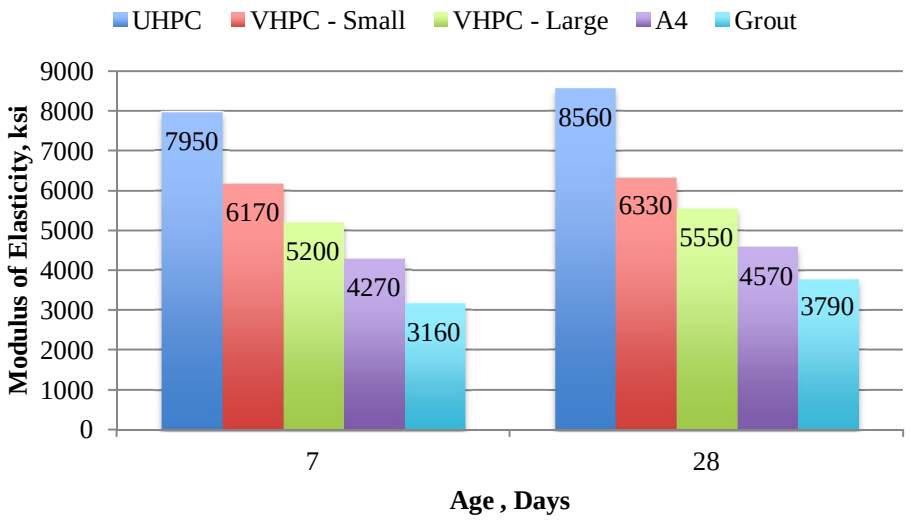

Figure 68. Modulus of elasticity

Reinforcing Steel Bond

The pull out tests were performed on VHPC-Large and VHPC-Small specimens at ages ranging from 12 hrs. to 7 days and the reinforcing steel ruptured each time as shown in Figure 69.

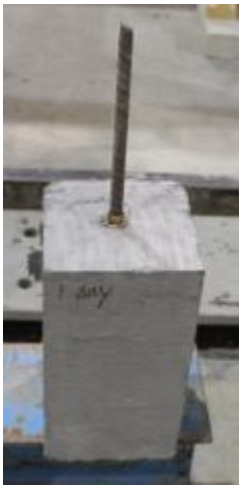

Figure 69. Ruptured reinforcing steel

Figure 70 and Figure 71 present the data for the VHPC-Large mixture from the wire pot and bottom LVDT respectively. The first test at 12 hours ruptured the reinforcing steel without exhibiting slipping at the bottom more than 0.005 in. During the second test at 1 day, the actuator began to leak oil so the specimen was unloaded and the actuator was temporarily fixed to finish testing. However at day 2 the actuator was still leaking oil causing the test to be postponed until day 7 when it was fixed.

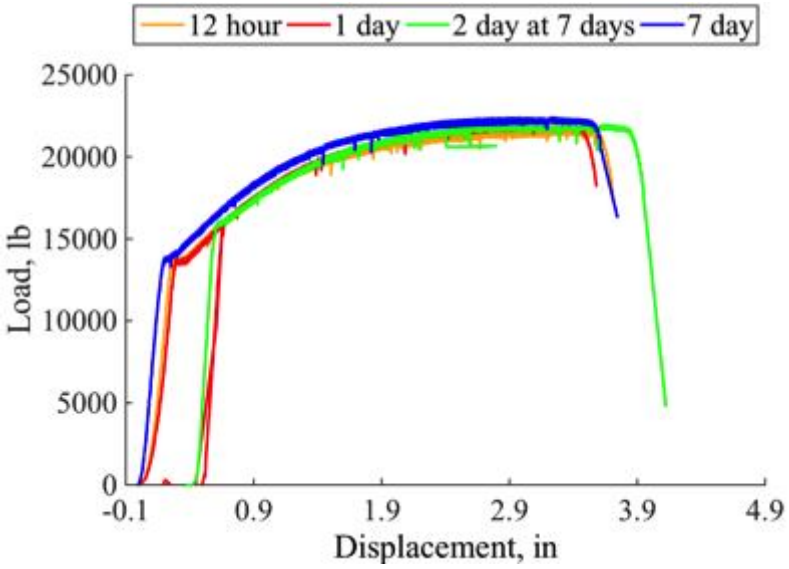

Figure 70. VHPC Large – Wire Pot vs Load

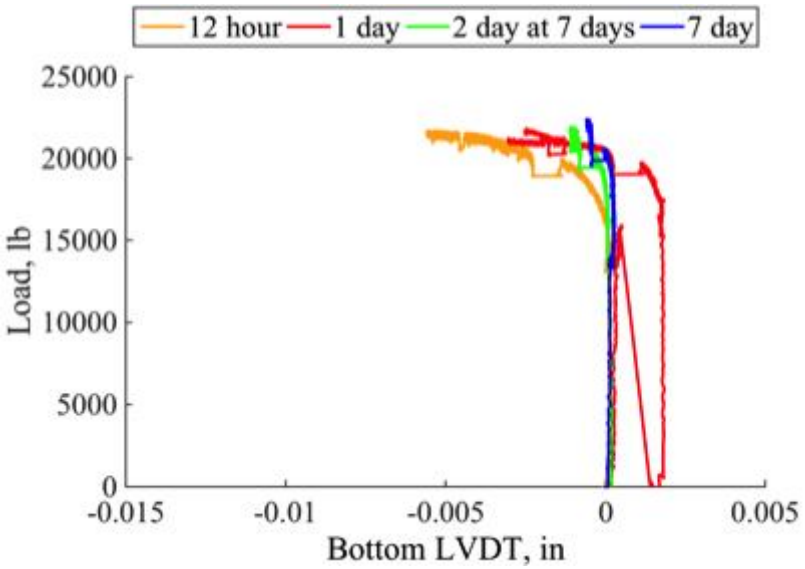

Figure 71. VHPC Large - Bottom LVDT vs Load

Figure 72 and Figure 73 present the data for the VHPC-Small mixture from the wire pot and bottom LVDT respectively. The first test at 12 hrs. ruptured the reinforcing steel and only had 0.01 in. slip at the bottom LVDT. The reinforcing steel used in the 1 day specimen ruptured at a load significantly lower than every other grade 60 steel bar used in testing which ruptured around the expected load of 15 kips. Because of this, the ruptured steel was examined after the test it was found that there was a deformity where the steel ruptured which precipitated early failure.

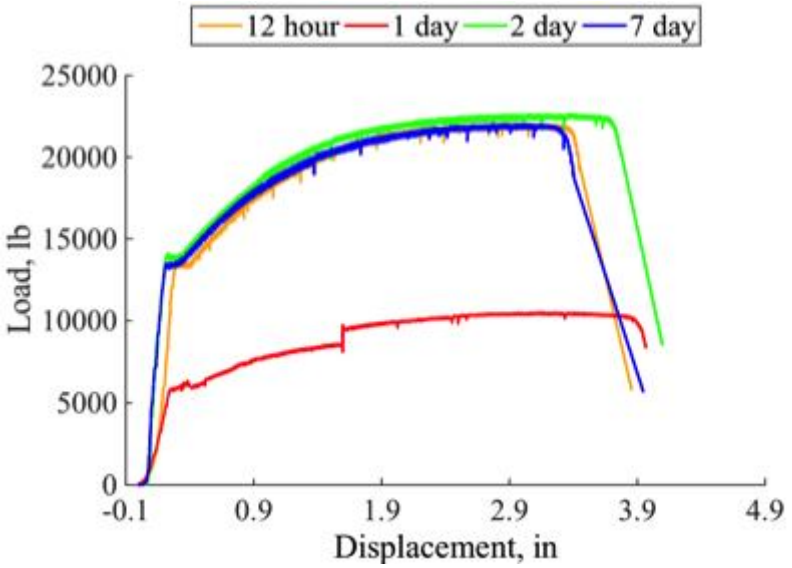

Figure 72. VHPC Small - Wire Pot vs Load

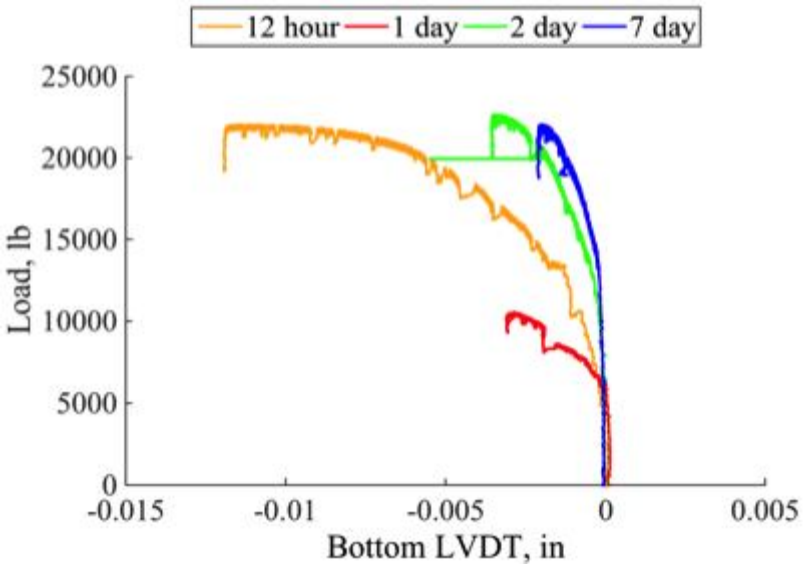

Figure 73. VHPC Small - Bottom LVDT vs Load

The results for both VHPC mixes show that the bond between the VHPC and reinforcing steel is obtained by 12 hours.

Bond with Concrete

The results of the pull off tests for both VHPC mixes are shown in Figure 74. The surface preparation that improved the bond strength the most was SSD. At 28 days, sand blasting only

improved the bond strength by 20 percent. However, the time and effort required to sand blast an entire shear key surface makes it an uneconomical option for only a 20 percent increase in strength. Whereas, the time and effort required to create a SSD shear key surface is minimal compared to the 94 percent increase in strength at seven days for the dry vs SSD results.

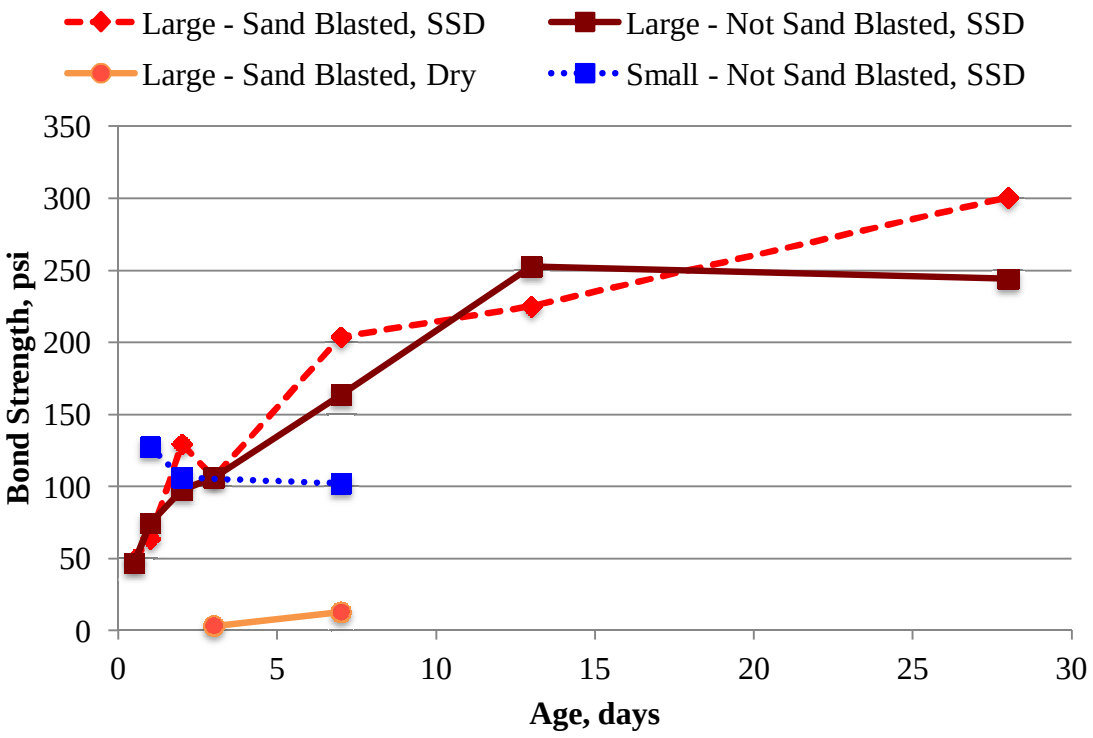

Figure 74. VHPC bond with concrete

Joyce (2014) performed the same pull off tests for UHPC, grout, and VHPC-Large with a sand blasted and SSD surface condition. The results are shown in Figure 75. With the same surface conditions, The UHPC and VHPC-Large had the same bond strength, while the grout had less than 10 percent of the bond strength at 15 days.

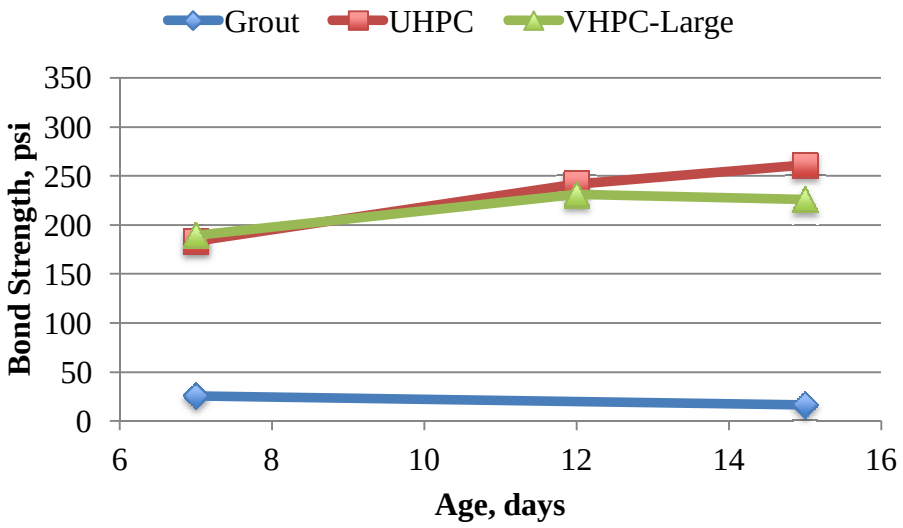

Figure 75. Joyce bond tests results

The classification for different bond failures are as specified in ASTM D7234 (2012) and the VHPC failure classifications experienced in these tests are presented. The typical failure mode observed in the VHPC at 12 hours and one day was substrate failure C in which the bond failed at a thin layer of cementitious material. This is shown in Figure 76 where a thin layer of cementitious material is still visible on the precast concrete. A few of the 12 hour tests failed at the epoxy because there was not adequate time for it to fully cure.

Figure 76. Typical VHPC 12 hour to 1 day failure

The typical failure mode observed in the VHPC at testing ages of two days to five days was substrate failure B in which the bond failed at the cement paste but was not strong enough to fracture the aggregate. This is shown in Figure 77 where the there is no longer a thin layer of cementitious material left on the precast concrete and the aggregate is still fully intact.

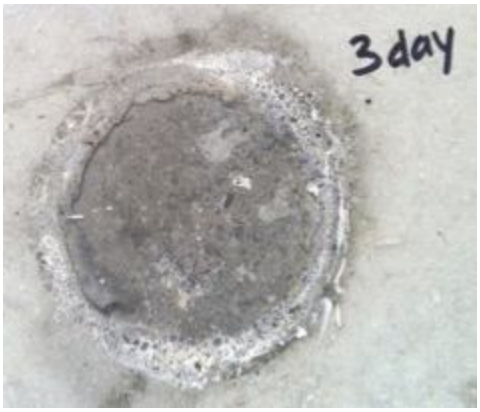

Figure 77. Typical VHPC 2 day to 5 day failure

The typical failure mode observed in the VHPC at seven days and older was substrate failure A in which the bulk of the cement paste was detached along with fracturing the aggregate inside the precast concrete member. This is shown in Figure 78 where the left two pictures were taken at seven day tests and the right one was taken at 28 days.

Figure 78. Typical VHPC 7 days and older failure

Workability and Flow

The results for the inverted slump tests are shown in Figure 79. Time zero represents when the VHPC was fully mixed and could be placed. The first test performed using the VHPC-Large mixture showed that by 30 minutes the spread had decreased to 14 in. and no longer flowed as designed. Increasing the workability of the VHPC by adding retarder to the mix was then investigated. The retarder was dosed in the same units as the HRWR (oz/cwt.) and is denoted in the plot by the number next to the mix, 0 meaning no retarder was added. After observing that the retarder did not improve the workability after the mix sat still for 20 minutes, continuously mixing the VHPC was examined. Originally, the VHPC was left in the mixer sitting still for 10 minutes in between tests. However for the mixed batches, the mixer was left on throughout the tests, which greatly improved the workability. The tests were also performed on a continuously mixed VHPC-Small mix without retarder. The VHPC-Small performed significantly better than the VHPC-Large and did not lose much of its workability after 40 minutes. The initial target spread for the VHPC was determined to be 19 in. to 21 in.

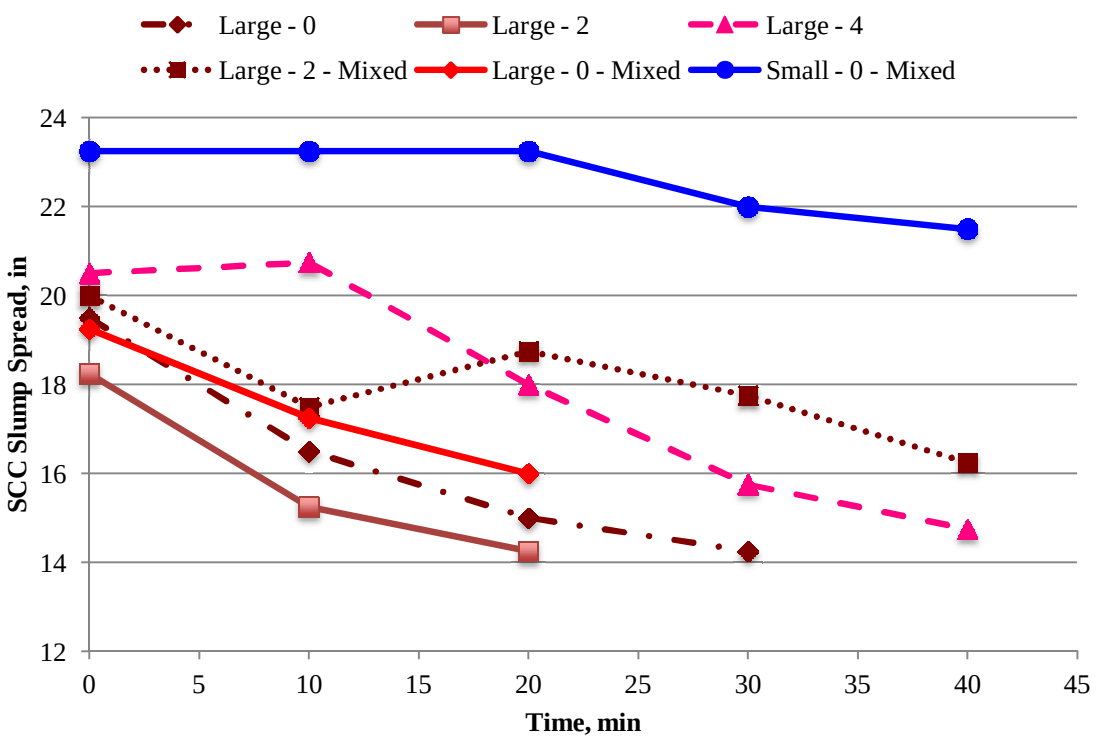

Figure 79. VHPC Slump Spread

The results of the box flow tests with the VHPC-Large mixture are shown in Figure 80. The objective was to determine how far the mixture could be reasonably expected to flow and how long it would remain that workable. In an attempt to increase the time in which the VHPC-Large is able to be placed, adding retarder was also examined. As can be seen, the addition of retarder along with continuously mixing the VHPC-Large greatly improved the workability of the mix.

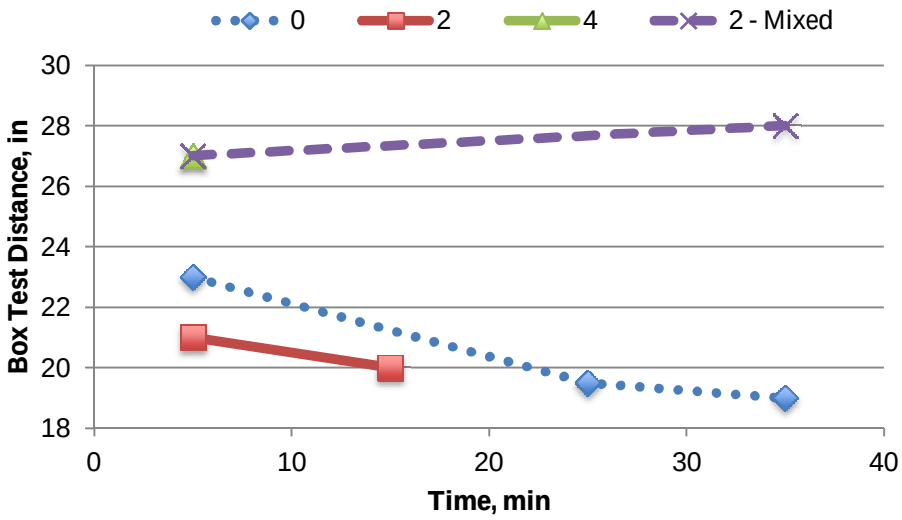

Figure 80. VHPC-Large box flow tests results

The results from the shear key flow test with the VHPC-Small mixture are shown in Figure 81. Placing the VHPC-Small began in the low end and moved toward the upper end. The majority of the shear key was placed continuously, however, the upper end was placed after a fifteen minute break.

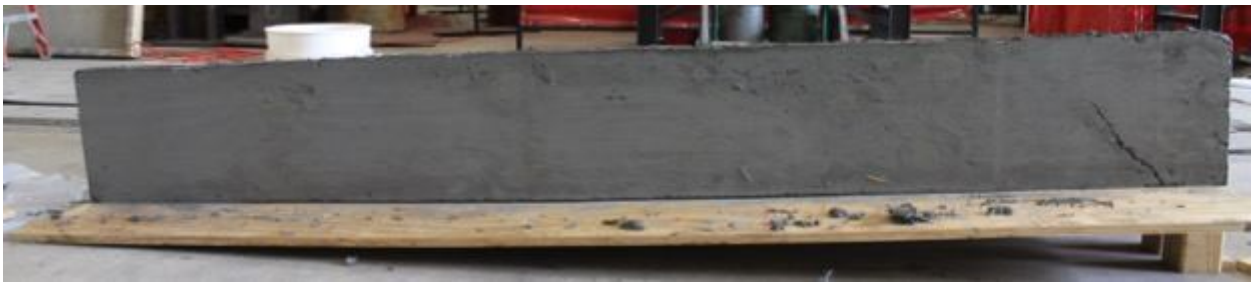

Figure 81. Shear key flow test overall after removing the formwork

To examine what happens when two batches are placed next to each other, the top half of the joint was rodded while the bottom half was not. The results of this are shown in Figure 82 and Figure 83. As can be seen, a cold joint formed on the bottom half of the upper end where the two batches were not rodded together.

Figure 82. Shear key flow test lower end

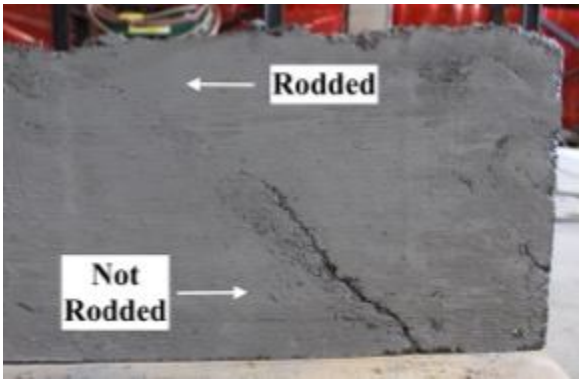

Figure 83. Shear key flow test upper end

The transverse slope of the geometric cutouts was also found to not cause the VHPC to overflow on the low end. A picture of this is shown in Figure 84 where the VHPC-Small is still level after being placed on an incline.

Figure 84. Dog bone slope results

Durability

The results from the freeze/thaw tests are shown in Figure 85 through Figure 87. Based on Lane and Ozyildirim (1999), the minimum passing relative dynamic modulus after 300 cycles is 60 for the Virginia Transportation Research Council (VTRC). As seen, all of the mixes tested meet this requirement as they are all above 90.

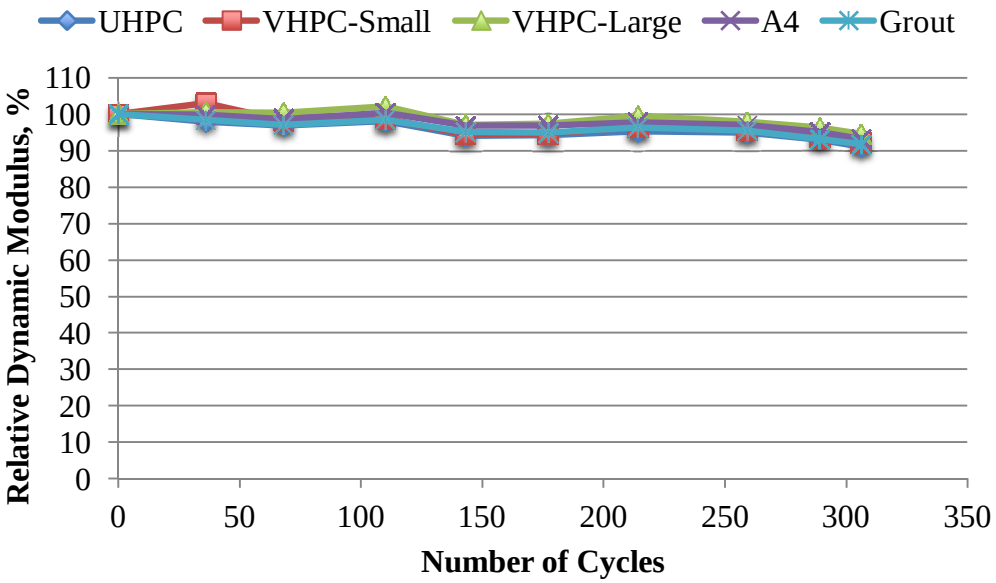

Figure 85. Freeze/Thaw relative dynamic modulus

The specimens were initially weighed dry, before being placed in the freeze/thaw machine. Each subsequent weight was measured after removing the specimen from the water filled bins, letting the surface dry off, and then wiping off the scaled surface. As seen in Figure 86, the weight measurements taken after the first group of cycles show that some of the specimen absorbed a large amount of water. The weights then remained constant until the surfaces of the specimen started scaling.

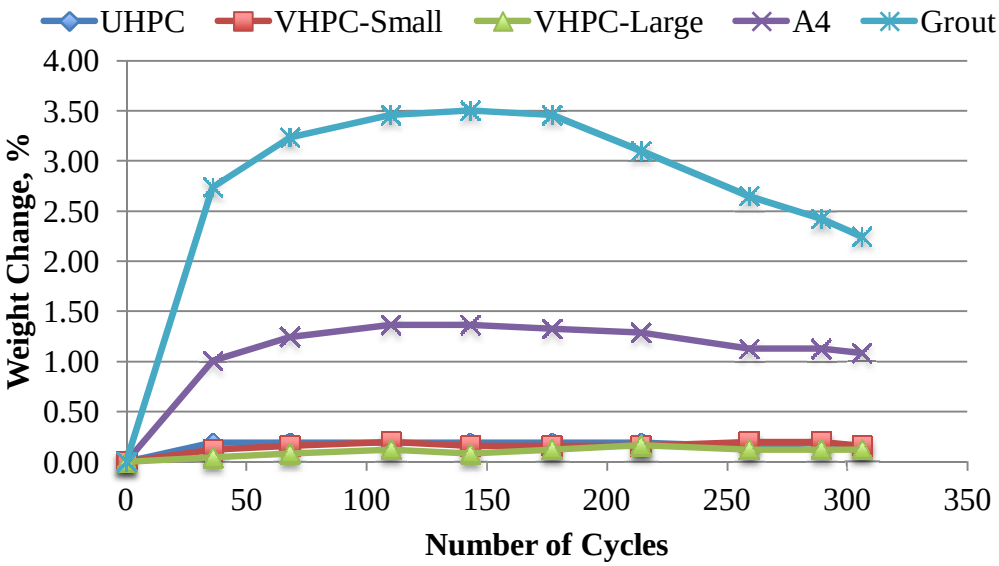

Figure 86. Freeze/Thaw weight change

The data presented in Figure 87 was the scaling of the bottom and side surfaces; none of the top surfaces exhibited scaling because they were not fully submerged for the entirety of testing. The VTRC rating system for scaling was as follows:

0 = no scaling

1 = light scaling where the aggregate could not be seen

2 = light to moderate scaling where the aggregate could be seen, but not felt

3 = moderate scaling where the surface between the aggregate started to scale

4 = moderate to heavy scaling where some of the aggregate was exposed, but not all

5= heavy scaling where the surface is rough with exposed aggregate

The grout and UHPC did not have aggregate to be exposed, so the rating system was adjusted to a judgment call of whether or not the amount of scaling would have caused the aggregate to be exposed. While the UHPC and both VHPC mixes did not exhibit any scaling in the first 300 cycles, the steel fibers that were exposed began to rust.

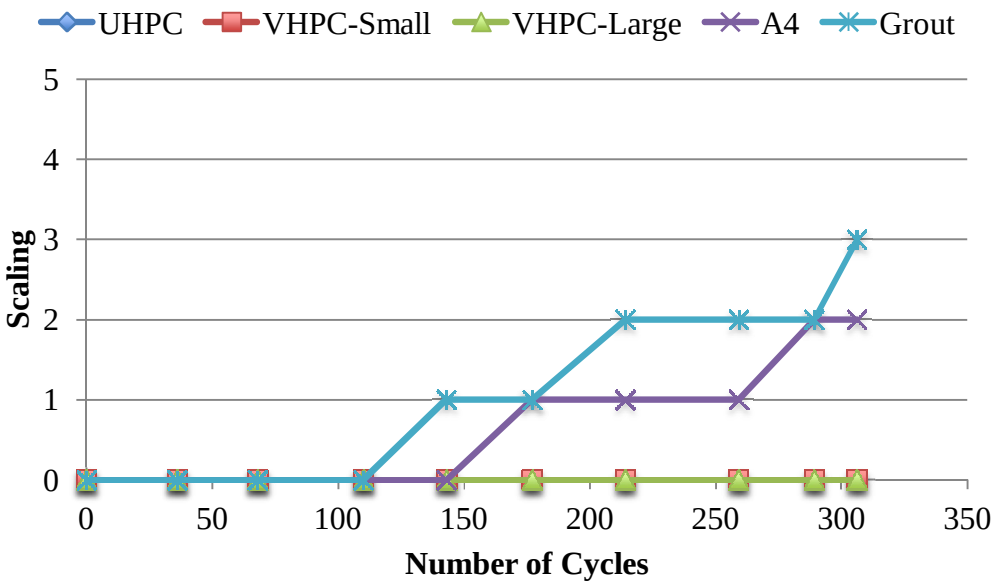

Figure 87. Freeze/Thaw scaling

Shrinkage

The shrinkage tests results are shown in Figure 88, Figure 89, and Figure 90. As mentioned before, not all of the specimen cast were able to be tested in the ASTM C157 testing comparator. The shrinkage results for the mixes that were tested in the ASTM C157 testing comparator are shown in Figure 88. The UHPC and VHPC mixes showed the highest shrinkage measured with ASTM C157 due to their higher concentration of cementitious materials.

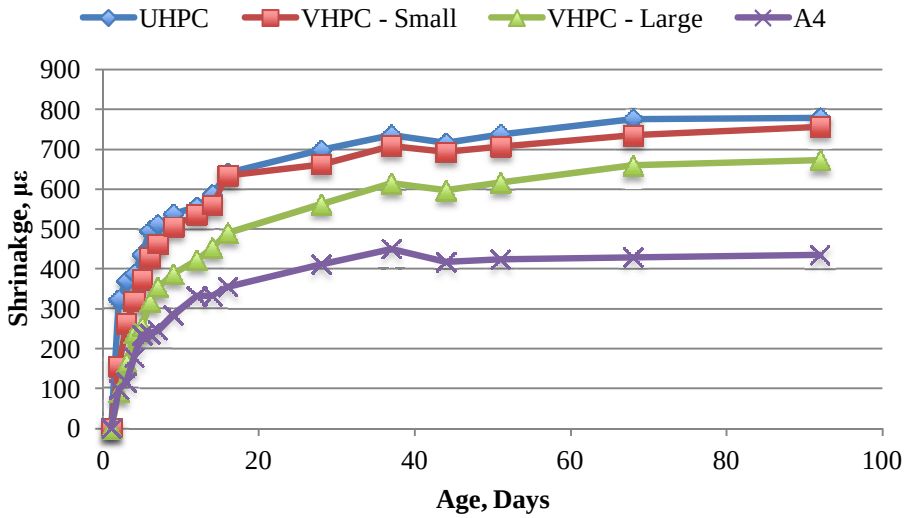

Figure 88. Shrinkage

The same surface shrinkage was measured using the DEMEC discs and the results are shown in Figure 89. The grout is marketed as non-shrink precision grout, however it exhibited shrinkage more than four times as much as the A4 deck concrete and over twice as much as the UHPC and VHPC mixes. This is one indicator that grout is not the best material to use in the shear keys because shrinkage cracks may form.

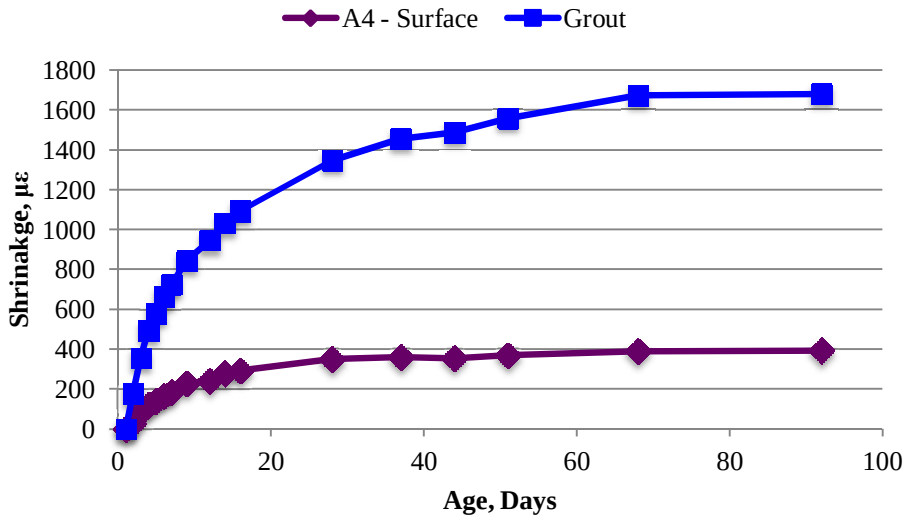

Figure 89. Surface shrinkage

One of the A4 deck concrete specimens was tested in both configurations, standard and surface shrinkage. Figure 90 shows the comparison of the two results. The difference of the two test methods for measuring shrinkage is very small and can be considered negligible. Therefore, the results of the grout shrinkage presented in the previous Figure 89, can be directly compared to the shrinkage results of the VHPC.

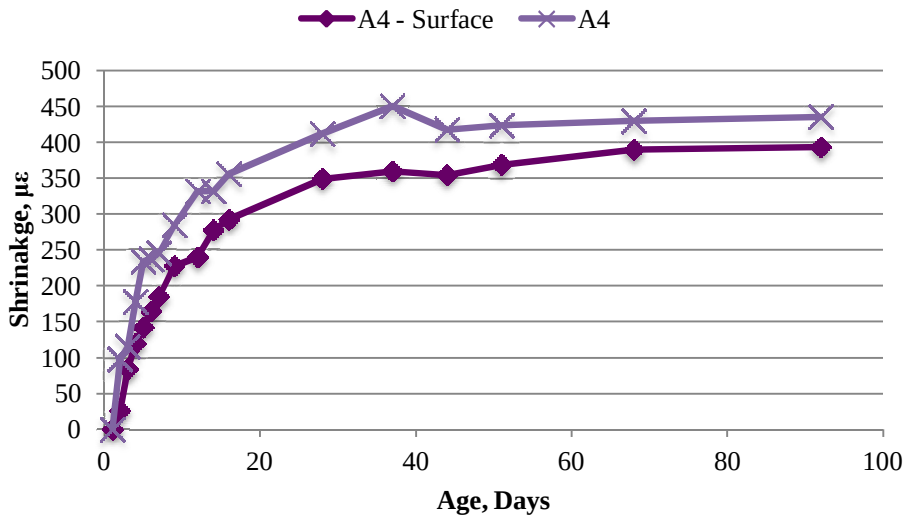

Figure 90. Shrinkage methods comparison

Cost and Benefits Assessment of VHPC

While the material properties for VHPC and UHPC are similar, the main advantage of VHPC as opposed to UHPC is the cost. VHPC is a non-proprietary mixture and can be easily mixed using readily available materials. The VHPC also has the addition of coarse aggregate, which helps to make it more economical. The cost of the materials required to make a cubic yd. of VHPC is presented in Table 32 and Table 33. The majority of the cost comes from the steel fibers.

Table 17. VHPC - Large cost

Material	Amount, lb/yd^3	Cost, $/lb	Total Cost, $
Water	319	0	0.00
Cement	1121	0.0625	70.03
Fly Ash	240	0.0300	7.21
Silica Fume	240	0.2100	50.46
Sand	1450	0.0098	14.14
¼ in. Limestone	621	0.0093	5.74
1.2 in. Fibers	265	1.1173	295.64
HRWR (25 oz/cwt)	11836	0.0040	46.47
		Total Cost:	**490**

Table 18. VHPC - Small cost

Material	Amount, lb/yd^3	Cost, $/lb	Total Cost, $
Water	319	0	0.00
Cement	1121	0.0625	70.06
Fly Ash	240	0.0300	7.20
Silica Fume	240	0.2100	50.40
Sand	1345	0.0098	13.11
⅛ in. Limestone	660	0.0610	40.26
½ in. Fibers	260	2.3100	600.60
HRWR (25 oz/cwt)	11727	0.0040	46.47
		Total Cost:	**828**

Material Tests Summary

A summary of the material test results for grout, UHPC, VHPC-Small, and VHPC-Large is presented in Table 19.

Table 19. Material properties summary

Average Material Properties	Age, days	UHPC	VHPC-Small	VHPC-Large	Grout
Compressive Strength, psi	7	16000	15600	13700	4600
	28	19900	16400	15700	8950
Splitting Tensile Strength, psi	7	1810	1920	1640	621
	28	2410	2140	1920	696
Modulus of Elasticity, ksi	7	7950	6170	5200	3160
	28	8560	6330	5500	3790
Bond with Concrete, psi (sand blasted, SSD)	7	183	102*	190	26
	15	261	N/A	226	17
Relative Dynamic Modulus, %	300 cycles	91	92	95	92
Shrinkage, με	7	511	462	354	724
	28	698	662	561	1347
	92	779	757	673	1680
Cost, $/yd^3	N/A	2000^	828	490	

*VHPC-Small Bond results were for non-sandblasted, SSD
^Cost estimate for proprietary UHPC, includes engineering with project

As observed, the UHPC and both VHPC mixes gained strength faster and achieved higher compressive and splitting tensile strengths than the grout. The splitting tensile tests for the UHPC and both VHPC mixes also exhibited some post cracking tensile strength where the steel fibers present bridged the cracks so that the cylinders continued to take load. The fibers also enabled the cylinders to remain intact after testing. While the grout cylinder split completely in half not long after initial cracking. Along with the increased strengths, the UHPC and both VHPC mixes also had larger modulus of elasticity than the grout. While the increased compressive and splitting tensile strengths make UHPC and both VHPC mixes a better option than grout, the bond strength with the concrete is the main advantage. Because the deterioration of the grout shear key begins at the bond with the precast concrete member, the increased bond strength could potentially make the joints last significantly longer. The bond strength of the UHPC and both VHPC mixes is much larger than the bond of the grout; the grout bond with the

concrete is only 10 percent of the strength of the UHPC and both VHPC mixes bond with the concrete. The durability presented portrayed with the relative dynamic modulus shows that after 300 cycles all of the mixes are still intact. However, of the four mixes, the grout is the only one that presented scaling. The shrinkage exhibited by the non-shrink grout far exceeded that of the UHPC and both VHPC mixes. The one area where grout was more advantageous than the UHPC and both VHPC mixes was the cost; the grout is significantly more economical up front. However, with the extended lifespan replacing the grout with VHPC could offer, the economical value of the VHPC could surpass the grout in the long run.

The UHPC and both VHPC mixes exhibited higher strengths, better bond, better durability and less shrinkage than the grout. Therefore, these mixes were investigated to be used in the rehabilitation of the Buffalo Branch Bridge. The deciding factor in using the VHPC instead of the UHPC was the cost; VHPC is a more economical option.

Non-Contact Lap Splice Test

An initial static test was performed and then the specimen was loaded with 1,000,000 cyclic tests as outlined in the methods section and finally a final static test was performed. Neither the contact nor the non-contact lap splice test specimens were able to be loaded to failure due to the load frame capacity.

According to Joyce (2014), in the contact lap splice specimen, cracks were first observed on both faces of the north joint at an actuator displacement of 0.09 in. while the south joint remained uncracked until 0.25 in. The largest joint opening measured before the test was stopped was 0.123 in. in the north joint. Cracks first formed at the interface of the precast concrete and the VHPC in the bottom of the shear keys. As the tests continued, the cracks propagated into the

precast concrete member instead of the stronger VHPC shear key. Splitting cracks were also observed in the VHPC on top of the south blockout above the lap splice bar.

Similarly to the contact lap splice test, the non-contact lap splice test specimen began to crack at an actuator displacement of 0.08 in. in the south joint and the north joint remained uncracked until 0.27 in. The non-contact lap splice test also had a largest joint opening of 0.123 in. with the cracks initiated at the interface of the precast concrete and the VHPC in the bottom of the shear keys and propagating into the precast concrete member as the test continued.

The objective of this test was to compare the overall performance of a contact and non-contact lap splice. Because of this, only the results from the final static tests are presented in this report. Figure 91 and Figure 92 show the displacements of the joint LVDTs during the final static tests.

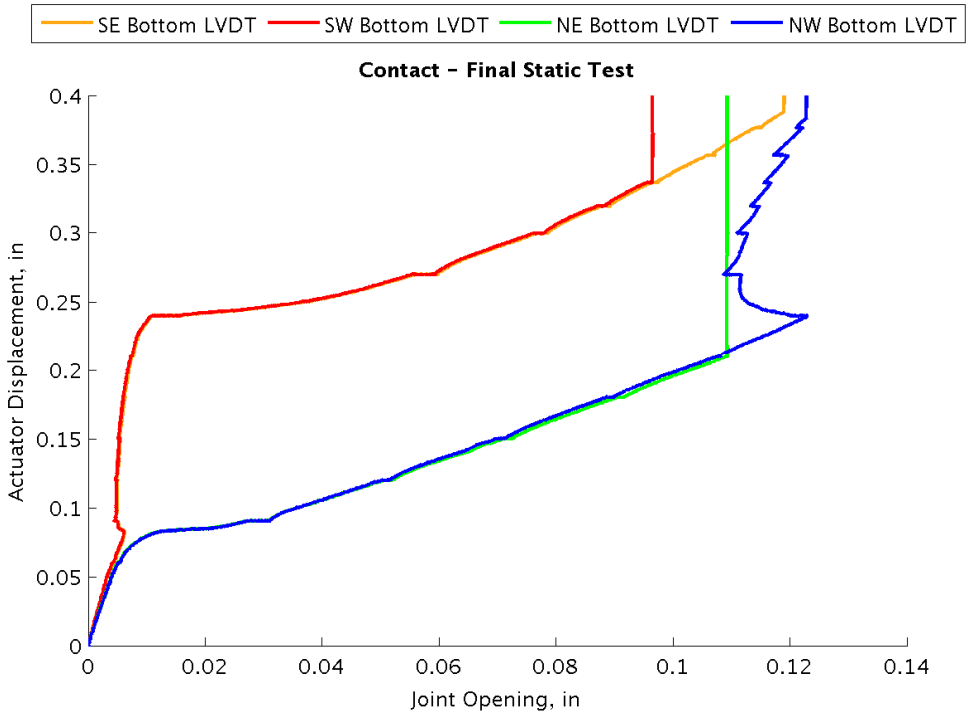

Figure 91. Contact final static test (Joyce, 2014)

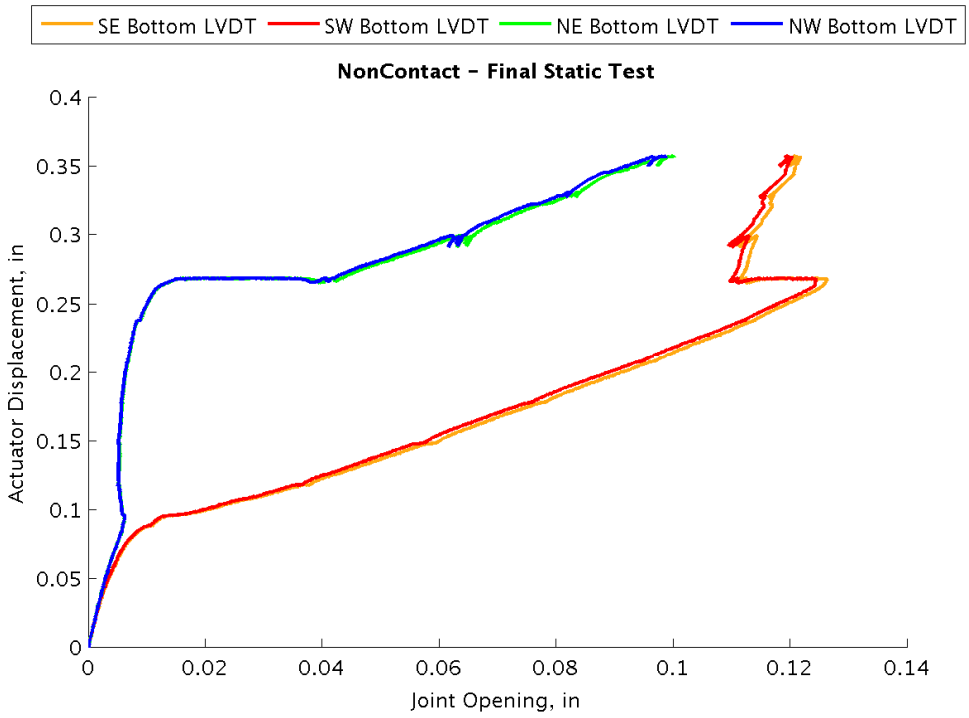

Figure 92. Non-Contact final static test

A comparison of the actuator load and displacement of the contact and non-contact lap splice tests is shown in Figure 93. Before the test had to be stopped, the maximum load reached and the corresponding actuator displacement for the contact lap splice test was 32,400 lbs at 0.44 in. and for the non-contact lap splice test was 25,600 lbs at 0.36 in. Neither specimen was loaded to failure due to the capacity of the test set up, the non-contact lap splice test was ended at a smaller load. According to Joyce, the service load was calculated to be 3800 lbs, which both specimens clearly exceeded. The displacement of the non-contact lap splice specimen was only slightly higher than that of the contact lap splice specimen under the same load and both followed the same linear slope. This is a good indicator that a shear key with a non-contact lap splice will perform as well as one with a contact lap splice. Although both test specimens exhibited cracking during testing, the water ponding tests showed no signs of water leaking through the joints.

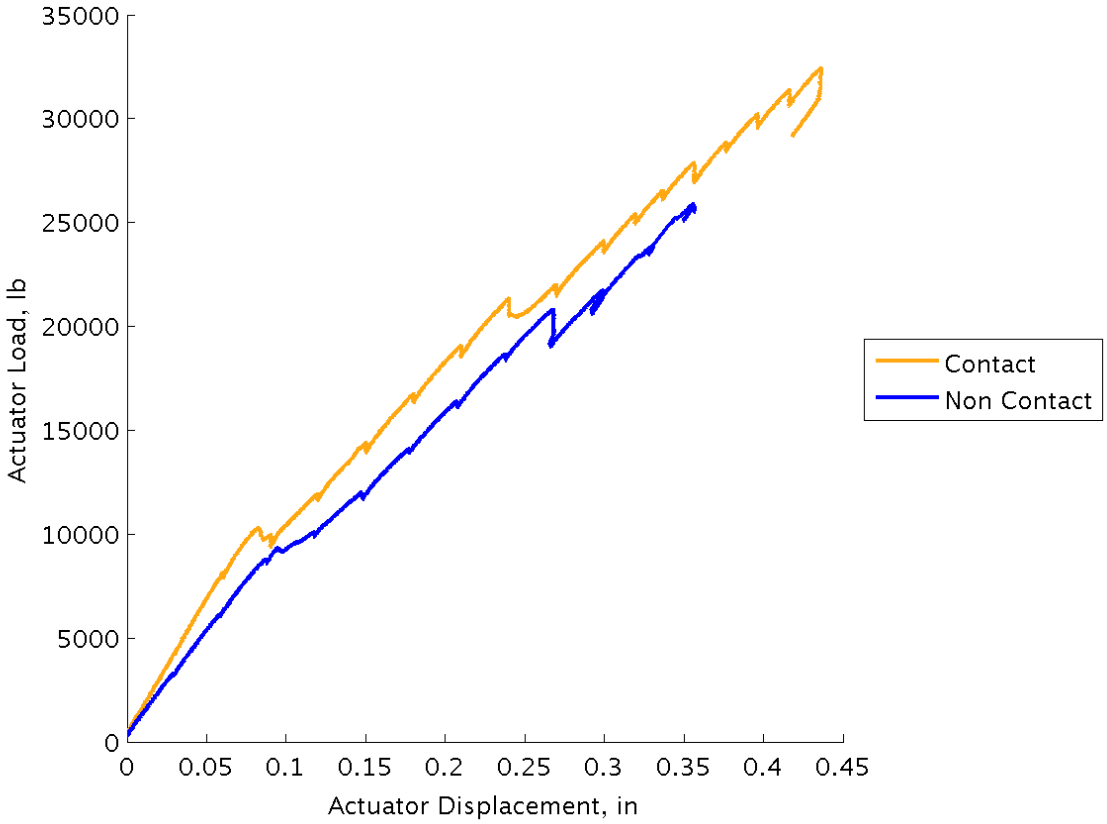

Figure 93. Contact vs non-contact final static test

Buffalo Branch Bridge Live Load Test

Strain Transducers and Deflectometers

Each load case was repeated three times in quasi-static runs of the loading truck. The midspan deflections and longitudinal strains for all nine of the box beams and all six of the load cases are presented in the Appendix. Representative plots of the typical deflections and strains are shown in Figure 94 and Figure 95. Each plot shows the results from an individual truck crossing where the vertical deflection or bottom longitudinal surface strain is plotted for each beam for each of the six locations of the loading truck described in Table 15 in the Experimental Methods section. Ideally, the magnitude and shape of the deflection and strain plots should

match for each load case. However, throughout all the load cases, the deflectometer measuring the deflection at B2 appears to be measuring lower deflections than expected. It should also be noted that the deflectometer measuring the deflection at B5 appeared to be measuring lower deflections than expected for the first two load cases, and during the third run of load case two, it fell off the bridge and had to be reattached. For the duration of the testing day, the deflectometer measuring the deflection on B5 gave results more in accordance with the expected values.

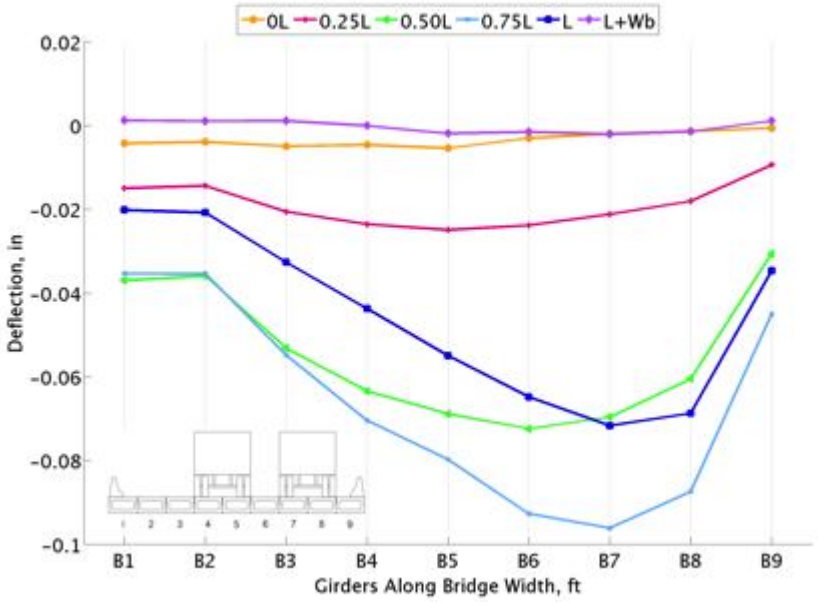

Figure 94. Load 6 run 1 deflection

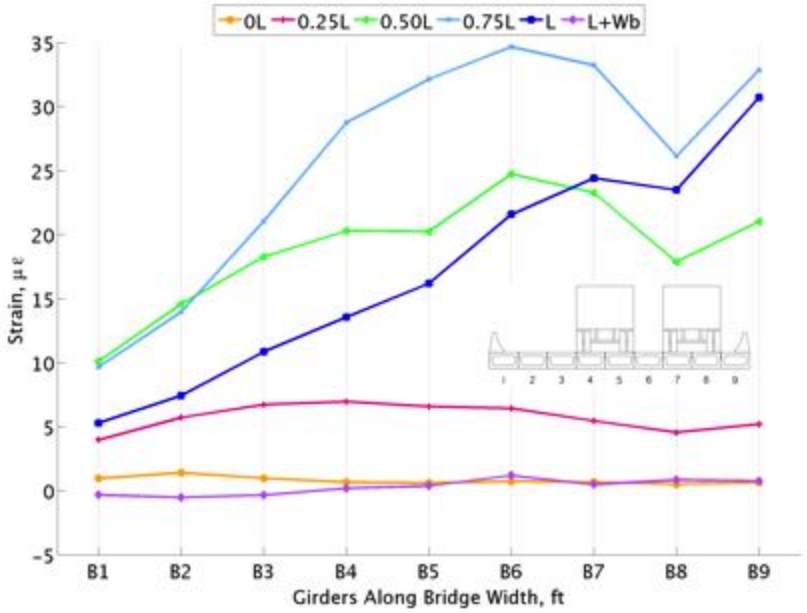

Figure 95. Load 6 run 1 strain

Linear Variable Differential Transformers

The horizontal and vertical relative displacements of adjacent box beam members were measured for each of the three quasi-static runs of the six load cases. The results are presented in Figure 96 through Figure 99. Load case 1 and load case 4 are presented as they are the same load case just mirrored to the opposite side of the bridge, so the results should be the same values just mirrored for both load cases. It should be noted that the LVDTs were calibrated at every 0.01 in. to a maximum range of 0.15 in., while the maximum relative displacement measured was 0.0037 in.

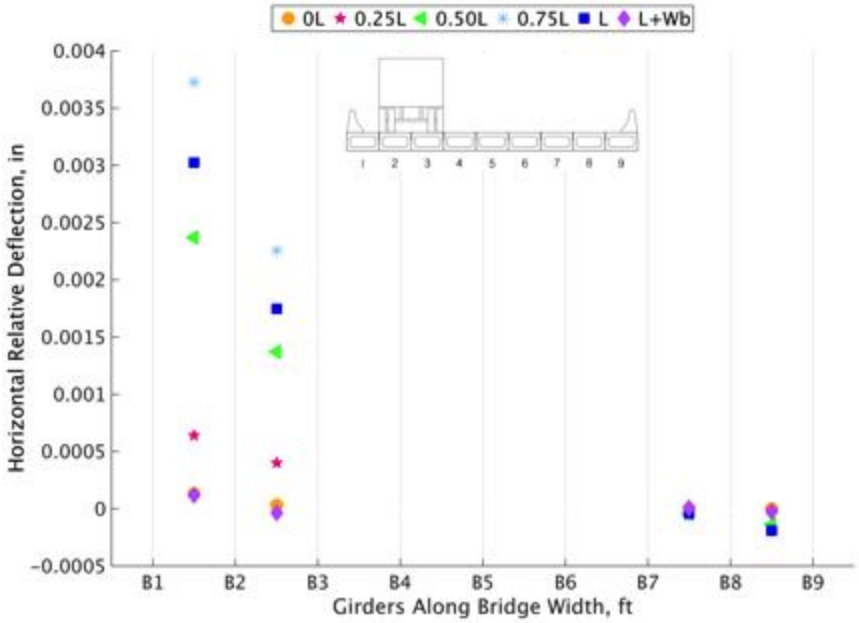

Figure 96. Load 1 run 3 relative horizontal deflection

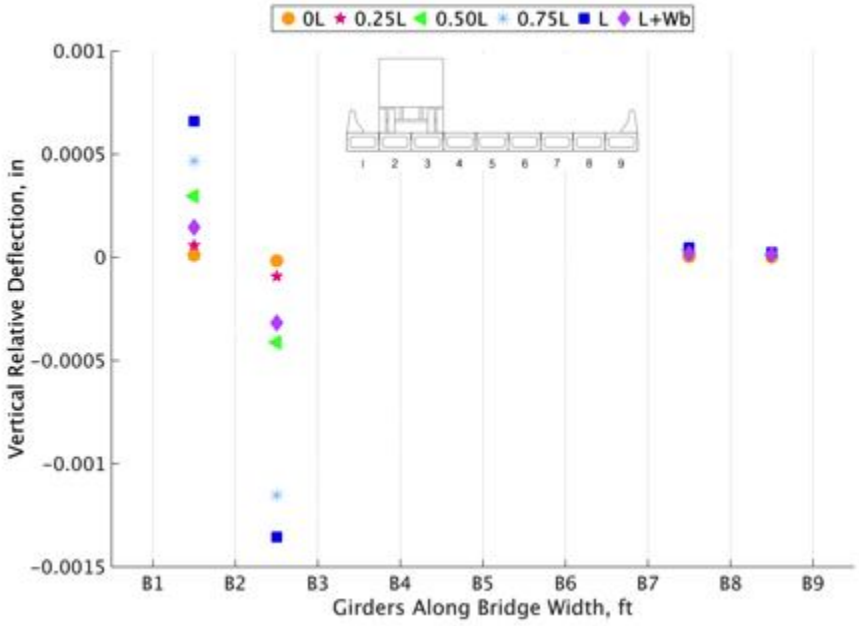

Figure 97. Load 1 run 1 relative vertical deflection

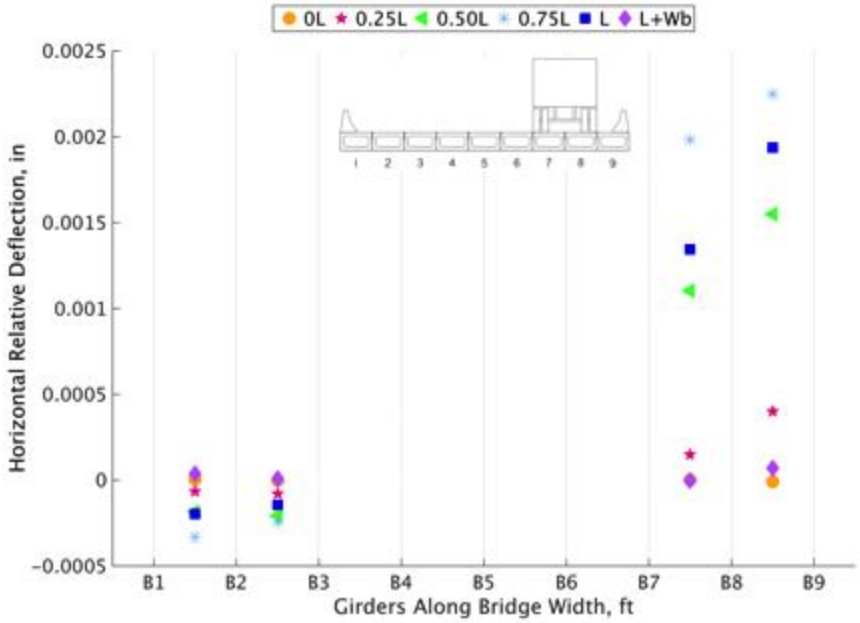

Figure 98. Load 4 run 2 relative horizontal deflection

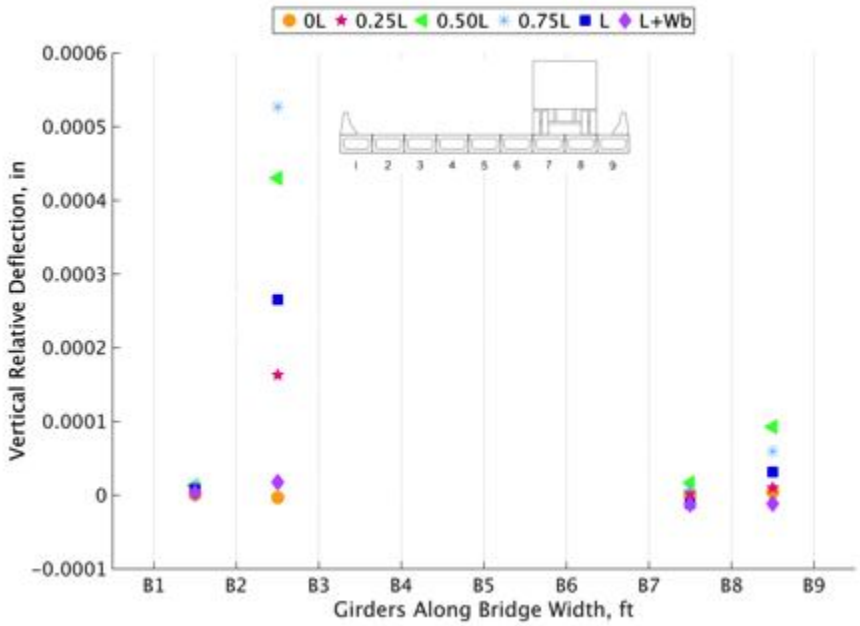

Figure 99. Load 4 run 2 relative vertical deflection

As observed, the relative horizontal deflections for the two load cases are mirrored as expected; the joints directly under the truck load had higher relative horizontal deflections than

those on the other side of the bridge. While the joints all deflected as expected, the downstream deteriorated joints deflected about 35 percent more than the upstream ones. This shows that the deterioration of the downstream joints is allowing for more relative horizontal deflections to occur. In contrast, the relative vertical deflections for the two load cases are not mirrored. In both load cases, the downstream deteriorated joints display larger relative vertical deflections, even when the truck load is applied on the other side of the bridge.

Halbe (2014) presents the results of live load tests of two similar adjacent box beam bridges. The Karr Valley Creek Bridge (KVCB) was a continuous two span two lane bridge in New York with a 24° skew and was constructed in 1990. The KVCB consisted of ten box girders connected with a partial depth grouted connection. The KVCB had a composite concrete topping that displayed reflective cracking at several locations which had been repaired using a sealant to prevent water from leaking through the joints. The second bridge tested was the Aden Road Bridge (ARB). The ARB consisted of three simply supported spans and was comprised of nine box girders connected with a partial depth grouted shear key and tied at the third span locations and was constructed in 1982. The ARB had a non-composite asphalt topping which displayed severe deterioration with reflective cracking and joints leaking along the entire length bridge. Several girders also showed signs of reinforcing steel corrosion with spalling and delamination of the concrete on the underside of the bridge. The maximum relative deflections Halbe collected are compared to the BBB results in Table 20. The BBB relative deflections are significantly smaller than the other two bridges Halbe tested.

Table 20. Maximum relative deflection comparison

	BBB	KVCB	ARB
Maximum Horizontal Relative Deflection, in.	0.0037	N/A	0.007
Maximum Vertical Relative Deflection, in.	0.0006	0.12	0.014

Girder Distribution Factors

Table 21 shows the values for the Buffalo Branch Bridge used to obtain the GDFs with AASHTO's method presented in the literature review.

Table 21. Values used in AASHTO method for Buffalo Branch Bridge

N_b	b, in.	L, ft.	I, in.^{4}	J, in.^{4}	d_e, ft.	θ, °
9	48	55	65941	141060	2.0	30

The GDFs calculated using AASHTO's method are shown in Table 22.

Table 22. GDFs calculated with AASHTO's method

	Interior Girders	Exterior Girders
One Lane Loaded	0.195	0.232
Two or More Lanes Loaded	0.327	0.366

The GDFs calculated from the results of the live load test and FEA model are shown in Table 23 and Table 24. To obtain these results, the GDFs for each beam were calculated for every run of each load case, discarding the outlier data from the instrumentation that was not working properly. The maximum values for each beam are presented as the GDFs.

Table 23. GDFs from live load test and FEA for one lane loaded

		B1	B2	B3	B4	B5	B6	B7	B8	B9
Live Load Test	Deflection	0.214	0.180	0.201	0.187	0.160	0.178	0.218	0.202	0.114
	Strain	0.145	0.222	0.193	0.170	0.132	0.189	0.195	0.164	0.207
FEA	Deflection	0.195	0.184	0.163	0.144	0.129	0.144	0.162	0.170	0.170
	Strain	0.199	0.204	0.173	0.150	0.127	0.157	0.177	0.190	0.175

Table 24. GDFs from live load test and FEA for two or more lanes loaded

		B1	B2	B3	B4	B5	B6	B7	B8	B9
Live Load Test	Deflection	0.257	0.223	0.283	0.285	0.273	0.301	0.310	0.283	0.151
	Strain	0.185	0.281	0.282	0.277	0.277	0.283	0.286	0.233	0.284
FEA	Deflection	0.273	0.276	0.272	0.261	0.247	0.257	0.257	0.247	0.235
	Strain	0.276	0.294	0.275	0.258	0.245	0.255	0.264	0.262	0.234

A comparison of the GDFs obtained using the three methods are shown in Figure 100 for one design lane loaded and in Figure 101 for two or more design lanes loaded. The maximum GDFs calculated from the live load test data and FEA model are presented in two groups, the maximum of the seven interior girders and the maximum of the two exterior girders. The plots of the data from the specific load cases that provided the maximum GDFs are shown in the appendix. Table 25 outlines which load cases and runs were used to calculate the GDFs presented in Figure 100 and Figure 101.

Table 25. Figures used to calculate GDFs

	One Lane Loaded		Two or More Lanes Loaded	
	Interior	**Exterior**	**Interior**	**Exterior**
Live Load Test Deflection	Figure 234 - Run 2	Figure 226 - Run 1	Figure 236 - Run 1	Figure 230 - Run 3
Live Load Test Strain	Figure 227 - Run 1	Figure 233 - Run 1	Figure 237 - Run 1	Figure 237 - Run 1
FEA Deflection	Figure 226	Figure 226	Figure 230	Figure 230
FEA Strain	Figure 227	Figure 227	Figure 231	Figure 231

The GDFs obtained from the AASHTO method, live load test, and FEA model are all similar. The AASHTO method over predicts the GDFs leading to a conservative design for all cases except the interior girders with one truck load.

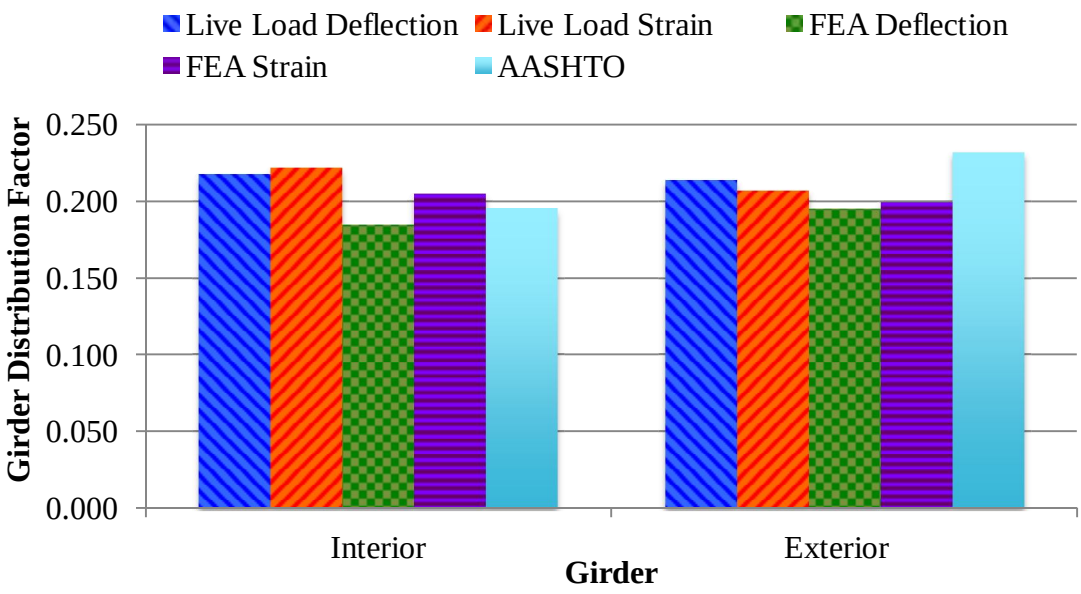

Figure 100. GDF comparison for one design lane loaded

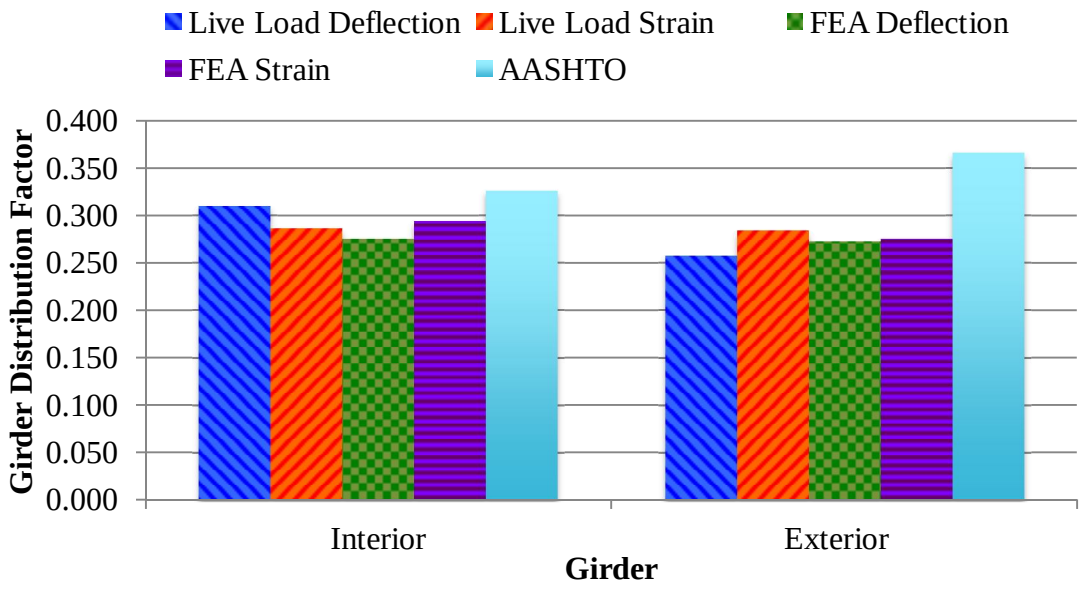

Figure 101. GDF comparison for two or more design lanes loaded

A comparison of the GDFs calculated for the BBB to the ones in Halbe (2014) for the KVCB and ARB are presented in Figure 102 and Figure 103. The GDFs calculated from the live load deflections are not presented for the ARB bridge because the deflectometers malfunctioned.

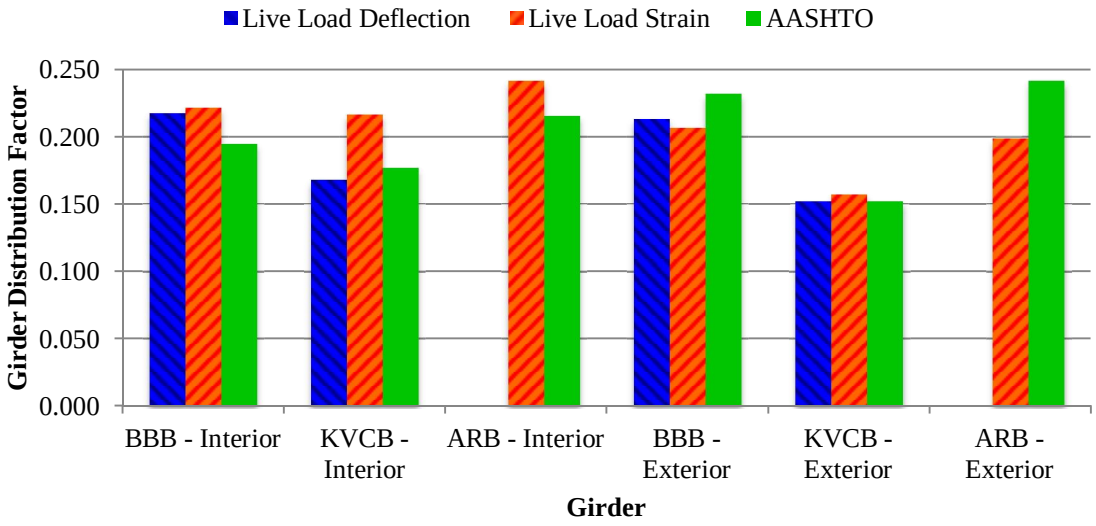

Figure 102. Bridge GDF comparison for one design lane loaded

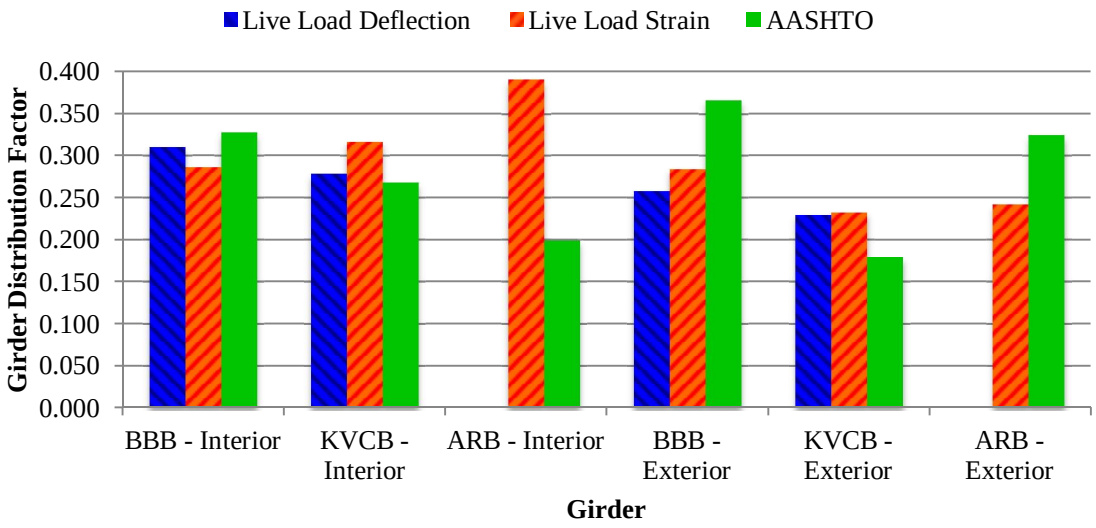

Figure 103. Bridge GDF comparison for two or more design lanes loaded

The GDFs obtained from the live load test compared to the AASHTO method were similar for the BBB and the KVCB showing that the two bridges were able to transfer load across the joints as designed. However, the GDFs calculated from the strains in the live load test for the ARB shows that the joints were deteriorated and not able to transfer the load as designed.

These measured GDFs correspond to the visual appearance of the bridges. The BBB and the KVCB both had relative cracking, but the joints were not completely failed and were still able to transfer loads. While the ARB had reflective cracking as well as severe damage to the asphalt deck and spalling and delamination on the underside of the concrete girders which is consistent with the measured GDFs being larger than the AASHTO calculated GDFs. This implies that the reflective cracking does not necessarily mean that the transverse load distribution is damaged to the point of adversely affecting the capacity of the bridge, but that the completely failed shear keys and corrosion of the reinforcing steel does.

FEA and Live Load Comparison

The results of the FEA and the live load test are presented in Figure 105 and Figure 106 by plotting the maximum deflections and strains measured for each of the three runs and the FEA model for each load case. The FEA model was an accurate representation for the deflections and strains experienced by the bridge due to the truck loading. Hand calculations were completed to predict the maximum strain. The loading, shear diagram, and moment diagrams were used to obtain the maximum moment that one truck would cause and are shown in Figure 104. The axle orientation used represented the trucks used in the live load tests and the location of the truck was used because it provided the maximum longitudinal strain along the bridge.

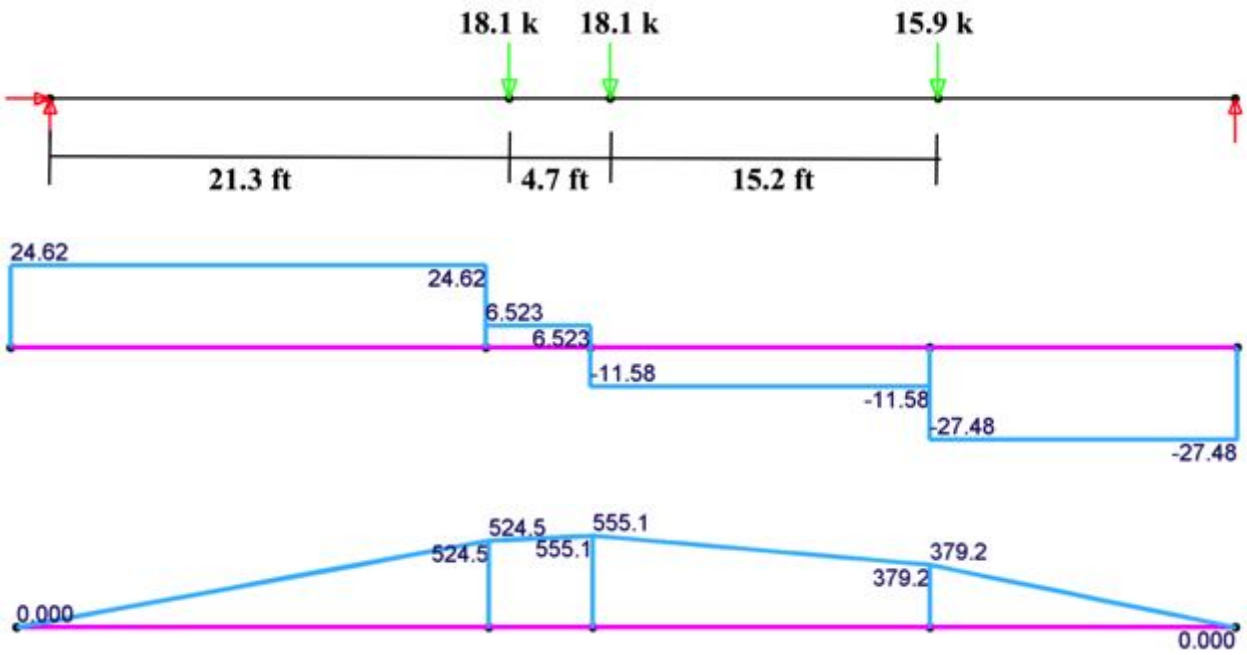

Figure 104. Loading, shear diagram, and moment diagram

Once the maximum moment was calculated, it was multipled by the AASHTO GDFs for interior and exterior girders presented in the previous section and presented in Table 26. These moments representing the moment experienced by each interior and exterior girder were then used to calculate the maximum stress using:

$$\sigma = \frac{M\,y}{I} \qquad \text{(Eq. 15)}$$

where, σ was the stress in ksi, y was the distance from the bottom of the precast concrete beam to the neutral axis in in., and I was the moment of inertia in in.^{4}. The maximum strain for the beam was then calculated using Hooke's law:

$$\varepsilon = \frac{\sigma}{E} \qquad \text{(Eq. 16)}$$

where ε was the strain in $\mu\varepsilon$ and E was the modulus of elasticity for the precast concrete beam in ksi. Table 26 presents the values used.

Table 26. Values used in hand calculations of strain at midspan

I, in.^{4}	E, ksi	y, in.	Mmax, k*ft	AASHTO GDF with One Lane Loaded for Interior Girders	AASHTO GDF with One Lane Loaded for Exterior Girders
65941	4100	13.37	555	0.195	0.232

Table 27 presents the predicted maximum strains for the interior and exterior girders determined by using the interior and exterior GDFs calculated by AASHTO method for a single truck load.

Table 27. Maximum strain predictions

Interior Girder Strain, με	Exterior Girder Strain, με
64	76

The maximum strains predicted using the hand calculations were larger than the actual strains measured during the live load test and FEA model for the interior and exterior girders.

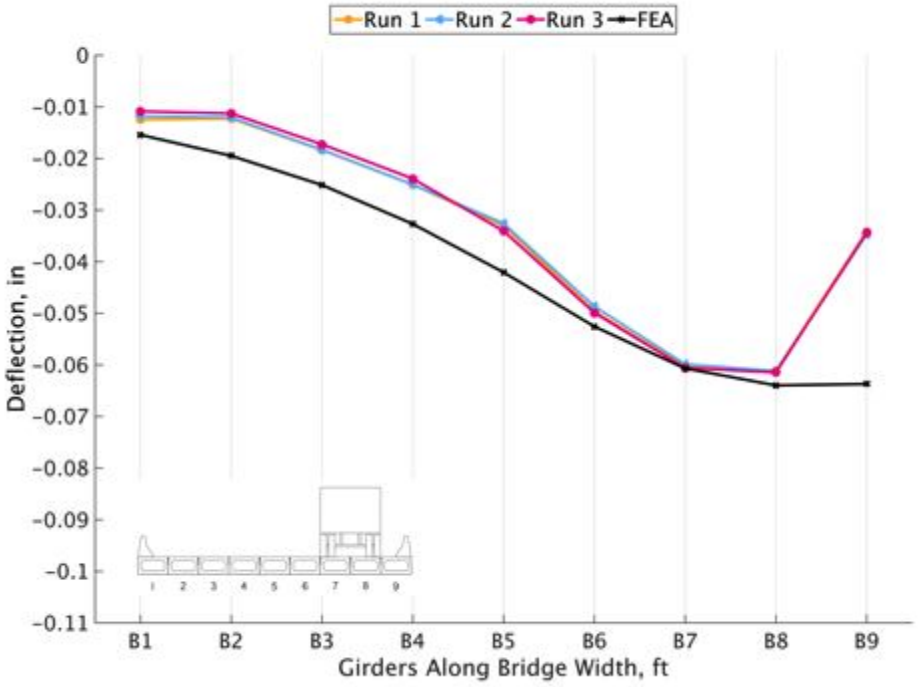

Figure 105. Load 4 deflection comparison

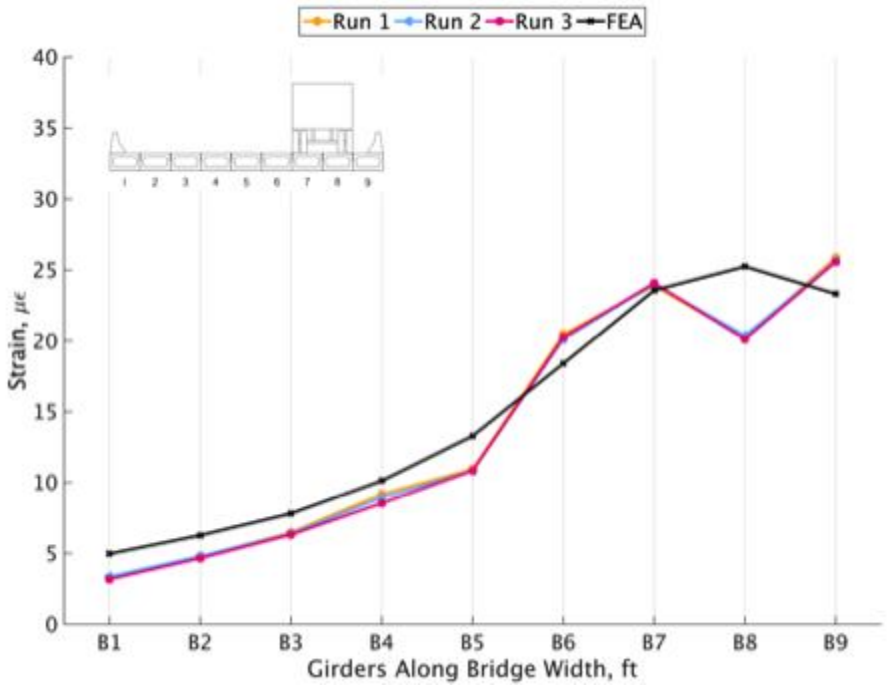

Figure 106. Load 4 strain comparison

BUFFALO BRANCH BRIDGE REHABILITATION

Proposed Rehabilitation Plan

The proposed rehabilitation plan for the Buffalo Branch Bridge is shown in Figure 107.

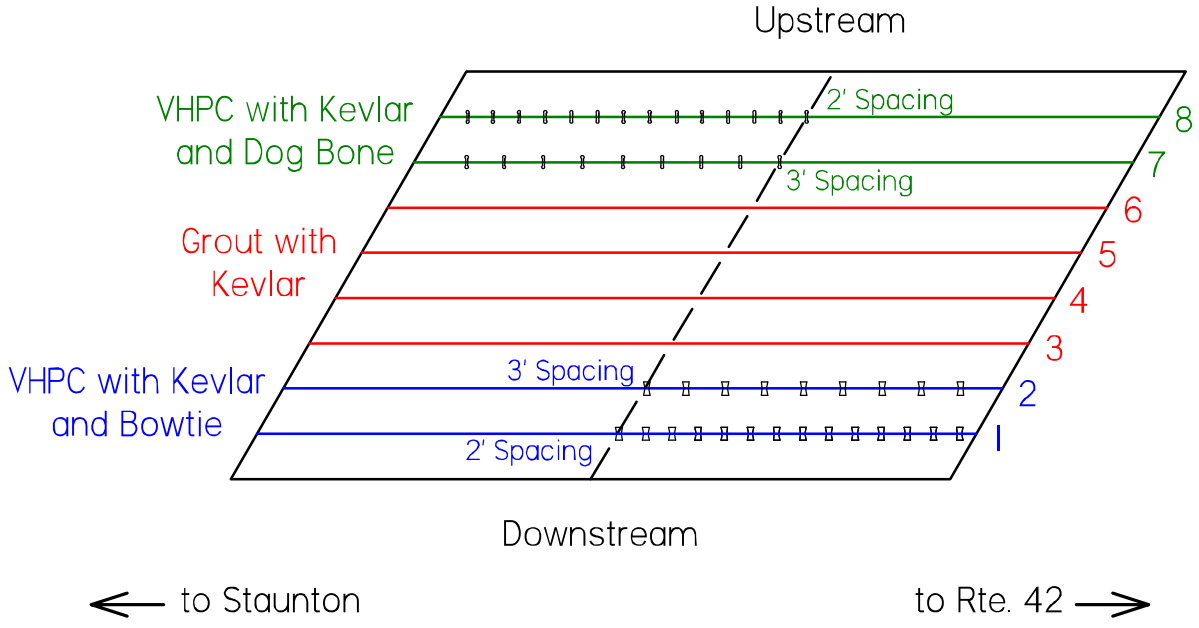

Figure 107. Buffalo Branch Bridge rehabilitation plan

The plan was for all of the joints to be completely cleaned out. The four interior joints were to be replaced with fresh grout and a Kevlar and epoxy topping. The four exterior joints were to be replaced with VHPC and the addition of geometric cutouts at the obtuse skew corners.

Figure 108 shows the dimensions for the dog bone cutouts to be used in the upstream joints. Figure 109 shows the dimensions for the bowtie cutouts to be used in the downstream joints.

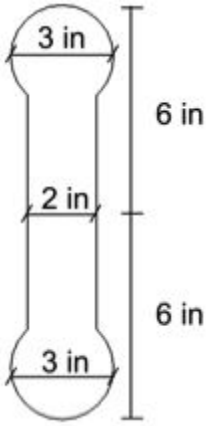

Figure 108. Dog bone geometry

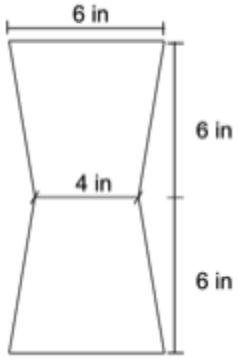

Figure 109. Bowtie geometry

The VHPC required for each joint was calculated and is presented in Table 28. Each batch was for 1.5 cubic ft. of VHPC.

Table 28. VHPC required for joint rehabilitation

Joint	Location	VHPC required, ft^3	Batches required
1	Downstream exterior	8.1	6
2	Downstream interior	7.1	6
7	Upstream interior	6.1	5
8	Upstream exterior	6.6	5

To assist the contractor in weighing out the materials beforehand, the mix design for each batch was provided and is shown in Table 29.

Table 29. Mix design for a 1.5 cu. ft. batch of VHPC-Small

Material	Details	Company	Amount (lbs)
Fly Ash	Class F	Titan America	13.3
Silica Fume	EMS-965	Silica Fume Association	13.3
½ in. Fibers	Dramix OL 13/.20	Bekaert	14.5
Cement	Type I/II		62.3
Sand	Wytheville Sand (Passing the No. 8 Sieve)		74.7
1/8 in. Aggregate	Epoxy Overlay (EP5 - Modified Sand)	Lanford Brothers	36.7
Water			17.7
High Range Water Reducer	Sika - Visco Crete 2100		650 mL
Retarder	Sika - Plastiment Water Reducing Retarder		VT will provide

To ensure placing the VHPC went smoothly, the following mixing procedure presented in Table 30 was provided to the contractor. It was recommended that the contractor acquire two 9 cu. ft. capacity mortar mixers two wheelbarrows and weigh everything beforehand.

Table 30. VHPC mixing procedure for Buffalo Branch Bridge rehabilitation

Start Time (min)	Mixer 1		Mixer 2	
	Task	Duration (min)	Task	Duration (min)
0	**Mixer 1 – Batch 1** • Wet mixer and pour out excess water • Add sand, 1/8 in. aggregate, and approximately half of the water • Let mix	5		
5	• Add cement, fly ash, silica fume, and remaining water • Let mix	5		
10	• Add HRWR • Let mix • (look at consistency and decide if more HRWR is desired)	3	**Mixer 2 – Batch 1** • Wet mixer and pour out excess water • Add sand, 1/8 in. aggregate, and approximately half of the water • Let mix	5
13	• Add fibers • Let mix	2		
15	• Remove VHPC from mixer to place	5	• Add cement, fly ash, silica fume, and remaining water • Let mix	5
18			• Add HRWR • Let mix • (look at consistency and decide	3

			if more HRWR is desired)	
20	**Mixer 1 – Batch 2** • Wet mixer and pour out excess water • Add sand, 1/8 in. aggregate, and approximately half of the water • Let mix	5	• Add fibers • Let mix	2
25	• Add cement, fly ash, silica fume, and remaining water • Let mix	5	• Remove VHPC from mixer to place	5
30	• Add HRWR • Let mix • (look at consistency and decide if more HRWR is desired)	3	**Mixer 2 – Batch 2** • Wet mixer and pour out excess water • Add sand, 1/8 in. aggregate, and approximately half of the water • Let mix	5
33	• Add fibers • Let mix	2		
35	• Remove VHPC from mixer to place	5	• Add cement, fly ash, silica fume, and remaining water • Let mix	5
40	**Mixer 1 – Batch 3** • Wet mixer and pour out excess water • Add sand, 1/8 in. aggregate, and approximately half of the water • Let mix	5	• Add HRWR • Let mix • (look at consistency and decide if more HRWR is desired)	3
43			• Add fibers • Let mix	2
45	• Add cement, fly ash, silica fume, and remaining water • Let mix	5	• Remove VHPC from mixer to place	5
50	• Add HRWR • Let mix • (look at consistency and decide if more HRWR is desired)	3	**Mixer 2 – Batch 3** • Wet mixer and pour out excess water • Add sand, 1/8 in. aggregate, and approximately half of the water • Let mix	5
53	• Add fibers • Let mix	2		
55	• Remove VHPC from mixer to place	5	• Add cement, fly ash, silica fume, and remaining water • Let mix	5
60			• Add HRWR • Let mix • (look at consistency and decide if more HRWR is desired)	3
63			• Add fibers • Let mix	2
65			• Remove VHPC from mixer to place	5

Rehabilitation Performed

Rehabilitation Process

A construction crew, consisting of two traffic flagmen, a supervisor, and six other workers performed the rehabilitation process. Several VDOT and Virginia Tech employees were also present.

Preparing the Joints

Every step of the rehabilitation process was completed in two stages, the downstream half followed by the upstream half, so that traffic could continue to use one lane over the bridge. The rehabilitation process began with removing the asphalt topping to expose the adjacent box beams and the joints. The next two steps were completed in opposite sequence for the upstream and downstream halves of the bridge. For the downstream half, the joints were first cleared and then the reinforcing steel was located, whereas for the upstream half, the reinforcing steel was located and then the joints were cleared. The deteriorated grout that was cleared from the joints is shown in Figure 110. In the downstream exterior joints, the deteriorated grout closely resembled sand and could be scooped out barehanded without any effort. However, for the four interior joints, the grout was still securely bonded to the adjacent box beams and difficult to remove.

Figure 110. Deteriorated grout

While the shear keys were 12 in. deep, typically only 4 in. of grout was removed and is shown in Figure 111. On the exterior joints where the grout was clearly deteriorated four in. into the shear key, the top four in. of the shear key was still the only grout to be removed because that was as deep as the jackhammer could reach into the shear key. This is shown in Figure 112.

Figure 111. Typical depth of cleared joints

Figure 112. Removing grout from joints

Due to the varying width of the upstream joints shown in Figure 113 and the jackhammer being able to fit deeper, there were sections where the grout was cleared out up to 6 in. deep.

Figure 113. Varying width of joints

Locating the reinforcing steel began with measuring out where the dog bones would be cut. A dog bone was placed at midspan and the spacing was measured from there to the end of

the bridge at 2, 3, or 4 ft and is indicated by a red line in Figure 114. Next, a pachometer was used to locate the reinforcing steel on both sides of the dog bone location and is indicated by a black line in Figure 115.

Figure 114. Reinforcing steel locations

Figure 115. Locating steel with pachometer

After the initial spacing of the dog bones was positioned and the reinforcing steel marked, the final locations of the dog bones were marked by saw cutting into the adjacent box means shown in Figure 116.

Figure 116. Dog bone locations and surrounding reinforcing steel marked

Once the location of the dog bones were cut and the joints cleared, the dog bones were cut and are shown in Figure 117. Cutting the dog bones took approximately 20 minutes each and began by cutting both ends with a 3 in. core drill. Next, the inside was cut with a saw blade and the whole dog bone was chiseled out.

Figure 117. Dog bones

One bowtie, shown in Figure 118, was cut at midspan of joint 7 to determine how difficult it was to cut without cutting through the reinforcing steel. Cutting the bowtie also took

approximately 20 minutes. To avoid cutting completely through the reinforcing steel in the precast concrete member, the ends of the bowtie were chiseled out

Figure 118. Bowtie

Figure 119 shows joint 1 with dog bones spaced at 2 ft and joint 2 with dog bones spaced at 3 ft as specified in the proposed rehabilitation plan except using dog bones instead of bowties. Figure 120 shows joint 7 with only a bowtie at midspan and joint 8 with dog bones spaced at 4 ft.

Figure 119. Joints 1 and 2

Figure 120. Joints 7 and 8

The joints were sand blasted and sprayed with a hose to create a SSD condition immediately before placing the VHPC, shown in Figure 121.

Figure 121. SSD joints

Mixing

On the first day of placing, the first batch of VHPC began mixing at 9:30 am. The goal was to start mixing the VHPC before the temperature increased so that the VHPC would remain workable longer. Before mixing, the contractor weighed out the required amount of each material in buckets and aligned them on a tarp with a chart outlining the materials and batch number, shown in Figure 122. This allowed for the mixing process to start smoothly.

Figure 122. Materials pre-weighed

The mixing and placing procedure followed what was specified in the proposed rehabilitation plan except for only using one mixer. Only one mixer was used because the joints were only cleared 4 in. instead of all 12 in. causing not as much VHPC to be required which allowed for the joints to still be placed quickly with just one mixer. Figure 123 shows the pre-weighed materials being added to the mixer and the mixed VHPC being dumped into the wheelbarrow.

Figure 123. Mixing

After the VHPC was adequately mixed, the inverted slump test was performed to measure the spread. The original slump test from the first batch on day one of placing is shown in Figure 124. With a spread of 12 in., the VHPC was too stiff to place. It was returned to the mixer and more HRWR was added. Retarder was also added to improve the workability of the VHPC.

Figure 124. Slump test, VHPC too stiff

On the contrary, the original slump test from the first batch on day two of placing had too large of a spread at 27 in.. Figure 125 shows evidence of bleeding from the water sheen on the surface and the mortar halo surrounding the VHPC.

Figure 125. Slump test, VHPC too flowable

After noticing the bleeding in the first batch on day two, the materials were examined more closely. It rained at night between the first and second days of placing the joints and the

sand was not properly covered. Instead of using dry sand, the sand was wet enough to hold the shape of a ball as shown in Figure 126.

Figure 126. Wet sand

To measure the moisture content of the sand, a 4 in. x 8 in. cylinder sample of the wet sand was taken and immediately capped so that the moisture would not escape. The weight of the wet sand and metal bowl was 2410 g.. The bowl containing the sand sample was placed in the oven to dry and the dry weight of the bowl and sand was 2270 g.. The moisture content was then calculated to be 6.0 %. Figure 127 shows a VHPC batch with a slump test of 18 in. to illustrate what target spread looked like.

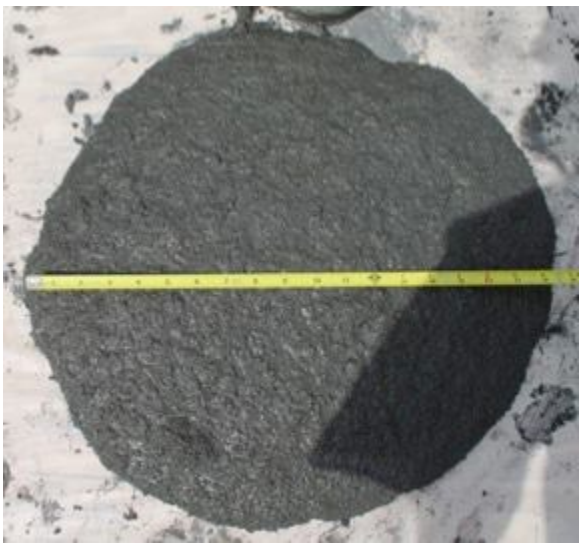

Figure 127. Slump test, VHPC target spread

The amount of HRWR and retarder that were added to each batch are presented in Table 31. The wet sand reduced the amount of HRWR and retarder that was required to achieve the target spread. The decision to not add retarder to the batches mixed on day two was also influenced by the short curing time expected before traffic was directed back on the rehabilitated joints.

Table 31. Actual HRWR and retarder doses

	Day 1					Day 2			
	Batch 1	Batch 2	Batch 3	Batch 4	Batch 5	Batch 1	Batch 2	Batch 3	Batch 4
HRWR (oz/cwt)	32	35	35	36	35	27	26	23	26
Retarder (oz/cwt)	1	1	1	1	1	0	0	0	0

Placing

After the workability of the VHPC was determined to be adequate, the wheelbarrow was filled and dumped at the joint, shown in Figure 128.

Figure 128. Dumping VHPC from wheelbarrow

Figure 129 shows the piles of dumped VHPC being spread along the joint using shovels and scoops.

Figure 129. Spreading VHPC with shovels and scoops

Because the contractor did not have chairs to sit the reinforcing steel on, approximately 1 in. of the VHPC was placed in the dog bone and then the reinforcing steel was set on top of it, shown in Figure 130 and Figure 131.

Figure 130. Placing reinforcing steel in dog bones

Figure 131. Reinforcing steel in dog bone

To prevent cold joints from forming where two batches of the VHPC met, it was rodded throughout the section where the two batches met, shown in Figure 132.

Figure 132. Rodding VHPC where batches meet

One area of concern that arose while placing was the contractor's interpretation of a SSD surface. The joints had a thin layer of water in the bottom of them when the VHPC was placed. The VHPC was placed starting at the higher elevation end and moving towards the lower

elevation end. This caused the layer of water to be pushed along the joint until it pooled at the end. Figure 133 shows the full four in. depth of the joint filled with the pooled water.

Figure 133. Water building up at the end of joint

Curing

The VHPC began to cure very quickly, as evident in Figure 134 and Figure 135 by the skin forming on the surface of the dog bone and bowtie before the VHPC was placed in the entire joint and covered with wet burlap.

Figure 134. Curing dog bone

Figure 135. Curing bowtie

Once the VHPC was placed in entire length of the joint, the joint was covered with wet burlap to moist cure the joints and improve the rate of curing. This is shown in Figure 136.

Figure 136. Wet burlap covered joints

On day one the downstream joints were completely placed by 12:00 pm and on day two the upstream joints were completely placed by 1:00 pm. At 5:00 pm each day, the traffic lane traveling over the newly placed joints was opened back up. Therefore, the VHPC was allowed to moist cure for five hours on day one and four hours on day two before traffic was directed back on it. Figure 137 and Figure 138 show the downstream joints that were placed on day one after being driven on from 5:00 pm to the following morning. The traffic does not appear to have affected the joints.

Figure 137. Cured joints

Figure 138. Cured dog bones

Material Properties

To measure the compressive strength, 2 in. cubes were made for each batch mixed except for the final batch mixed on day two and are shown in Figure 139. To measure the splitting tensile strength, six 3 in. x 6 in. cylinders were made from the final batch mixed on day two.

Figure 139. VHPC cubes

Figure 140 and Figure 141 present the compressive and splitting tensile strengths of VHPC-Small used in the Buffalo Branch Bridge rehabilitation compared to the average strength of the VHPC-Small. The compressive strengths were obtained by testing one cube from each batch at each age and the splitting tensile strengths were obtained by testing two of the cylinders at each age. Ideally, more samples would have been taken. However, due to a shortage of molds and material being placed, these were the only samples taken.

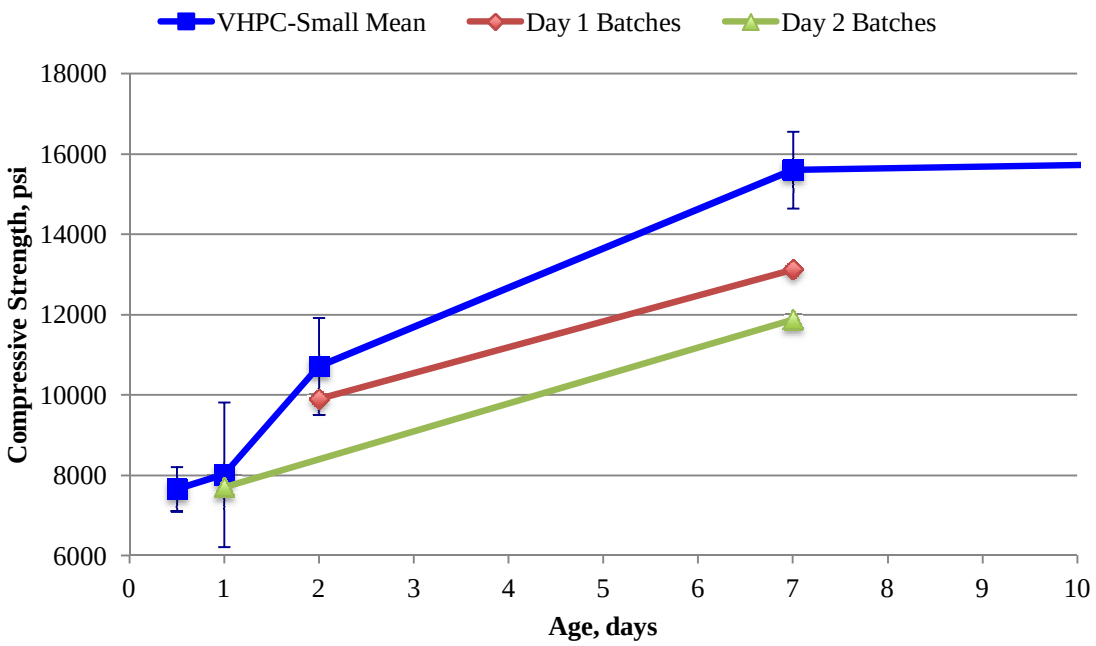

Figure 140. Bridge rehabilitation VHPC compressive strength

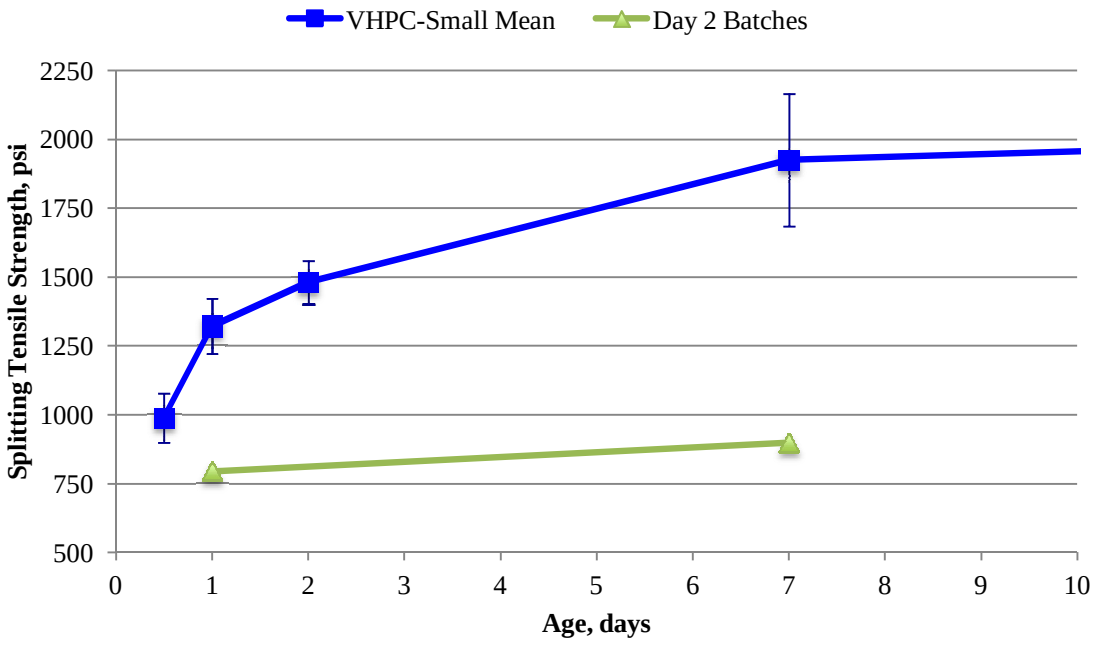

Figure 141. Bridge rehabilitation VHPC splitting tensile strength

CONCLUSIONS AND RECOMMENDATIONS

Project Summary

The objective of this research project was to design a rehabilitation plan for an adjacent box beam bridge with deteriorated joints using VHPC. First, a material characterization of both VHPC mixes was completed to determine if it was the best suited material to replace the grout used to connect the precast members in adjacent box beam bridges. Second, tests were completed to determine if non-contact lap splices performed comparably to contact lap splices in adjacent precast member bridges. Third, a FEA of the Buffalo Branch Bridge was completed to predict how the bridge would respond to the live load test if the grouted joints were not deteriorated and still fully bonded. Fourth, a live load test was performed on the Buffalo Branch Bridge to determine the actual condition of the joints and the initial performance of the bridge before the rehabilitation. Finally, the Buffalo Branch Bridge rehabilitation was designed and implemented.

Conclusions from Material Tests

- Grout was easier to mix and place than all of the concrete mixtures tested.
- The VHPC and UHPC gain strength faster and achieve higher strengths than the grout and A4 deck concrete.
- Due to the steel fibers present, the VHPC and UHPC have strong splitting tensile strengths and post cracking behavior.
- The VHPC bonded to 5 in. of reinforcing steel after 12 hours of curing adequately enough for the reinforcing steel to rupture when a tensile force was applied before slipping out of the VHPC.
- After seven days, the bond between the VHPC and the precast concrete member was strong enough to fracture the aggregate in the precast concrete member. As opposed to

the grout, which developed too low of a bond strength to successfully remove the paste from the surface of the precast concrete member.

- With continual mixing, the VHPC remained workable for approximately 30 minutes. When mixing outside in the heat, the addition of retarder helped to extend the workability of the VHPC. While the VHPC is self-consolidating, it did not flow so much that it overflows out of the top of the lower end of joints with a slight slope.
- The durability measured by scaling of the surface of the VHPC and UHPC were immensely better than the durability of the grout and A4 deck concrete. To extend the lifespan of adjacent box beam bridges, the durability of the material used in the joints is essential.
- Even though the grout is marketed as non-shrinkage, the tests performed in this project indicated that it shrinks more than the other mixtures tested in this investigation.

Conclusions from Non-Contact Lap Splice Test

- The joints for both specimens, the contact lap splice and the non-contact lap splice, both began opening and cracking at similar actuator displacements. The cracks also propagated in similar patterns.
- At the same actuator load, the actuator displacement of the non-contact lap splice specimen was only slightly larger than the contact lap splice.
- For both specimens, the water ponding tests showed no signs of the joints leaking.
- A 6 in. non-contact lap splice is recommended to fully develop the reinforcing steel.

Conclusions from Finite Element Analysis

- The FEA results predict the midspan deflections and strains accurately compared to the live load test results.

Conclusions from Buffalo Branch Bridge Live Load Test

- Even though the two exterior downstream joints exhibited signs that they had deteriorated significantly, the load was still transferred across them.
- The relative displacement of the upstream and downstream joints at midspan were comparable and smaller than expected, also indicating that the bridge was still acting compositely.
- The GDFs measured for the BBB compared to the AASHTO GDFs indicate that the bridge was able to sufficiently transfer the load across the joints.

Conclusions from Buffalo Branch Bridge Rehabilitation

- Meeting with the contractor before the rehabilitation to validate that they understand the proposed plan and that it is constructible is a necessity.

Recommendations

- VDOT should use VHPC as an economical alternative to the proprietary UHPC.
- An additional live load test of the Buffalo Branch Bridge should be done after the rehabilitation has cured for at least a month.
- The AASHTO formulas for calculating the GDFs are accurate when only reflective cracking is present. However, when the shear keys are completely failed and spalling and delamination have occurred, the AASHTO method is no longer an accurate representation of the GDFs.
- Further research should be done to determine an easier way to cut the dog bone and bowtie shapes into the shear keys without damaging the existing reinforcing steel in the precast concrete members.
- A better method to mix and place the VHPC should be researched.

- Finding a way to increase the bond of the grout with the precast concrete members could also be an economical way to extend the lifespan of the adjacent box beam bridges.
- Further research should be conducted to determine the time to cracking of UHPC and VHPC mixes.

REFERENCES

Abaqus, I. (2013). "Abaqus/Standard User's Manual." Dassaults Systemes.

Akhnoukh, A. K. (2008). “Development of High Performance Precast/Prestressed Bridge Girders.” Ph.D. Dissertation, University of Nebraska.

American Association of State Highway Transportation Officials (AASHTO) (2012). AASHTO LRFD Bridge Design Specifications, Sixth Edition. Washington, D.C.

AASHTO Standard T 132-87 (2004). "Tensile Strength of Hydraulic Cement Mortars." American Association of State Highway and Transportation Officials, Washington, D.C.

American Institute of Steel Construction (2010). “Manual of Steel Construction.” 14th Edition. Chicago: AISC.

ASTM Standard C39/C39M, 2014a, “Standard Test Method for Compressive Strength of Cylindrical Concrete Specimens,” ASTM International, West Conshohocken, PA, 2014, DOI: 10.1520/C0039_C0039M, www.astm.org.

ASTM Standard C109/C109M, 2013, "Test Method for Compressive Strength of Hydraulic Cement Mortars (Using 2-in. or [50-mm] Cube Specimens)" ASTM International, West Conshohocken, PA, DOI: 10.1520/C0109_C0109M-13, www.astm.org

ASTM Standard C192/C192M, 2013, “Standard Practice for Making and Curing Concrete Test Specimens in the Laboratory,” ASTM International, West Conshohocken, PA, 2013, DOI: 10.1520/C0192_C0192M, www.astm.org.

ASTM Standard C469/C469M, 2014, “Standard Test Method for Static Modulus of Elasticity and Poisson's Ratio of Concrete in Compression,” ASTM International, West Conshohocken, PA, 2010, DOI: 10.1520/C0469_C0469M-14, www.astm.org.

ASTM Standard C490/C490M, 2011e1, "Standard Practice for Use of Apparatus for the Determination of Length Change of Hardened Cement Paste, Mortar, and Concrete" ASTM International, West Conshohocken, PA, DOI: 10.1520/C0490_C0490M-11E01, www.astm.org

ASTM Standard C496/C496M, 2011, "Test Method for Splitting Tensile Strength of Cylindrical Concrete Specimens" ASTM International, West Conshohocken, PA, DOI: 10.1520/C0496_C0496M-11, www.astm.org

ASTM Standard C666/C666M, 2003 (2008), "Standard Test Method for Resistance of Concrete to Rapid Freezing and Thawing" ASTM International, West Conshohocken, PA, 10.1520/C0666_C0666M-03R08, www.astm.org

ASTM Standard C1611/C1611M, 2014, "Standard Test Method for Slump Flow of Self-Consolidating Concrete" ASTM International, West Conshohocken, PA, DOI: 10.1520/C1611_C1611M-14, www.astm.org

ASTM Standard D7234, 2012, "Standard Test Method for Pull-Off Adhesion Strength of Coatings on Concrete Using Portable Pull-Off Adhesion Testers " ASTM International, West Conshohocken, PA, DOI: 10.1520/D7234-12, www.astm.org

Collins, W. N. (2010). "Live Load Testing and Analysis of the Southbound Span of U.S. Route 15 Over Interstate-66." M.S. Thesis, Virginia Tech.

Graybeal, Benjamin, (2014). "Design and Construction of Field-Cast UHPC Connections." Report No. FHWA-HRT-14-084, Federal Highway Administration, McLean, VA.

Halbe, K. R. (2014). "New Approach to Connection Details Between Adjacent Box Beam Bridges." Ph.D. Dissertation, Virginia Tech.

Halbe, K. R., Field, C. S., Cousins, T. E., and Roberts-Wollmann, C. L. (2014). "Splice Lengths for No. 4 and No. 6 Bars in UHPC and VHPC." Virginia Center for Transportation Innovation and Research. Charlottesville, VA.

Johnson, J. B. (2010). "Bond Strength of Corrosion Resistant Steel Reinforcement in Concrete." M.S. Thesis, Virginia Tech.

Joyce, P. C. (2014). "Development of Improved Connection Details for Voided Slab Bridges." M.S. Thesis, Virginia Tech.

Lane, D. S., Ozyildirim, C. (1999). "Combinations of Pozzolans and Ground, Granulated, Blast-Furnace Slag for Durable Hydraulic Cement Concrete." Report No. VTRC 00-R1. Virginia Transportation Research Council. Charlottesville, VA.

Scholz, D. P., Wallenfelsz, J. A., Lijeron, C., and Roberts-Wollmann, C. L. (2007). "Recommendations for the Connection Between Full-Depth Precast Bridge Deck Panel Systems and Precast I-Beams." Report No. FHWA/VTRC 07-CR17, Virginia Transportation Research Council. Charlottesville, VA.

Virginia Department of Transportation (VDOT) (2007). "Road and Bridge Specification." Richmond, VA.

VDOT (2015). "Manual of Structure and Bridge Division Volume V." Richmond, VA.

APPENDIX

FEA Midspan Vertical Deflection and Longitudinal Strain Plots

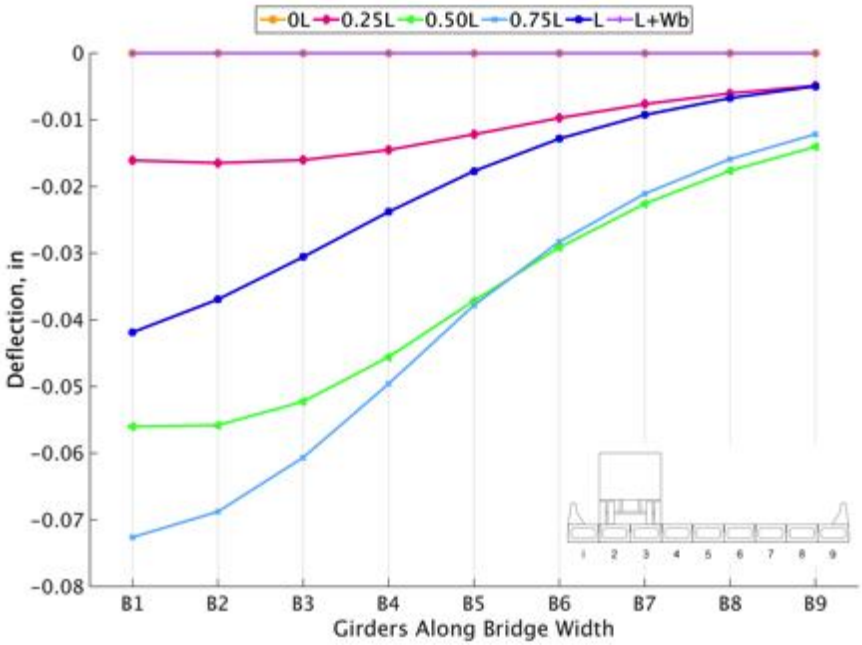

Figure 142. FEA Load case 1 deflection

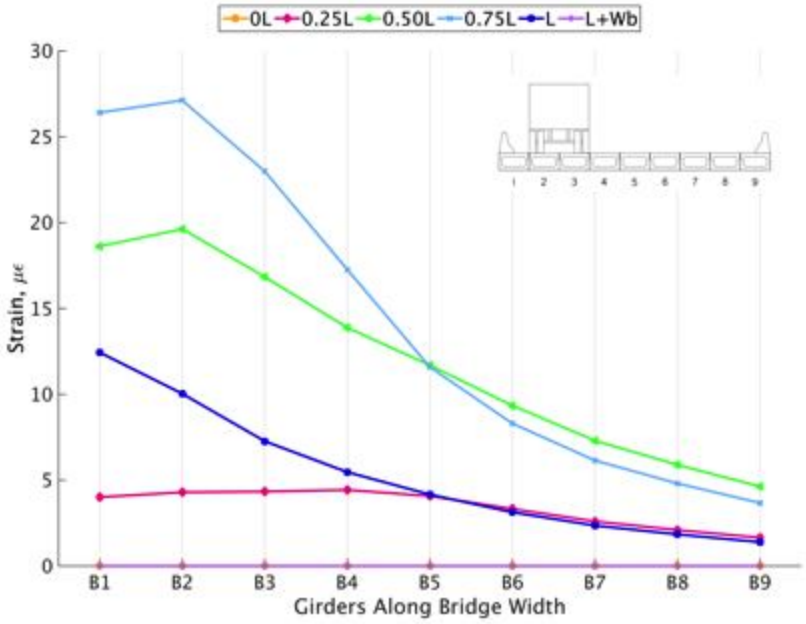

Figure 143. FEA Load case 1 strain

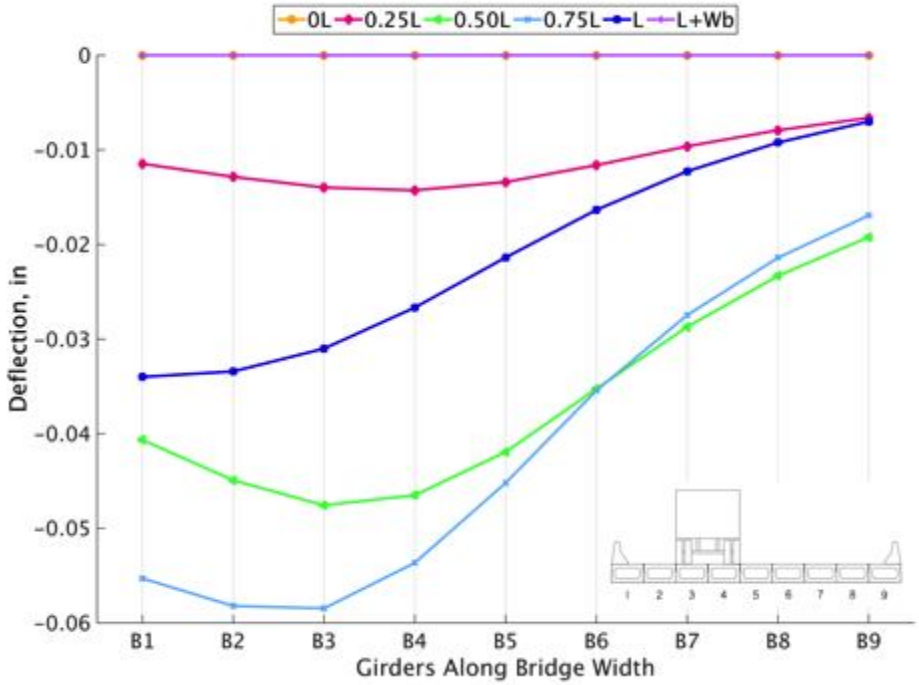

Figure 144. FEA Load case 2 deflection

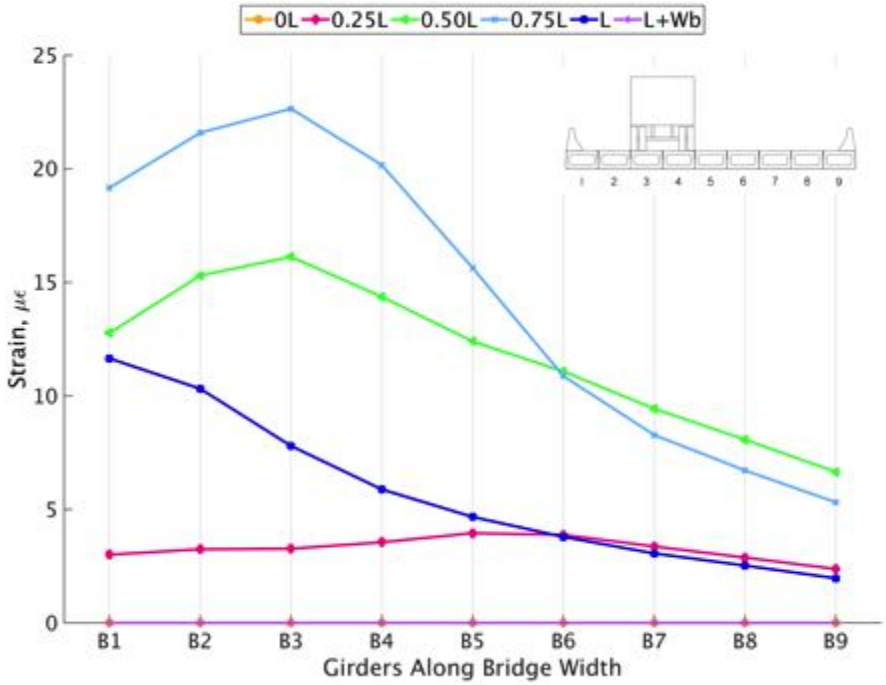

Figure 145. FEA Load case 2 strain

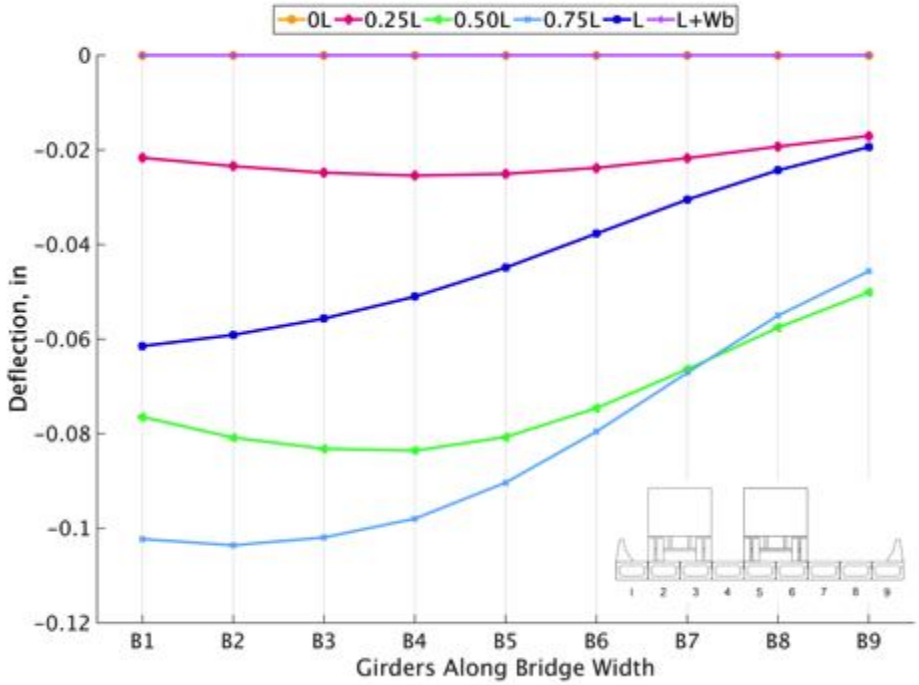

Figure 146. FEA Load case 3 deflection

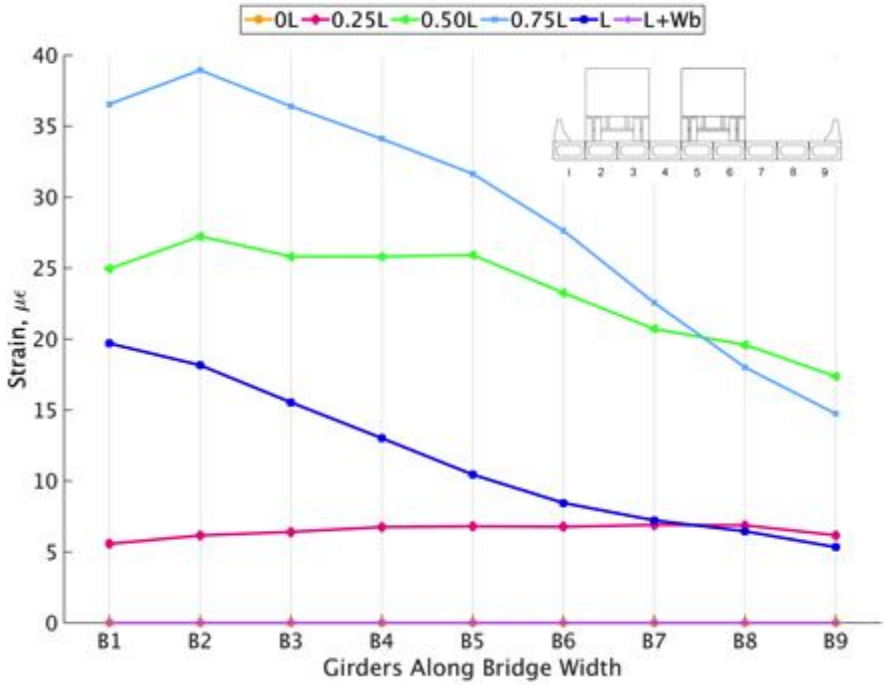

Figure 147. FEA Load case 3 strain

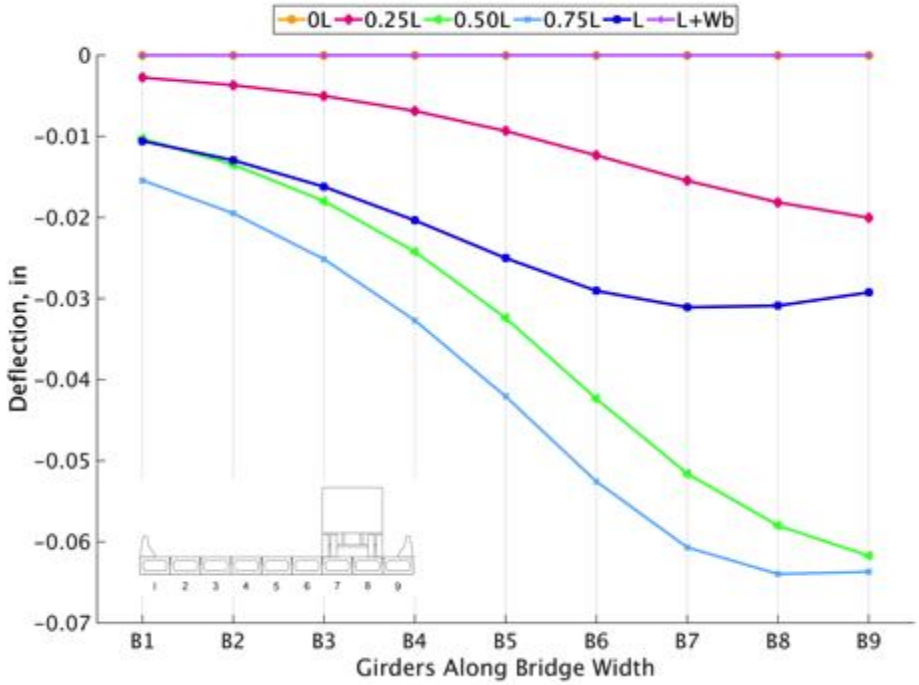

Figure 148. FEA Load case 4 deflection

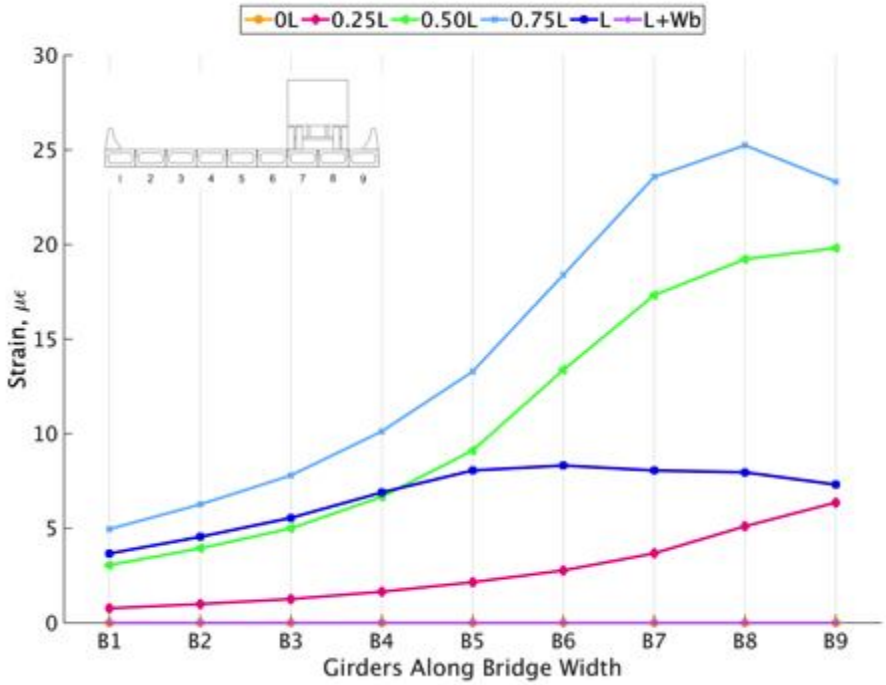

Figure 149. FEA Load case 4 strain

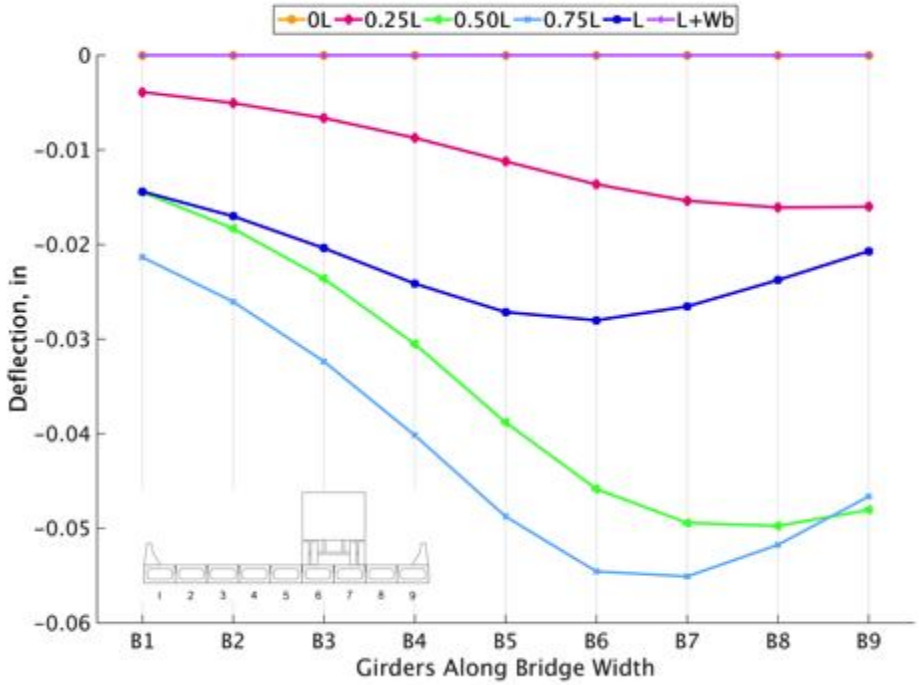

Figure 150. FEA Load case 5 deflection

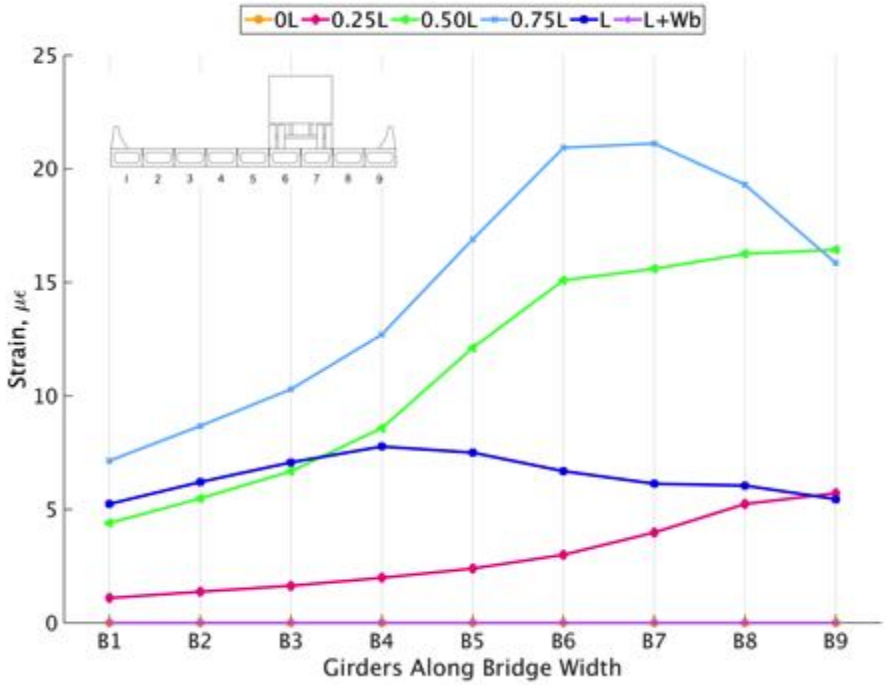

Figure 151. FEA Load case 5 strain

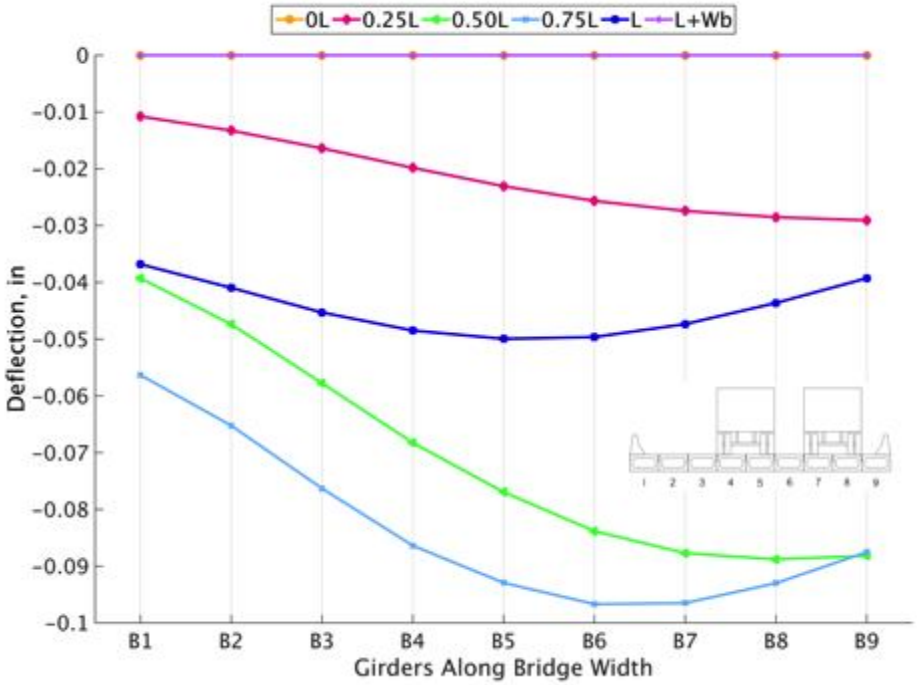

Figure 152. FEA Load case 6 deflection

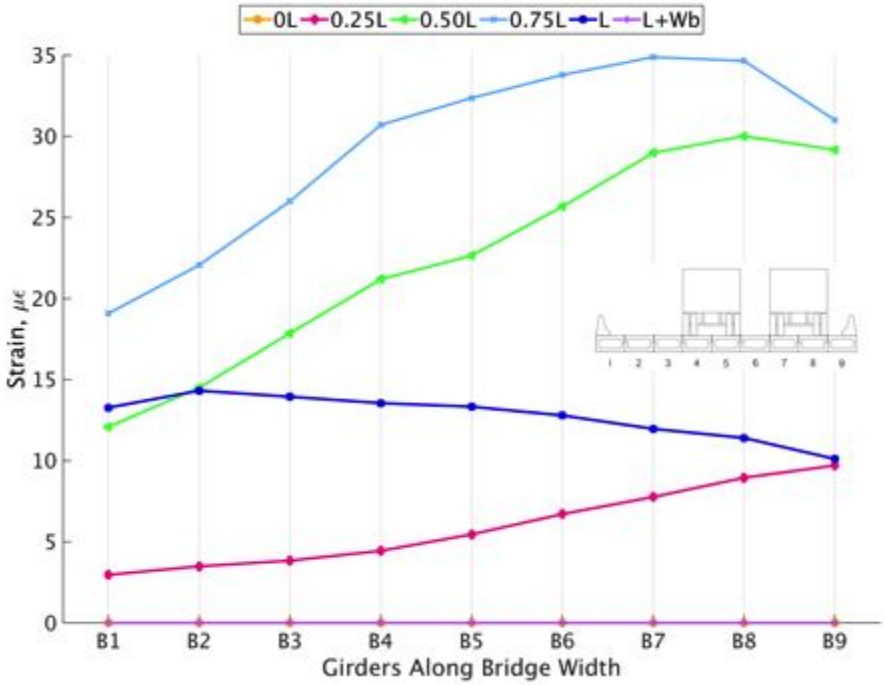

Figure 153. FEA Load case 6 strain

Live Load Test Midspan Vertical Deflection and Longitudinal Strain Plots

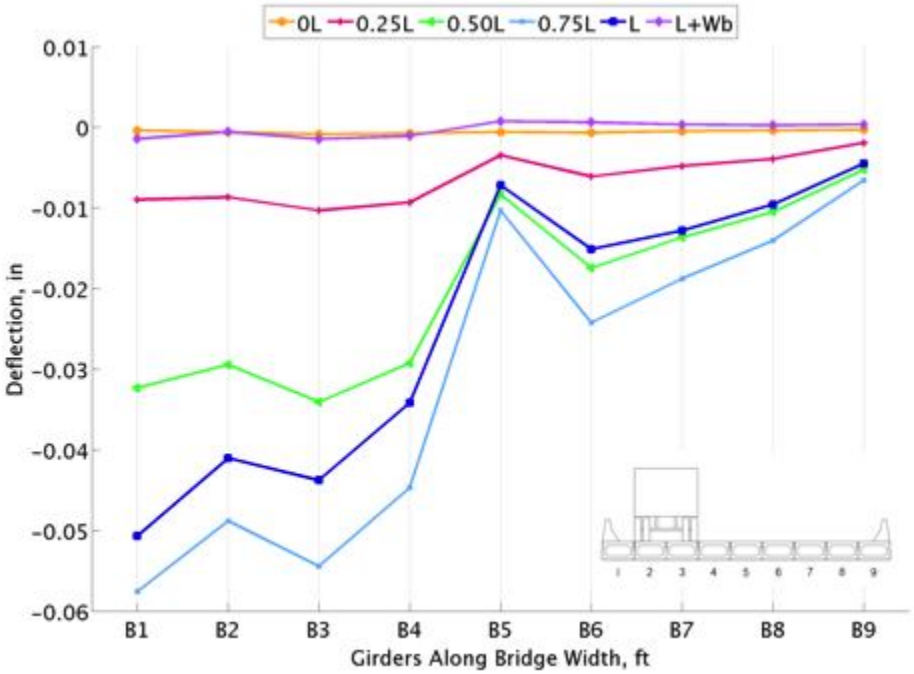

Figure 154. Load case 1 run 1 deflection

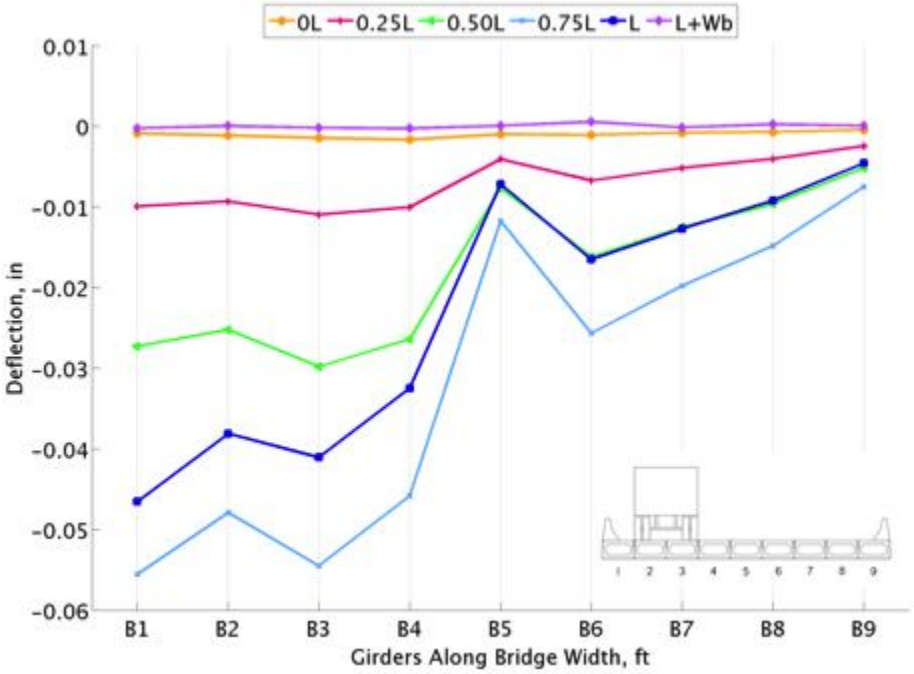

Figure 155. Load case 1 run 2 deflection

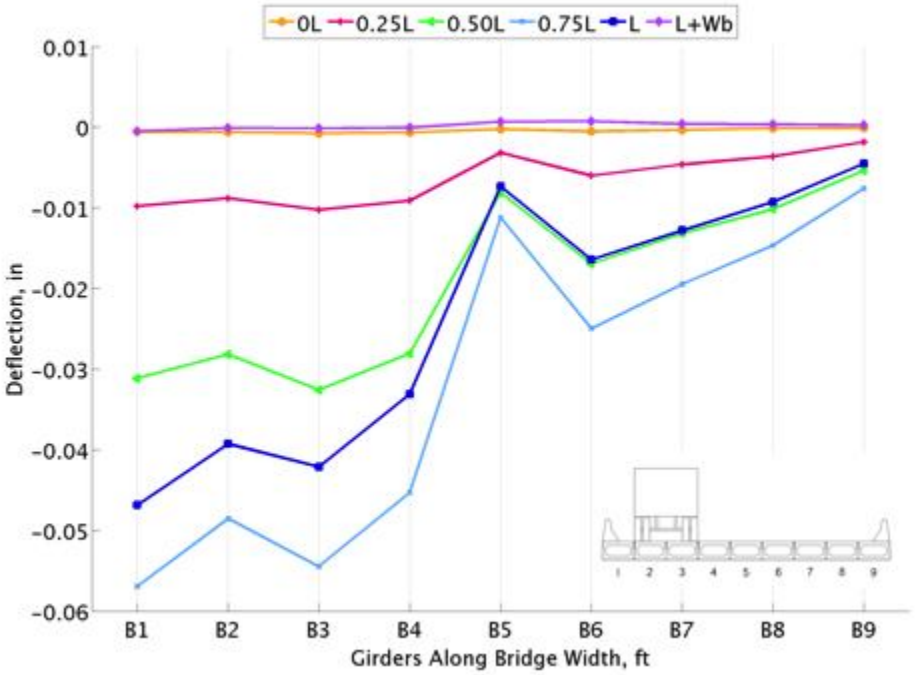

Figure 156. Load case 1 run 3 deflection

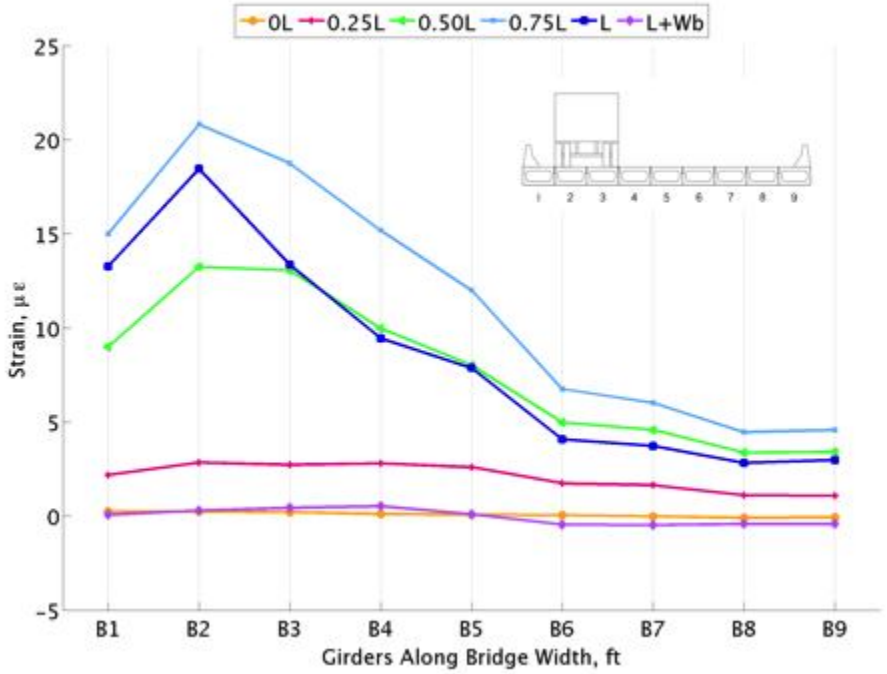

Figure 157. Load case 1 run 1 strain

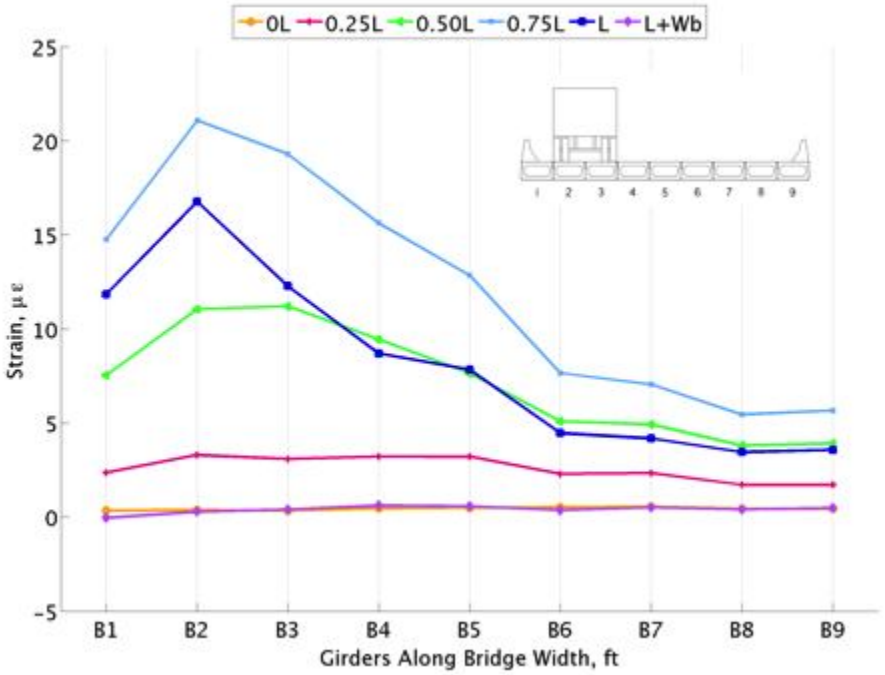

Figure 158. Load case 1 run 2 strain

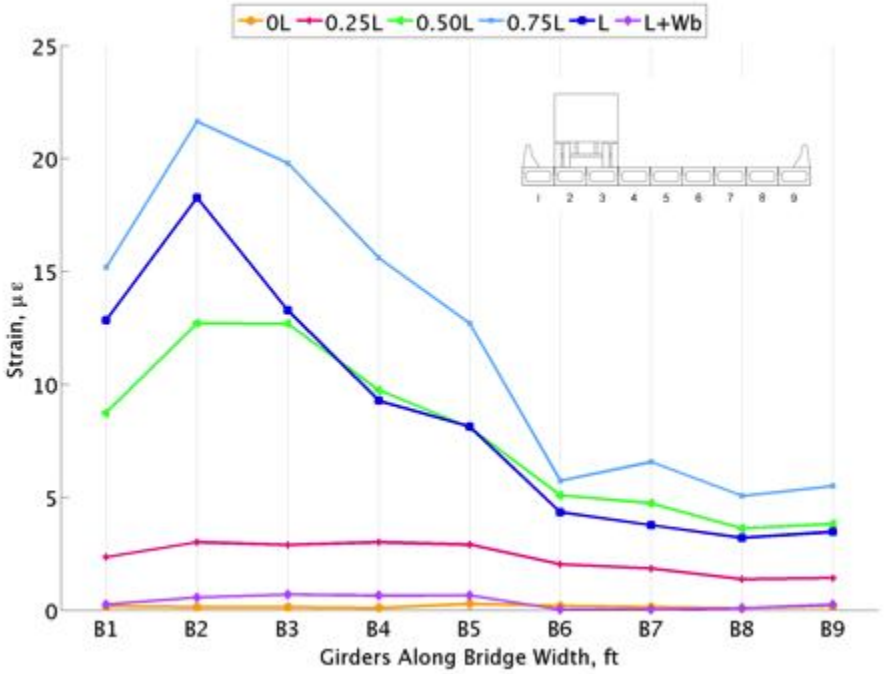

Figure 159. Load case 1 run 3 strain

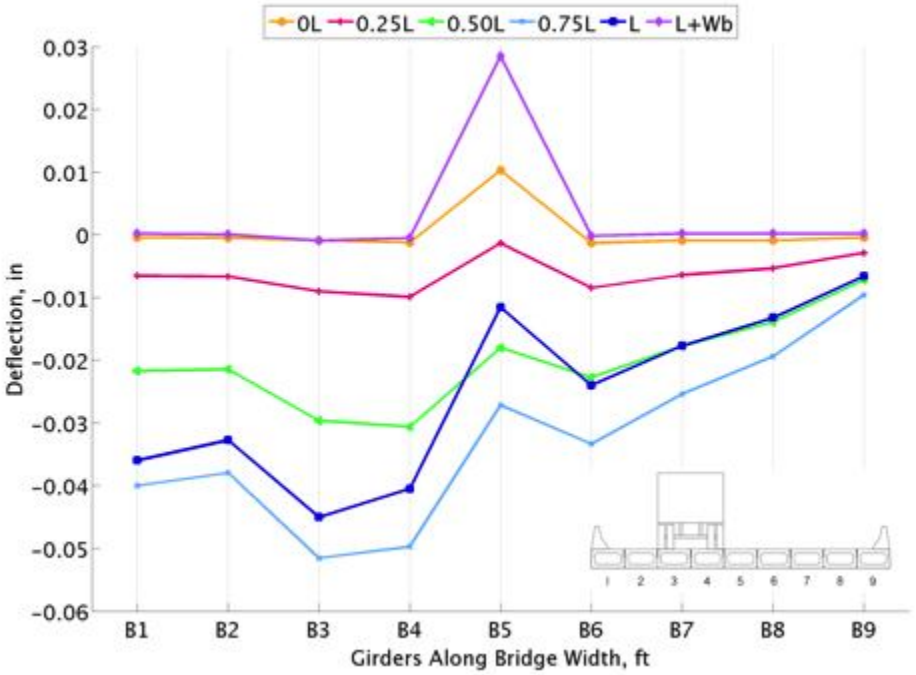

Figure 160. Load case 2 run 1 deflection

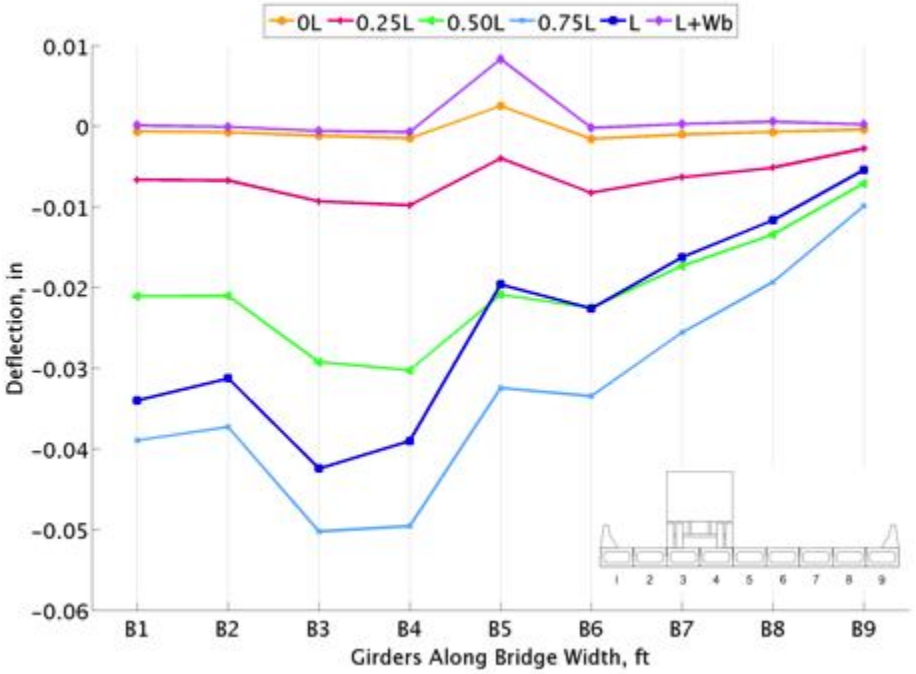

Figure 161. Load case 2 run 2 deflection

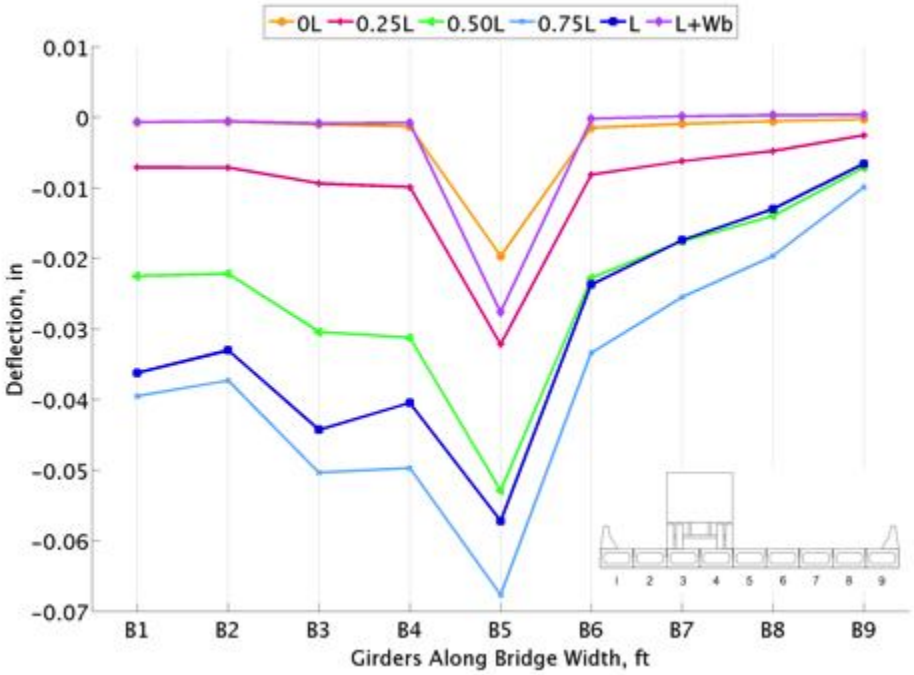

Figure 162. Load case 2 run 3 deflection

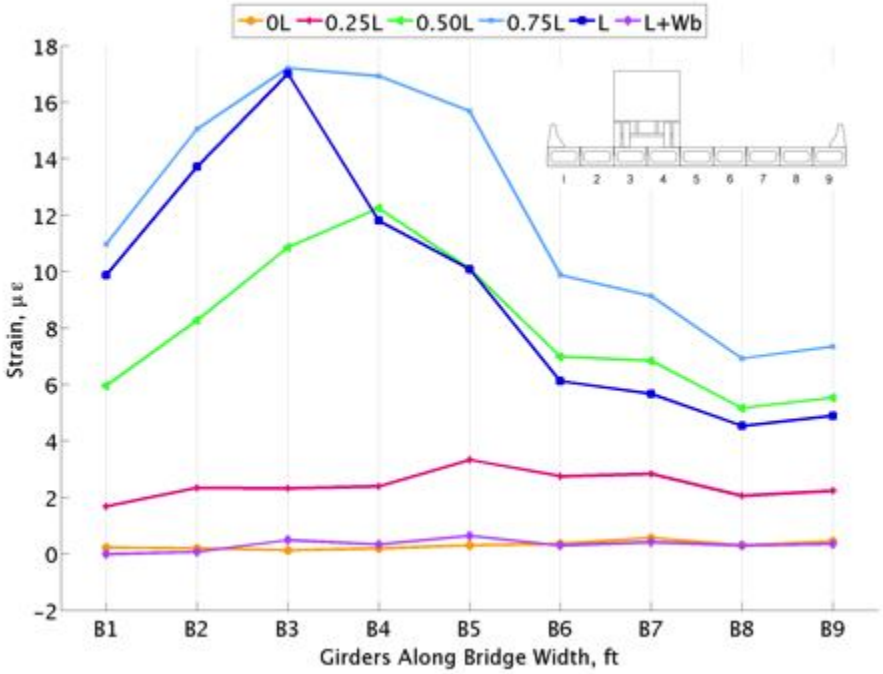

Figure 163. Load case 2 run 1 strain

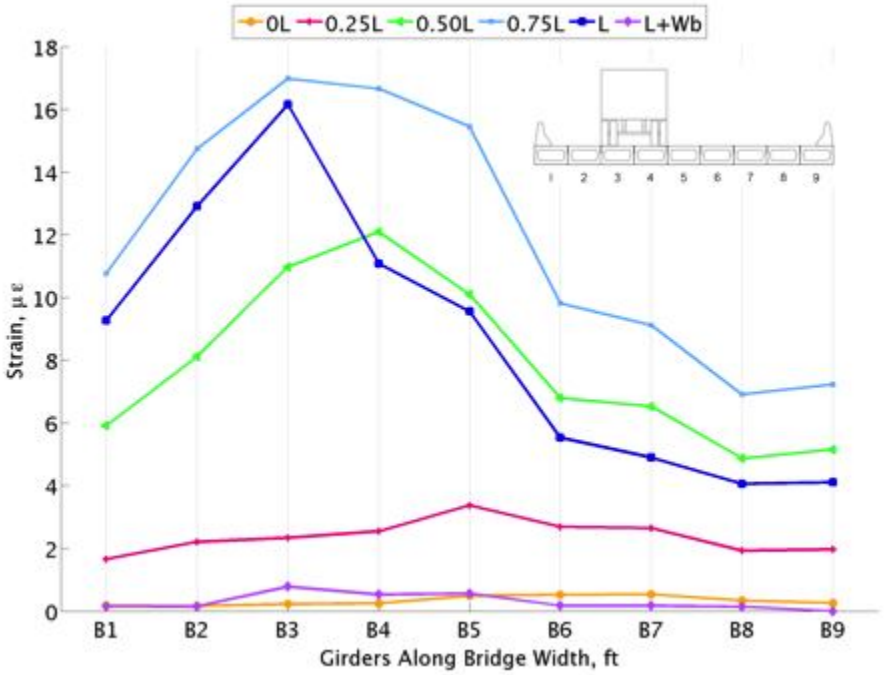

Figure 164. Load case 2 run 2 strain

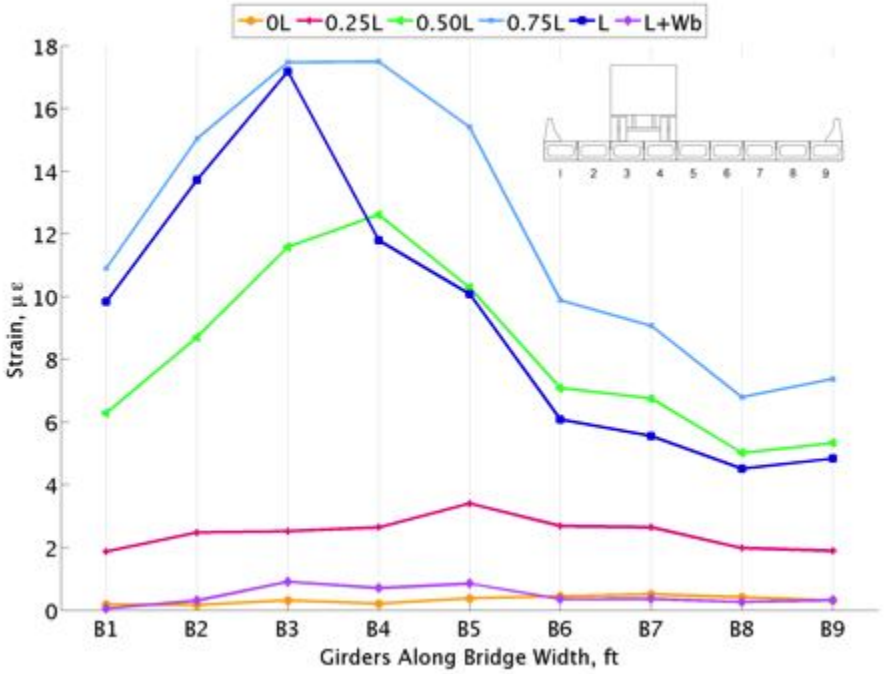

Figure 165. Load case 2 run 3 strain

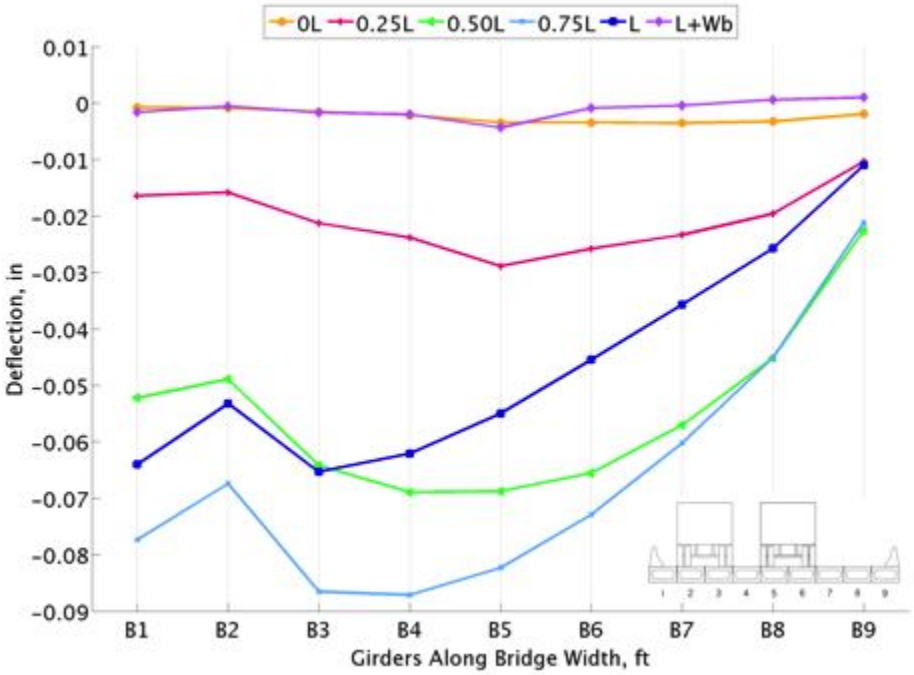

Figure 166. Load case 3 run 1 deflection

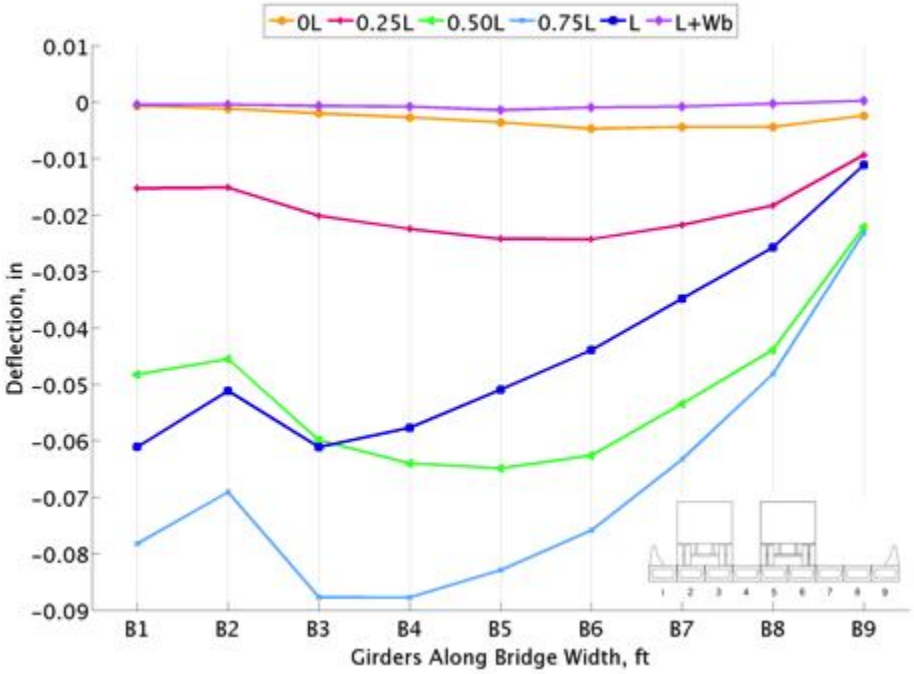

Figure 167. Load case 3 run 2 deflection

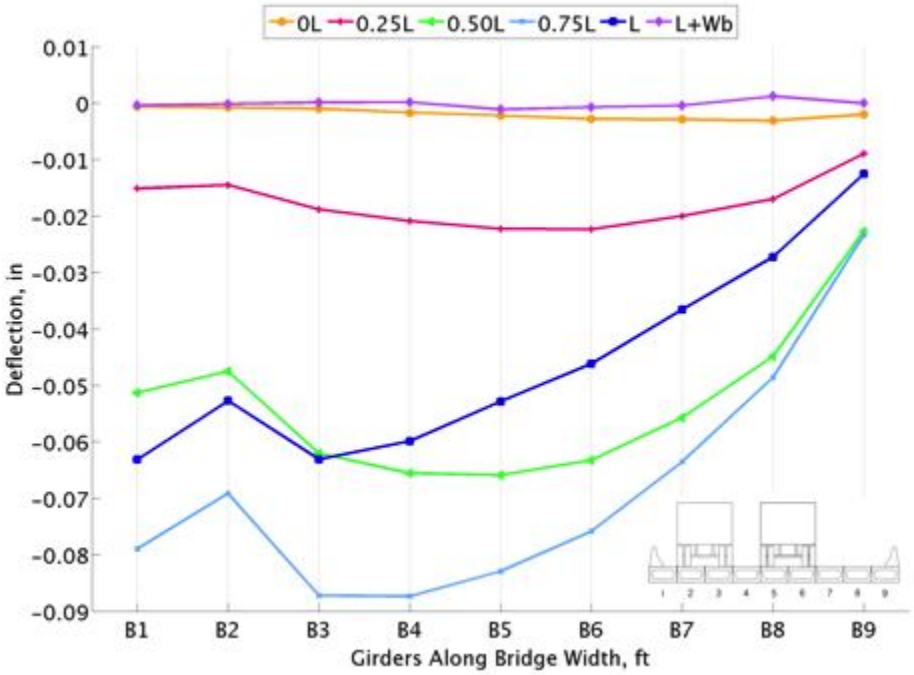

Figure 168. Load case 3 run 3 deflection

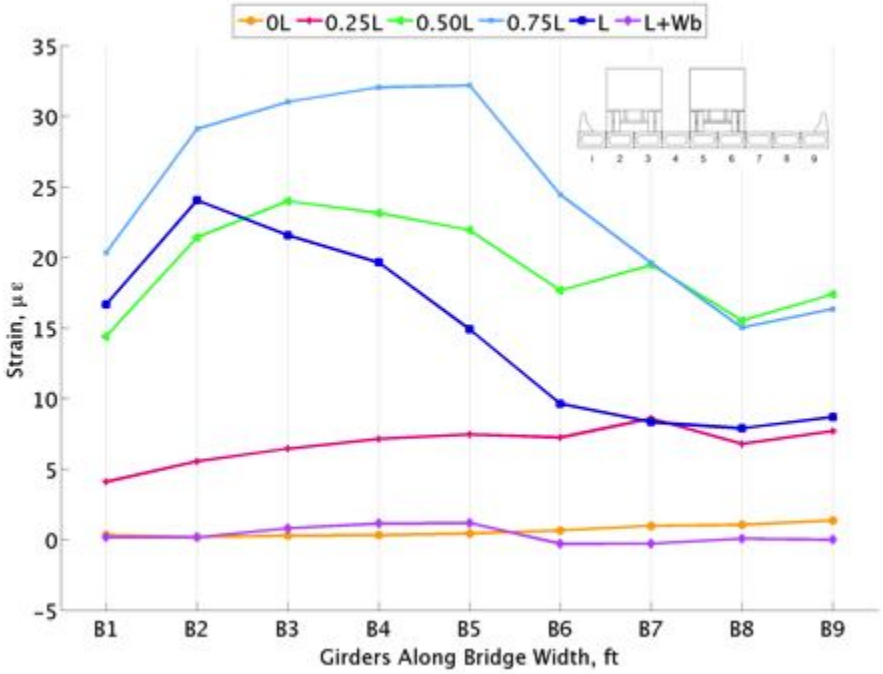

Figure 169. Load case 3 run 1 strain

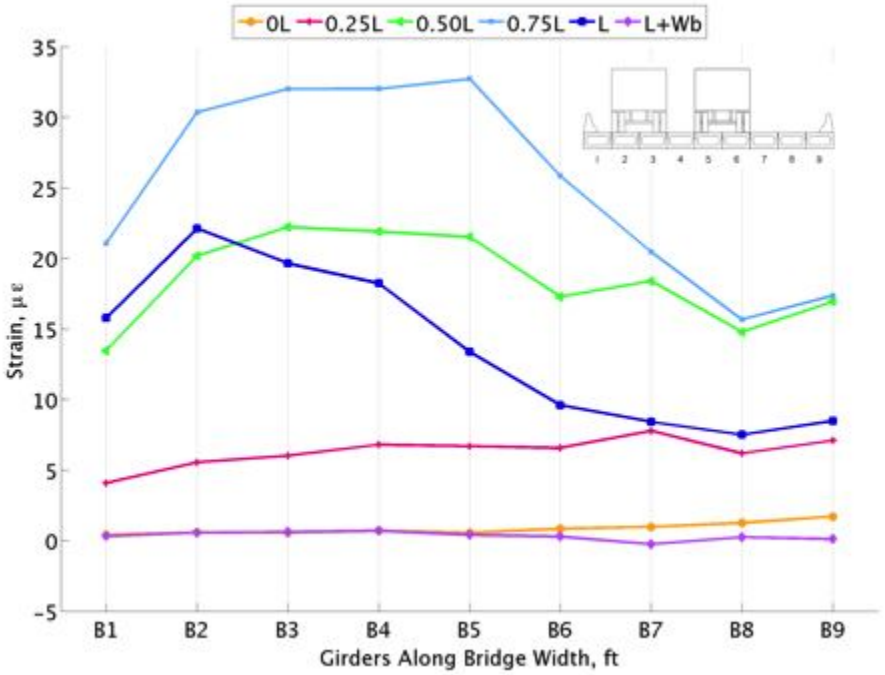

Figure 170. Load case 3 run 2 strain

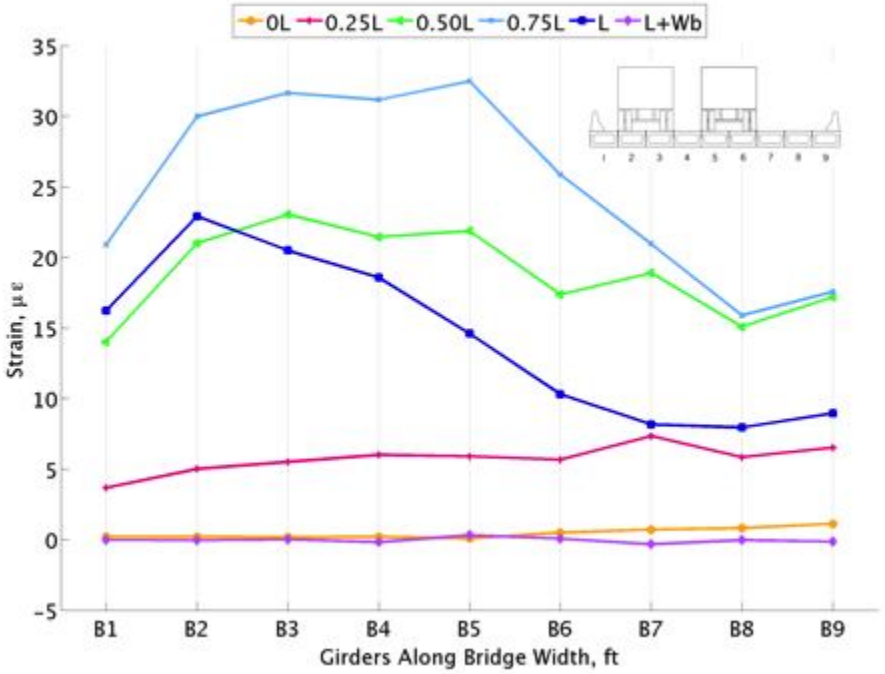

Figure 171. Load case 3 run 3 strain

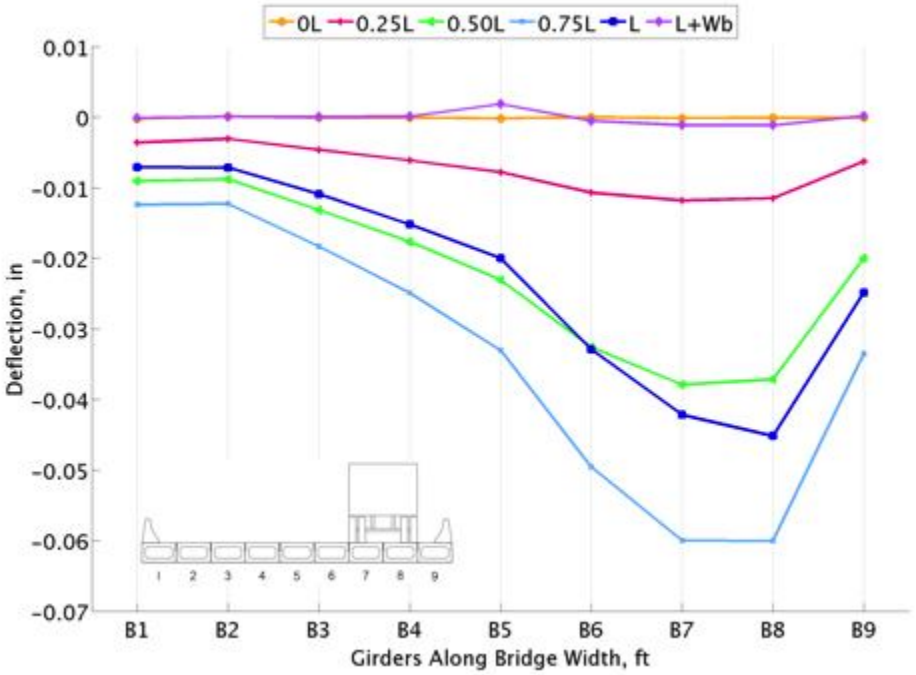

Figure 172. Load case 4 run 1 deflection

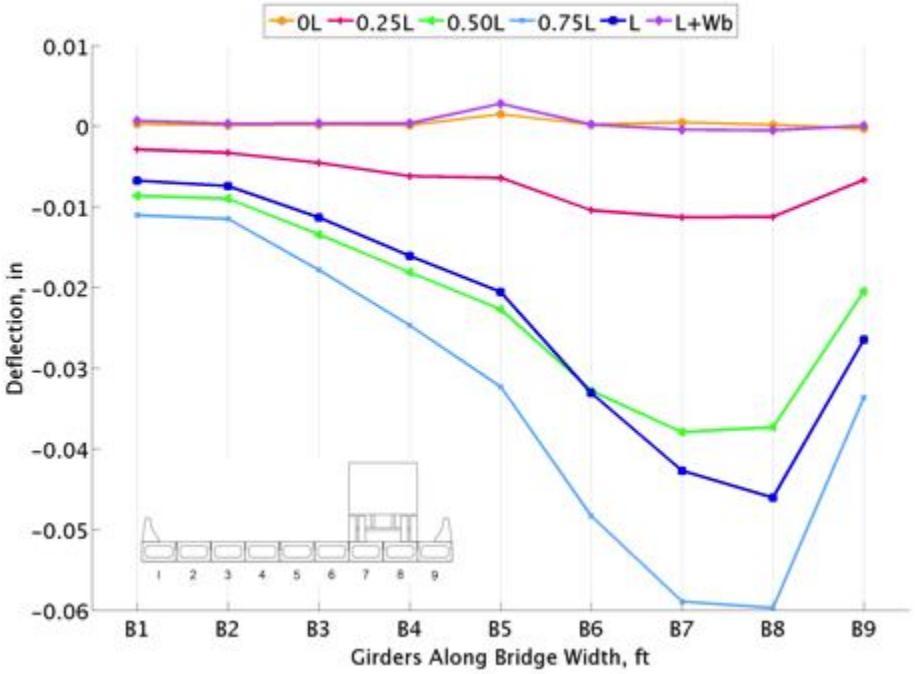

Figure 173. Load case 4 run 2 deflection

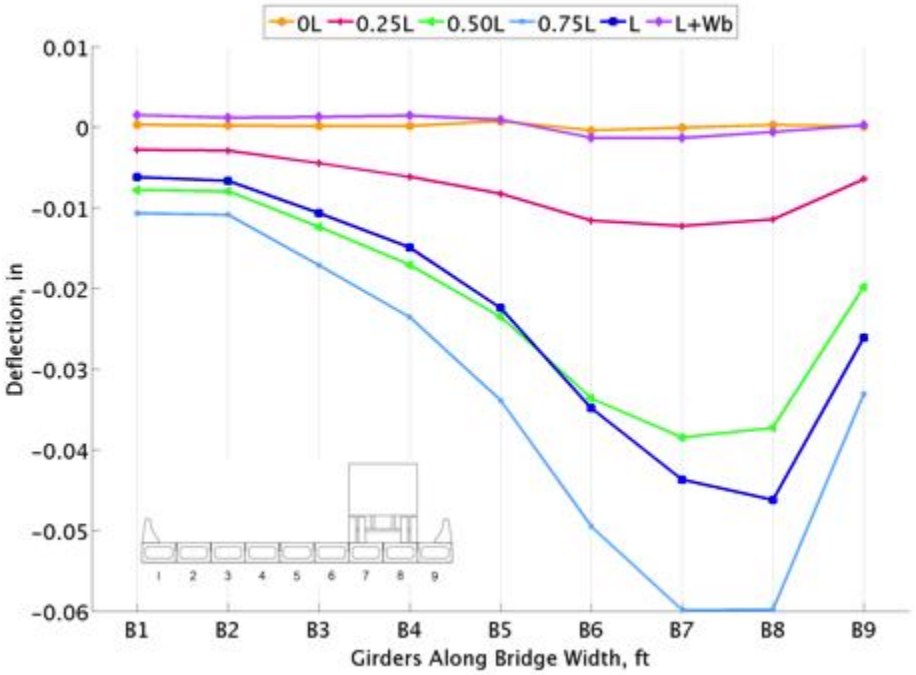

Figure 174. Load case 4 run 3 deflection

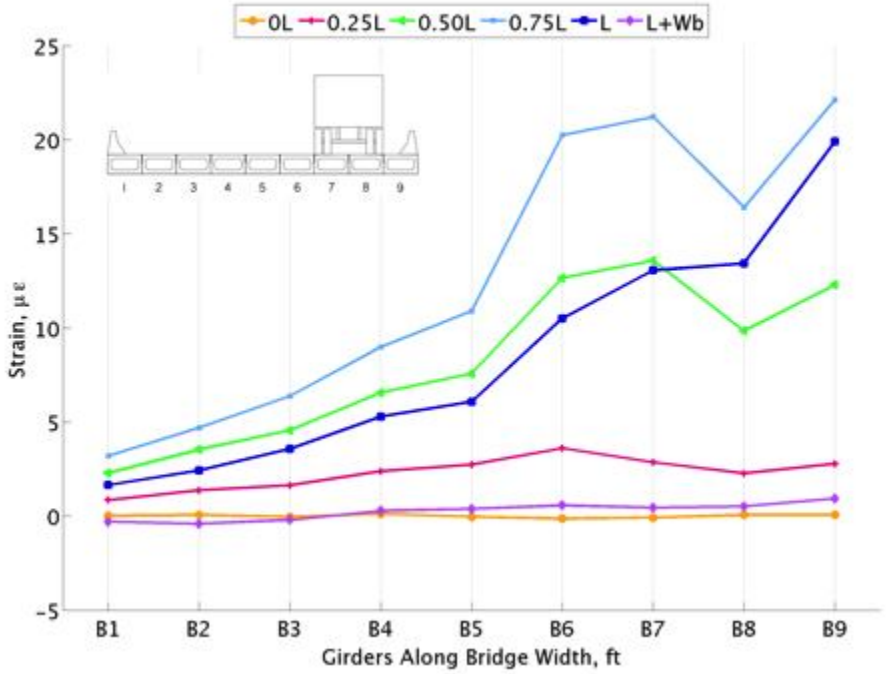

Figure 175. Load case 4 run 1 strain

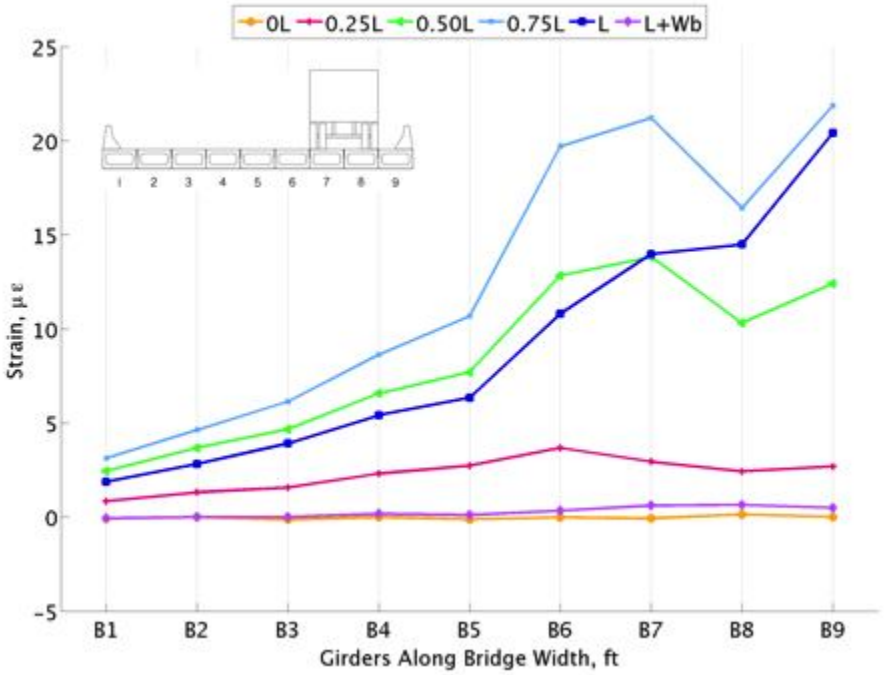

Figure 176. Load case 4 run 2 strain

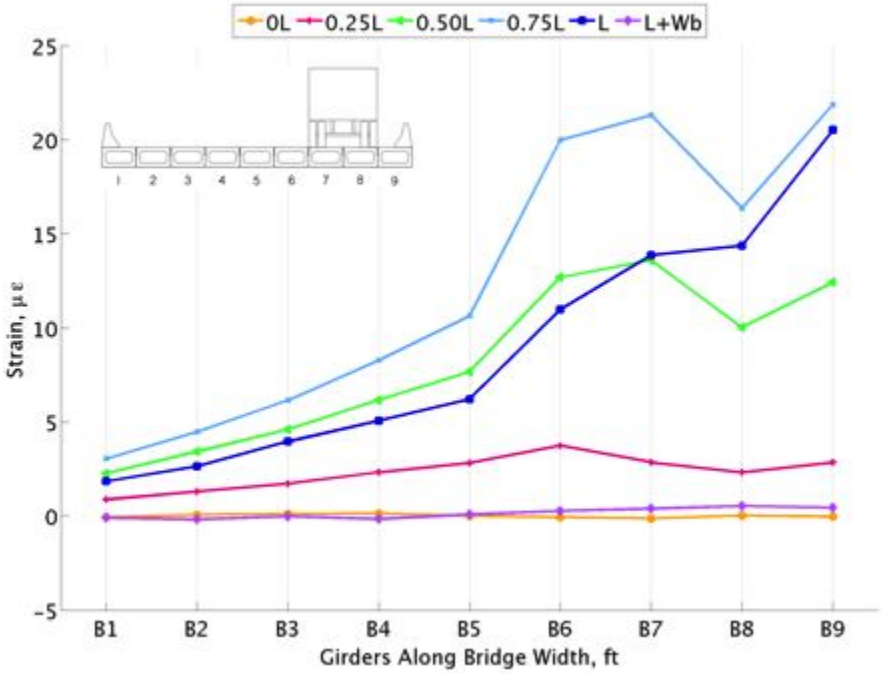

Figure 177. Load case 4 run 3 strain

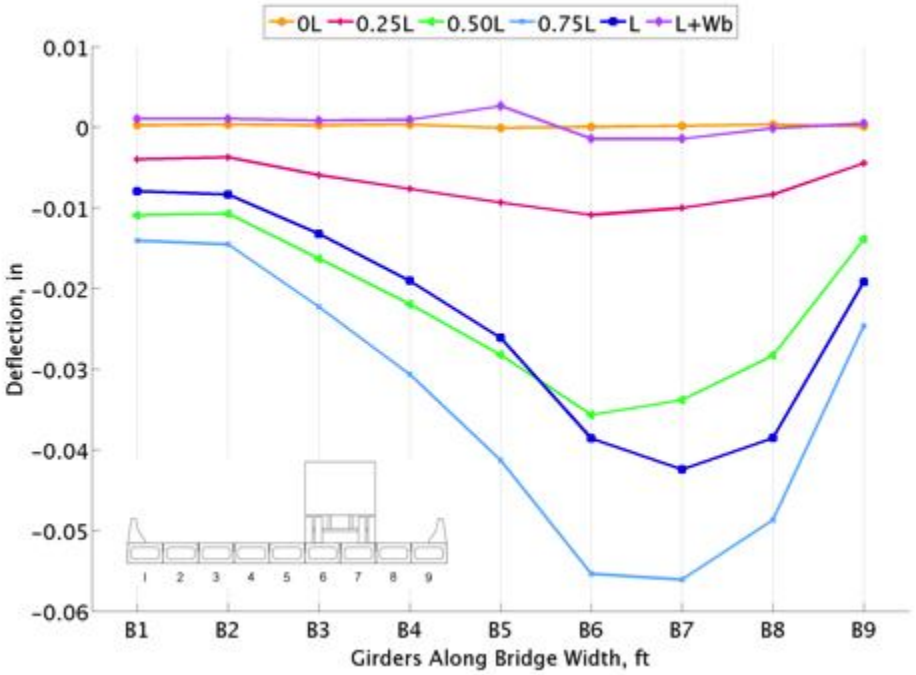

Figure 178. Load case 5 run 1 deflection

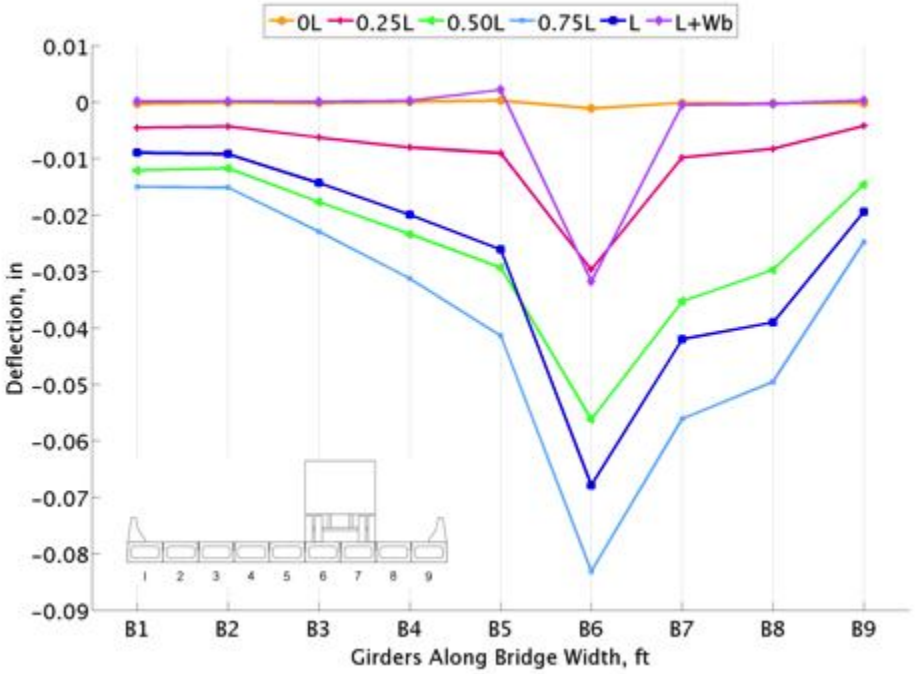

Figure 179. Load case 5 run 2 deflection

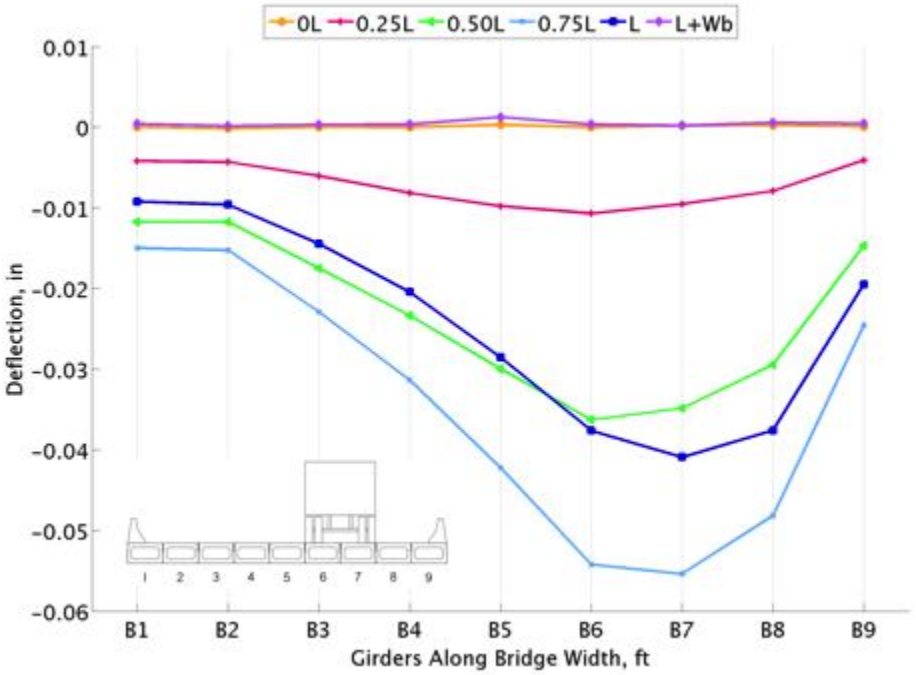

Figure 180. Load case 5 run 3 deflection

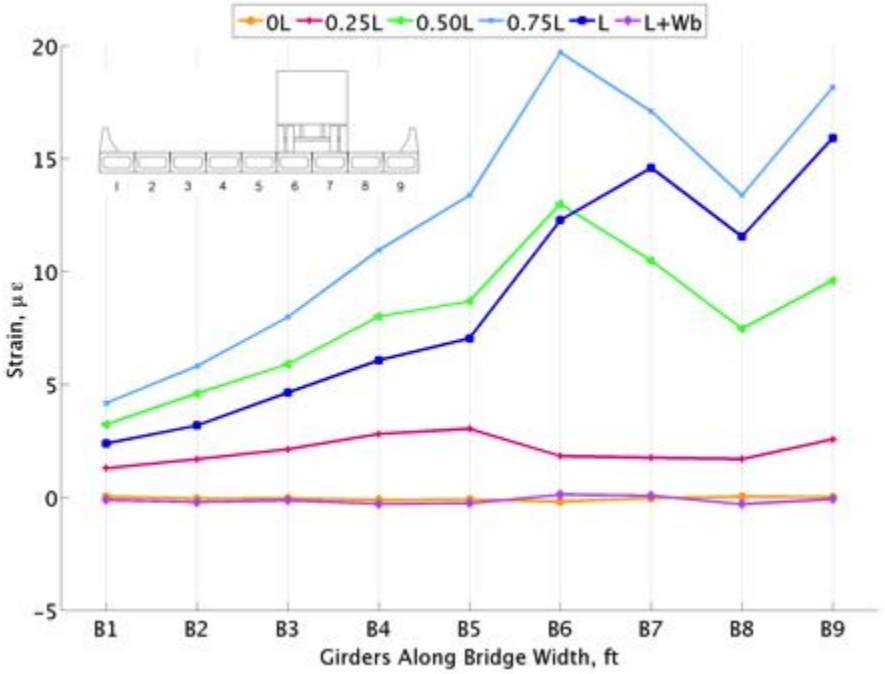

Figure 181. Load case 5 run 1 strain

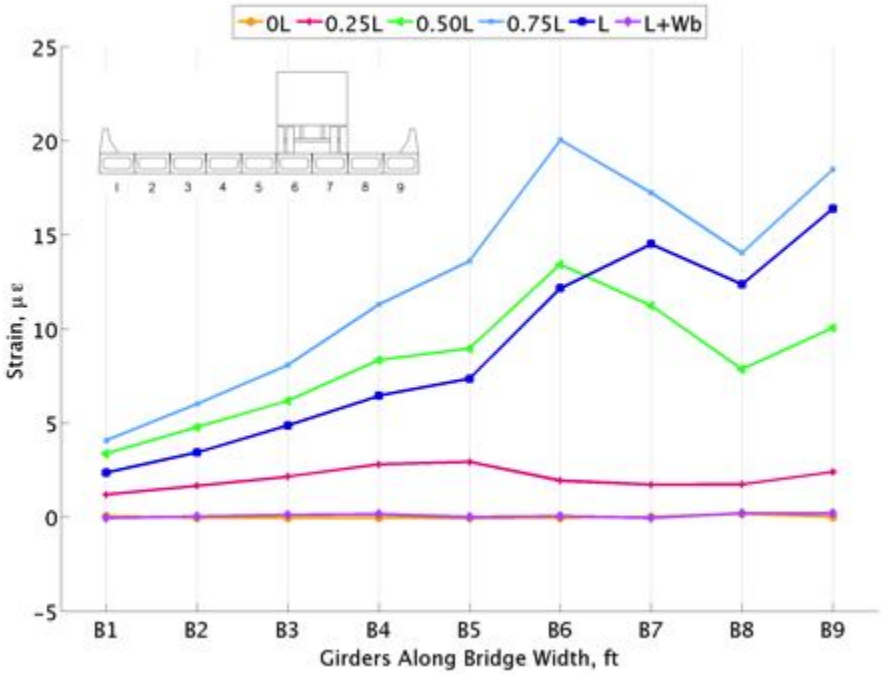

Figure 182. Load case 5 run 2 strain

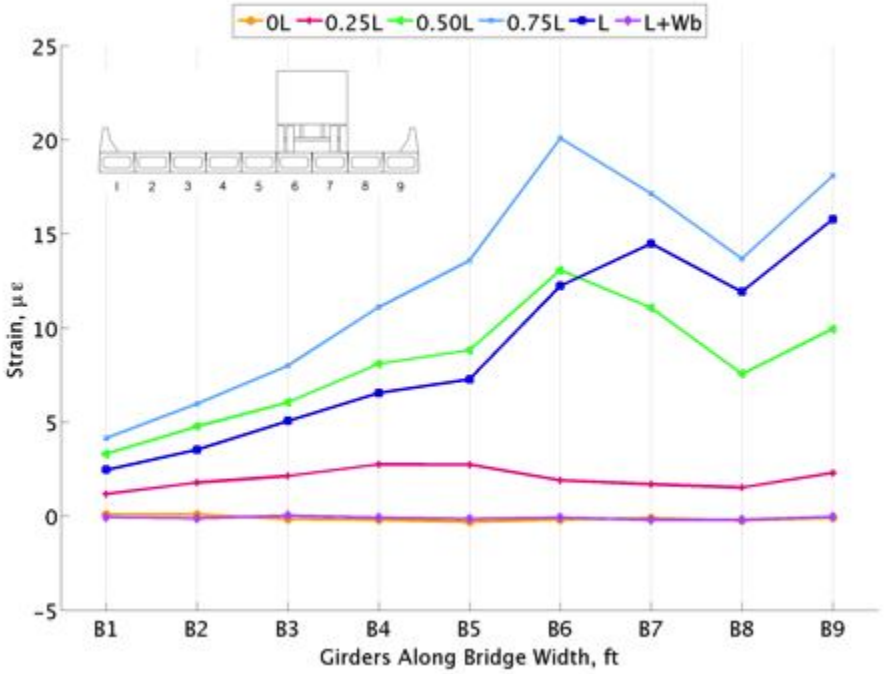

Figure 183. Load case 5 run 3 strain

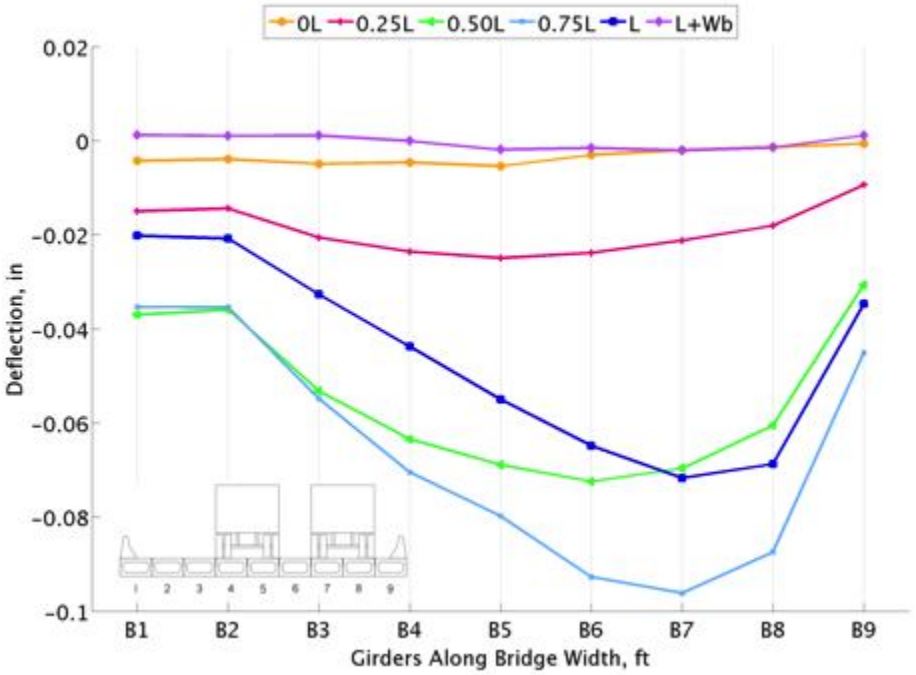

Figure 184. Load case 6 run 1 deflection

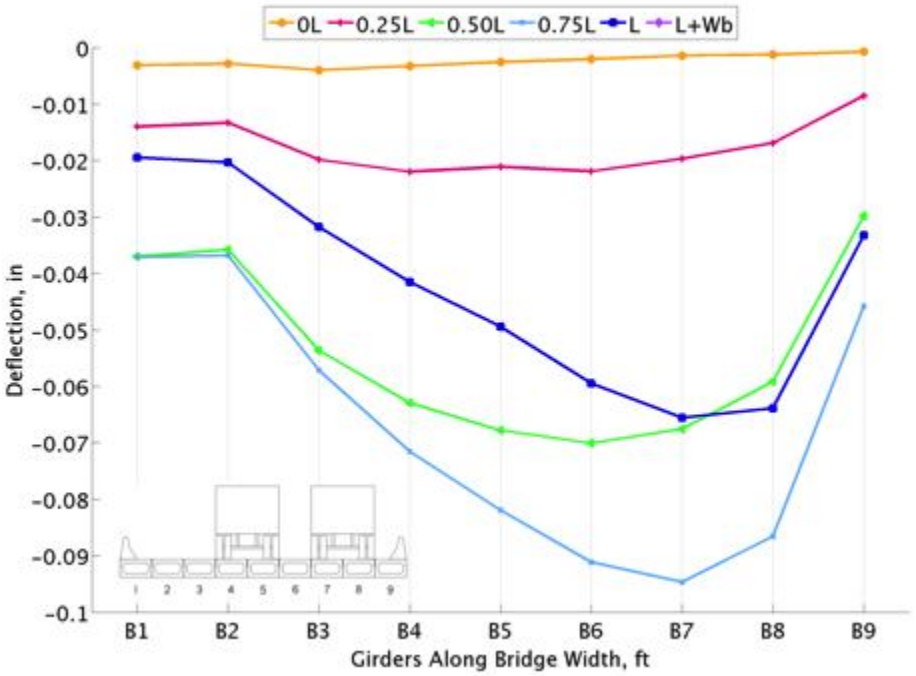

Figure 185. Load case 6 run 2 deflection

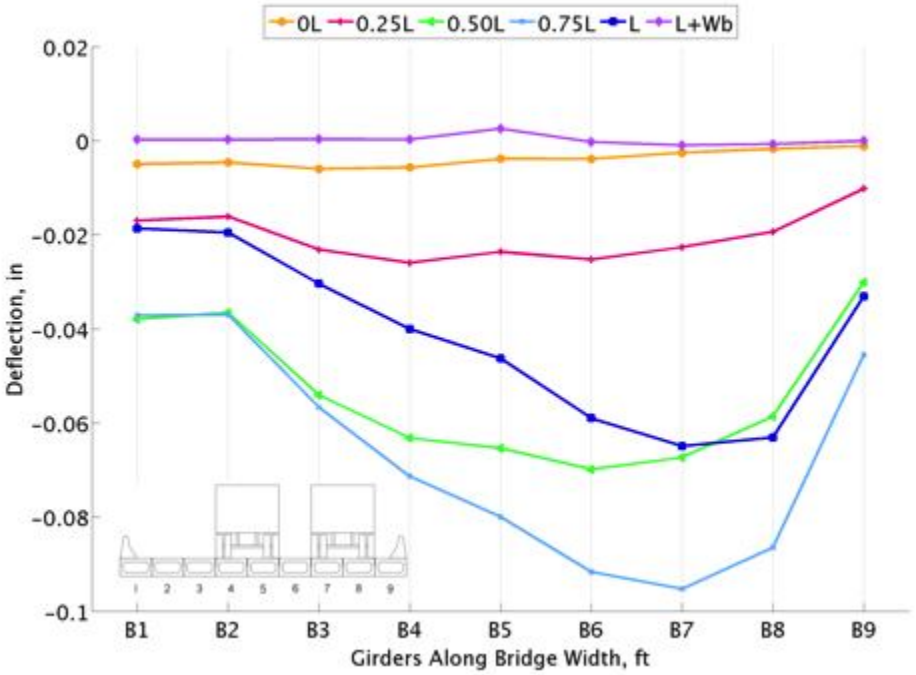

Figure 186. Load case 6 run 3 deflection

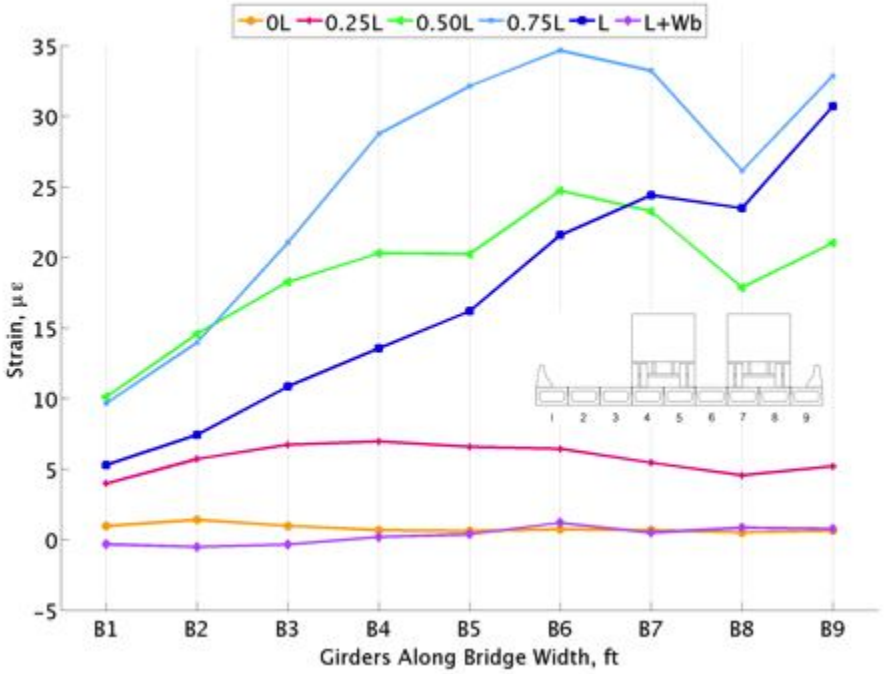

Figure 187. Load case 6 run 1 strain

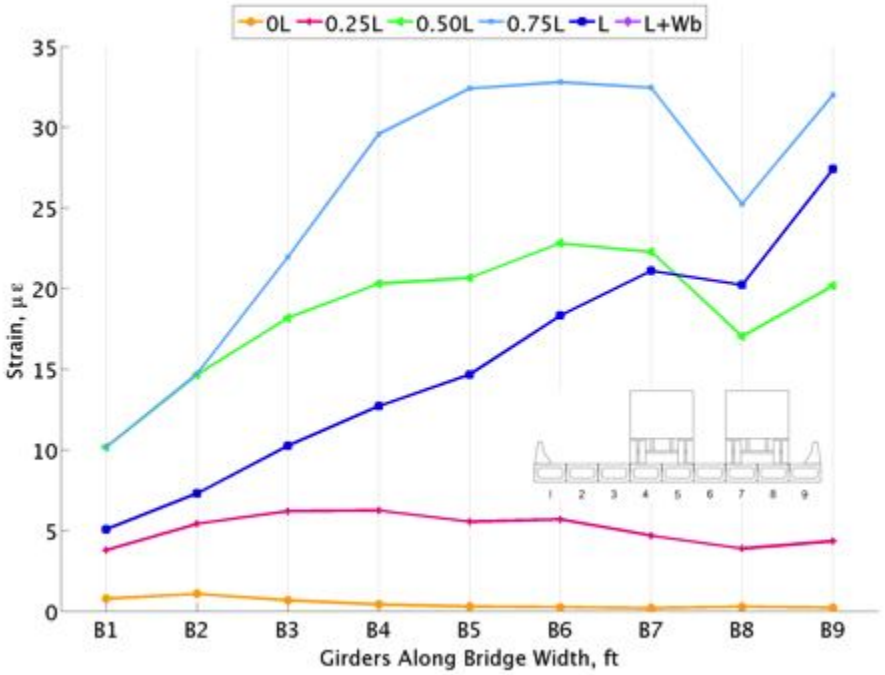

Figure 188. Load case 6 run 2 strain

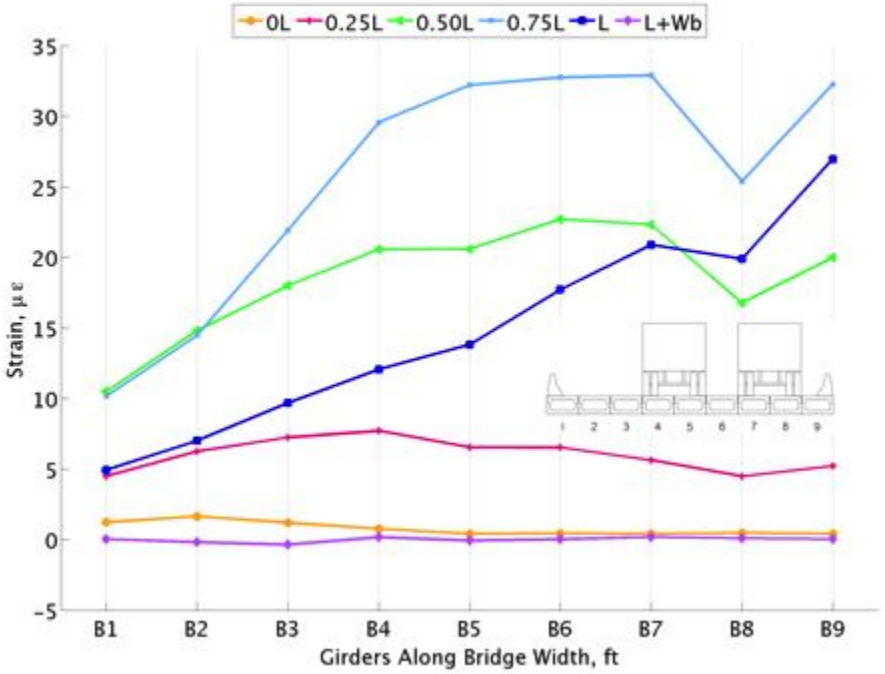

Figure 189. Load case 6 run 3 strain

Live Load Test Relative Horizontal and Vertical Deflection Plots

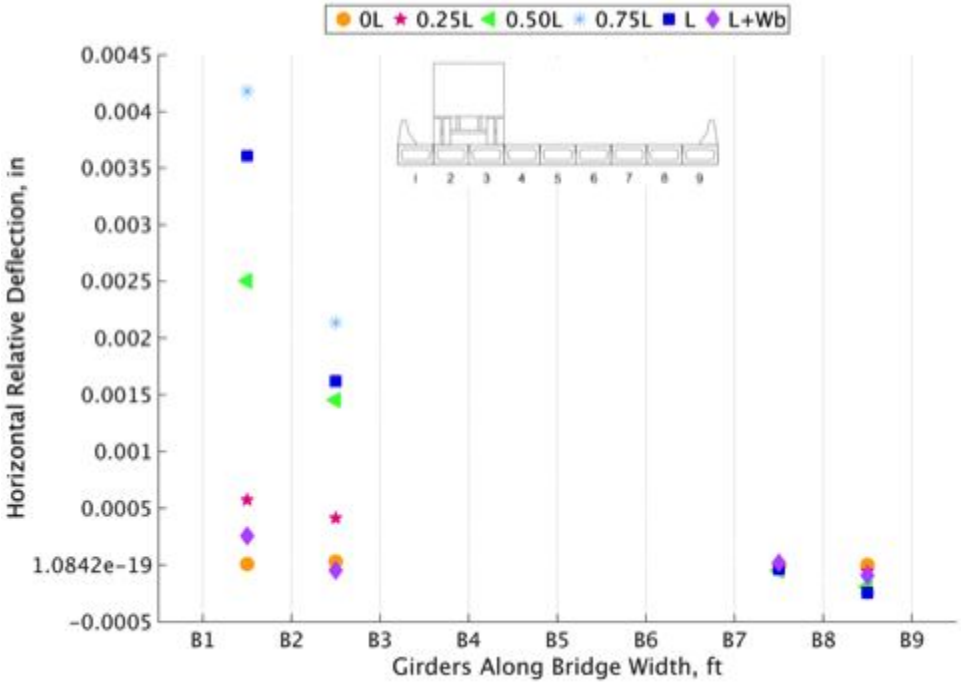

Figure 190. Load case 1 run 1 relative horizontal deflection

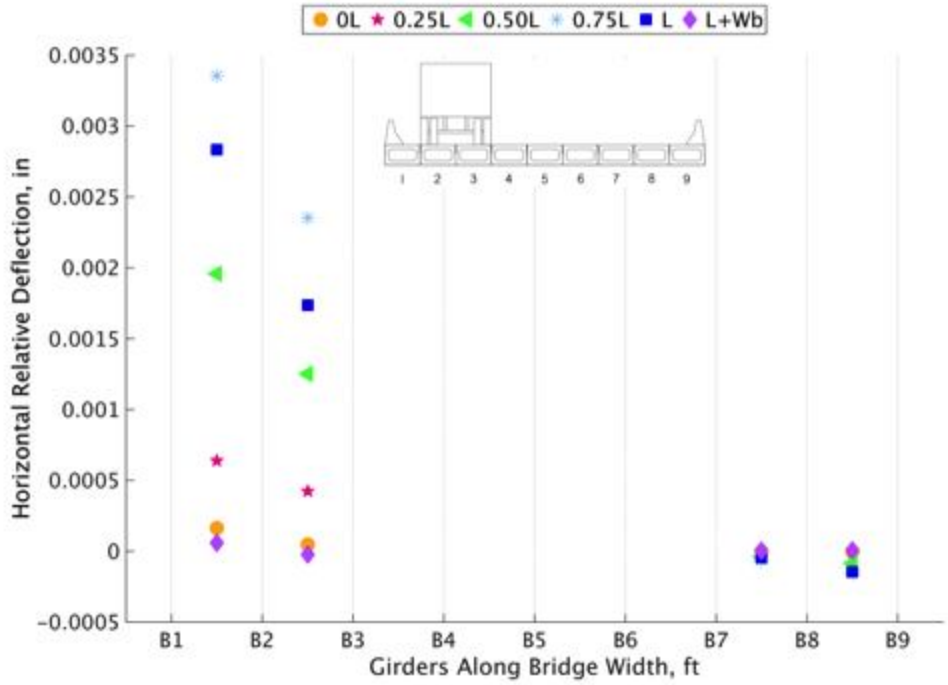

Figure 191. Load case 1 run 2 relative horizontal deflection

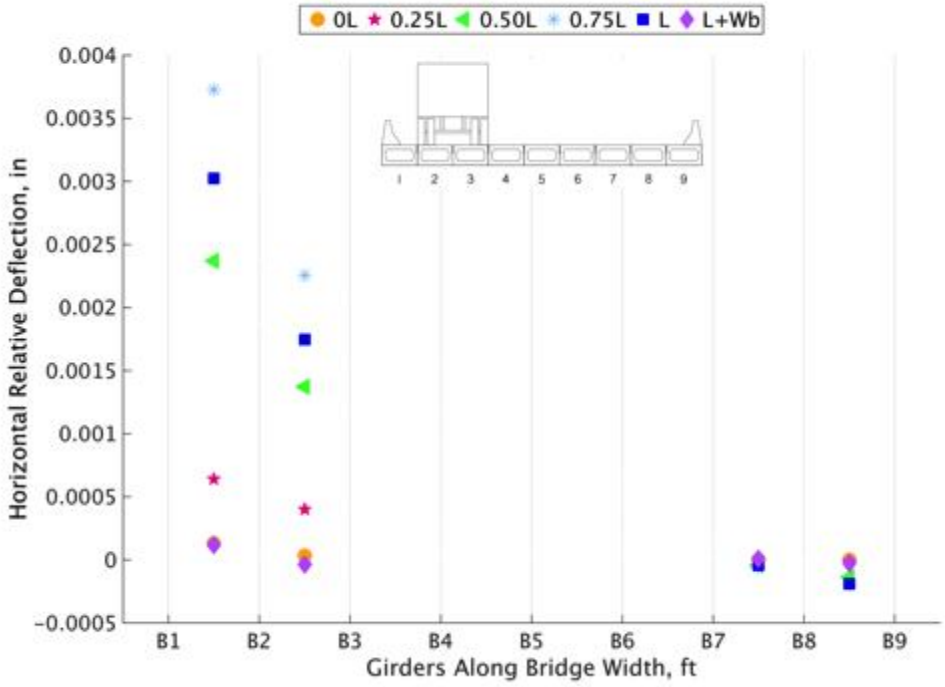

Figure 192. Load case 1 run 3 relative horizontal deflection

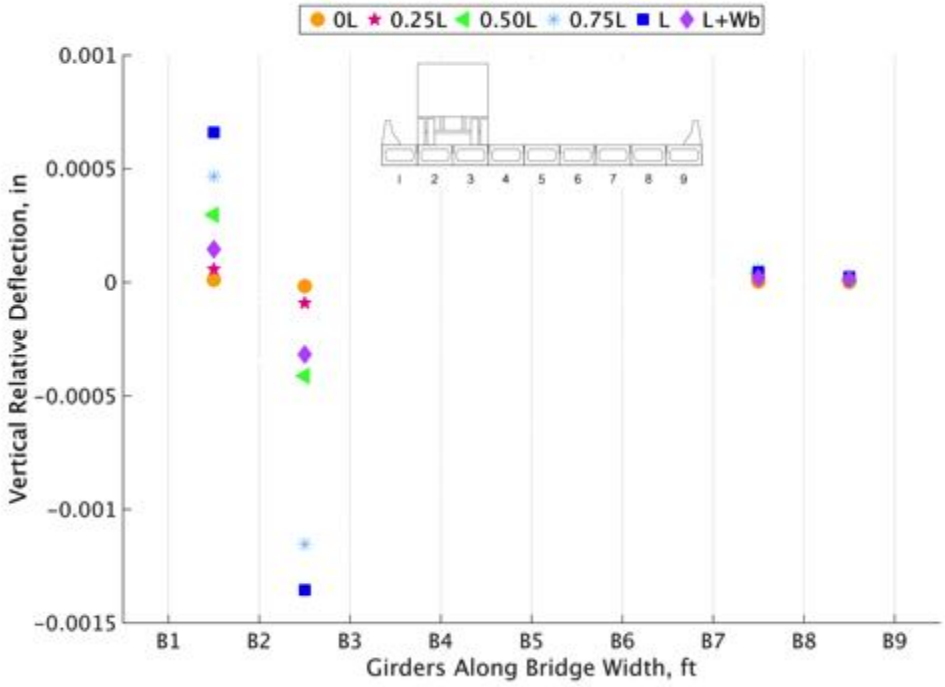

Figure 193. Load case 1 run 1 relative vertical deflection

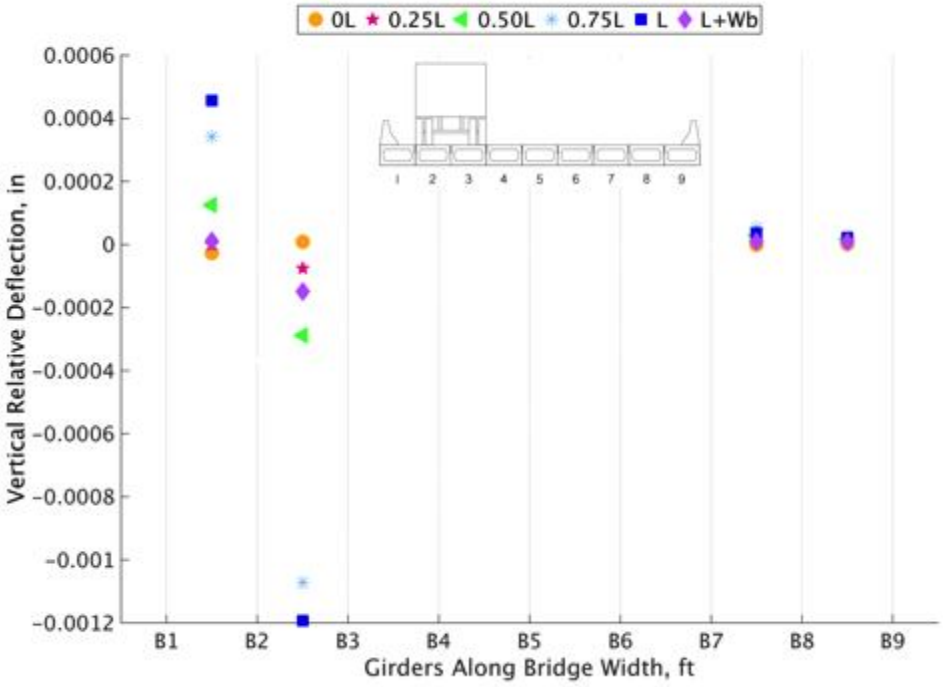

Figure 194. Load case 1 run 2 relative vertical deflection

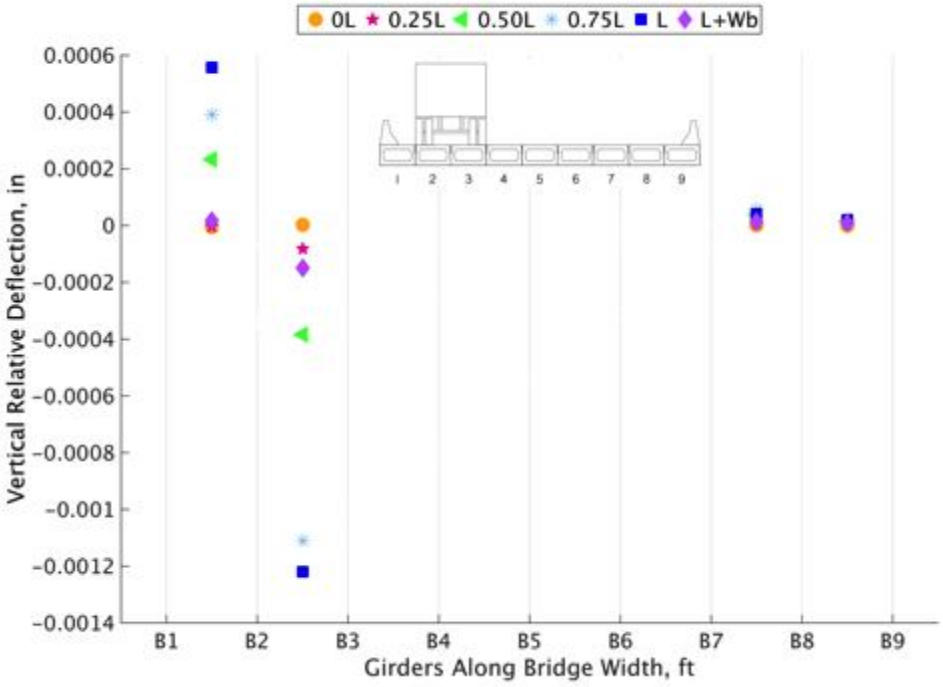

Figure 195. Load case 1 run 3 relative vertical deflection

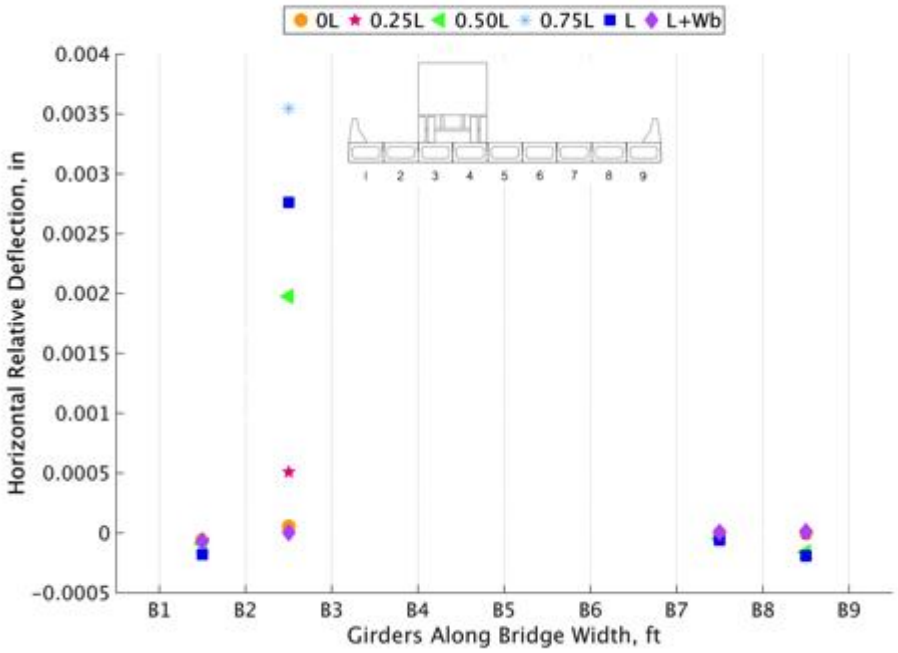

Figure 196. Load case 2 run 1 relative horizontal deflection

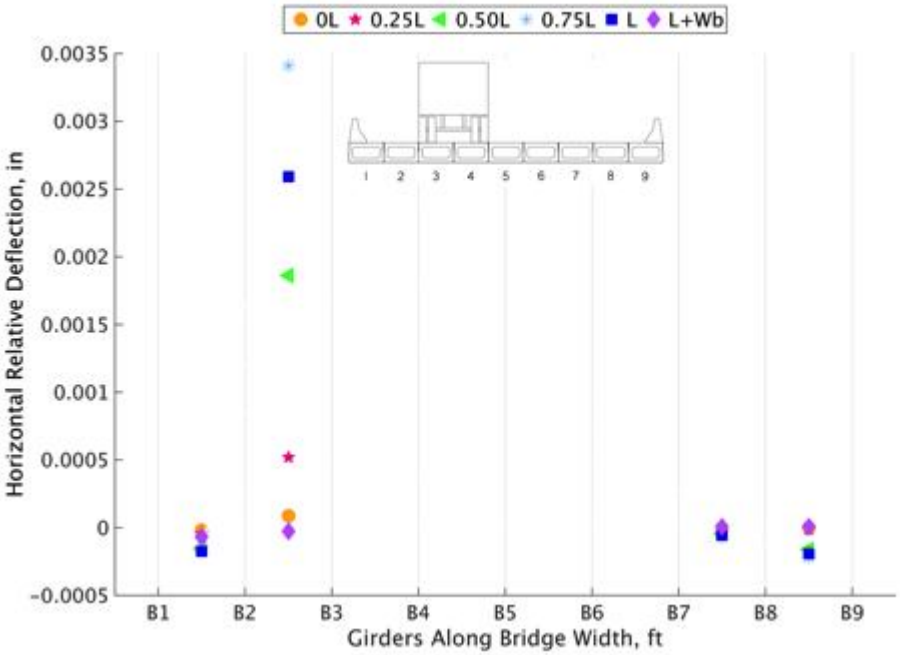

Figure 197. Load case 2 run 2 relative horizontal deflection

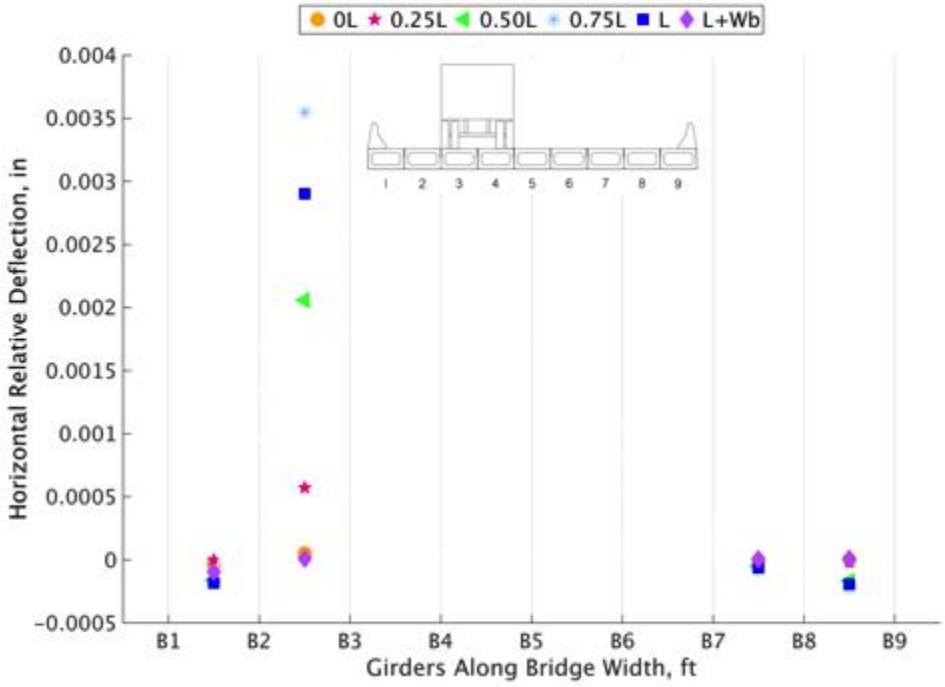

Figure 198. Load case 2 run 3 relative horizontal deflection

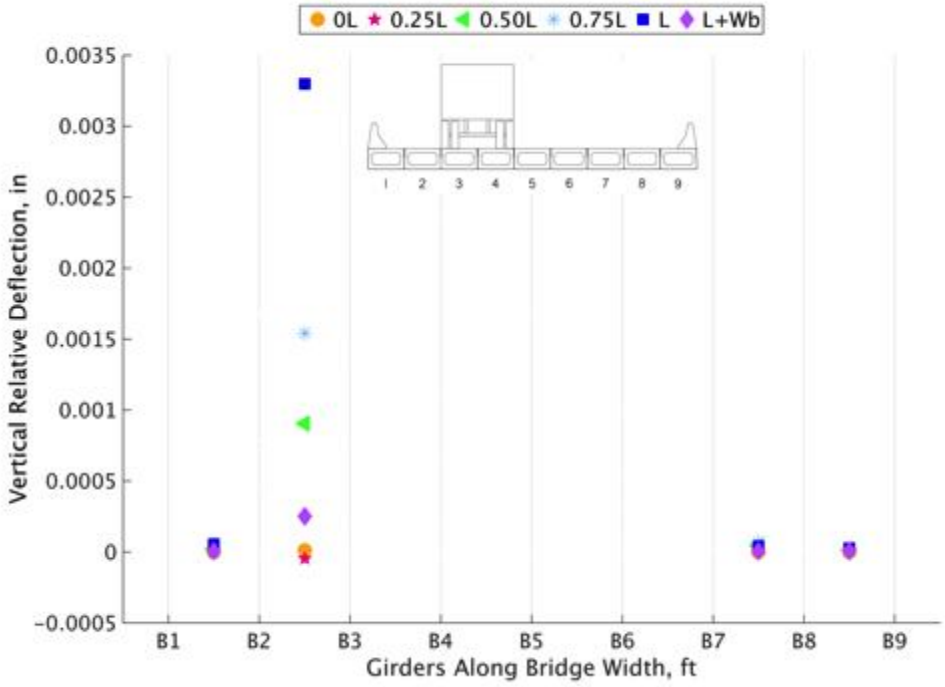

Figure 199. Load case 2 run 1 relative vertical deflection

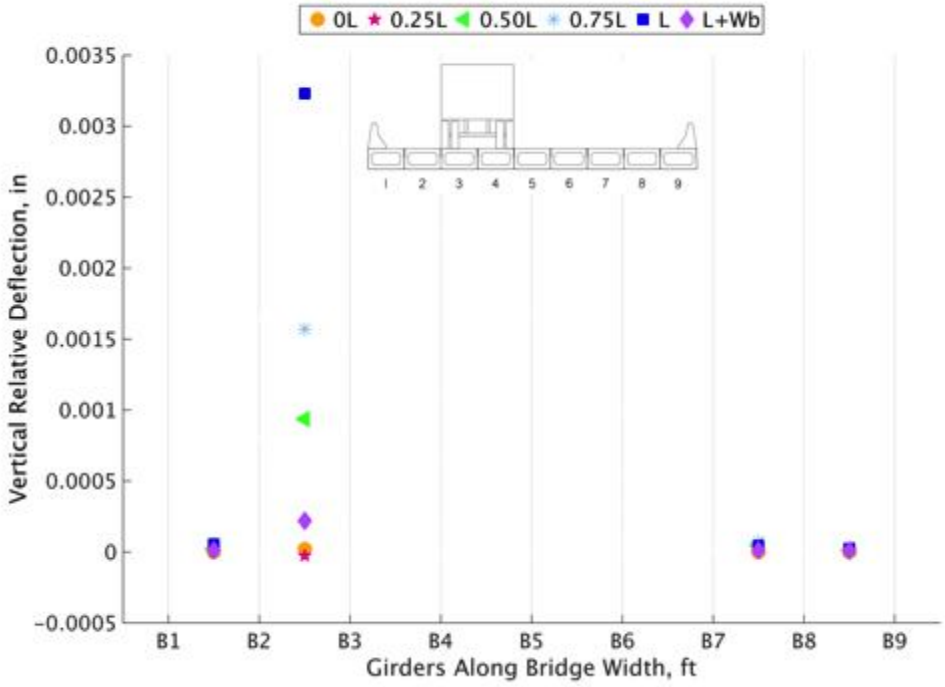

Figure 200. Load case 2 run 2 relative vertical deflection

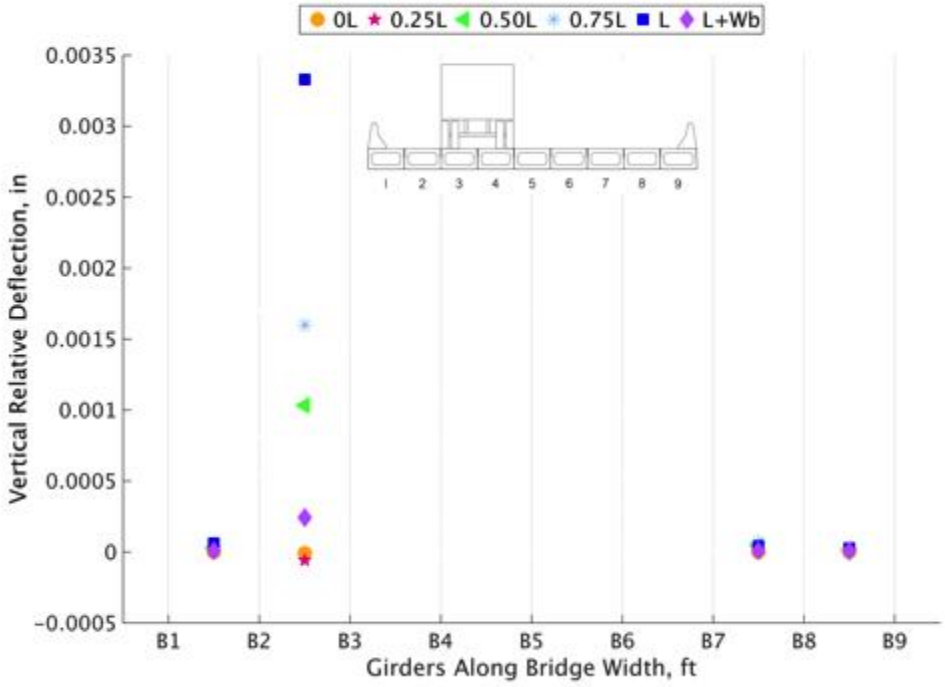

Figure 201. Load case 2 run 3 relative vertical deflection

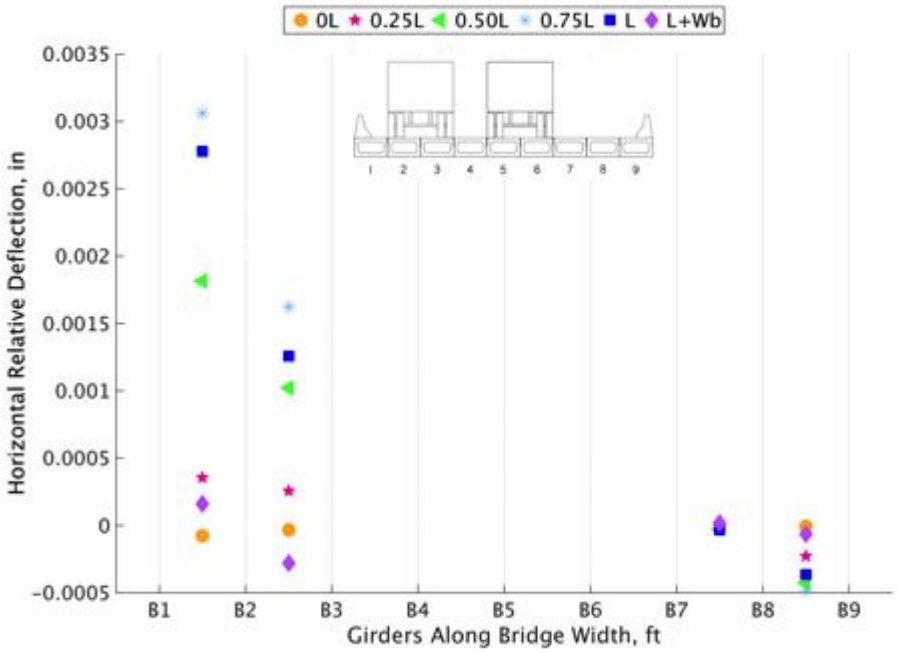

Figure 202. Load case 3 run 1 relative horizontal deflection

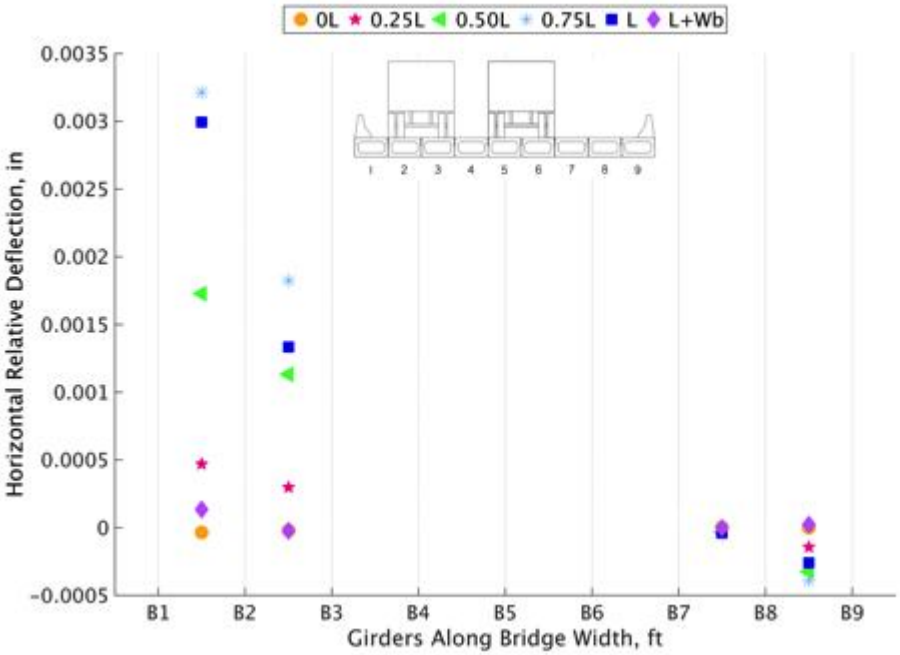

Figure 203. Load case 3 run 2 relative horizontal deflection

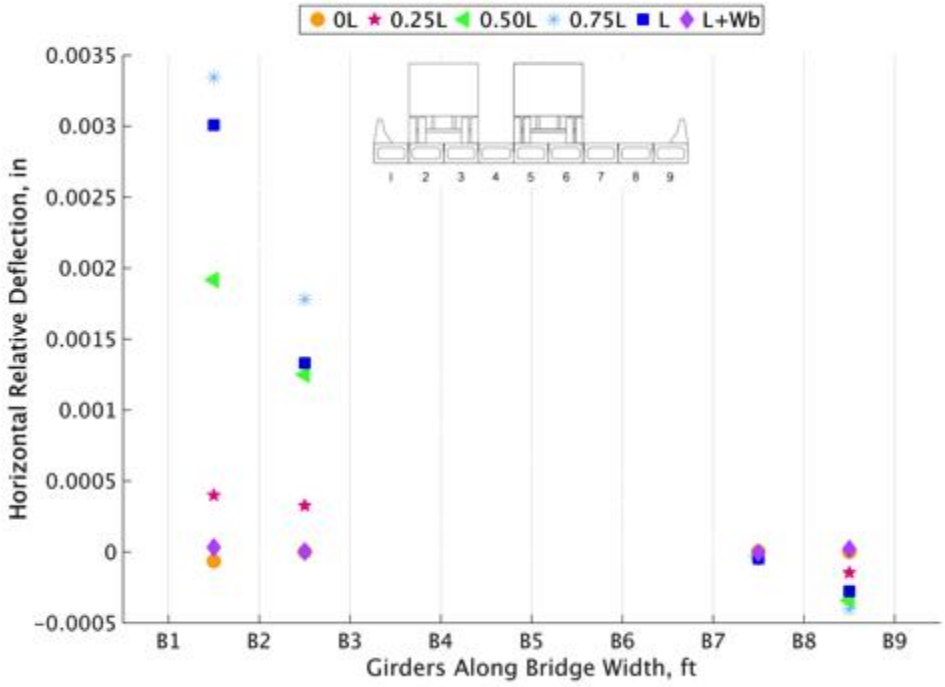

Figure 204. Load case 3 run 3 relative horizontal deflection

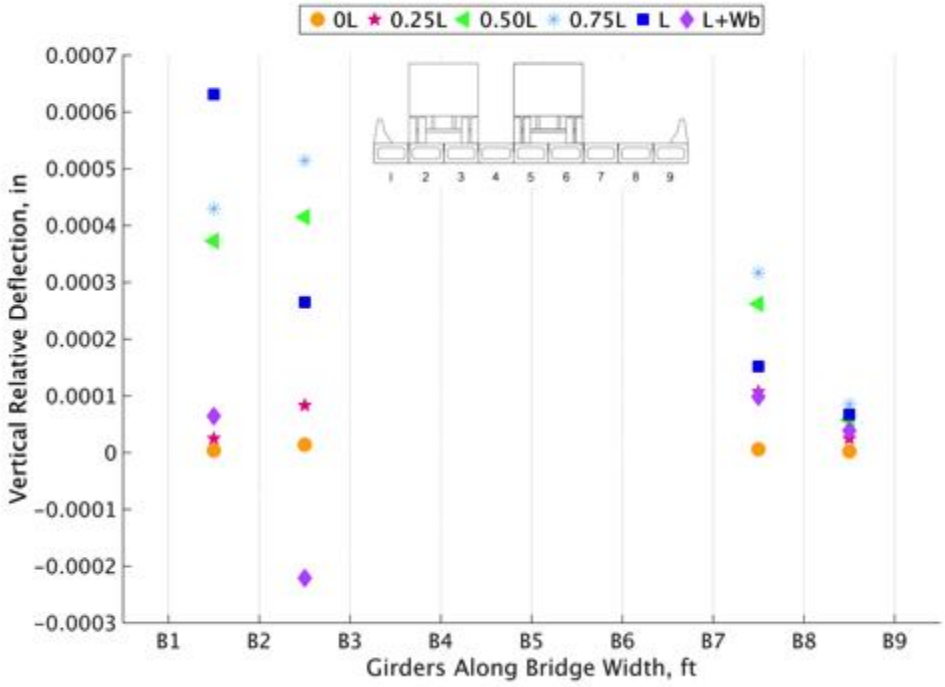

Figure 205. Load case 3 run 1 relative vertical deflection

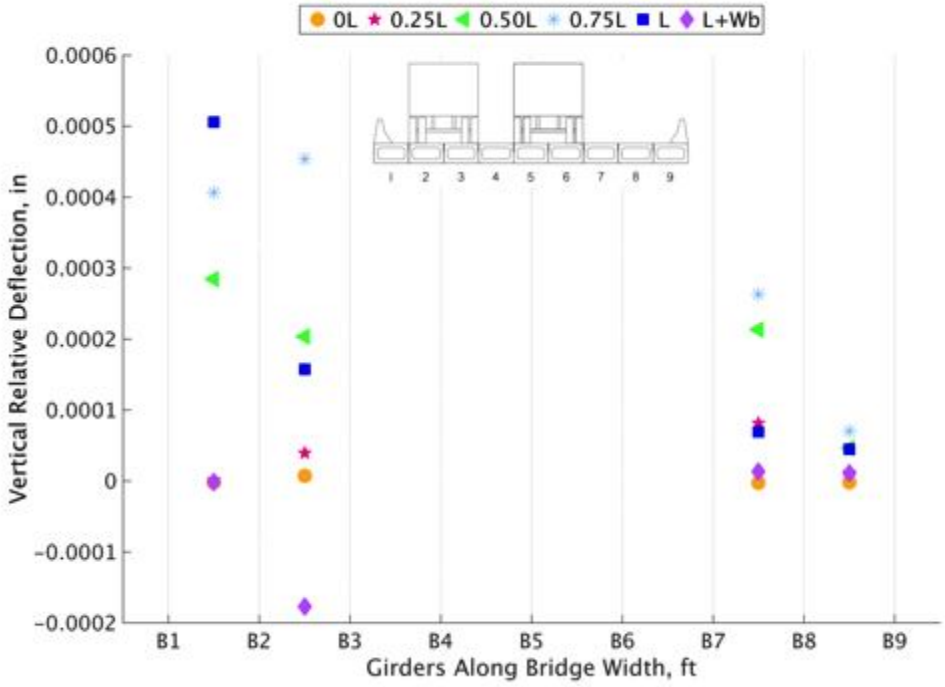

Figure 206. Load case 3 run 2 relative vertical deflection

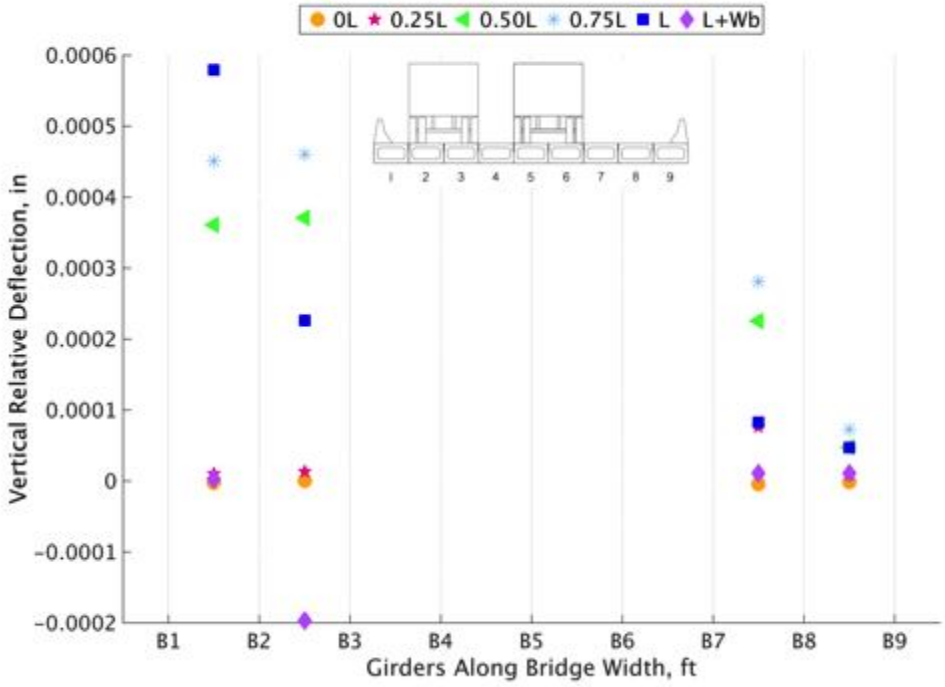

Figure 207. Load case 3 run 3 relative vertical deflection

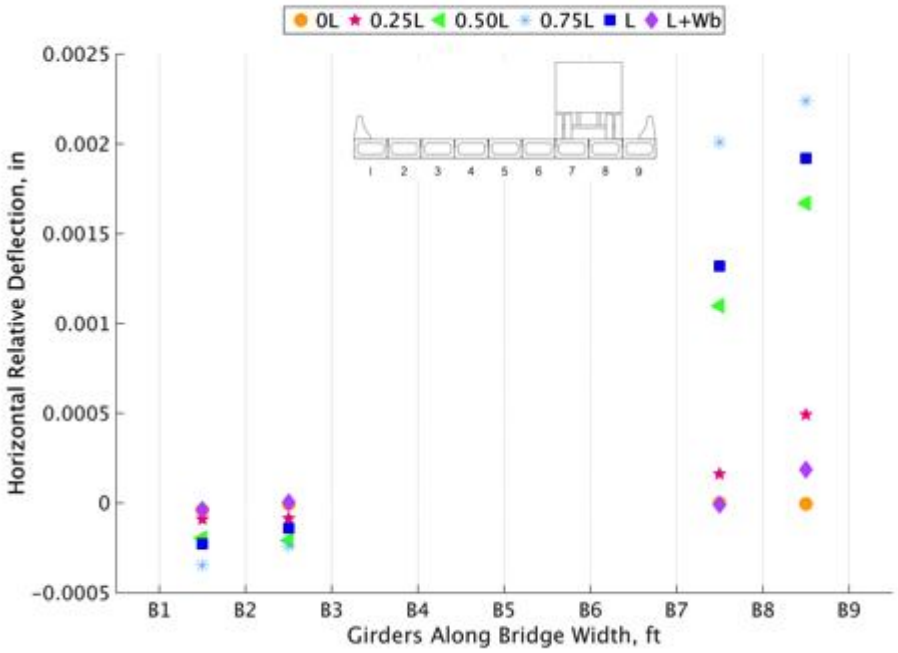

Figure 208. Load case 4 run 1 relative horizontal deflection

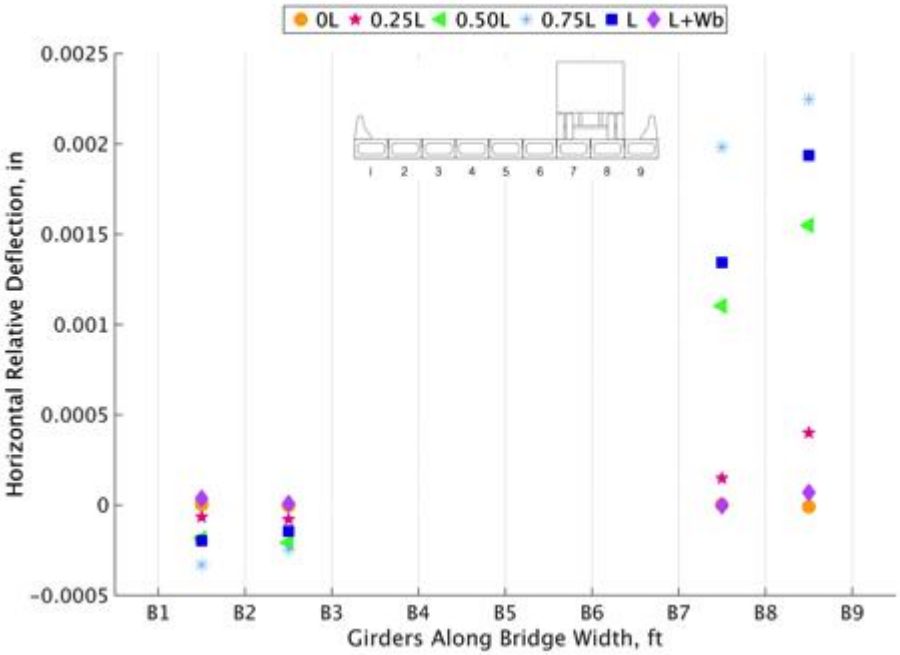

Figure 209. Load case 4 run 2 relative horizontal deflection

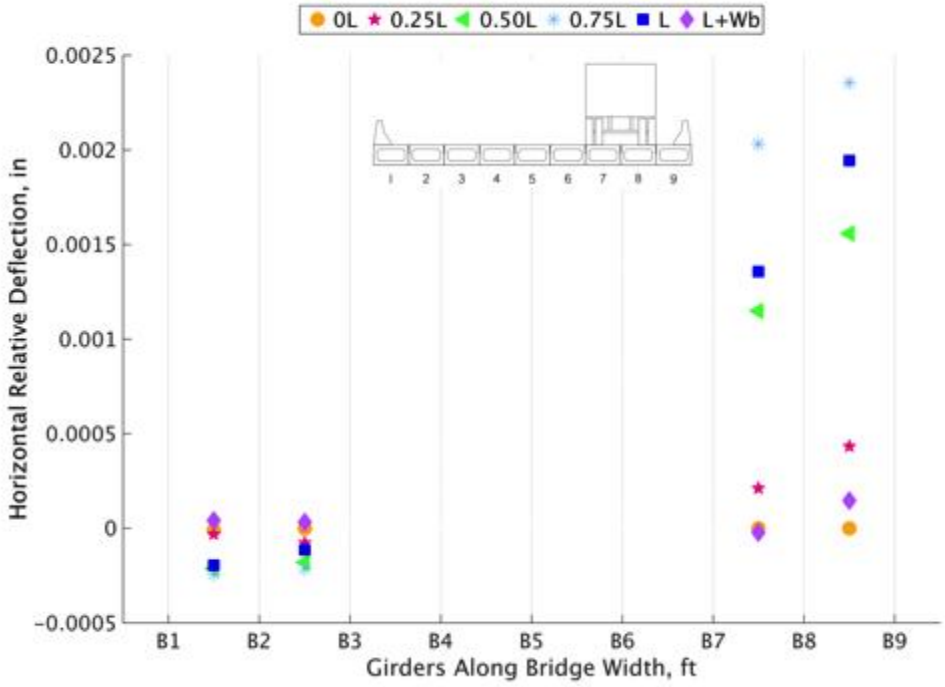

Figure 210. Load case 4 run 3 relative horizontal deflection

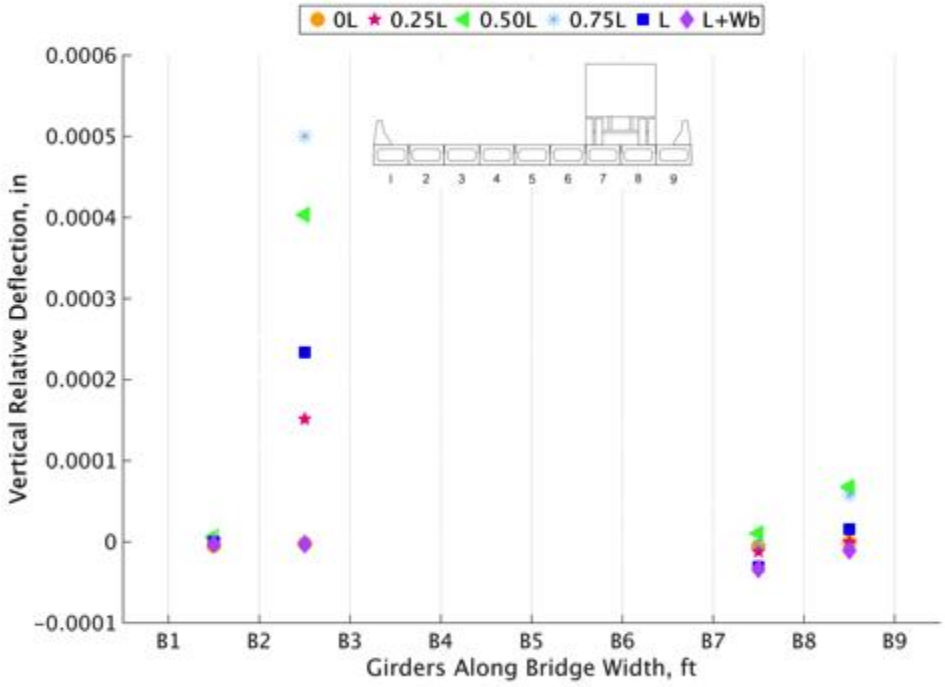

Figure 211. Load case 4 run 1 relative vertical deflection

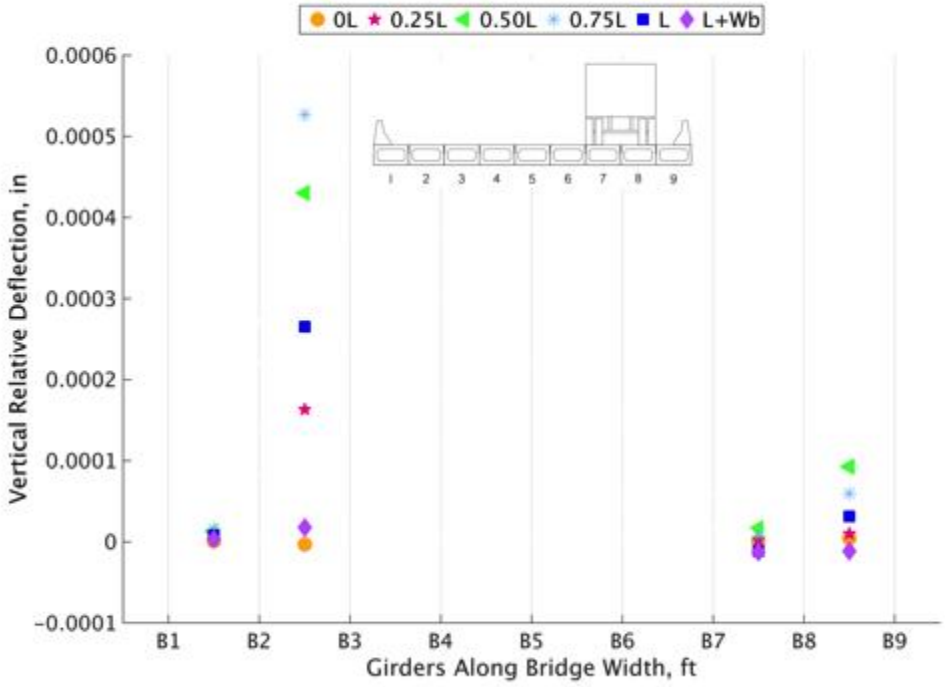

Figure 212. Load case 4 run 2 relative vertical deflection

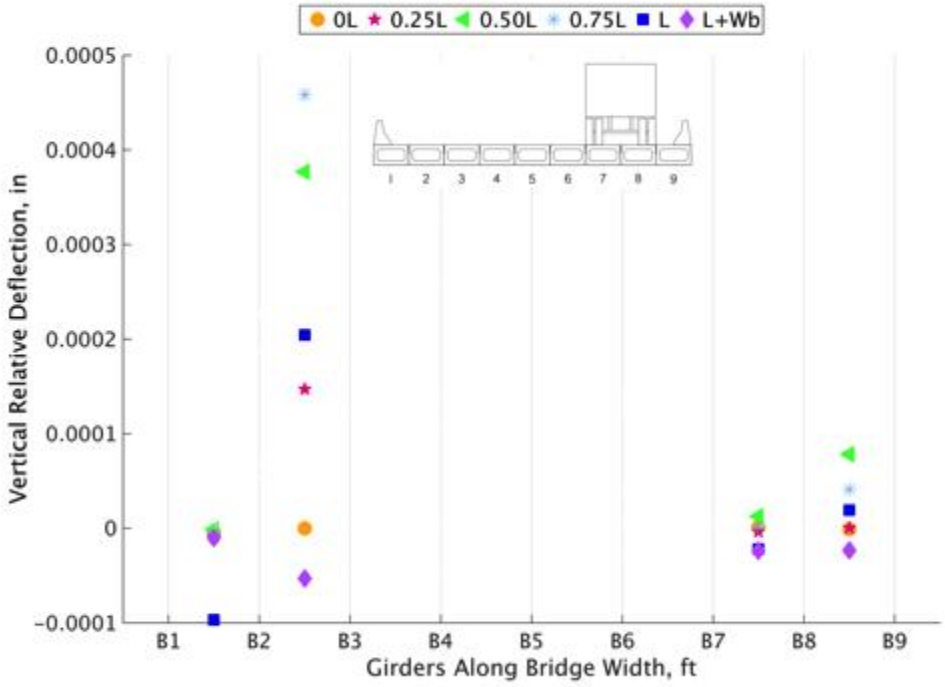

Figure 213. Load case 4 run 3 relative vertical deflection

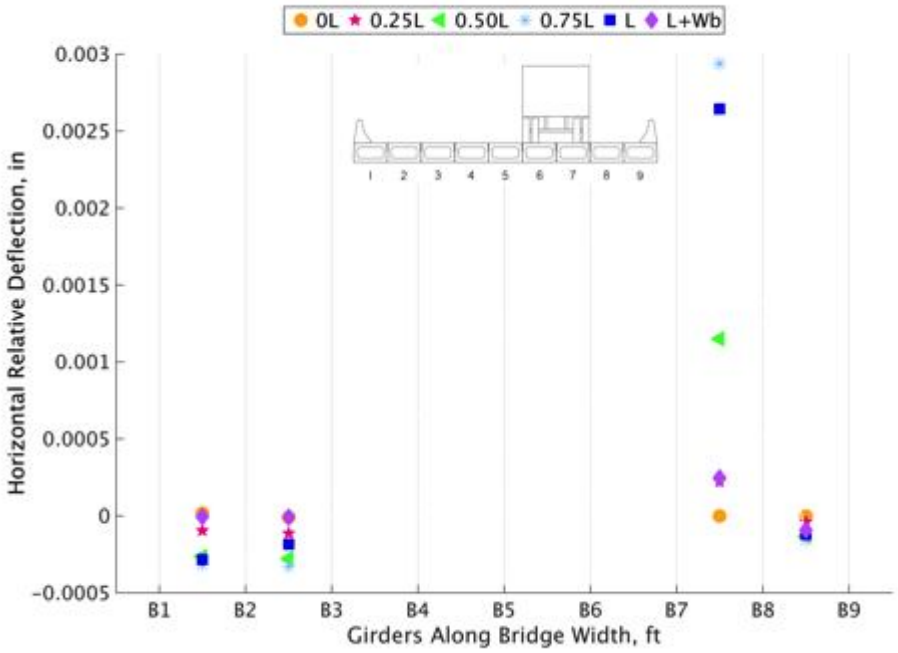

Figure 214. Load case 5 run 1 relative horizontal deflection

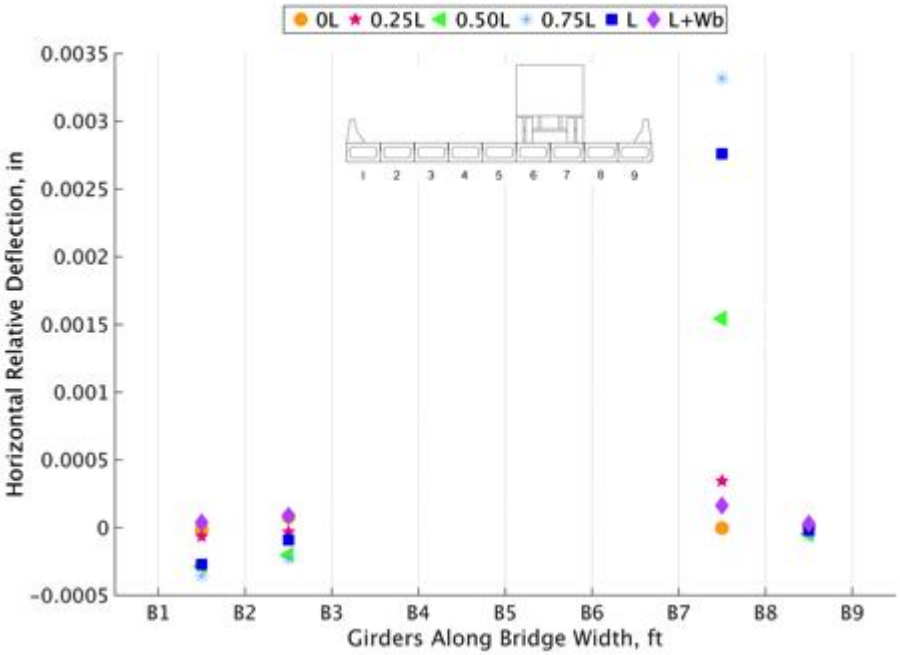

Figure 215. Load case 5 run 2 relative horizontal deflection

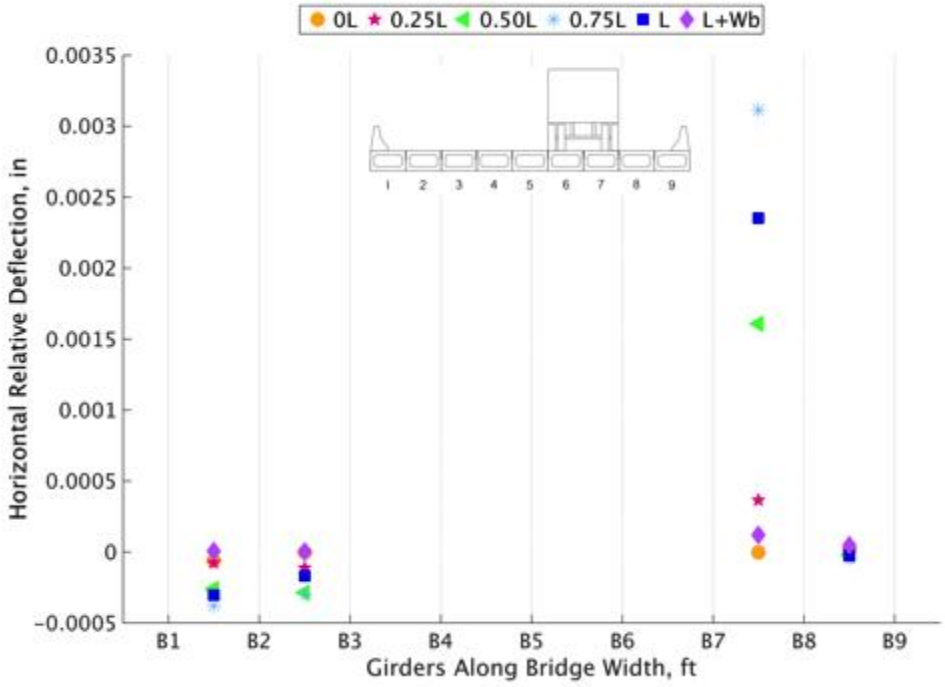

Figure 216. Load case 5 run 3 relative horizontal deflection

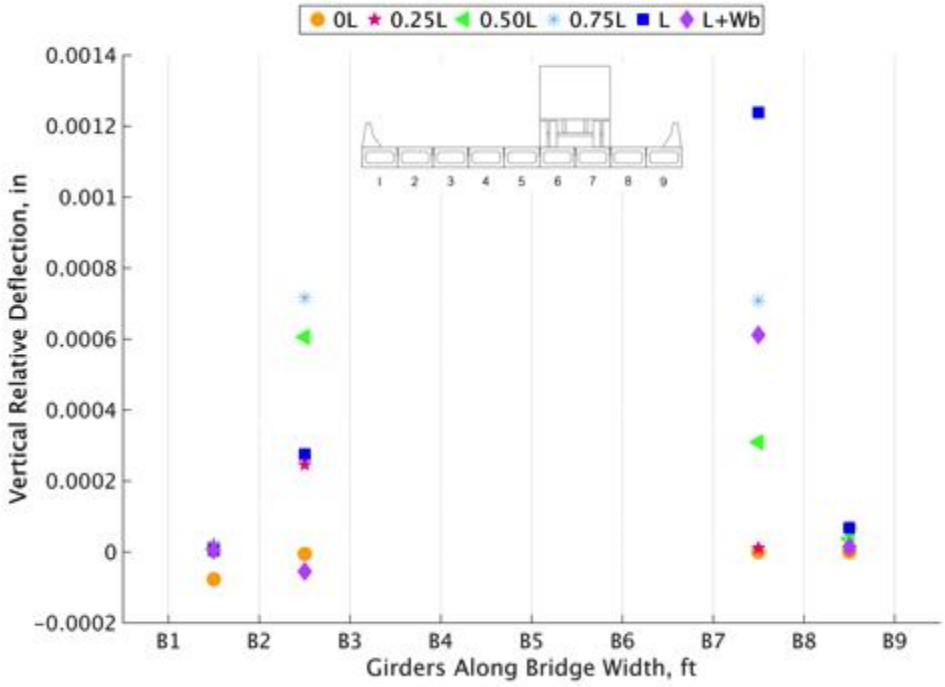

Figure 217. Load case 5 run 1 relative vertical deflection

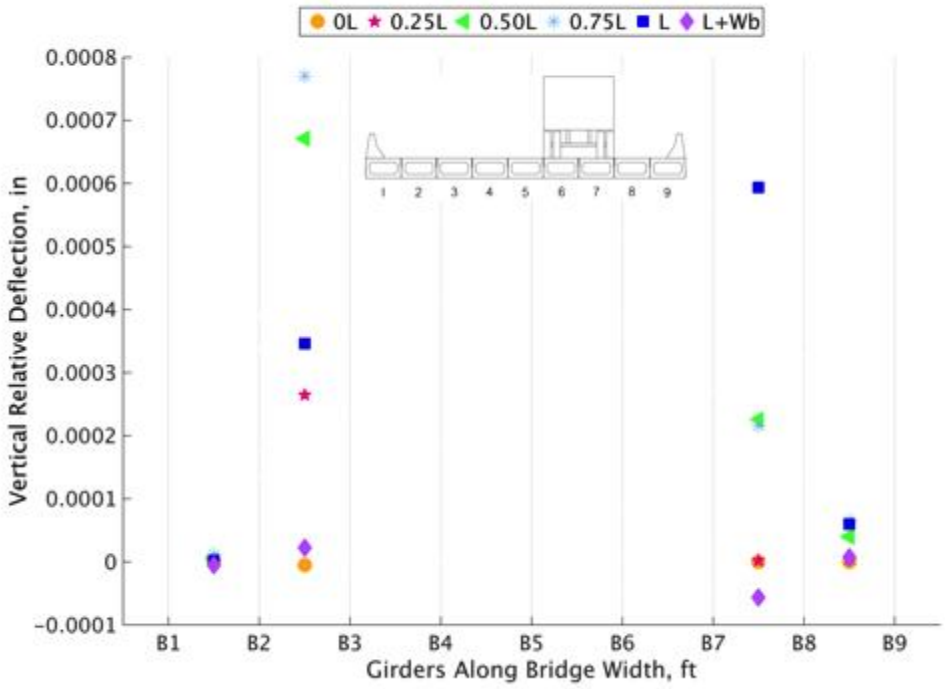

Figure 218. Load case 5 run 2 relative vertical deflection

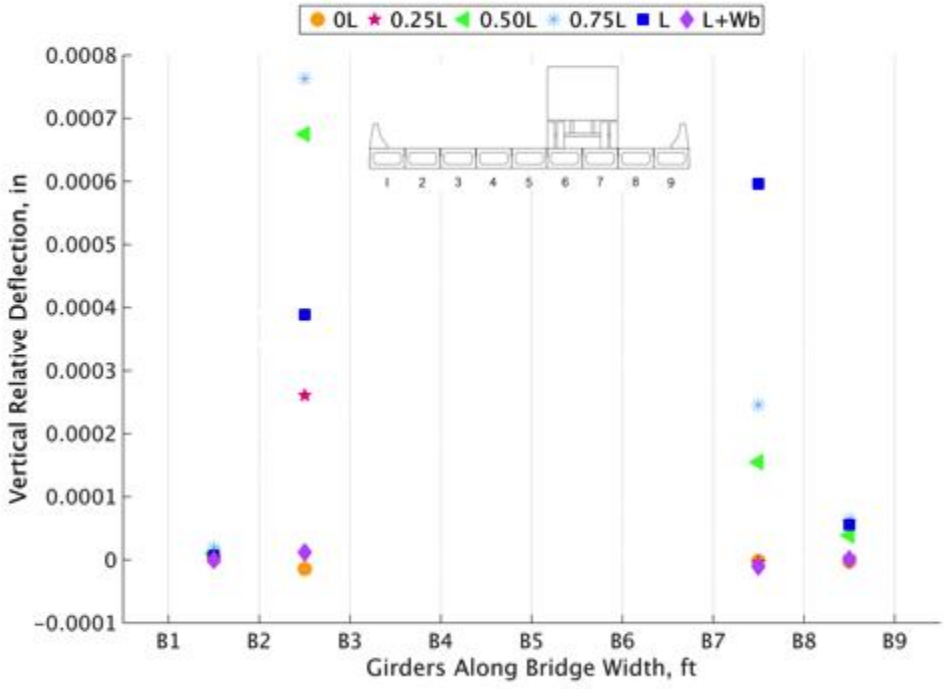

Figure 219. Load case 5 run 3 relative vertical deflection

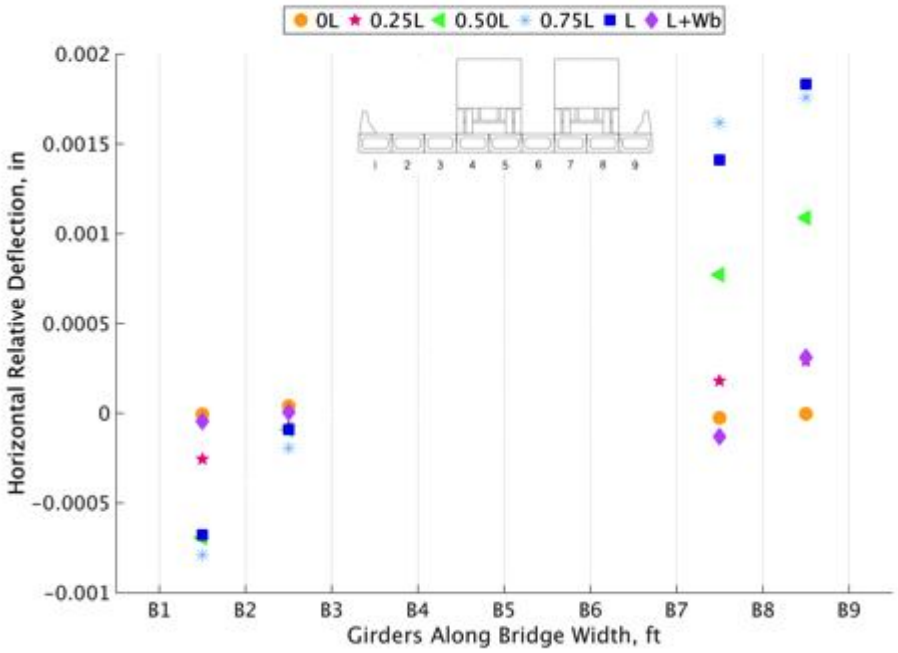

Figure 220. Load case 6 run 1 relative horizontal deflection

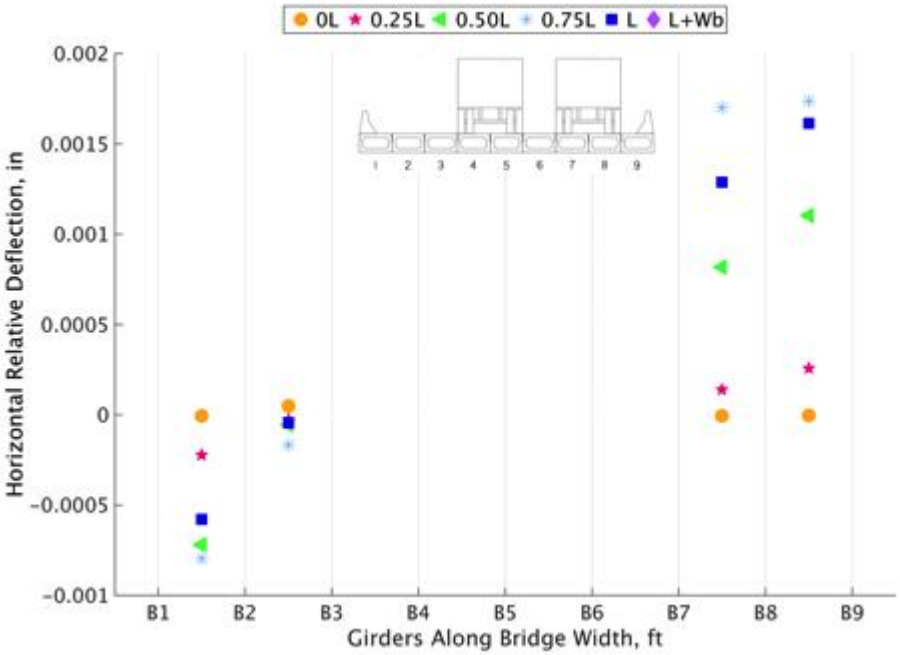

Figure 221. Load case 6 run 2 relative horizontal deflection

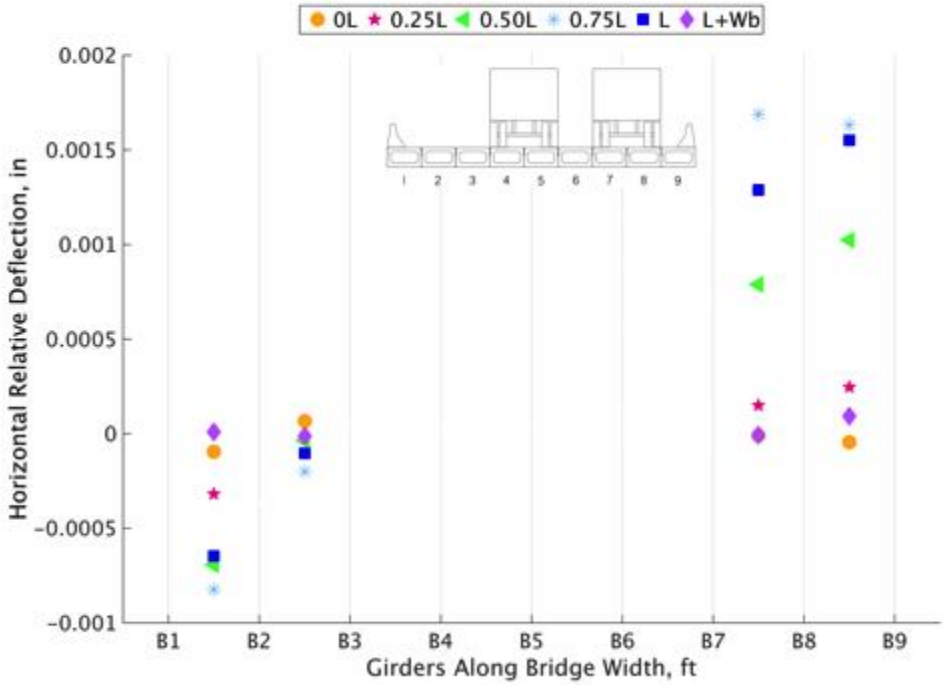

Figure 222. Load case 6 run 3 relative horizontal deflection

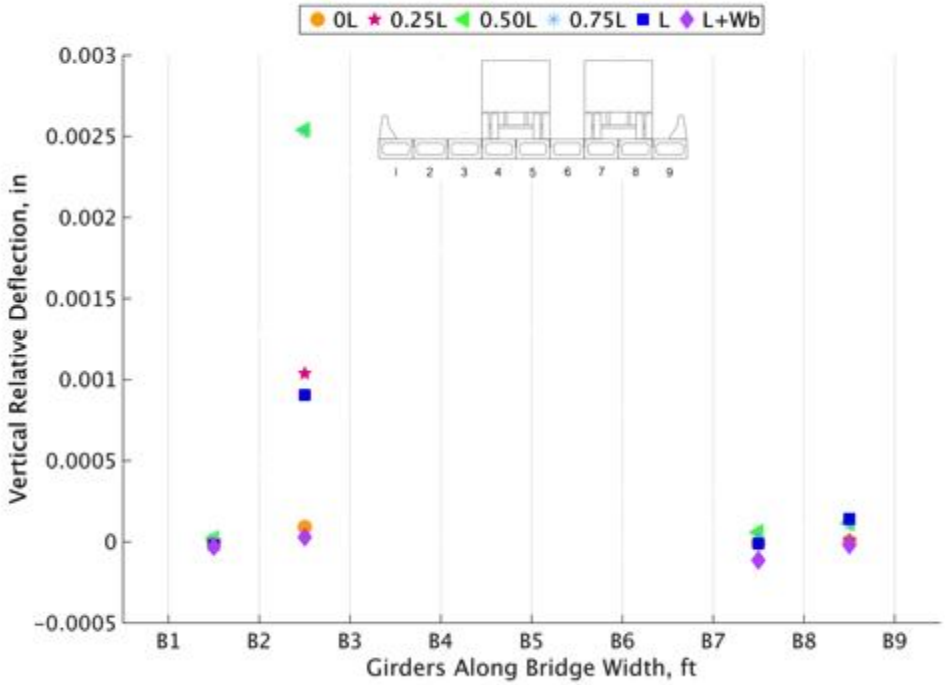

Figure 223. Load case 6 run 1 relative vertical deflection

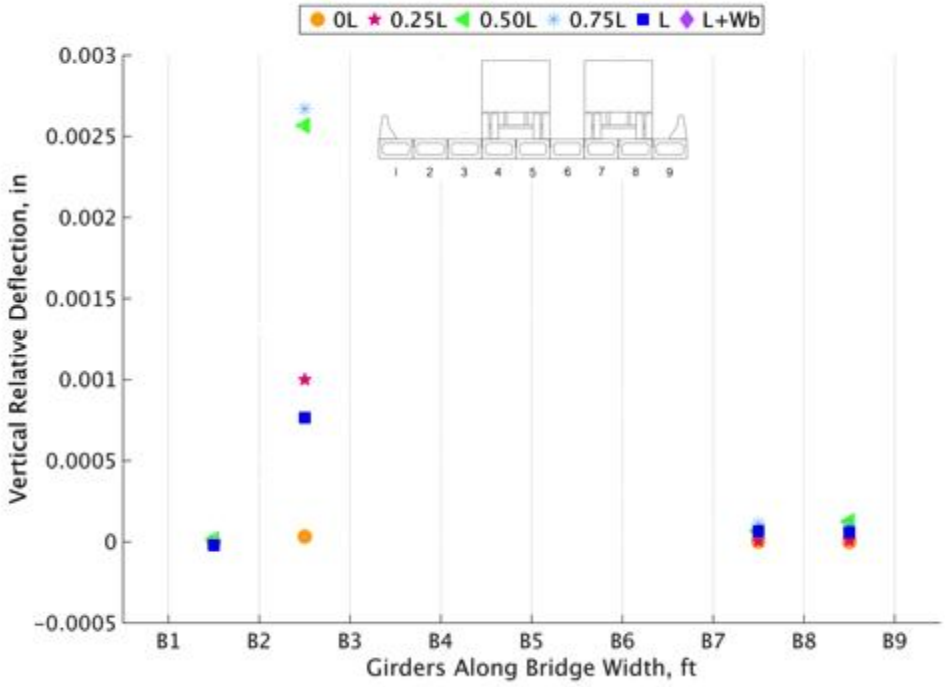

Figure 224. Load case 6 run 2 relative vertical deflection

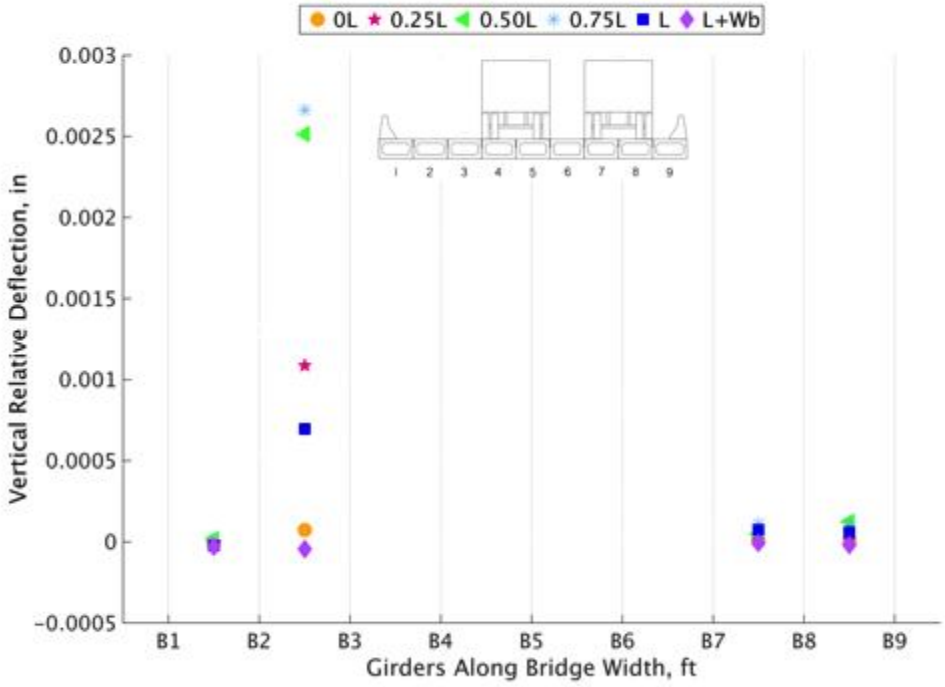

Figure 225. Load case 6 run 3 relative vertical deflection

FEA and Live Load Test Comparison Plots

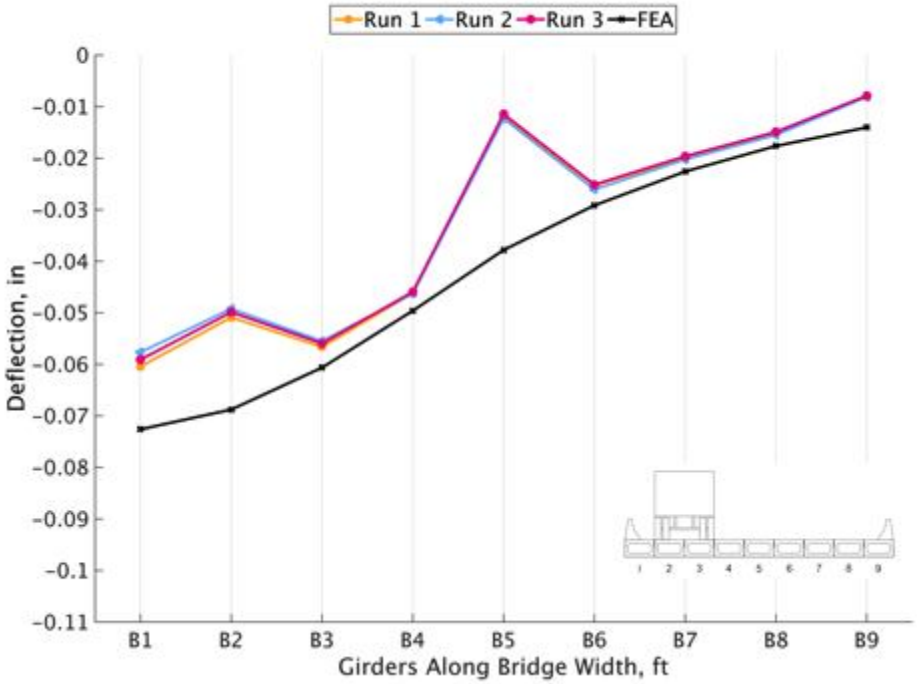

Figure 226. Load 1 deflection comparison

Table 32. Load 1 deflection comparison

	B1	B2	B3	B4	B5	B6	B7	B8	B9
FEA (in)	-0.073	-0.069	-0.061	-0.050	-0.038	-0.029	-0.023	-0.018	-0.014
Run 2 (in)	-0.056	-0.048	-0.055	-0.046	-0.012	-0.026	-0.020	-0.015	-0.007
% Diff.	**27**	**36**	**11**	**8**	**105**	**13**	**13**	**17**	**61**

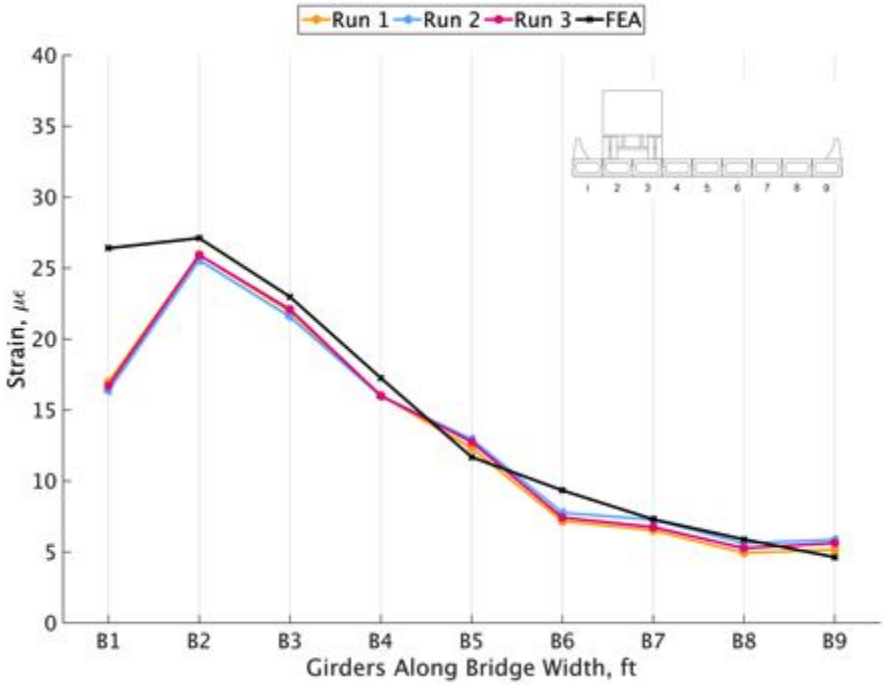

Figure 227. Load 1 strain comparison

Table 33. Load 1 strain comparison

	B1	B2	B3	B4	B5	B6	B7	B8	B9
FEA (με)	26.4	27.1	23.0	17.3	11.7	9.3	7.3	5.9	4.6
Run 3 (με)	15.2	21.6	19.8	15.6	12.7	5.7	6.6	5.1	5.5
% Diff.	**54**	**22**	**15**	**10**	**8**	**48**	**11**	**15**	**17**

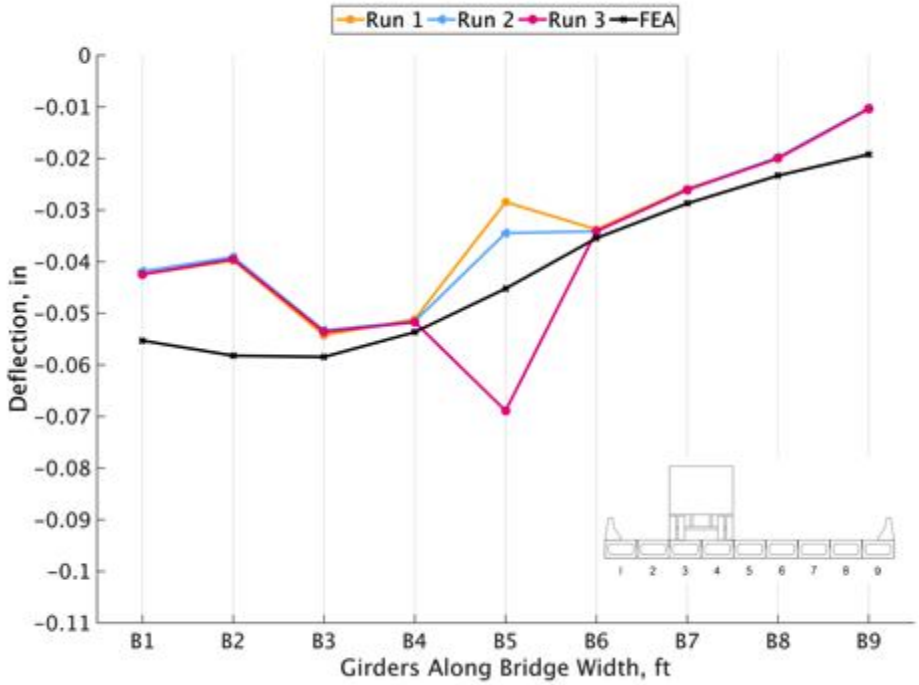

Figure 228. Load 2 deflection comparison

Table 34. Load 2 deflection comparison

	B1	B2	B3	B4	B5	B6	B7	B8	B9
FEA (in)	-0.055	-0.058	-0.058	-0.054	-0.045	-0.035	-0.029	-0.023	-0.019
Run 2 (in)	-0.039	-0.037	-0.050	-0.050	-0.032	-0.033	-0.026	-0.019	-0.010
% Diff.	**35**	**44**	**15**	**8**	**33**	**6**	**12**	**19**	**64**

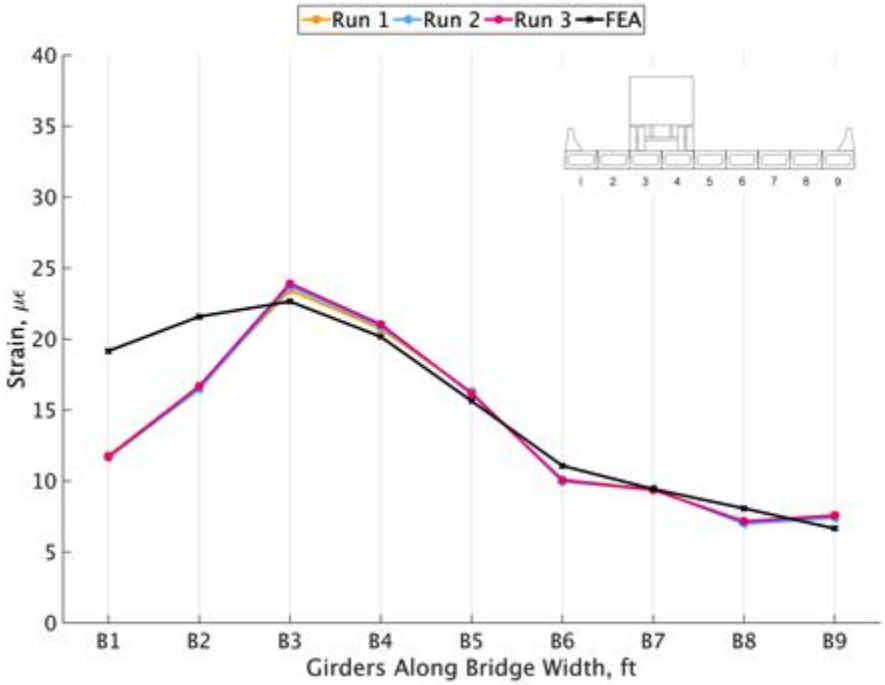

Figure 229. Load 2 strain comparison

Table 35. Load 2 strain comparison

	B1	B2	B3	B4	B5	B6	B7	B8	B9
FEA (με)	19.2	21.6	22.6	20.2	15.6	11.1	9.4	8.1	6.7
Run 3 (με)	10.9	15.0	17.5	17.5	15.4	9.9	9.1	6.8	7.4
% Diff.	**55**	**36**	**26**	**14**	**2**	**11**	**4**	**17**	**10**

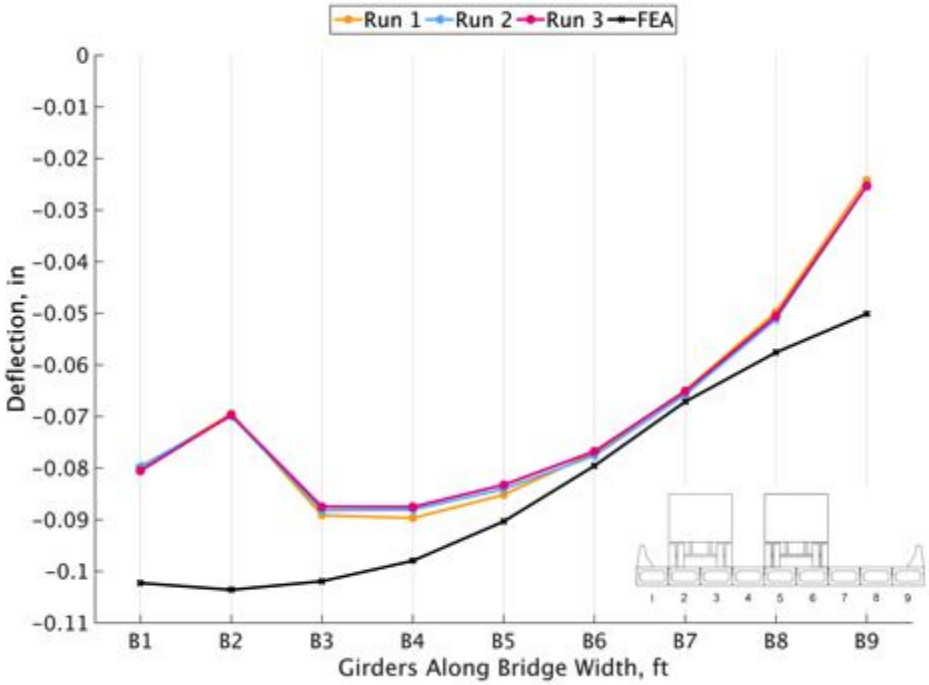

Figure 230. Load 3 deflection comparison

Table 36. Load 3 deflection comparison

	B1	B2	B3	B4	B5	B6	B7	B8	B9
FEA (in)	-0.102	-0.104	-0.102	-0.098	-0.090	-0.080	-0.067	-0.058	-0.050
Run 3 (in)	-0.079	-0.069	-0.087	-0.087	-0.083	-0.076	-0.064	-0.049	-0.023
% Diff.	**26**	**40**	**16**	**11**	**9**	**5**	**6**	**17**	**73**

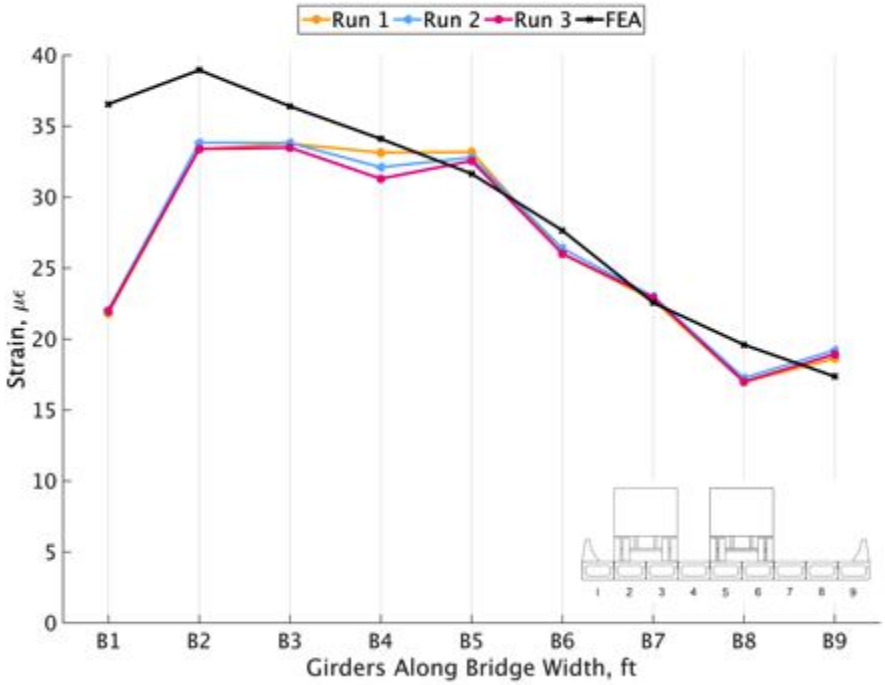

Figure 231. Load 3 strain comparison

Table 37. Load 3 strain comparison

	B1	B2	B3	B4	B5	B6	B7	B8	B9
FEA (με)	36.6	39.0	36.4	34.1	31.7	27.7	22.6	19.6	17.4
Run 3 (με)	20.9	30.0	31.6	31.2	32.5	25.9	21.0	15.9	17.6
% Diff.	**55**	**26**	**14**	**9**	**3**	**7**	**7**	**21**	**1**

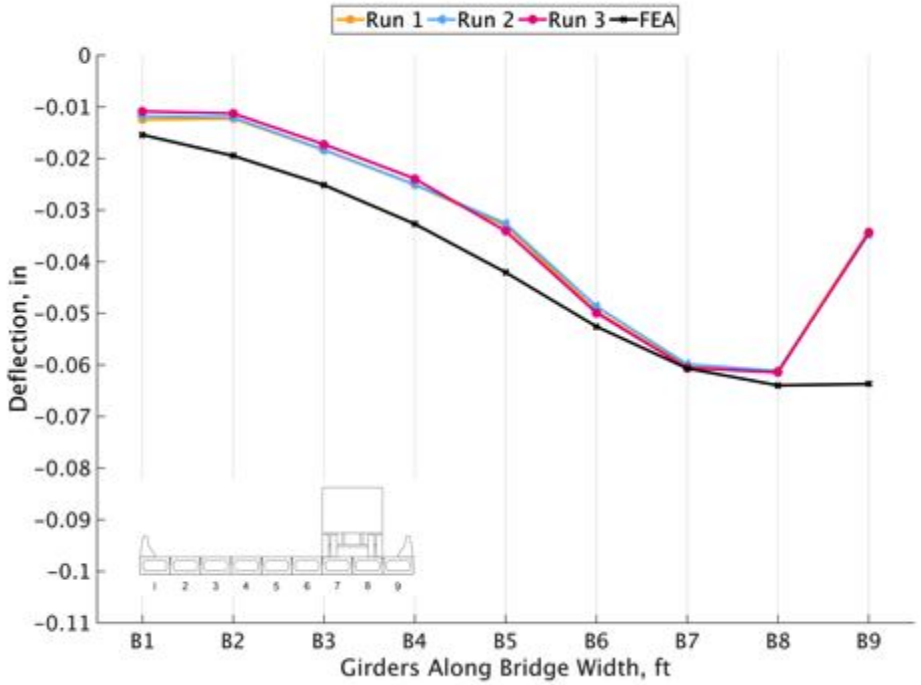

Figure 232. Load 4 deflection comparison

Table 38. Load 4 deflection comparison

	B1	B2	B3	B4	B5	B6	B7	B8	B9
FEA, in.	-0.015	-0.019	-0.025	-0.033	-0.042	-0.053	-0.061	-0.064	-0.064
Run 1, in.	-0.012	-0.012	-0.018	-0.025	-0.033	-0.050	-0.060	-0.060	-0.034
% Diff.	**22**	**45**	**31**	**27**	**24**	**6**	**1**	**6**	**62**

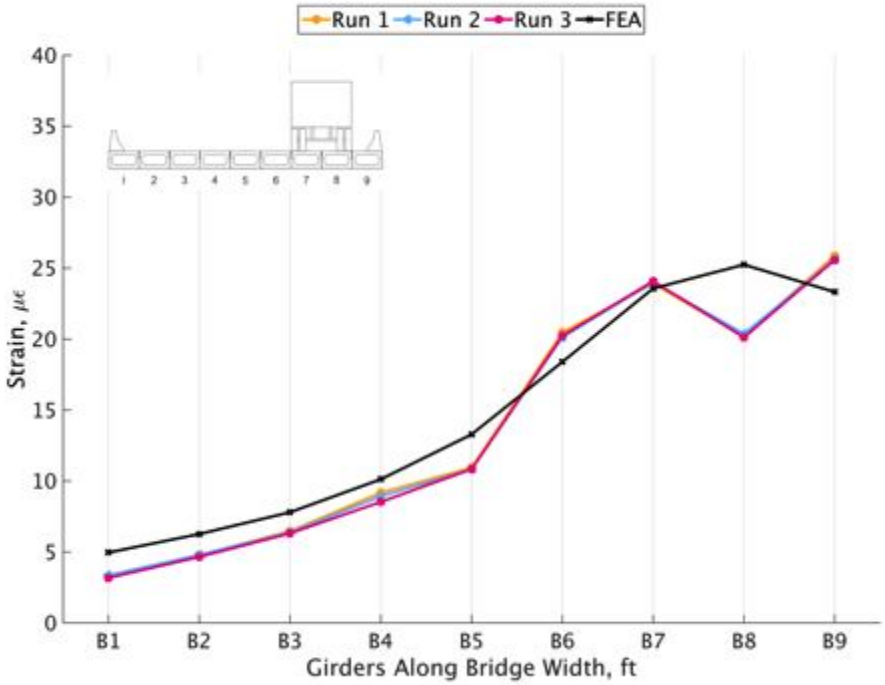

Figure 233. Load 4 strain comparison

Table 39. Load 4 strain comparison

	B1	B2	B3	B4	B5	B6	B7	B8	B9
FEA, με	5.0	6.3	7.8	10.1	13.3	18.4	23.6	25.2	23.3
Run 2, με	3.1	4.6	6.1	8.6	10.7	19.7	21.2	16.4	21.9
% Diff.	**45**	**30**	**24**	**16**	**22**	**7**	**11**	**42**	**6**

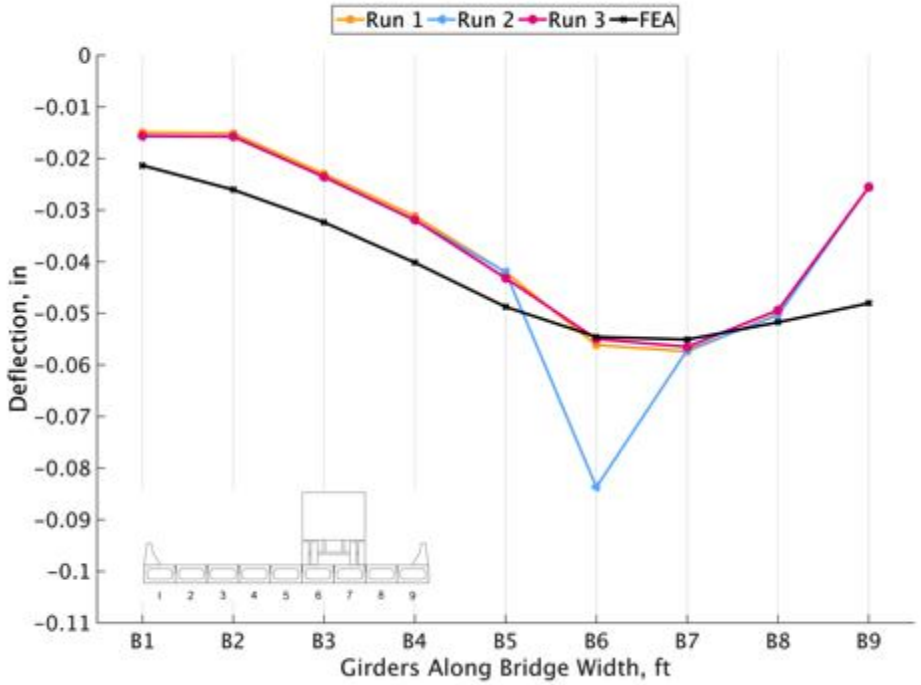

Figure 234. Load 5 deflection comparison

Table 40. Load 5 deflection comparison

	B1	B2	B3	B4	B5	B6	B7	B8	B9
FEA (in)	-0.021	-0.026	-0.032	-0.040	-0.049	-0.055	-0.055	-0.052	-0.048
Run 3 (in)	-0.015	-0.015	-0.023	-0.031	-0.042	-0.054	-0.055	-0.048	-0.025
% Diff.	**35**	**52**	**34**	**25**	**14**	**1**	**0**	**7**	**65**

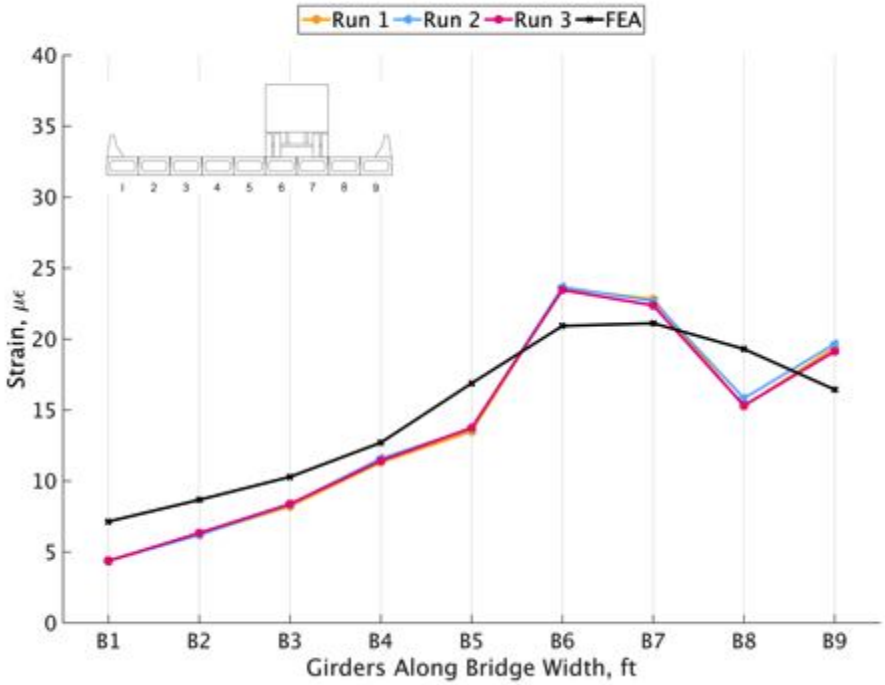

Figure 235. Load 5 strain comparison

Table 41. Load 5 strain comparison

	B1	B2	B3	B4	B5	B6	B7	B8	B9
FEA (με)	7.1	8.7	10.3	12.7	16.9	20.9	21.1	19.3	16.4
Run 2 (με)	4.1	6.0	8.1	11.3	13.6	20.0	17.2	14.0	18.5
% Diff.	**55**	**36**	**24**	**12**	**22**	**4**	**20**	**32**	**12**

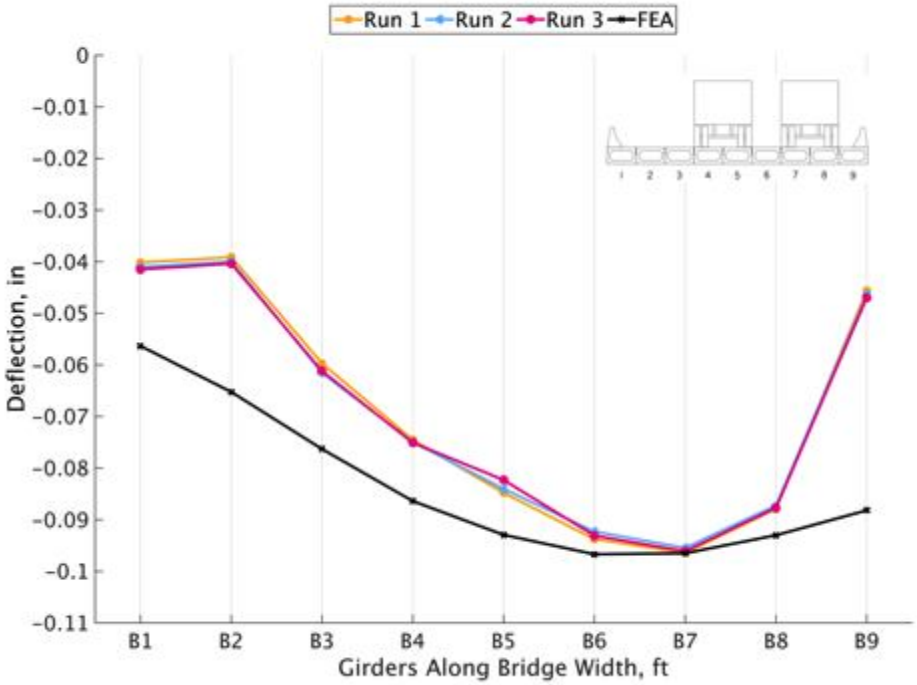

Figure 236. Load 6 deflection comparison

Table 42. Load 6 deflection comparison

	B1	B2	B3	B4	B5	B6	B7	B8	B9
FEA (in)	-0.056	-0.065	-0.076	-0.086	-0.093	-0.097	-0.096	-0.093	-0.088
Run 1 (in)	-0.037	-0.036	-0.055	-0.070	-0.080	-0.093	-0.096	-0.087	-0.045
% Diff.	**41**	**58**	**33**	**20**	**15**	**4**	**0**	**6**	**65**

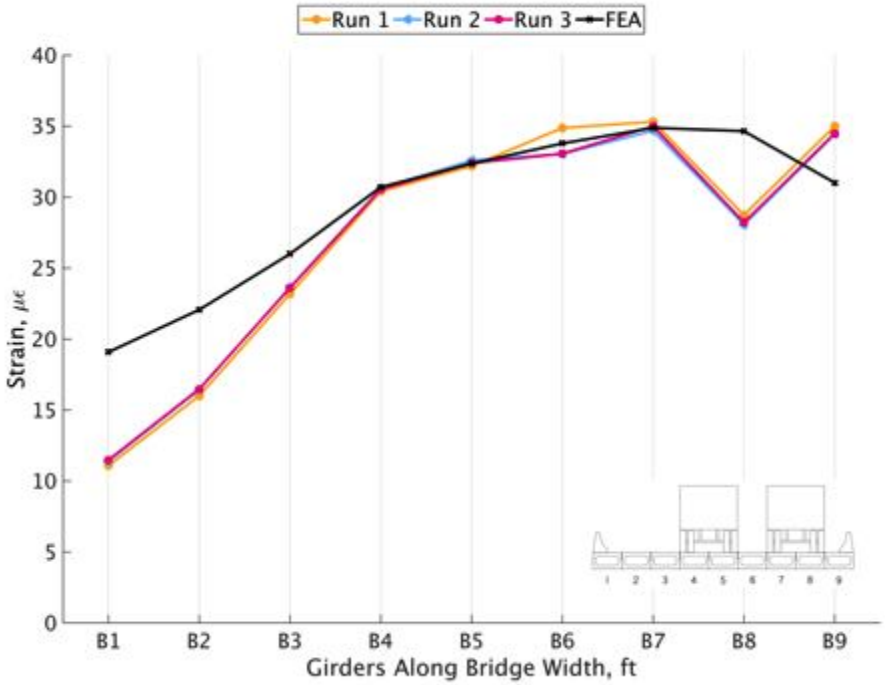

Figure 237. Load 6 strain comparison

Table 43. Load 6 strain comparison

	B1	B2	B3	B4	B5	B6	B7	B8	B9
FEA (με)	19.1	22.1	26.0	30.7	32.4	33.8	34.9	34.7	31.0
Run 1 (με)	10.1	14.6	21.1	28.7	32.1	34.7	33.2	26.1	32.8
% Diff.	**61**	**41**	**21**	**7**	**1**	**3**	**5**	**28**	**6**

Raw Data

Material Properties

Compressive Strength

Table 44. VHPC-Large compressive strength data

Compressive Cylinder Strength (psi)										
VHPC - Large										
Age (days)	**1/13/14**	**2/3/14**	**2/11/14**	**3/31/14**	**5/2/14**	**5/16/14**	**7/10/14**	**7/16/14**	**7/17/14**	**1/28/15**
0.5				1592	5570	4775				

0.5				1512	5968	5173				
0.5				1910	5650					
1				6565	8435	8157	8754	7958	9549	
1				5968	7759	7759	7560	7958	8952	
1				6366	8157		9549	7759	9151	
2				7560	8356	9947				
2				6963	10146	9151				
2					8754					
3				8952	11539	9350				
3				9151	11937	7799				
3				9549	10942	10146				
7		12533	14006	11220	12136	14324	14324	16512	17109	12533
7		12732	13727	10783	12414	14324	16313	11141	16711	12732
7		13329	13727	11738	12335	13926	15319	15120	16711	12335
8	14324									
8	12494									
8	10265									
9	13926									
9	14125									
9	12573									
12				11897						
12				12693						
12				11618						
13						16313				
13						16114				
13						14722				
28		15915		14006	16114	16512				16711
28		16313		14722	15518	17109				14722
28		15319		14404	15120	16313				16512

Table 45. VHPC-Large compressive strength calculations

VHPC - Large					In confidence interval	
Age (days)	**Mean**	**Standard Deviation**	**Sample Size**	**Confidence Interval**	**Min**	**Max**
0.5	4019	1978	8	1371	2648	5390
1	8021	1033	17	491	7530	8512
2	8697	1175	7	871	7826	9567
3	9930	1336	9	873	9057	10802
7	13708	1840	27	694	13014	14402
8	12361	2032	3	2300	10061	14661
9	13541	844	3	955	12586	14497
12	12069	558	3	631	11438	12700

13	15717	867	3	981	14735	16698
28	15687	936	15	474	15213	16161

Table 46. VHPC-Small compressive strength data

Compressive Cylinder Strength (psi)				
VHPC - Small				
Age (days)	**6/16/14**	**7/1/14**	**9/23/14**	**1/28/15**
0.5	6764	8754		
0.5	7361	7560		
0.5	7361	8157		
1	9151	10743	4377	
1	8952	11141	4974	
1	9748	11340	4974	
1			4775	
2	11539	12931	8555	
2	10743	13130	8952	
2	11340	12931	8356	
2			8674	
7	15915	17109		13130
7	16114	16512		14523
7	15717	17507		13926
7				
8				
8				
8				
9				
9				
9				
12				
12				
12				
13				
13				
13				
28				17706
28				14523
28				17109

Table 47. VHPC-Small compressive strength calculations

VHPC - Small					**In confidence interval**

Age (days)	Mean	Standard Deviation	Sample Size	Confidence Interval	Min	Max
0.5	7659	698	6	558	7101	8218
1	8017	2900	10	1797	6220	9815
2	10715	1950	10	1209	9506	11924
7	15606	1466	9	958	14648	16564
28	16446	1692	3	1915	14531	18361

Splitting Tensile Strength

Table 48. VHPC-Large splitting tensile strength data

VHPC - Large							
Age (days)	**1/13/14**	**2/3/14**	**2/11/14**	**3/31/14**	**5/2/14**	**5/16/14**	**1/28/15**
0.5					1243		
0.5					1094		
0.5					1094		
1					1442		
1					1293		
1					1343		
2					1393		
2					1343		
2					1542		
3					1566		
3					1516		
3					1194		
7		1536	1718	2122	1869	1718	1213
7		1741	1566	1540	1940	1667	1194
7		1592	1970	1415	1415		
8							
8							
8							
9	1592						
9	1830						
9	1552						
12							
12							
12							
13						2173	
13						1516	
13						2476	
28				2348	2089		
28		1819		2308	1940	1790	1741

28		1955		1860	1592	1890	1741
28		1855		1741	1592	2387	

Table 49. VHPC-Large splitting tensile strength calculations

VHPC - Large					In confidence interval	
Age (days)	**Mean**	**Standard Deviation**	**Sample Size**	**Confidence Interval**	**Min**	**Max**
0.5	1144	86	3	97	1046	1241
1	1359	76	3	86	1273	1445
2	1426	104	3	117	1309	1543
3	1425	202	3	229	1197	1654
7	1638	261	16	128	1511	1766
9	1658	151	3	170	1487	1828
13	2055	491	3	555	1499	2610
28	1915	249	16	122	1793	2037

Table 50. VHPC-Small splitting tensile strength data

Splitting Tensile Strength (psi)				
VHPC - Small				
Age (days)	**6/16/14**	**7/1/14**	**9/23/14**	**1/28/15**
0.5	945	909		
0.5	895	1094		
0.5		1103		
1	1243	1492		
1	1343	1343		
1		1194		
2	1492	1592		
2	1393	1393		
2		1542		
3				
3				
3				
7	1704	2324		1718
7	1718	2356		1566
7		2089		
8				
8				
8				
9				
9				

9				
12				
12				
12				
13				
13				
13				
28				2089
28				2188
28				

Table 51. VHPC-Small splitting tensile strength calculations

VHPC - Small					**In confidence interval**	
Age (days)	**Mean**	**Standard Deviation**	**Sample Size**	**Confidence Interval**	**Min**	**Max**
0.5	989	101	5	89	901	1078
1	1323	115	5	100	1223	1423
2	1482	89	5	78	1404	1560
7	1925	325	7	241	1684	2166
28	2139	70	2	97	2041	2236

Modulus of Elasticity

Table 52. VHPC-Large modulus data

Modulus (psi)							
VHPC - Large							
Age (days)	1/13/14	2/3/14	2/11/14	3/31/14	5/2/14	5/16/14	1/28/15
0.5					4070		
0.5					5269		
0.5					3755		
1					4736		
1					3677		
1					5108		
2					5292		
2					4793		
2					5246		
3					5014		
3					4453		
3					5813		
7		5316	5137	4576	4905	5193	5597

7		5784	5393	4459	4683	4842	5548
7		6156	5210	5023	4678	5963	
8	5481						
8	5404						
8	5435						
9	5509						
9	5878						
9	5653						
12				5042			
12				4634			
12				4678			
13						5569	
13						5402	
13						5735	
28		5862		5324	5283	5718	5811
28		6259		4823	5354	5661	5880
28		6275		4758	5295	5328	

Table 53. VHPC-Large modulus calculations

VHPC - Large					**In confidence interval**	
Age (days)	**Mean**	**Standard Deviation**	**Sample Size**	**Confidence Interval**	**Min**	**Max**
0.5	4365	799	3	904	3461	5269
1	4507	742	3	840	3667	5347
2	5110	276	3	312	4798	5422
3	5093	684	3	773	4320	5867
7	5204	493	17	235	4969	5438
8	5440	39	3	44	5396	5484
9	5680	186	3	211	5469	5891
12	4785	224	3	253	4531	5038
13	5569	166	3	188	5380	5757
28	5545	462	14	242	5303	5787

Table 54. VHPC-Small modulus data

Modulus (psi)				
VHPC - Small				
Age (days)	**6/16/14**	**7/1/14**	**9/23/14**	**1/28/15**
0.5	5151	4922		
0.5	4442	4735		
0.5	4331	5347		
1	5218	5291		

1	5237	5755		
1	5669	5567		
2	5645	4363		
2	5529	6082		
2	5442	5643		
3				
3				
3				
7	6172	5819		5881
7	5680	6320		6456
7	5799	6049		
8				
8				
8				
9				
9				
9				
12				
12				
12				
13				
13				
13				
28				6405
28				6257
28				

Table 55. VHPC-Small modulus calculations

VHPC - Small					**In confidence interval**	
Age (days)	**Mean**	**Standard Deviation**	**Sample Size**	**Confidence Interval**	**Min**	**Max**
0.5	4821	397	6	317	4504	5139
1	5456	236	6	189	5267	5645
2	5451	577	6	462	4989	5912
7	6022	275	8	190	5832	6212
28	6331	105	2	145	6186	6476

Shrinkage

Table 56. Internal shrinkage

Age	UHPC	VHPC - Small	VHPC - Large	A4
1	0	0	0	0
2	323	156	90	98
3	369	262	163	116
4	387	319	239	178
5	436	373	255	234
6	495	428	317	237
7	511	462	354	246
9	538	505	387	284
12	556	536	422	332
14	587	560	453	332
16	640	634	490	356
28	698	662	561	412
37	736	708	615	450
44	716	693	597	418
51	738	707	616	424
68	776	735	659	430
92	779	757	673	436

Table 57. External shrinkage

Age	A4 - Surface	Grout
1	0	0
2	26	176
3	84	356
4	120	494
5	142	579
6	164	664
7	185	724
9	228	843
12	240	946
14	278	1033
16	292	1093
28	349	1347
37	360	1456
44	354	1487
51	369	1559
68	390	1673

92	393	1680

Table 58. Shrinkage comparison

Age	A4 - Surface	A4
1	0	0
2	26	98
3	84	116
4	120	178
5	142	234
6	164	237
7	185	246
9	228	284
12	240	332
14	278	332
16	292	356
28	349	412
37	360	450
44	354	418
51	369	424
68	390	430
92	393	436

Freeze/Thaw Bar Weight

Table 59. Freeze/thaw weight

Mat.	Beam	2/25/15	3/9/15	3/19/15	3/31/15	4/10/15	4/21/15	5/1/15	5/14/15	5/27/15	6/5/15
		0	**36**	**68**	**110**	**143**	**177**	**214**	**259**	**289**	**306**
UHPC	**A**	17.74	17.76	17.76	17.76	17.78	17.76	17.76	17.76	17.76	17.76
	B	17.56	17.60	17.60	17.60	17.60	17.60	17.60	17.60	17.60	17.60
	C	17.64	17.68	17.68	17.68	17.66	17.68	17.68	17.66	17.68	17.66
VHPC - Small	**A**	16.76	16.78	16.78	16.78	16.78	16.78	16.78	16.78	16.78	16.78
	B	16.92	16.94	16.96	16.96	16.96	16.96	16.96	16.98	16.96	16.96
	C	16.82	16.84	16.84	16.86	16.84	16.84	16.84	16.84	16.86	16.84
VHPC - Large	**A**	16.30	16.30	16.30	16.32	16.30	16.30	16.32	16.32	16.32	16.32
	B	16.26	16.26	16.26	16.26	16.26	16.28	16.28	16.28	16.28	16.28
	C	16.42	16.44	16.46	16.46	16.46	16.46	16.46	16.44	16.44	16.44
A4	**A**	16.80	16.96	17.02	17.04	17.04	17.04	17.02	17.00	17.00	16.98

	B	16.66	16.82	16.84	16.86	16.86	16.86	16.86	16.82	16.82	16.82
	C	16.28	16.46	16.50	16.52	16.52	16.50	16.50	16.48	16.48	16.48
Grout	**A**	14.96	15.34	15.42	15.46	15.46	15.46	15.42	15.36	15.34	15.32
	B	14.78	15.22	15.28	15.30	15.30	15.30	15.22	15.14	15.08	15.04
	C	14.78	15.18	15.26	15.30	15.32	15.30	15.26	15.20	15.18	15.16

Resonance Frequency

Table 60. Resonance frequency data

Mat.		**2/25/15**	**3/9/15**	**3/19/15**	**3/31/15**	**4/10/15**	**4/21/15**	**5/1/15**	**5/14/15**	**5/27/15**	**6/5/15**
		0	**36**	**68**	**110**	**143**	**177**	**214**	**259**	**289**	**306**
UHPC	**A**	746.5	735.7	729.4	734.3	724.1	722.5	721.4	725.2	717.8	708.5
	B	744.4	738.7	735.2	740.7	725.4	723.7	732.0	729.4	722.2	714.1
	C	747.6	740.6	738.3	741.7	722.8	726.2	732.3	726.3	719.6	713.3
VHPC - Small	**A**	745.3	738.6	737.8	742.6	724.4	726.9	733.0	726.5	722.2	714.9
	B	747.2	789.1	740.1	738.1	722.9	726.1	732.8	726.6	719.8	714.9
	C	744.0	741.7	739.8	742.1	726.6	722.3	730.9	732.8	721.4	717.6
VHPC - Large	**A**	734.6	736.6	736.2	745.8	725.6	724.3	734.5	726.5	721.7	715.6
	B	735.5	738.0	735.8	745.7	721.9	725.6	733.3	727.1	723.4	713.2
	C	736.2	739.0	739.4	739.3	726.7	727.2	733.3	729.3	719.9	717.0
A4	**A**	488.9	499.1	494.6	501.0	491.5	490.8	493.4	489.4	486.0	482.8
	B	504.5	499.1	494.8	499.1	491.6	490.6	493.5	492.8	487.9	482.6
	C	504.4	497.7	498.5	500.4	490.3	492.0	494.2	493.4	486.0	480.7
Grout	**A**	504.4	499.2	496.0	498.7	490.0	489.2	493.8	490.4	487.1	483.8
	B	500.3	498.9	493.7	498.2	491.2	489.9	493.1	491.1	485.1	480.9
	C	504.0	498.4	497.0	500.4	489.7	490.7	494.7	493.3	484.4	480.4

BBB Data

Midspan Deflections

Table 61. Load case 1 deflection

	Load Case 1									
	Beam	**1**	**2**	**3**	**4**	**5**	**6**	**7**	**8**	**9**
FEA	0	0.000	0.000	0.000	0.000	0.000	0.000	0.000	0.000	0.000
	0.25	-0.016	-0.016	-0.016	-0.015	-0.012	-0.010	-0.008	-0.006	-0.005
	0.5	-0.056	-0.056	-0.052	-0.046	-0.037	-0.029	-0.023	-0.018	-0.014
	0.75	-0.073	-0.069	-0.061	-0.050	-0.038	-0.028	-0.021	-0.016	-0.012
	1	-0.042	-0.037	-0.031	-0.024	-0.018	-0.013	-0.009	-0.007	-0.005
	1.25	0.000	0.000	0.000	0.000	0.000	0.000	0.000	0.000	0.000
	Beam	**1**	**2**	**3**	**4**	**5**	**6**	**7**	**8**	**9**
Test result	0	-0.001	-0.001	-0.001	-0.002	-0.001	-0.001	-0.001	-0.001	0.000
	0.25	-0.010	-0.009	-0.011	-0.010	-0.004	-0.007	-0.005	-0.004	-0.002
	0.5	-0.027	-0.025	-0.030	-0.026	-0.008	-0.016	-0.013	-0.010	-0.005
	0.75	-0.056	-0.048	-0.055	-0.046	-0.012	-0.026	-0.020	-0.015	-0.007
	1	-0.047	-0.038	-0.041	-0.032	-0.007	-0.016	-0.013	-0.009	-0.005
	1.25	0.000	0.000	0.000	0.000	0.000	0.001	0.000	0.000	0.000
	Beam	**1**	**2**	**3**	**4**	**5**	**6**	**7**	**8**	**9**
Diff. (%)	0	-200.0	-200.0	-200.0	-200.0	-200.0	-200.0	-200.0	-200.0	-200.0
	0.25	47.4	55.5	37.6	36.7	100.0	36.6	39.0	39.9	66.7
	0.5	68.9	75.4	54.7	53.3	131.7	57.2	57.4	58.6	92.4
	0.75	26.6	35.8	10.6	7.9	105.2	9.8	6.4	6.9	47.6
	1	-10.6	-3.1	-29.3	-30.8	84.6	-25.0	-31.3	-30.9	8.1
	1.25	-200.0	-200.0	-200.0	-200.0	-200.0	-200.0	-200.0	-200.0	-200.0
	Beam	**1**	**2**	**3**	**4**	**5**	**6**	**7**	**8**	**9**
FEA	Min	-0.073	-0.069	-0.061	-0.050	-0.038	-0.029	-0.023	-0.018	-0.014
Test Result	Min	-0.056	-0.048	-0.055	-0.046	-0.012	-0.026	-0.020	-0.015	-0.007
Difference (%)			27	36	11	8	105	13	13	17

Table 62. Load case 2 deflection

	Load									

	Case 2									
	Beam	**1**	**2**	**3**	**4**	**5**	**6**	**7**	**8**	**9**
FEA	0	0	0	0	0	0	0	0	0	0
	0.25	-0.011	-0.013	-0.014	-0.014	-0.013	-0.012	-0.010	-0.008	-0.007
	0.5	-0.041	-0.045	-0.048	-0.046	-0.042	-0.035	-0.029	-0.023	-0.019
	0.75	-0.055	-0.058	-0.058	-0.054	-0.045	-0.035	-0.027	-0.021	-0.017
	1	-0.034	-0.033	-0.031	-0.027	-0.021	-0.016	-0.012	-0.009	-0.007
	1.25	0	0	0	0	0	0	0	0	0
	Beam	**1**	**2**	**3**	**4**	**5**	**6**	**7**	**8**	**9**
Test result	0	-0.001	-0.001	-0.001	-0.001	0.003	-0.002	-0.001	-0.001	0.000
	0.25	-0.007	-0.007	-0.009	-0.010	-0.004	-0.008	-0.006	-0.005	-0.003
	0.5	-0.021	-0.021	-0.029	-0.030	-0.021	-0.022	-0.017	-0.013	-0.007
	0.75	-0.039	-0.037	-0.050	-0.050	-0.032	-0.033	-0.026	-0.019	-0.010
	1	-0.034	-0.031	-0.042	-0.039	-0.020	-0.023	-0.016	-0.012	-0.005
	1.25	0.000	0.000	-0.001	-0.001	0.008	0.000	0.000	0.001	0.000
	Beam	**1**	**2**	**3**	**4**	**5**	**6**	**7**	**8**	**9**
Diff. (%)	0	-200.0	-200.0	-200.0	-200.0	-200.0	-200.0	-200.0	-200.0	-200.0
	0.25	53.2	62.8	40.0	37.2	108.2	33.7	41.7	43.0	82.3
	0.5	63.5	72.5	47.8	42.4	67.0	44.2	49.6	54.0	92.1
	0.75	34.7	43.8	15.1	7.9	32.8	5.7	7.2	10.2	52.6
	1	0.0	6.7	-31.1	-37.6	8.6	-32.1	-27.9	-23.2	25.9
	1.25	-200.0	-200.0	-200.0	-200.0	-200.0	-200.0	-200.0	-200.0	-200.0
	Beam	**1**	**2**	**3**	**4**	**5**	**6**	**7**	**8**	**9**
FEA	MAX	-0.055	-0.058	-0.058	-0.054	-0.045	-0.035	-0.029	-0.023	-0.019
Test Result	MAX	-0.039	-0.037	-0.050	-0.050	-0.032	-0.033	-0.026	-0.019	-0.010
Difference (%)			35	44	15	8	33	6	12	19

Table 63. Load case 3 deflection

	Load Case 3									
	Beam	**1**	**2**	**3**	**4**	**5**	**6**	**7**	**8**	**9**
FEA	0	0	0	0	0	0	0	0	0	0
	0.25	-0.022	-0.023	-0.025	-0.025	-0.025	-0.024	-0.022	-0.019	-0.017
	0.5	-0.076	-0.081	-0.083	-0.084	-0.081	-0.075	-0.066	-0.058	-0.050
	0.75	-0.102	-0.104	-0.102	-0.098	-0.090	-0.080	-0.067	-0.055	-0.046
	1	-0.061	-0.059	-0.056	-0.051	-0.045	-0.038	-0.031	-0.024	-0.019
	1.25	0	0	0	0	0	0	0	0	0

	Beam	**1**	**2**	**3**	**4**	**5**	**6**	**7**	**8**	**9**
Test result	0	-0.001	-0.001	-0.001	-0.002	-0.002	-0.003	-0.003	-0.003	-0.002
	0.25	-0.015	-0.014	-0.019	-0.021	-0.022	-0.022	-0.020	-0.017	-0.009
	0.5	-0.051	-0.048	-0.062	-0.066	-0.066	-0.063	-0.056	-0.045	-0.023
	0.75	-0.079	-0.069	-0.087	-0.087	-0.083	-0.076	-0.064	-0.049	-0.023
	1	-0.063	-0.053	-0.063	-0.060	-0.053	-0.046	-0.037	-0.027	-0.013
	1.25	0.000	0.000	0.000	0.000	-0.001	-0.001	0.000	0.001	0.000
	Beam	**1**	**2**	**3**	**4**	**5**	**6**	**7**	**8**	**9**
Diff. (%)	0	-200.0	-200.0	-200.0	-200.0	-200.0	-200.0	-200.0	-200.0	-200.0
	0.25	35.5	47.2	27.4	19.7	11.8	6.3	8.4	12.5	62.3
	0.5	39.3	51.9	29.1	24.2	20.2	16.4	17.5	24.8	75.2
	0.75	25.7	39.9	15.6	11.5	8.5	4.8	5.5	12.3	64.6
	1	-2.7	11.4	-12.6	-16.0	-16.4	-20.2	-18.0	-11.5	42.8
	1.25	-200.0	-200.0	-200.0	-200.0	-200.0	-200.0	-200.0	-200.0	-200.0
	Beam	**1**	**2**	**3**	**4**	**5**	**6**	**7**	**8**	**9**
FEA	MAX	-0.102	-0.104	-0.102	-0.098	-0.090	-0.080	-0.067	-0.058	-0.050
Test Result	MAX	-0.079	-0.069	-0.087	-0.087	-0.083	-0.076	-0.064	-0.049	-0.023
Difference (%)			26	40	16	11	9	5	6	17

Table 64. Load case 4 deflection

	Load Case 4									
	Beam	**1**	**2**	**3**	**4**	**5**	**6**	**7**	**8**	**9**
FEA	0	0	0	0	0	0	0	0	0	0
	0.25	-0.003	-0.004	-0.005	-0.007	-0.009	-0.012	-0.015	-0.018	-0.020
	0.5	-0.010	-0.013	-0.018	-0.024	-0.032	-0.042	-0.052	-0.058	-0.062
	0.75	-0.015	-0.019	-0.025	-0.033	-0.042	-0.053	-0.061	-0.064	-0.064
	1	-0.011	-0.013	-0.016	-0.020	-0.025	-0.029	-0.031	-0.031	-0.029
	1.25	0	0	0	0	0	0	0	0	0
	Beam	**1**	**2**	**3**	**4**	**5**	**6**	**7**	**8**	**9**
Test result	0	0.000	0.000	0.000	0.000	0.000	0.000	0.000	0.000	0.000
	0.25	-0.004	-0.003	-0.005	-0.006	-0.008	-0.011	-0.012	-0.011	-0.006
	0.5	-0.009	-0.009	-0.013	-0.018	-0.023	-0.033	-0.038	-0.037	-0.020
	0.75	-0.012	-0.012	-0.018	-0.025	-0.033	-0.050	-0.060	-0.060	-0.034
	1	-0.007	-0.007	-0.011	-0.015	-0.020	-0.033	-0.042	-0.045	-0.025
	1.25	0.000	0.000	0.000	0.000	0.002	-0.001	-0.001	-0.001	0.000
	Beam	**1**	**2**	**3**	**4**	**5**	**6**	**7**	**8**	**9**

Diff. (%)	0	-200.0	-200.0	-200.0	-200.0	-200.0	-200.0	-200.0	-200.0	-200.0
	0.25	-27.0	18.4	8.2	11.5	17.9	14.3	26.9	44.9	104.9
	0.5	12.8	42.2	30.9	31.3	33.7	26.0	30.5	43.8	102.2
	0.75	21.7	45.5	31.5	27.0	24.0	5.9	1.2	6.3	62.1
	1	39.5	57.7	39.1	29.0	22.2	-12.5	-30.3	-37.6	16.2
	1.25	-200.0	-200.0	-200.0	-200.0	-200.0	-200.0	-200.0	-200.0	-200.0
	Beam	**1**	**2**	**3**	**4**	**5**	**6**	**7**	**8**	**9**
FEA	MAX	-0.015	-0.019	-0.025	-0.033	-0.042	-0.053	-0.061	-0.064	-0.064
Test Result	MAX	-0.012	-0.012	-0.018	-0.025	-0.033	-0.050	-0.060	-0.060	-0.034
Difference (%)			22	45	31	27	24	6	1	6

Table 65. Load case 5 deflection

	Load Case 5									
	Beam	**1**	**2**	**3**	**4**	**5**	**6**	**7**	**8**	**9**
FEA	0	0	0	0	0	0	0	0	0	0
	0.25	-0.004	-0.005	-0.007	-0.009	-0.011	-0.014	-0.015	-0.016	-0.016
	0.5	-0.014	-0.018	-0.024	-0.031	-0.039	-0.046	-0.049	-0.050	-0.048
	0.75	-0.021	-0.026	-0.032	-0.040	-0.049	-0.055	-0.055	-0.052	-0.047
	1	-0.014	-0.017	-0.020	-0.024	-0.027	-0.028	-0.027	-0.024	-0.021
	1.25	0	0	0	0	0	0	0	0	0
	Beam	**1**	**2**	**3**	**4**	**5**	**6**	**7**	**8**	**9**
Test result	0	0.000	0.000	0.000	0.000	0.000	0.000	0.000	0.000	0.000
	0.25	-0.004	-0.004	-0.006	-0.008	-0.010	-0.011	-0.010	-0.008	-0.004
	0.5	-0.012	-0.012	-0.017	-0.023	-0.030	-0.036	-0.035	-0.029	-0.015
	0.75	-0.015	-0.015	-0.023	-0.031	-0.042	-0.054	-0.055	-0.048	-0.025
	1	-0.009	-0.010	-0.014	-0.020	-0.029	-0.038	-0.041	-0.038	-0.019
	1.25	0.000	0.000	0.000	0.000	0.001	0.000	0.000	0.001	0.000
	Beam	**1**	**2**	**3**	**4**	**5**	**6**	**7**	**8**	**9**
Diff. (%)	0	-200.0	-200.0	-200.0	-200.0	-200.0	-200.0	-200.0	-200.0	-200.0
	0.25	-7.2	16.1	9.9	7.0	13.7	24.5	47.1	68.3	118.9
	0.5	20.9	44.0	29.9	26.6	25.7	23.3	34.6	51.3	106.4
	0.75	35.0	52.4	34.3	24.7	14.4	0.6	-0.5	7.2	62.1
	1	44.1	55.8	34.2	16.6	-5.0	-29.3	-42.6	-45.1	6.2
	1.25	-200.0	-200.0	-200.0	-200.0	-200.0	-200.0	-200.0	-200.0	-200.0
	Beam	**1**	**2**	**3**	**4**	**5**	**6**	**7**	**8**	**9**
FEA	MAX	-0.021	-0.026	-0.032	-0.040	-0.049	-0.055	-0.055	-0.052	-0.048

Test Result	MAX	-0.015	-0.015	-0.023	-0.031	-0.042	-0.054	-0.055	-0.048	-0.025
Difference (%)			35	52	34	25	14	1	0	7

Table 66. Load case 6 deflection

	Load Case 6									
	Beam	**1**	**2**	**3**	**4**	**5**	**6**	**7**	**8**	**9**
FEA	0	0	0	0	0	0	0	0	0	0
	0.25	-0.011	-0.013	-0.016	-0.020	-0.023	-0.026	-0.027	-0.029	-0.029
	0.5	-0.039	-0.047	-0.058	-0.068	-0.077	-0.084	-0.088	-0.089	-0.088
	0.75	-0.056	-0.065	-0.076	-0.086	-0.093	-0.097	-0.096	-0.093	-0.088
	1	-0.037	-0.041	-0.045	-0.048	-0.050	-0.050	-0.047	-0.044	-0.039
	1.25	0	0	0	0	0	0	0	0	0
	Beam	**1**	**2**	**3**	**4**	**5**	**6**	**7**	**8**	**9**
Test result	0	-0.004	-0.004	-0.005	-0.005	-0.005	-0.003	-0.002	-0.001	-0.001
	0.25	-0.015	-0.014	-0.021	-0.024	-0.025	-0.024	-0.021	-0.018	-0.009
	0.5	-0.037	-0.036	-0.053	-0.063	-0.069	-0.072	-0.070	-0.060	-0.031
	0.75	-0.035	-0.035	-0.055	-0.070	-0.080	-0.093	-0.096	-0.087	-0.045
	1	-0.020	-0.021	-0.033	-0.044	-0.055	-0.065	-0.072	-0.069	-0.035
	1.25	0.001	0.001	0.001	0.000	-0.002	-0.002	-0.002	-0.001	0.001
	Beam	**1**	**2**	**3**	**4**	**5**	**6**	**7**	**8**	**9**
Diff. (%)	0	-200.0	-200.0	-200.0	-200.0	-200.0	-200.0	-200.0	-200.0	-200.0
	0.25	-32.8	-8.1	-22.7	-17.3	-7.8	7.4	25.5	44.9	102.4
	0.5	6.1	27.5	8.2	7.3	11.0	14.5	23.0	37.9	96.9
	0.75	45.7	59.3	32.7	20.3	15.2	4.1	0.3	6.2	64.0
	1	58.3	65.3	32.4	10.3	-9.6	-26.5	-40.9	-44.7	12.3
	1.25	-200.0	-200.0	-200.0	-200.0	-200.0	-200.0	-200.0	-200.0	-200.0
	Beam	**1**	**2**	**3**	**4**	**5**	**6**	**7**	**8**	**9**
FEA	MAX	-0.056	-0.065	-0.076	-0.086	-0.093	-0.097	-0.096	-0.093	-0.088
Test Result	MAX	-0.037	-0.036	-0.055	-0.070	-0.080	-0.093	-0.096	-0.087	-0.045
Difference (%)			41	58	33	20	15	4	0	6

Midspan Strain

Table 67. Load case 1 strain

	Load Case 1									
	Beam	**1**	**2**	**3**	**4**	**5**	**6**	**7**	**8**	**9**
FEA	0	0	0	0	0	0	0	0	0	0
	0.25	4.0	4.3	4.3	4.4	4.1	3.3	2.6	2.1	1.6
	0.5	18.6	19.6	16.8	13.9	11.7	9.3	7.3	5.9	4.6
	0.75	26.4	27.1	23.0	17.3	11.6	8.3	6.1	4.8	3.7
	1	12.4	10.0	7.3	5.5	4.2	3.1	2.4	1.8	1.4
	1.25	0	0	0	0	0	0	0	0	0
	Beam	**1**	**2**	**3**	**4**	**5**	**6**	**7**	**8**	**9**
Test result	0	0.2	0.1	0.1	0.1	0.3	0.2	0.1	0.1	0.2
	0.25	2.4	3.0	2.9	3.0	2.9	2.0	1.8	1.4	1.4
	0.5	8.7	12.7	12.7	9.8	8.1	5.1	4.7	3.6	3.8
	0.75	15.2	21.6	19.8	15.6	12.7	5.7	6.6	5.1	5.5
	1	12.8	18.3	13.3	9.3	8.1	4.3	3.8	3.2	3.5
	1.25	0.3	0.6	0.7	0.6	0.7	0.0	0.0	0.1	0.2
	Beam	**1**	**2**	**3**	**4**	**5**	**6**	**7**	**8**	**9**
Diff. (%)	0	-200.0	-200.0	-200.0	-200.0	-200.0	-200.0	-200.0	-200.0	-200.0
	0.25	52.0	35.2	39.9	38.2	33.5	48.5	33.8	41.7	14.3
	0.5	72.2	42.8	28.1	34.9	36.5	58.9	42.7	47.7	19.3
	0.75	54.0	22.5	14.9	10.1	-9.2	36.7	-6.6	-5.1	-39.9
	1	-3.2	-58.2	-58.5	-51.7	-64.6	-32.4	-45.9	-53.9	-85.6
	1.25	-200.0	-200.0	-200.0	-200.0	-200.0	-200.0	-200.0	-200.0	-200.0
	Beam	**1**	**2**	**3**	**4**	**5**	**6**	**7**	**8**	**9**
FEA	MAX	26.4	27.1	23.0	17.3	11.7	9.3	7.3	5.9	4.6
Test Result	MAX	15.2	21.6	19.8	15.6	12.7	5.7	6.6	5.1	5.5
Difference (%)		54	22	15	10	8	48	11	15	17

Table 68. Load case 2 strain

	Load Case 2									
	Beam	**1**	**2**	**3**	**4**	**5**	**6**	**7**	**8**	**9**
FEA	0	0	0	0	0	0	0	0	0	0
	0.25	3.0	3.2	3.3	3.6	4.0	3.9	3.4	2.9	2.4
	0.5	12.8	15.3	16.1	14.4	12.4	11.1	9.4	8.1	6.7
	0.75	19.2	21.6	22.6	20.2	15.6	10.9	8.3	6.7	5.3

	1	11.6	10.3	7.8	5.9	4.7	3.8	3.1	2.5	2.0
	1.25	0	0	0	0	0	0	0	0	0
	Beam	**1**	**2**	**3**	**4**	**5**	**6**	**7**	**8**	**9**
Test result	0	0.2	0.2	0.3	0.2	0.4	0.4	0.5	0.4	0.3
	0.25	1.9	2.5	2.5	2.6	3.4	2.7	2.6	2.0	1.9
	0.5	6.3	8.7	11.6	12.6	10.3	7.1	6.8	5.0	5.3
	0.75	10.9	15.0	17.5	17.5	15.4	9.9	9.1	6.8	7.4
	1	9.8	13.7	17.2	11.8	10.1	6.1	5.6	4.5	4.8
	1.25	0.0	0.3	0.9	0.7	0.8	0.4	0.4	0.3	0.3
	Beam	**1**	**2**	**3**	**4**	**5**	**6**	**7**	**8**	**9**
Diff. (%)	0	-200.0	-200.0	-200.0	-200.0	-200.0	-200.0	-200.0	-200.0	-200.0
	0.25	46.7	26.9	26.0	29.5	15.0	36.5	24.2	37.0	23.0
	0.5	68.0	54.9	32.9	13.0	18.6	44.0	33.2	46.7	21.9
	0.75	55.0	35.8	25.8	14.2	1.5	9.6	-9.1	-1.1	-32.3
	1	16.9	-28.4	-75.1	-66.9	-73.4	-46.4	-57.8	-56.4	-84.3
	1.25	-200.0	-200.0	-200.0	-200.0	-200.0	-200.0	-200.0	-200.0	-200.0
	Beam	**1**	**2**	**3**	**4**	**5**	**6**	**7**	**8**	**9**
FEA	MAX	19.2	21.6	22.6	20.2	15.6	11.1	9.4	8.1	6.7
Test Result	MAX	10.9	15.0	17.5	17.5	15.4	9.9	9.1	6.8	7.4
Difference (%)			55	36	26	14	2	11	4	17

Table 69. Load case 3 strain

	Load Case 3									
	Beam	**1**	**2**	**3**	**4**	**5**	**6**	**7**	**8**	**9**
FEA	0	0	0	0	0	0	0	0	0	0
	0.25	5.6	6.2	6.4	6.8	6.8	6.8	6.9	6.9	6.2
	0.5	25.0	27.2	25.8	25.8	25.9	23.3	20.7	19.6	17.4
	0.75	36.6	39.0	36.4	34.1	31.7	27.7	22.6	18.0	14.7
	1	19.7	18.2	15.5	13.0	10.5	8.5	7.2	6.5	5.3
	1.25	0	0	0	0	0	0	0	0	0
	Beam	**1**	**2**	**3**	**4**	**5**	**6**	**7**	**8**	**9**
Test result	0	0.2	0.2	0.2	0.2	0.1	0.5	0.7	0.8	1.1
	0.25	3.7	5.0	5.5	6.0	5.9	5.7	7.3	5.8	6.5
	0.5	14.0	21.0	23.0	21.4	21.9	17.4	18.9	15.1	17.2
	0.75	20.9	30.0	31.6	31.2	32.5	25.9	21.0	15.9	17.6
	1	16.2	22.9	20.5	18.6	14.6	10.3	8.2	7.9	9.0

	1.25	0.0	-0.1	0.0	-0.2	0.3	0.1	-0.3	0.0	-0.1
	Beam	**1**	**2**	**3**	**4**	**5**	**6**	**7**	**8**	**9**
Diff. (%)	0	-200.0	-200.0	-200.0	-200.0	-200.0	-200.0	-200.0	-200.0	-200.0
	0.25	41.2	20.7	15.2	11.7	14.3	17.8	-6.0	16.2	-5.4
	0.5	56.1	25.9	11.4	18.5	17.0	29.0	9.2	26.1	1.0
	0.75	54.6	26.0	14.0	9.0	-2.5	6.7	7.4	12.5	-17.4
	1	19.3	-23.1	-27.5	-35.1	-33.1	-19.7	-12.2	-20.4	-50.5
	1.25	-200.0	-200.0	-200.0	-200.0	-200.0	-200.0	-200.0	-200.0	-200.0
	Beam	**1**	**2**	**3**	**4**	**5**	**6**	**7**	**8**	**9**
FEA	MAX	36.6	39.0	36.4	34.1	31.7	27.7	22.6	19.6	17.4
Test Result	MAX	20.9	30.0	31.6	31.2	32.5	25.9	21.0	15.9	17.6
Difference (%)			55	26	14	9	3	7	7	21

Table 70. Load case 4 strain

	Load Case 4									
	Beam	**1**	**2**	**3**	**4**	**5**	**6**	**7**	**8**	**9**
FEA	0	0	0	0	0	0	0	0	0	0
	0.25	0.8	1.0	1.3	1.7	2.2	2.8	3.7	5.1	6.4
	0.5	3.1	3.9	5.0	6.7	9.1	13.4	17.3	19.2	19.8
	0.75	5.0	6.3	7.8	10.1	13.3	18.4	23.6	25.2	23.3
	1	3.7	4.6	5.6	6.9	8.1	8.3	8.1	8.0	7.3
	1.25	0	0	0	0	0	0	0	0	0
	Beam	**1**	**2**	**3**	**4**	**5**	**6**	**7**	**8**	**9**
Test result	0	-0.1	0.0	-0.1	0.0	-0.1	0.0	-0.1	0.1	0.0
	0.25	0.8	1.3	1.6	2.3	2.7	3.7	2.9	2.4	2.7
	0.5	2.5	3.7	4.7	6.6	7.7	12.8	13.8	10.3	12.4
	0.75	3.1	4.6	6.1	8.6	10.7	19.7	21.2	16.4	21.9
	1	1.9	2.8	3.9	5.4	6.3	10.8	14.0	14.5	20.4
	1.25	-0.1	0.0	0.0	0.2	0.1	0.3	0.6	0.6	0.5
	Beam	**1**	**2**	**3**	**4**	**5**	**6**	**7**	**8**	**9**
Diff. (%)	0	-200.0	-200.0	-200.0	#DIV/0!	-200.0	-200.0	-200.0	-200.0	-200.0
	0.25	-8.6	-27.7	-21.6	-33.3	-23.8	-27.8	22.0	71.0	81.1
	0.5	22.0	6.8	6.7	1.4	16.7	4.1	22.4	60.3	45.9
	0.75	45.0	29.8	23.8	15.9	21.8	-6.8	10.5	42.3	6.5
	1	64.7	46.8	34.6	24.2	24.0	-26.0	-53.7	-58.2	-94.5
	1.25	-200.0	-200.0	-200.0	-200.0	-200.0	-200.0	-200.0	-200.0	-200.0

	Beam	**1**	**2**	**3**	**4**	**5**	**6**	**7**	**8**	**9**
FEA	MAX	5.0	6.3	7.8	10.1	13.3	18.4	23.6	25.2	23.3
Test Result	MAX	3.1	4.6	6.1	8.6	10.7	19.7	21.2	16.4	21.9
Difference (%)			45	30	24	16	22	7	11	42

Table 71. Load case 5 strain

	Load Case 5									
	Beam	**1**	**2**	**3**	**4**	**5**	**6**	**7**	**8**	**9**
FEA	0	0	0	0	0	0	0	0	0	0
	0.25	1.1	1.4	1.6	2.0	2.4	3.0	4.0	5.2	5.7
	0.5	4.4	5.5	6.7	8.6	12.1	15.1	15.6	16.3	16.4
	0.75	7.1	8.7	10.3	12.7	16.9	20.9	21.1	19.3	15.8
	1	5.2	6.2	7.1	7.8	7.5	6.7	6.1	6.0	5.5
	1.25	0	0	0	0	0	0	0	0	0
	Beam	**1**	**2**	**3**	**4**	**5**	**6**	**7**	**8**	**9**
Test result	0	0.0	0.0	0.0	0.0	0.0	0.0	0.0	0.2	0.0
	0.25	1.2	1.7	2.2	2.8	2.9	1.9	1.7	1.7	2.4
	0.5	3.4	4.8	6.2	8.3	9.0	13.4	11.2	7.9	10.1
	0.75	4.1	6.0	8.1	11.3	13.6	20.0	17.2	14.0	18.5
	1	2.4	3.4	4.9	6.4	7.4	12.2	14.5	12.4	16.4
	1.25	0.0	0.0	0.1	0.2	0.0	0.1	0.0	0.2	0.2
	Beam	**1**	**2**	**3**	**4**	**5**	**6**	**7**	**8**	**9**
Diff. (%)	0	-200.0	-200.0	-200.0	-200.0	-200.0	-200.0	-200.0	-200.0	-200.0
	0.25	-8.2	-19.7	-27.4	-34.0	-20.1	43.2	79.2	100.3	81.7
	0.5	26.6	13.7	7.8	2.8	29.9	11.6	32.5	69.6	48.2
	0.75	54.7	36.2	24.1	11.8	21.6	4.4	20.2	31.6	-15.3
	1	75.9	57.5	36.8	18.7	1.9	-58.1	-81.2	-68.6	-100.2
	1.25	-200.0	-200.0	-200.0	-200.0	-200.0	-200.0	-200.0	-200.0	-200.0
	Beam	**1**	**2**	**3**	**4**	**5**	**6**	**7**	**8**	**9**
FEA	MAX	7.1	8.7	10.3	12.7	16.9	20.9	21.1	19.3	16.4
Test Result	MAX	4.1	6.0	8.1	11.3	13.6	20.0	17.2	14.0	18.5
Difference (%)			55	36	24	12	22	4	20	32

Table 72. Load case 6 strain

	Load Case 6									
	Beam	**1**	**2**	**3**	**4**	**5**	**6**	**7**	**8**	**9**
FEA	0	0	0	0	0	0	0	0	0	0
	0.25	3.0	3.5	3.8	4.4	5.5	6.7	7.8	9.0	9.7
	0.5	12.1	14.5	17.9	21.2	22.6	25.7	29.0	30.0	29.2
	0.75	19.1	22.1	26.0	30.7	32.4	33.8	34.9	34.7	31.0
	1	13.3	14.3	13.9	13.6	13.3	12.8	12.0	11.4	10.1
	1.25	0	0	0	0	0	0	0	0	0
	Beam	**1**	**2**	**3**	**4**	**5**	**6**	**7**	**8**	**9**
Test result	0	1.0	1.4	1.0	0.7	0.6	0.7	0.7	0.5	0.6
	0.25	4.0	5.7	6.7	7.0	6.6	6.4	5.5	4.6	5.2
	0.5	10.1	14.6	18.3	20.3	20.2	24.7	23.3	17.9	21.0
	0.75	9.7	14.0	21.1	28.7	32.1	34.7	33.2	26.1	32.8
	1	5.3	7.4	10.8	13.6	16.2	21.6	24.4	23.5	30.7
	1.25	-0.3	-0.5	-0.4	0.2	0.4	1.2	0.5	0.8	0.8
	Beam	**1**	**2**	**3**	**4**	**5**	**6**	**7**	**8**	**9**
Diff. (%)	0	-200.0	-200.0	-200.0	-200.0	-200.0	-200.0	-200.0	-200.0	-200.0
	0.25	-29.0	-48.3	-54.5	-44.0	-18.6	4.2	35.0	65.0	60.5
	0.5	17.8	-0.6	-2.2	4.3	11.2	3.7	21.9	50.7	32.5
	0.75	65.5	45.0	21.0	6.6	0.7	-2.5	4.9	28.0	-5.7
	1	86.0	63.3	25.0	0.0	-19.3	-51.1	-68.4	-69.2	-100.9
	1.25	-200.0	-200.0	-200.0	-200.0	-200.0	-200.0	-200.0	-200.0	-200.0
	Beam	**1**	**2**	**3**	**4**	**5**	**6**	**7**	**8**	**9**
FEA	MAX	19.1	22.1	26.0	30.7	32.4	33.8	34.9	34.7	31.0
Test Result	MAX	10.1	14.6	21.1	28.7	32.1	34.7	33.2	26.1	32.8
Difference (%)			61	41	21	7	1	3	5	28